

AD-A204 145

DTIC
ELECTED

JAN 27 1989

533016 01 87

(1)

cb H

MODEL TESTS ON THE
CERC FULL SCALE TEST FLOATING BREAKWATER
Final Report

by

A. Tørum, C.T. Stansberg,
G.O. Otterå, O.H. Slættelid

June 1987

United States Army
European Research Office of the U.S. Army
London England

Contract number: DAJA45-86-C-0035

Work carried out by:
Norwegian Marine Technology Research Institute A/S
(MARINTEK)

Approved for public release,
distribution unlimited

MARINTEK
THE SINTEF GROUP



REPORT
REPORT



MARINTEK
THE SINTEF GROUP

REPORT

Norwegian Marine Technology Research Institute A/S

MAIN OFFICE
Haakon Haakonsensgt 34 Tel. +47-7-59 55 00 SANDEFJORD
P O Box 4125 Valentinslyst Telex 55 146 nsfln P O Box 173 Asnes
N-7001 Trondheim, Norway Telefax -47-7-59 57 76 N-3201 Sandefjord, Norway
Tel. +47-34-73 033

File no	87-0166		
Report no	533016 01 87		
Accessibility	Restricted		
No. of pages	216	Model no	

Report title: MODEL TESTS ON THE CERC FULL SCALE TEST FLOATING BREAKWATER
Final Report, ~~Draft~~

Commission project title:
Model Tests on the CERC Full Scale Test Floating Breakwater

Client:	Department of the Army (U.S.A.) Headquarters, 47th Area Support Group P.O. Box 160, Warrington Cheshire WA5 1UW, ENGLAND	Client's ref.:	Dennis P. Foley Peter Grace (CERC)
---------	-----------------------------------------------------------------------------------------------------------------------------------	----------------	---------------------------------------

Commission project manager:	Work carried out by:
Alf Tørum	Carl Trygve Stansberg Geir Olav Otterå Olav H. Slættelid

External cooperation with:	Represented by:
----------------------------	-----------------

Summary of the report:

Model tests with a floating breakwater in short-crested waves have been performed in scale 1:10. The breakwater is a model of a 2-pontoon CERC prototype. 2 versions are tested: fendered and stiff. Some tests in long-crested waves are also included. Wave elevation, anchor line forces, breakwater motions and hydrodynamic pressures have been measured. Simple numerical simulations of forces and motions are made. Experimental wave reduction is studied through maximum and RMS values and wave spectra. Wave transmission varies from 30% for 2s waves to 100% for 6s waves (full scale). Control of wave statistics and grouping is included. Waves in front of the model is also studied. Maximum and RMS values, auto- and cross-spectra, linear transfer functions and amplitude statistics of forces and motions are presented. The maximum force in a single sensor was 102 kN, while in a single anchor line it was larger than 150 kN. Non-linearities in motions and forces result in significantly larger extremes than predicted by linear theory.

Other documentation:

Appendices: 30 Data Reports including all data from the analysis.

Subject words: Flytemolo
(in Norwegian) Modellforsøk
Kortkammede bølger
Numeriske simuleringer

City/date: Trondheim, 1987.06.11.

Reported by

Carl Trygve Stansberg
Alf Tørum
Project manager/Head of department

BUFRUM database

While the Institute exercises all possible care to see that assignments are carried out as conscientiously as the circumstances allow, no economical responsibility for the results or their application will be accepted by the Institute or its responsible bodies. Complete reports may be used in customer relations, but any excerpts must be approved by the Institute.

Unclassified

SECURITY CLASSIFICATION OF THIS PAGE (When Data Entered)

REPORT DOCUMENTATION PAGE		READ INSTRUCTIONS BEFORE COMPLETING FORM
1. REPORT NUMBER 533016 01 87	2. GOVT ACCESSION NO.	3. RECIPIENT'S CATALOG NUMBER
4. TITLE (and Subtitle) Model Tests on the CERC Full Scale Test Floating Breakwater Final Report, Draft		5. TYPE OF REPORT & PERIOD COVERED Open Final. Aug. 1986 - June 1987
7. AUTHOR(s) Alf Tørum Carl Trygve Stansberg		6. PERFORMING ORG. REPORT NUMBER DAJA45-86-C-0035
9. PERFORMING ORGANIZATION NAME AND ADDRESS Norwegian Marine Technology Research Institute A/S P.O. Box 4125 - Valentinslyst N-7001 Trondheim, NORWAY		10. PROGRAM ELEMENT, PROJECT, TASK AREA & WORK UNIT NUMBERS
11. CONTROLLING OFFICE NAME AND ADDRESS Department of the Army Headquarters, 47th Area Support Group P.O. Box 160, Warrington, Cheshire WA 5 1UW, England		12. REPORT DATE 1987.06.11
14. MONITORING AGENCY NAME & ADDRESS (if different from Controlling Office) US Army Corps of Engineers Waterways Experimental Station Coastal Engineering Research Center P.O. Box 631, Vicksburg, Mississippi 39180-0631, USA		13. NUMBER OF PAGES 216
16. DISTRIBUTION STATEMENT (of this Report) <i>Up</i> Distribution Limited		18. SECURITY CLASS. (of this report) Classified
17. DISTRIBUTION STATEMENT (of the abstract entered in Block 20, if different from Report)		
18. SUPPLEMENTARY NOTES		
19. KEY WORDS (Continue on reverse side if necessary and identify by block number) Floating Breakwater Model Tests Short-crested Waves Numerical Simulations		
20. ABSTRACT (Continue on reverse side if necessary and identify by block number) Model tests with a floating breakwater in short-crested waves have been performed in scale 1:10. The breakwater is a model of a 2-pontoon CERC prototype. 2 versions are tested: fendered and stiff. Some tests in long-crested waves are also included. Wave elevation, anchor line forces, breakwater motions and hydrodynamic pressures have been measured. Simple numerical simulations of forces and motions are made.		

(Continued)

DD FORM 1 JAN 71 1473 EDITION OF 1 NOV 68 IS OBSOLETE

Unclassified
SECURITY CLASSIFICATION OF THIS PAGE (When Data Entered)

Unclassified

SECURITY CLASSIFICATION OF THIS PAGE(When Data Entered)

20 (Continued from previous page)

Experimental wave reduction is studied through maximum and significant wave heights and wave spectra. Wave transmission varies from ~30% for 2s waves to ~100% for 6s waves (full scale). Control of wave statistics and grouping is included. Waves in front of the model are also studied. Maximum and RMS values, auto- and cross-spectra, linear transfer functions and amplitude statistics of forces and motions are presented. The maximum force in a single sensor was 102 kN, while in a single anchor line it was larger than 150 kN. Non-linearities in motions and forces result in significantly larger extremes than predicted by linear theory.

INSPECTED

Accession For	
NTIS	BR&I <input checked="" type="checkbox"/>
DTIC TAB	<input type="checkbox"/>
Unpublished	<input type="checkbox"/>
Classification:	
Distribution:	
Availability Codes	
Normal and/or	
Dist	Special
A-1	

Unclassified

SECURITY CLASSIFICATION OF THIS PAGE(When Data Entered)

CONTENTS

	Page
1. INTRODUCTION	1
2. TEST CONDITIONS	2
2.1 Test facilities	2
2.2 The breakwater model and the instrumentation	2
2.3 Test program	14
2.4 Generation of irregular, short-crested waves	16
2.5 Data processing	17
3. EXPERIMENTAL RESULTS	19
3.1 Results for fendered model	20
3.1.1 Photographs of fendered breakwater model in irregular waves	20
3.1.2 Wave reduction/amplification around fendered breakwater model	21
3.1.3 Mooring line forces	49
3.1.4 Motions analysis	80
3.2 Results for stiff model	105
3.2.1 Photographs of stiff breakwater model in irregular waves	105
3.2.2 Wave reduction/amplification around stiff breakwater model	106
3.2.3 Mooring line forces	134
3.2.4 Motions analysis	165

.89 1 27 006

	Page
4. COMPUTER SIMULATIONS WITH A SIMPLE NUMERICAL MODEL	190
4.1 Brief introduction	190
4.2 System description	191
4.2.1 Floating breakwaters	191
4.2.2 Mooring system data	192
4.2.3 Mooring system	193
4.2.4 Wave conditions	195
4.3 Results	196
4.3.1 Wave frequency response	196
4.3.2 Mooring analysis	200
4.3.3 First order motion transfer functions	204
5. DISCUSSION AND CONCLUSIONS	211
6. REFERENCES	216

APPENDICES: 30 Data Reports (in separate volumes)

1. INTRODUCTION

This report presents results from a 1:10 model scale experiment with a floating breakwater concept proposed by CERC/US Army Corps of Engineers. The experiment is carried out in the MARINTEK Ocean Basin, mainly in short-crested irregular waves. The breakwater is a model of a full-scale prototype which has been tested earlier by CERC in a 4-year test program in Puget Sound, Seattle, U.S.A./1/. Thus a main objective of the model test is to verify the full scale results. In addition, the model test include more severe wave conditions than those observed in Puget Sound. The model test presented in this report include measurements of wave elevation behind and in front of the breakwater, mooring line forces, breakwater motions, and hydrodynamic pressures at the front and back sides of the breakwater. A total number of 20 different test runs were made with the model, + 10 wave calibration runs. All results from the subsequent analysis are put together in separate Data Reports, one for each test run (Appendix 1-30). The most essential results are presented in this Main Report.

All recorded data are stored on magnetic tapes at MARINTEK. Parts of each of the 20 model test runs are also recorded on video tapes.

The CERC prototype, as well as the model, was made up by two rigid, rectangular boxes (pontoons). A good description of the prototype test details is found in the resulting CERC report /1/. Two different pontoon connection types are used in the present model test: fendered (no bolting) and stiff (pontoons welded together).

Additional, similar model tests with 6 pontoons were later made for the Norwegian Coastal Directorate. Results from that test are presented in a separate report /2/.

Computer simulations of the linear motions of the stiff breakwater, based on a simple numerical model, are also presented.

The work presented in the present report and in /2/ follows mainly the lines described in the Proposal /3/, except from some changes in the test program (see chapter 2.4).

2. TEST CONDITIONS

2.1 Test facilities

The laboratory test was performed in MARINTEK's large Ocean Basin which measures 50m x 80m. See the schematical drawing in fig. 2.1. For this test, the model scale was chosen to be 1:10. In order to simulate the average bottom depth of 18.3m in Puget Sound, the adjustable bottom was therefore set at 1.83m.

The Ocean Basin is equipped with 2 wavemaker systems (see fig. 2.1). One of the 50m short side-walls consists of a large, horizontally double-hinged hydraulic wavemaker (wavemaker 1). In the present experiment, however, we used the multiflap wavemaker (wavemaker 2) located along one of the long sides, in order to be able to generate shortcrested as well as long-crested waves. This wavemaker consists of 144 electromechanical, individually computer controlled flaps. The generation of irregular, short-crested waves is briefly described in section 2.4.

Along the 2 sidewalls opposite to the wavemakers, rigid and impermeable beaches are installed. The beach slope is curved (zero slope at still water level).

2.2. The breakwater model and the instrumentation

The full scale prototype breakwater was made up of air-filled concrete boxes, see fig. 2.2. and the CERC Report /1/. Since the model test included no measurements of structural dynamics of the model, it was for simplicity decided to construct the model scale breakwater pontoons with steel kernels surrounded by a stiff, impermeable foamy material ("divinycell"). See fig. 2.3. The short ends were made of steel plates. The waves, hydrodynamics, mooring line forces and the breakwater motions are expected not to be affected by this structural difference between the prototype and the model, as long as the size, shape, weight and moments of inertia are reproduced in model scale (see Appendix A of the Proposal /3/).

The breakwater model was tested in fendered condition (figs. 2.4.a, 2.6, 2.7, 2.16 and 2.17) as well as in stiff condition (fig. 2.4.b). The fen-

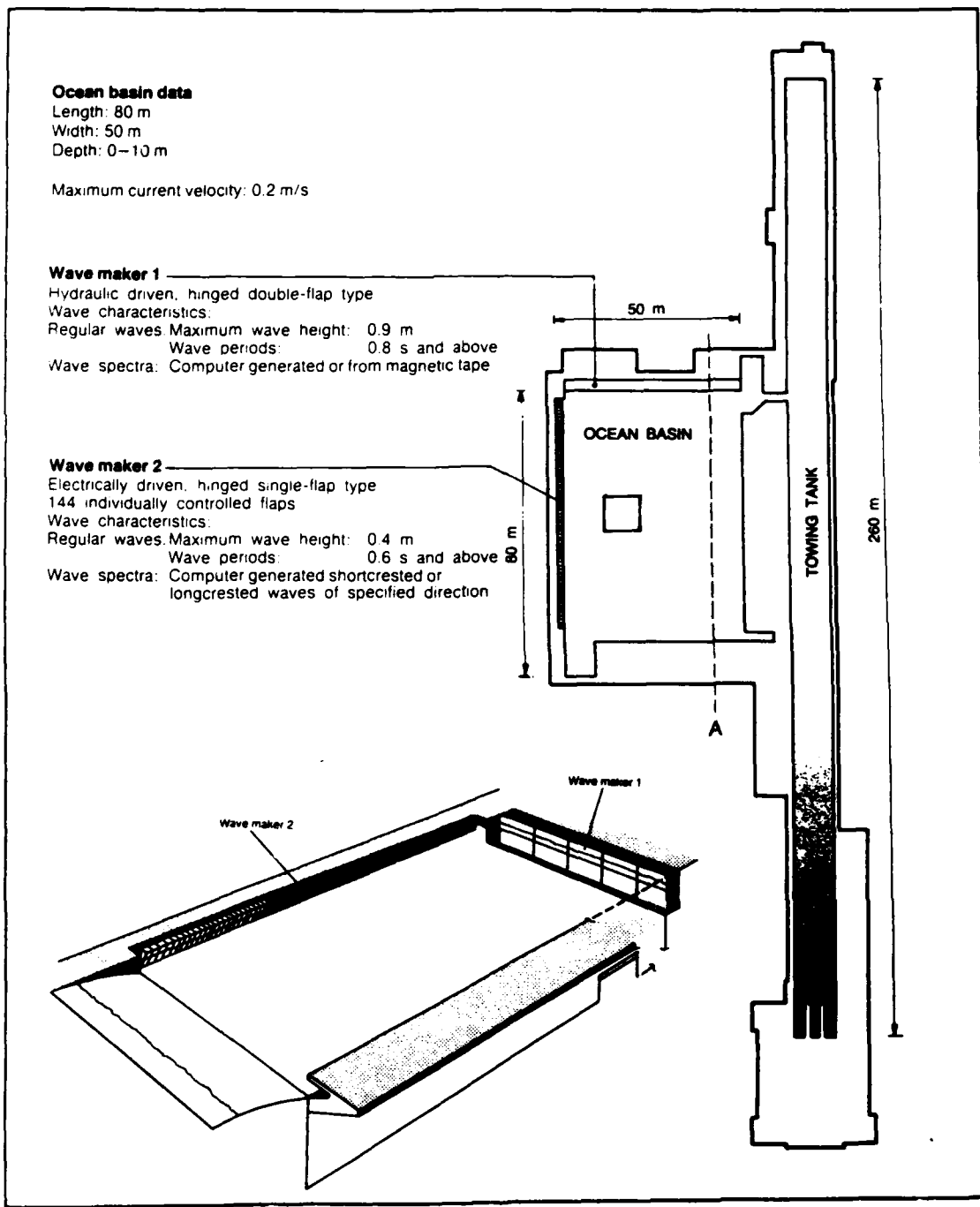


Fig. 2.1 Principle drawing of the ocean basin where the experiments were done. The measurement area for these tests is indicated as a square in the basin.

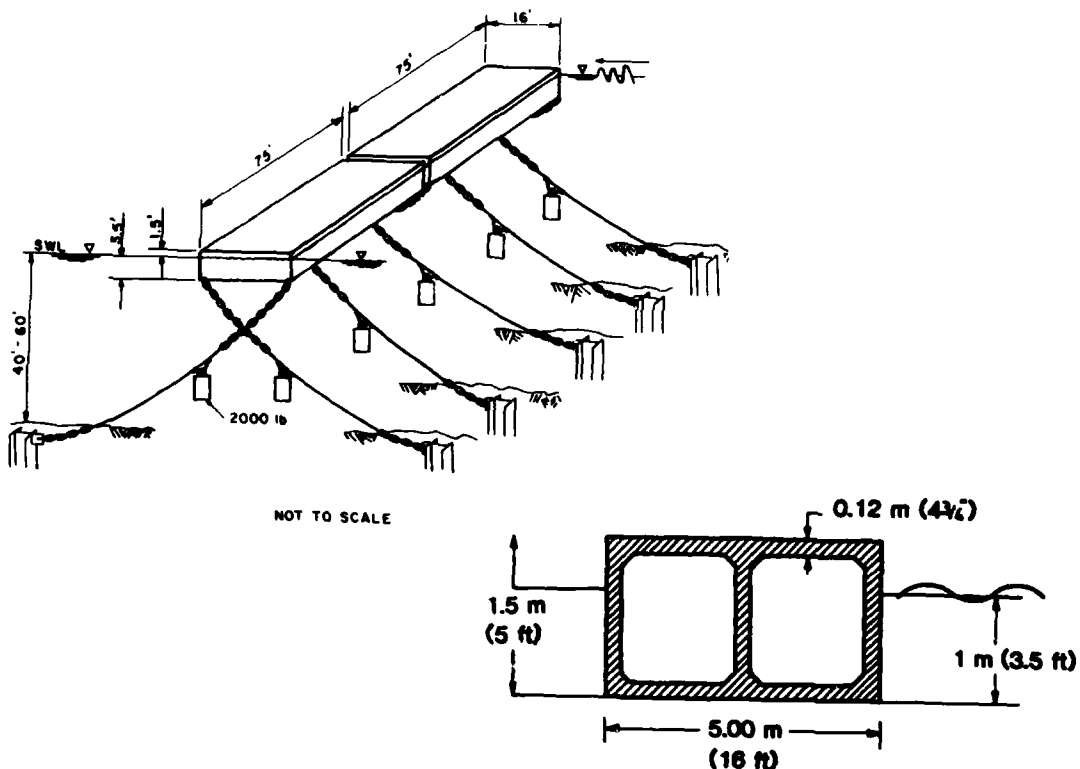


Fig. 2.2 Illustrating the prototype breakwater (from /1/ and /3/).

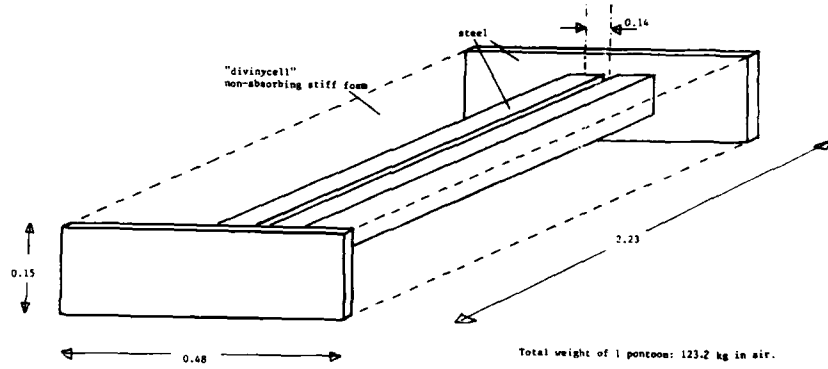


Fig. 2.3 Schematical drawing of a pontoon model

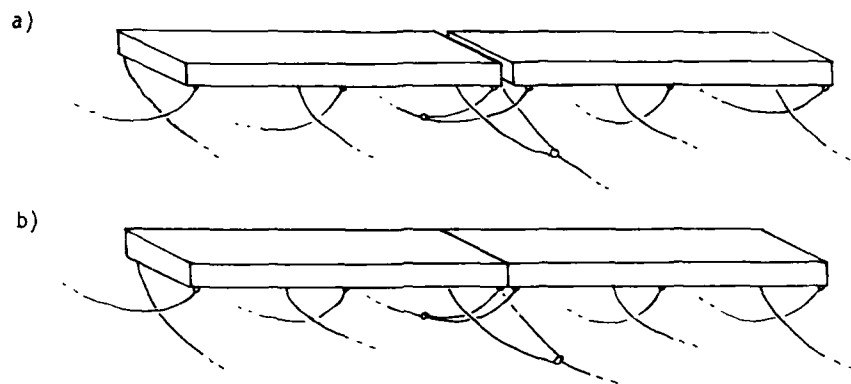


Fig. 2.4 a) Fendered breakwater model
b) Stiff breakwater model

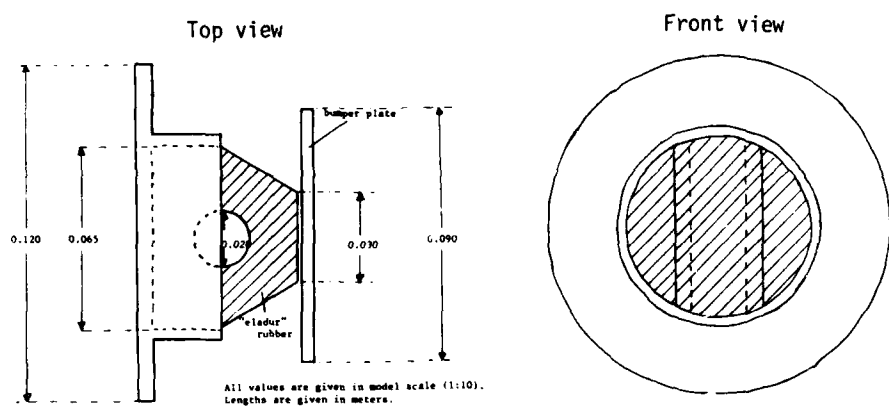


Fig. 2.5 Schematical illustration of a fender model



Fig. 2.6 Installing the breakwater model in the Ocean Basin (fendered breakwater).



Fig. 2.7 Viewing the breakwater from the short end. The mooring line connection to the pontoon can be observed.

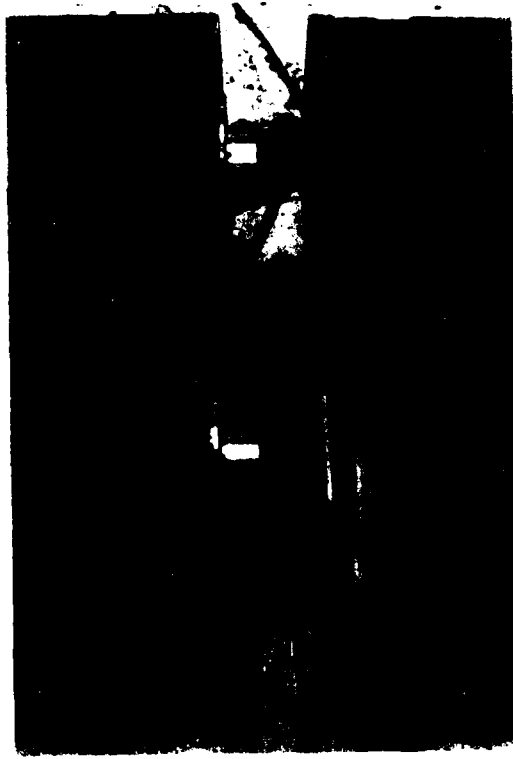


Fig. 2.8 The fender system.

fenders (figs. 2.5 and 2.8) were made of a hard synthetic rubber material ("eladur"). The stiff breakwater was obtained by removing the fenders and welding the pontoons together at the short ends, which means that the total length of the breakwater was 5 cm less than for the fendered model (model scale).

A tilt test of a free floating pontoon gave a roll period equal to 1.0s, model scale. The freeboard of a free pontoon was 5 cm, while in moored condition it was 4 cm, model scale.

The mooring lines were modelled with wires and chains, as shown in fig. 2.9 and the photographs figs. 2.7, 2.11 - 2.14. They were modelled to simulate, as closely as possible, the prototype lines /1/ with respect to weight, size and stiffness. The stiffness was modelled with a proper spring at the bottom end of each line (see fig. 2.12, 2.13). Fig. 2.10 shows the geometry of the mooring system. A force measuring sensor was included in the chain of each line just beneath the breakwater (fig. 2.14). Static tension force in each line was measured to be \sim 18 N (the corresponding prototype tension was 22 kN /1/). (For the central y-coupled lines, this was divided into \sim 9 k N for each of the chains between the y-coupling and the breakwater bottom).

Pressure transducers were placed on either long vertical side of the pontoons, see fig. 2.15. An optical positioning system developed at MARINTEK,/4/ OPTOPOS, was used to measure 6 motional components (x-, y-, z-position, roll, pitch, yaw) of each pontoon. (For the stiff model, only the 6 components of the whole structure were measured). See fig. 2.18 for the definition of the coordinate system.

23 wave staffs were used to measure the wave elevation: 12 staffs in front and 11 behind the breakwater. See fig. 2.19 for the location of the staffs. The actual design of the staffs may be observed from the photographs in figs. 2.6, 2.16 and 2.17.

Table 2.1 shows the measuring channels used throughout the experiment. The 6 last channels, ch. 48-53, are, however, used only for the fendered model.

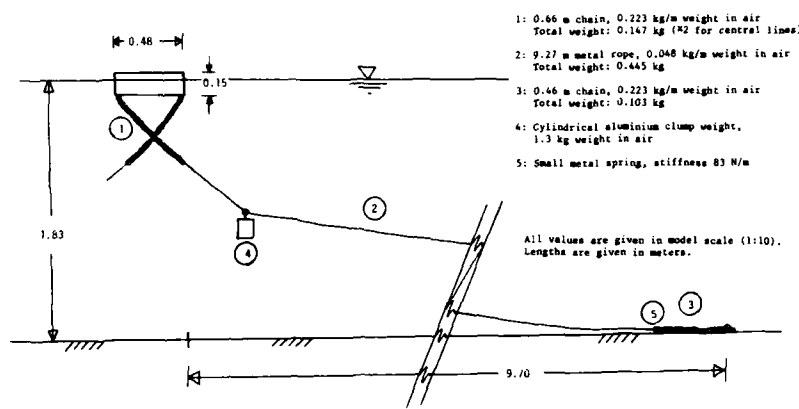


Fig. 2.9 A mooring line of the breakwater model.

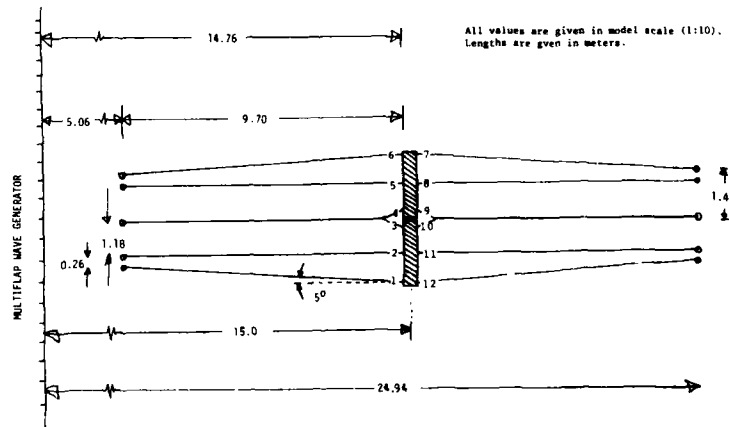


Fig. 2.10 The mooring system of the model, seen from above.
The numbers marked at the breakwater denote the force sensors
at the bottom of the pontoons (the corresponding mooring lines
are crossing beneath the breakwater and are seen on the other
side of the breakwater on this figure).



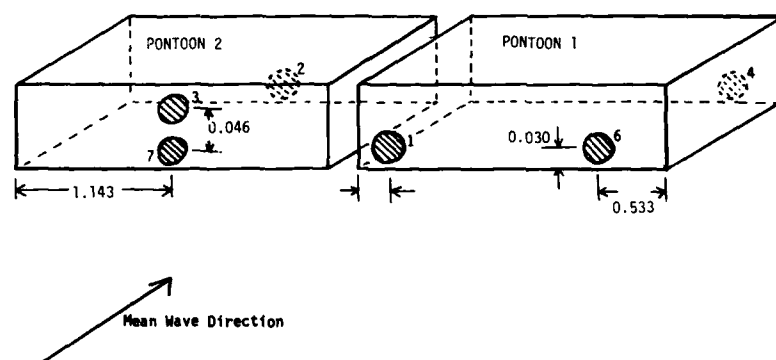
Fig. 2.11 The central mooring lines with the y-coupling and the clump-weights.



Fig. 2.12 Fig. 2.13
The bottom-end of a mooring line,
with the spring modelling the
stiffness.



Fig. 2.14 A force sensor.



All values are given in model scale (1:10).
Lengths are given in meters.

Fig. 2.15 Pressure cell locations.

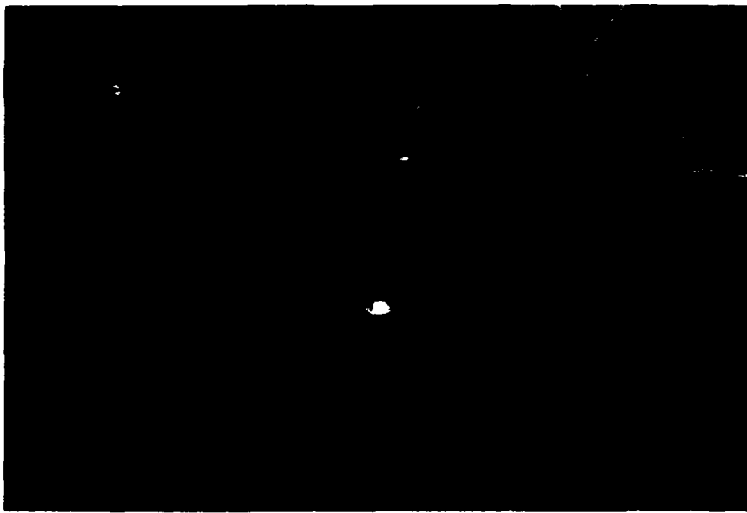


Fig. 2.16 The moored floating breakwater (fendered) in still water.

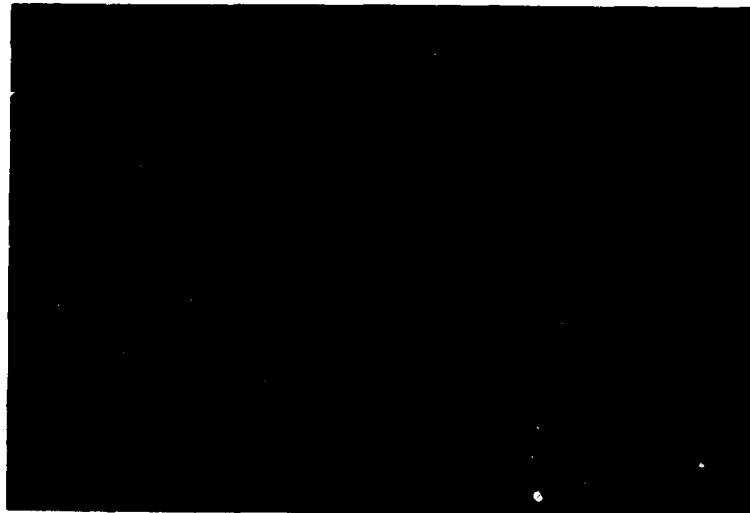


Fig. 2.17 Detailed picture of the floating breakwater.

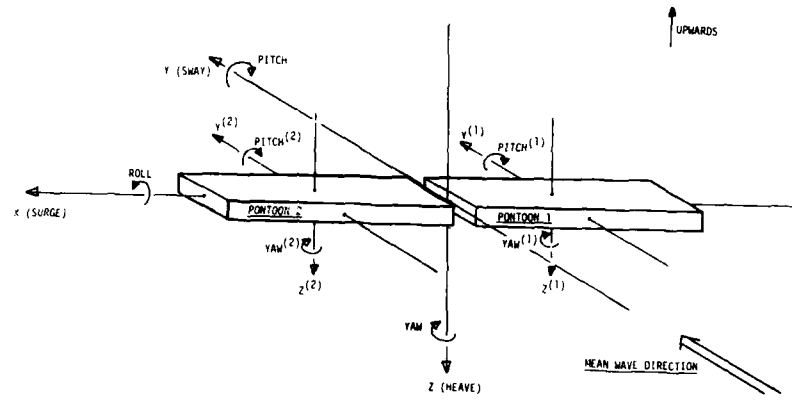


Fig. 2.18 The coordinate system.

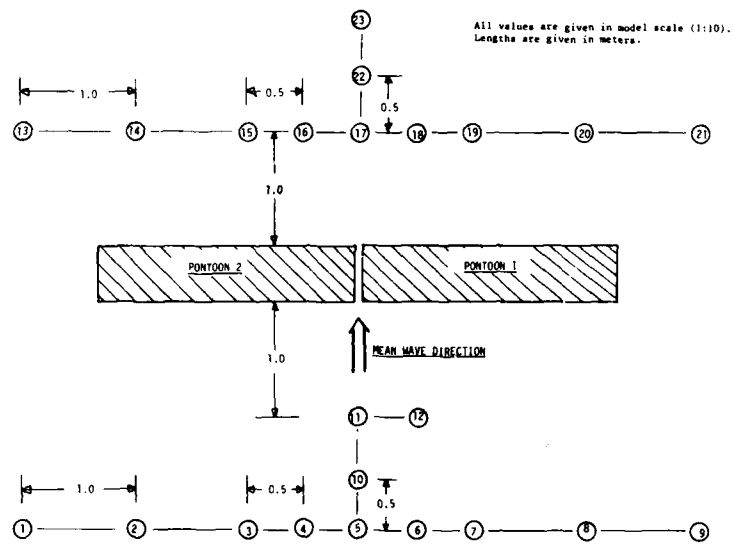


Fig. 2.19 Wave staff locations

No. of chans: 53

Channels:

NR	NAME	UNIT
1	WAVE 1	M
2	WAVE 2	M
3	WAVE 3	M
4	WAVE 4	M
5	WAVE 5	M
6	WAVE 6	M
7	WAVE 7	M
8	WAVE 8	M
9	WAVE 9	M
10	WAVE 10	M
11	WAVE 11	M
12	WAVE 12	M
13	WAVE 13	M
14	WAVE 14	M
15	WAVE 15	M
16	WAVE 16	M
17	WAVE 17	M
18	WAVE 18	M
19	WAVE 19	M
20	WAVE 20	M
21	WAVE 21	M
22	WAVE 22	M
23	WAVE 23	M
24	RING 1(force)	k N
25	RING 2	k N
26	RING 3	k N
27	RING 4	k N
28	RING 5	k N
29	RING 6	k N
30	RING 7	k N
31	RING 8	k N
32	RING 9	k N
33	RING 10	k N
34	RING 11	k N
35	RING 12	k N
36	P.CELL 1	PA
37	P.CELL 2	PA
38	P.CELL 3	PA
39	P.CELL 4	PA
40	P.CELL 6	PA
41	P.CELL 7	PA
42	X-POS 1	M
43	Y-POS 1	M
44	Z-POS 1	M
45	ROLL 1	DEG
46	PITCH 1	DEG
47	YAW 1	DEG
48	X-POS 2	M
49	Y-POS 2	M
50	Z-POS 2	M
51	ROLL 2	DEG
52	PITCH 2	DEG
53	YAW 2	DEG

Table 2.1

2.3 Test program

A total number of 30 test runs were made:

10 wave calibration runs with no model (No. 101-115)

10 runs with fendered model (No. 201-215)

10 runs with stiff model (No. 351-365)

Table 2.2 explains the different tests. Test runs 107-108-109, 207-208-209, 357-358-359 were chosen to reproduce 3 CERC prototype wave records. (This reproduction is not perfectly accurate, since some of the waves of the 3 actual input spectra are somewhat shorter than recommended for the wavemaker. In addition, the 3 prototype wave records used as input waves in those 9 test runs must be expected to be disturbed by the prototype breakwater).

Registration of signals started simultaneously with the start of the wavemaker and lasted 16 minutes (model scale) (regular waves: 6 minutes). Plots of the start-up sequence (51.2s model scale) for each channel are included in the Data Reports Appendix 1-30, to serve as a tool in e.g. technical control and offset studies. In the main analysis, however, the last 12 minutes (2 minutes for regular waves) were used, in order to let the wave field have 4 minutes to build up to more or less stationary conditions. Sampling interval used is 0.050s (model scale). All signals passed through a Butterworth 4th order analog filter with cut-off at 6 Hz (model scale).

533016 FLOATING BREAKWATER MODEL TEST, 2 PONTOONS

List of all the test runs.

Wave Calibration Runs:

Run no.	Wave Condition (Full scale)
101	Jonswap spectr. $T_p=3.2s$ $H_s=0.75m$ $\gamma=3.3 \cos^2\theta$ dir.sp.
102	Jonswap spectr. $T_p=4.3s$ $H_s=1.00m$ $\gamma=3.3 \cos^2\theta$ dir.sp.
103	Jonswap spectr. $T_p=5.0s$ $H_s=1.50m$ $\gamma=3.3 \cos^2\theta$ dir.sp.
107	Jonswap spectr. $T_p=3.0s$ $H_s=0.93m$ $\gamma=2.0 \cos^2\theta$ dir.sp.
108	Jonswap spectr. $T_p=2.8s$ $H_s=0.65m$ $\gamma=2.0 \cos^2\theta$ dir.sp.
109	Jonswap spectr. $T_p=2.4s$ $H_s=0.65m$ $\gamma=2.7 \cos^2\theta$ dir.sp.
111	Jonswap spectr. $T_p=3.2s$ $H_s=0.75m$ $\gamma=3.3 \cos^2\theta$ dir.sp.
112	Jonswap spectr. $T_p=3.2s$ $H_s=0.75m$ $\gamma=3.3$ long-crested
113	Regular waves $T = 6.3s$ $H = 1.00m$
115	Regular waves $T = 3.2s$ $H = 0.75m$

The mean wave direction is 90 deg (perpendicular to the long sides of the breakwater) for all the test runs.

Tests with fendered breakwater model:

Run no.	Wave condition
201	As run no. 101
202	As run no. 102
203	As run no. 103
207	As run no. 107
208	As run no. 108
209	As run no. 109
211	As run no. 111
212	As run no. 112
213	As run no. 113
215	As run no. 115

Tests with stiff breakwater model:

Run no.	Wave condition
351	As run no. 101
352	As run no. 102
353	As run no. 103
357	As run no. 107
358	As run no. 108
359	As run no. 109
361	As run no. 111
362	As run no. 112
363	As run no. 113
365	As run no. 115

Table 2.2

2.4 Generation of irregular, short-crested waves

Basically, the simulation starts with the specification of a directional frequency spectrum $S(f, \theta)$ of the surface wave elevation $\eta(t)$. The spectrum is modelled as a monomodal JONSWAP- $\cos^2\theta$ spectrum, defined by the following formulas:

$$S(f, \theta) = S(f) \cdot D(\theta) \quad (2.1)$$

$$S(f) = K_1 \cdot f^{-5} \exp -1.25(f/f_p)^2 - 4 \cdot \gamma \beta$$

$$\beta = \exp -(f-f_p)^2/(2\sigma^2 f_p^2) \quad (2.2)$$

$$\begin{aligned} \sigma &= 0.07 \quad f < f_p \\ &= 0.09 \quad f > f_p \end{aligned}$$

$$D(\theta) = K_2 \cos^2 s(\theta - \theta_0) \quad (2.3)$$

where γ = peak enhancement factor
 f_p = peak frequency
 θ_0 = mean wave direction
 s = directional spreading parameter
 K_1, K_2 are scaling factors

Note that this model assumes the same directional spectrum $D(\theta)$ for all frequencies.

The spectrum is specified by the 5 input parameters H_s , f_p , γ , θ_0 and s , where the last 4 are defined above, and

$$H_s = H_{mo} = 4/m_0$$

$$m_0 = \int_0^\infty df S(f) \quad (2.4)$$

The time series generation is then based on linear superposition of harmonic (plane) wave components with weight functions based on eq. (2.1) - eq. (2.3) and the actual frequency increments. The software for the multiflap generator combines 100 components, each with a random phase and a random direction according to the chosen directional spectrum $D(\theta)$. The frequencies chosen for the spectrum generation are non-equidistant, with a high frequency density around the spectral peak, and a lower density in the spectral tails.

2.5 Data processing

The following analysis is made:

1. Listing of simple statistics (data available immediately after each test run) - model scale.
2. Plotting of autospectra of each channel (based on FFT of blocks consisting of 2048 data points each) - full scale.
3. Plotting of the first 1024 time history points of each channel (the start-up sequence) - full scale.
4. Plotting of a block of 1250 (280 for regular waves) time history points of the following channels: Wave Staff 1, 8, 11, 13, 18, 21 + all other channels. Full scale.

The time window is chosen to include the maximum force (or wave elevation if wave calibration) recorded in the run (the same time window is used for all channels in the run).

For regular waves, additional time history plots with 280 points (for the same set of channels) are presented, showing an early stage of the wave train (after the transient, before reflection).

5. Listings of spectral and zero-up-crossing peak-to-peak parameter values for at least the following channels:
Wave staff no. 11 and 18, 3 force sensors, all motional

measurements. Full scale.
All 23 wave staffs. Model scale.

6. Spectra of wave staff no. 11 and 18 are compared to theoretical JONSWAP plots, and to corresponding calibrated spectra. Wave amplitude transmission (and amplification in front) curves are plotted. Full scale.
7. Wave group spectra based on the Hilbert envelope /5/, for ch. 11 & 18 are plotted and compared to theoretical curves calculated from the measured wave spectrum. "Pinkster" formula /5,6/). Full scale.
8. Plots with zero-up-crossing wave height statistics are compared to the Rayleigh distribution (wave 11 & 18). Full scale.
9. Plots with statistics of force & motion maxima are compared to the Rayleigh distribution (3 force sensors, 6 motional components). Full scale.
10. Plots of transfer/functions between wave 11 and 3 force sensors + 3 motional components, (Wave 11 signal is taken from wave calibration - not from the actual model test run). Full scale.
11. Plots of cross spectra (coherence & phase) between wave 11 and 3 force sensors + 3 motional components (Wave 11 signal is taken from the same test run as the force & motions measurement). Full scale.

All motions measurements (Channel 42-53) are digitally filtered at 0.99 Hz (full scale) after the recording and before the main analysis. (Data in the first listings, item 1 above are however not filtered).

Complete results from the analysis described above are presented in the Data Reports - Appendix 1-30. Main results have been selected for presentation in this Main Report.

3. EXPERIMENTAL RESULTS

The breakwater model experiment in the Ocean Basin resulted in a large amount of data. One of the reasons for this is the long registration period used in the irregular wave tests (~ 1000-1500 wave periods, of which the last ~ 700-1000 were used in the main analysis), which was chosen in order to give reliable statistics of the results. During the planning of the experiment, it was considered to be important to emphasize long records because moored structures like this floating breakwaters often have significant non-linear motions in the low-frequency region.

As a consequence, one had to be selective when planning the analysis and the presentation in this Main Report. We have emphasized the irregular wave tests (although some analysis is done also for the regular wave tests - see the Data Reports). It is the intention of this Main Report to point out the following essential features of the breakwater model in irregular waves:

- Wave reduction
- Wave amplification in front
- Change of wave spectrum due to model
- Wave statistics/grouping, with/without model
- Wave pattern around model
- Effect of wave short-crestedness on waves and responses
- Force and motion maximum/RMS value vs. significant wave height and peak period.
- Force and motion spectra
- Linear transfer functions
- Coherence analysis (i.e. coupling between waves-forces-motions)
- Deviations from linear (1. order) behaviour

The presentation is divided into 2 main parts:

Fendered model analysis
Stiff model analysis

which each is split up into 3 parts:

Waves
Forces
Motions

3.1 Results for fendered model

3.1.1 Photographs of fendered breakwater model in irregular waves

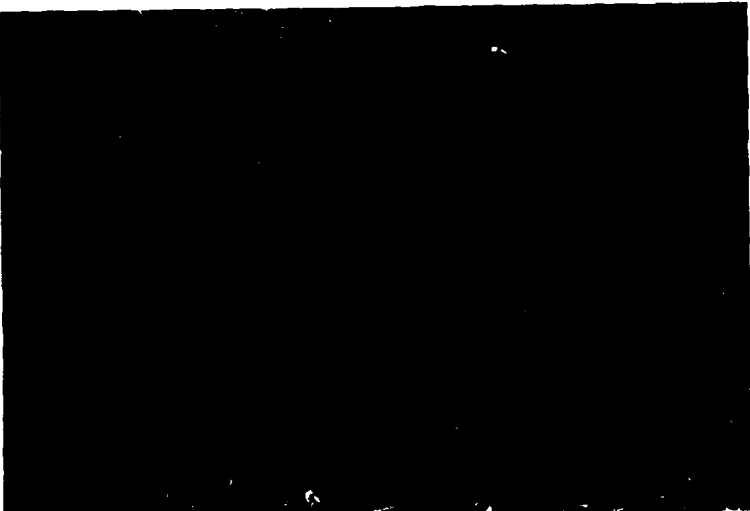


Fig. 3.1
Run no. 203



Fig. 3.2
Run no. 203



Fig. 3.3
Run no. 207

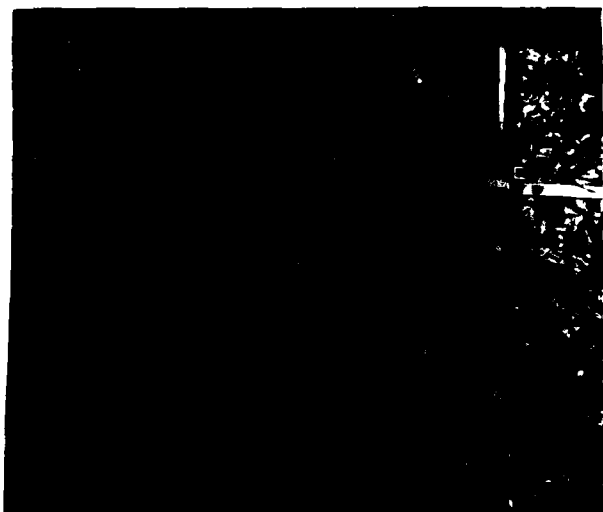


Fig. 3.4 Relative motion of pontoons, run no. 203.
Picture no. 1, in a series of 3.



Fig. 3.5 Relative motion of pontoons, run no. 203.
Picture no. 2 in a series of 3.



Fig. 3.6 Relative motion of pontoons, run no. 203.
Picture no. 3 in a series of 3.

3.1.2 Wave reduction/amplification around fendered breakwater model

The first plot (fig. 3.7) shows the normalized maximum wave height $H_{max,n} = H_{max}/H_{max,o}$ and normalized significant wave height $H_{mo,n} = H_{mo}/H_{mo,o}$ behind the model (wave staff 18, see fig. 2.19) as a function of the input peak wave period T_p . $H_{max,o}$ and $H_{mo,o}$ are wave height values obtained from calibration without model. Next, figs. 3.8-3.15 show plots of the distribution of $H_{max,n}$ and $H_{mo,n}$ 1m behind (wave staffs 1-9), and 2m in front of (wave staffs 13-21), the breakwater, for each of the 8 irregular sea states. Figs. 3.16 - 3.21 show wave spectra for wave staff 18 (1m behind) and 11 (1m in front) with and without model, compared to theoretical input values, together with resulting amplitude transmission/ amplification functions. Wave height statistics, (compared to the Rayleigh distribution) and wave group spectra (compared to theoretical "Pinkster" curve /5, 6/), with and without model, are finally presented in figs. 3.22 - 3.33. Wave group spectra are calculated as the spectra of the square Hilbert envelope of the wave elevation /5/.

WAVE REDUCTION VS PEAK PERIOD OF INPUT WAVE
 WAVE STAFF NO. 18 FENDERED MODEL

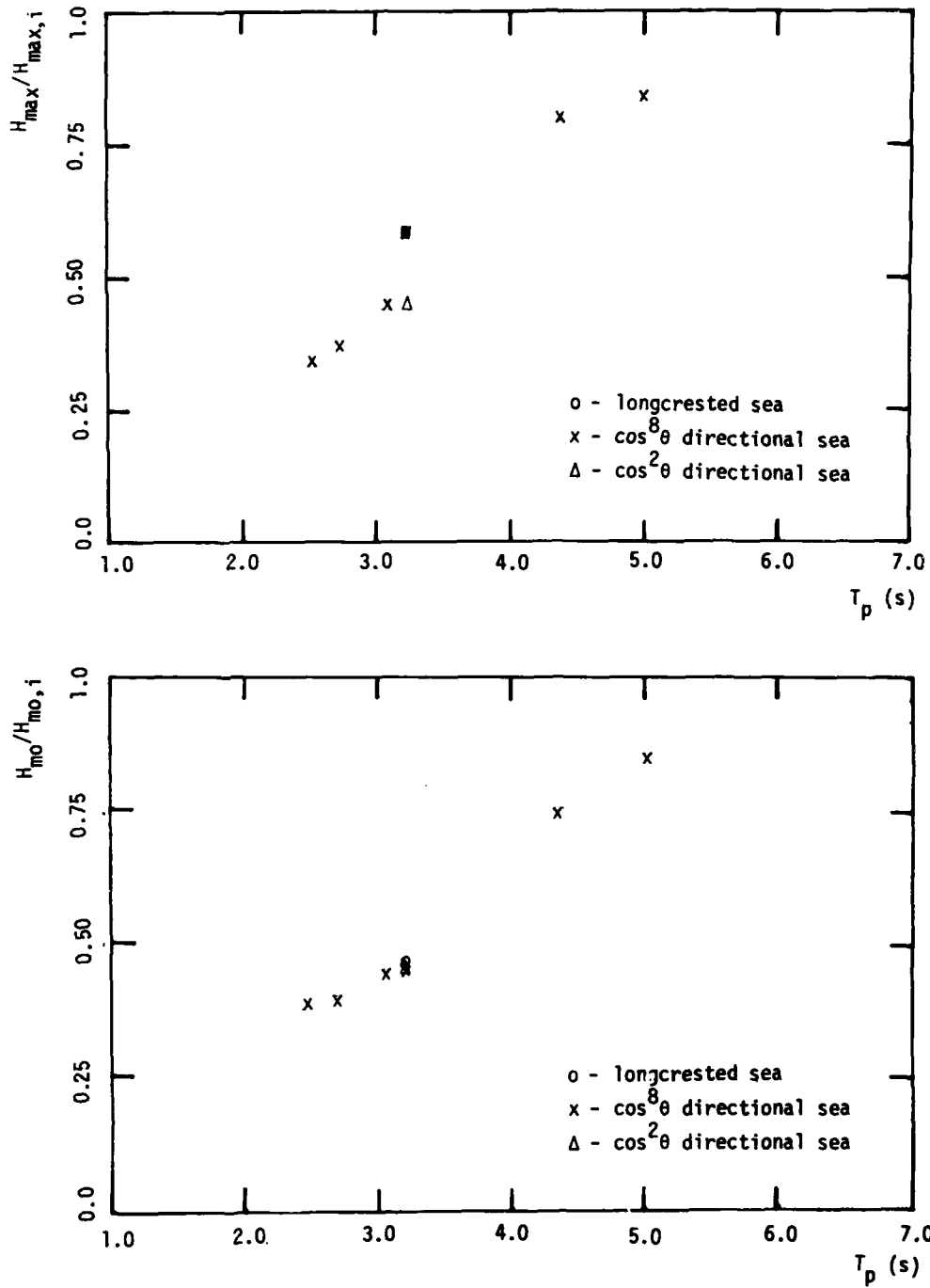


Fig. 3.7

WAVE REDUCTION/AMPLIFICATION NEAR THE BREAKWATER MODEL

TEST NO. 201:

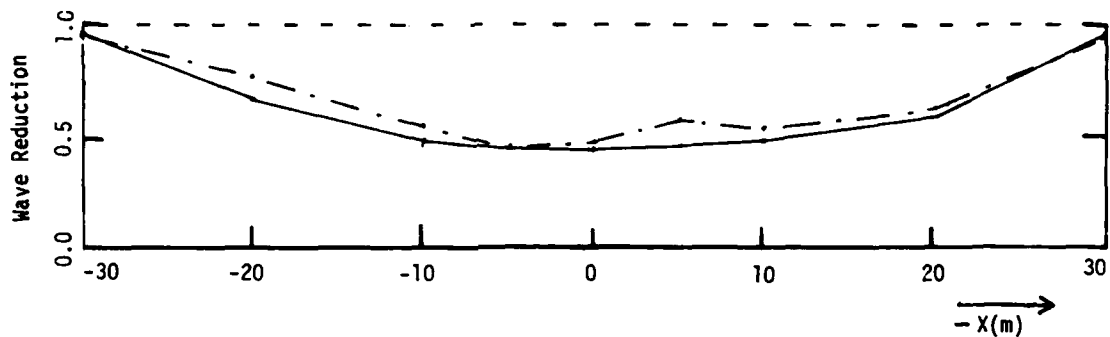
$$T_p = 3.2 \text{ s} \quad H_s = 0.75 \text{ m} \quad \text{Gam} = 3.3 \quad \cos^8 \theta$$

Fendered Model

$$\frac{H_{mo} \text{ with model}}{H_{mo} \text{ without model}}$$

$$\frac{H_{max} \text{ with model}}{H_{max} \text{ without model}}$$

10 M BEHIND:



20 M IN FRONT:

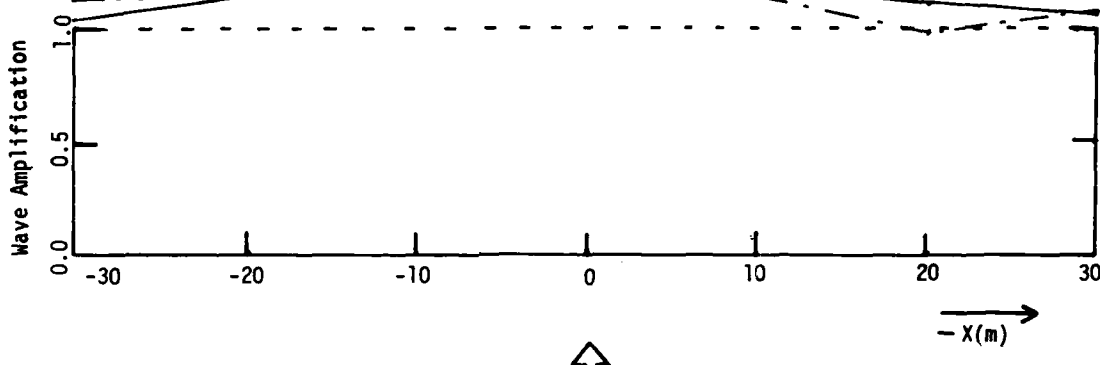


Fig. 3.8

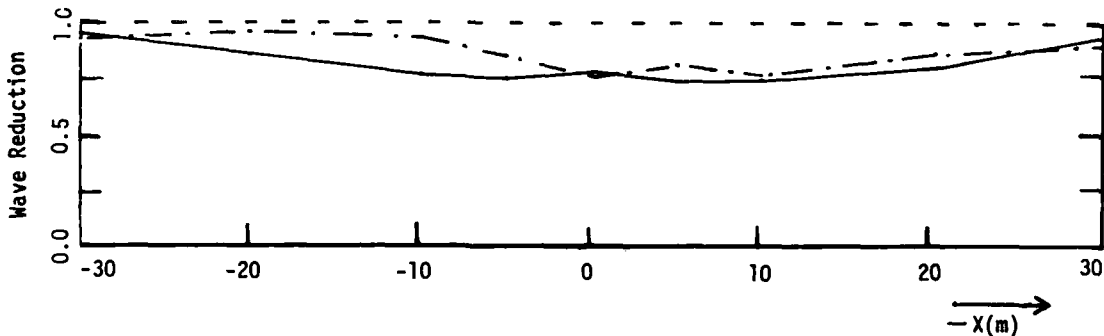
WAVE REDUCTION/AMPLIFICATION NEAR THE BREAKWATER MODEL

TEST NO. 202:

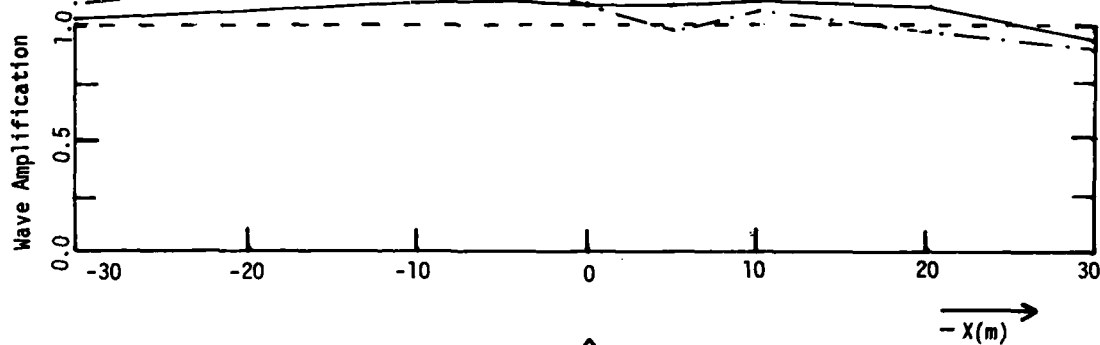
$$T_p = 4.3 \text{ s} \quad H_s = 1.0 \text{ m} \quad \text{Gam} = 3.3 \quad \cos^8 \theta$$

Fendered Model

10 M BEHIND:



20 M IN FRONT:



Mean Wave Direction

Fig. 3.9

WAVE REDUCTION/AMPLIFICATION NEAR THE BREAKWATER MODEL

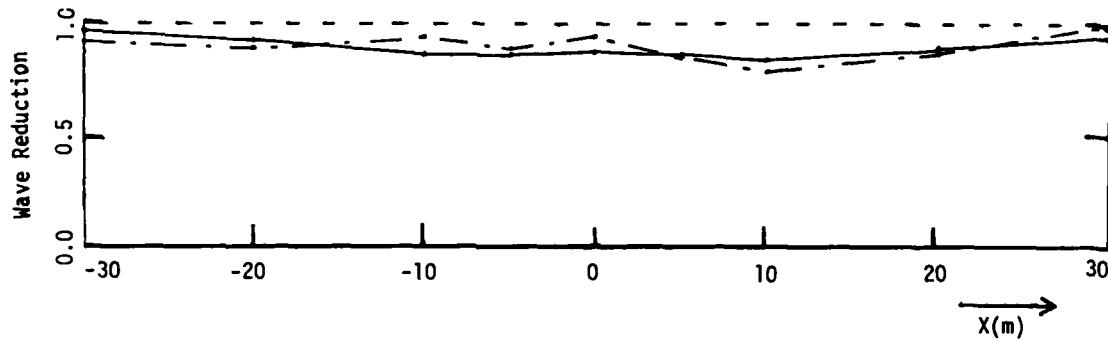
TEST NO. 203:

$T_p = 5.0\text{s}$ $H_s = 1.5\text{m}$ $\Gamma_m = 3.3 \cos^8 \theta$

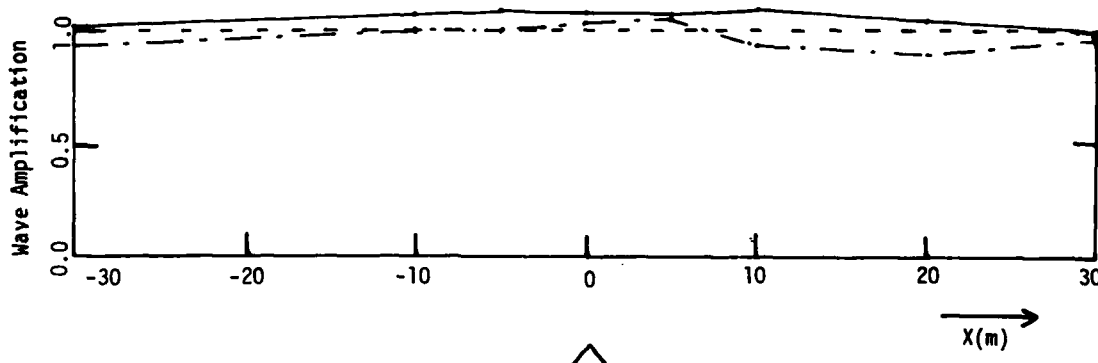
Fendered Model

$\frac{H_{mo} \text{ with model}}{H_{mo} \text{ without model}}$

10 M BEHIND:



20 M IN FRONT:



Mean Wave Direction

Fig. 3.10

WAVE REDUCTION/AMPLIFICATION NEAR THE BREAKWATER MODEL

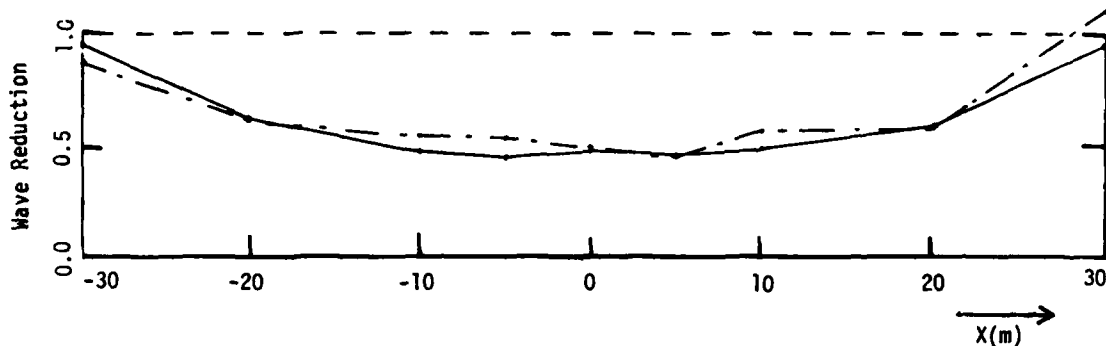
TEST NO. 207:

$T_p = 3.0\text{s}$ $H_s = 0.93\text{m}$ $\text{Gam} = 2.0 \cos^8 \theta$
Fendered Model

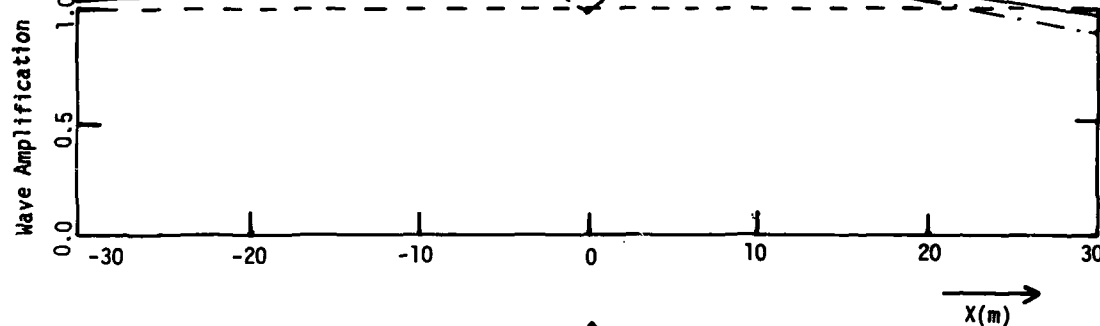
$\frac{H_{mo} \text{ with model}}{H_{mo} \text{ without model}}$

$\frac{H_{max} \text{ with model}}{H_{max} \text{ without model}}$

10 M BEHIND:



20 M IN FRONT:



Mean Wave Direction

Fig. 3.11

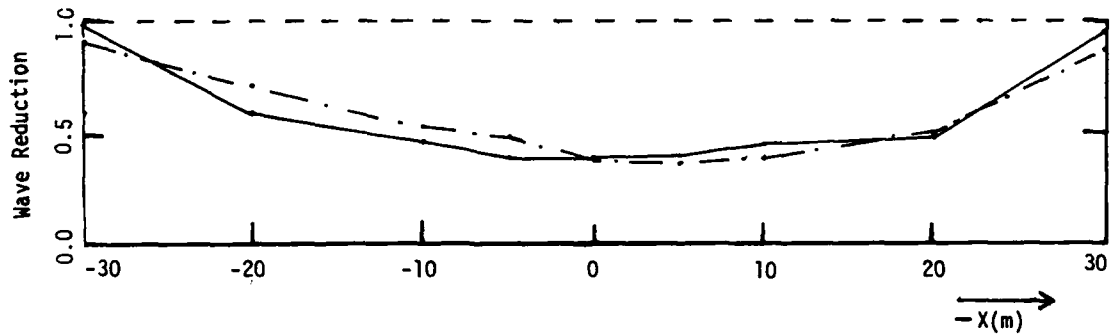
WAVE REDUCTION/AMPLIFICATION NEAR THE BREAKWATER MODEL

TEST NO. 208:

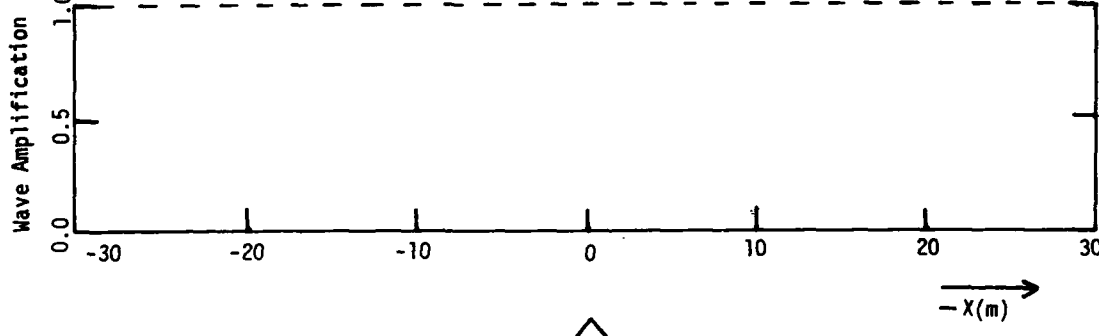
$$T_p = 2.8 \text{ s} \quad H_s = 0.65 \text{ m} \quad \Gamma_m = 2.0 \quad \cos^8 \theta$$

Fendered Model

10 M BEHIND:



20 M IN FRONT:



Mean Wave Direction

Fig. 3.12

WAVE REDUCTION/AMPLIFICATION NEAR THE BREAKWATER MODEL

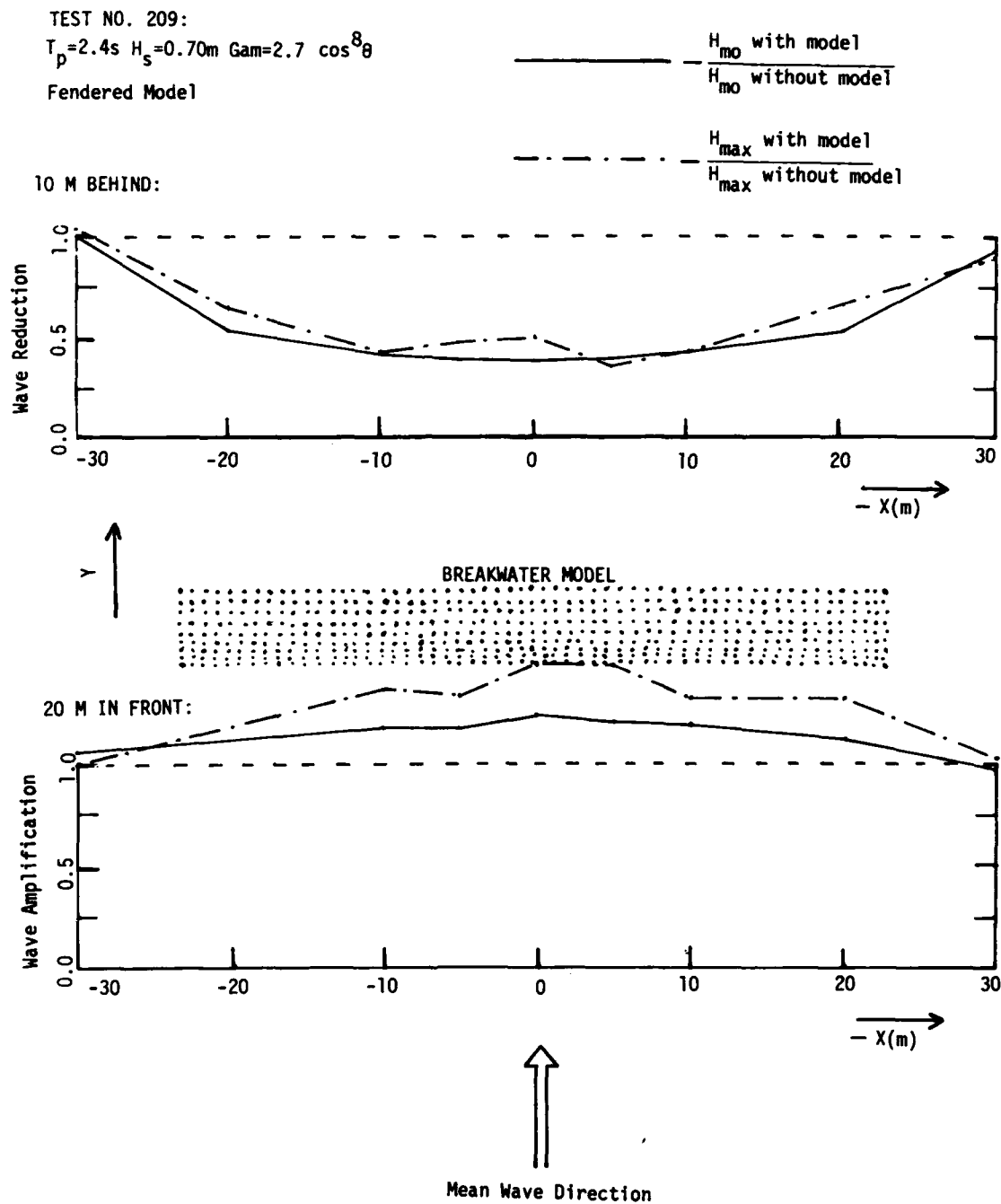


Fig. 3.13

WAVE REDUCTION/AMPLIFICATION NEAR THE BREAKWATER MODEL

TEST NO. 211:

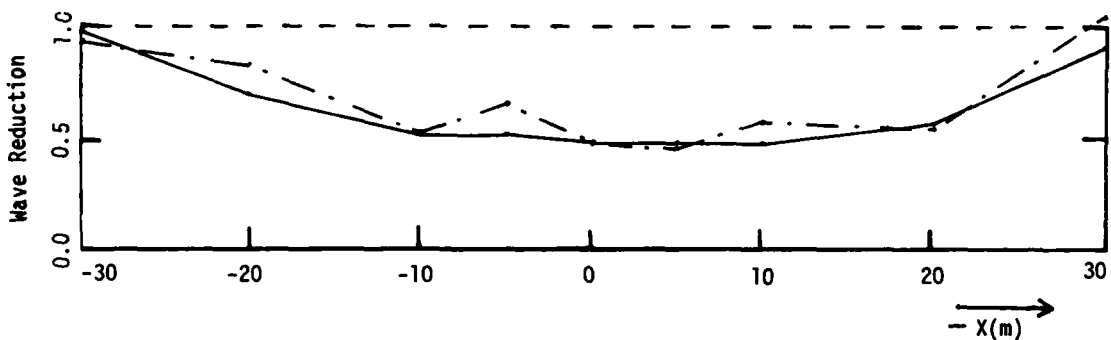
$$T_p = 3.2 \text{ s} \quad H_s = 0.75 \text{ m} \quad \Gamma_m = 3.3 \cos^2 \theta$$

Fendered Model

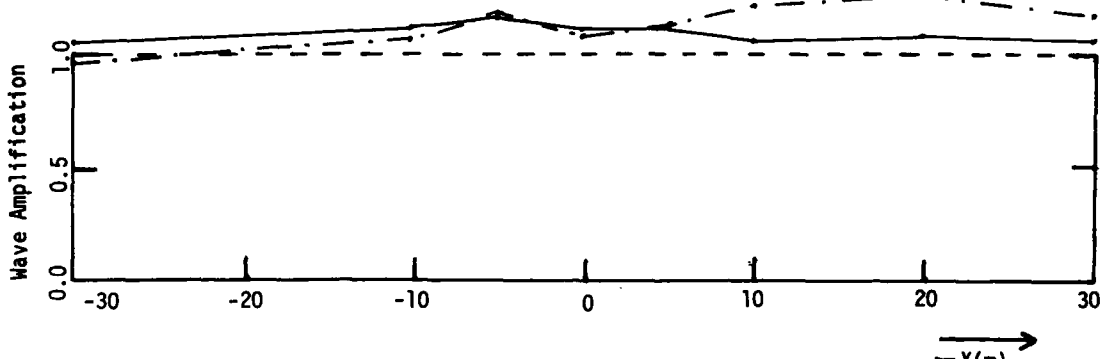
$$\frac{H_{mo}}{H_{mo \text{ without model}}}$$

10 M BEHIND:

$$\frac{H_{max}}{H_{max \text{ without model}}}$$



20 M IN FRONT:



Mean Wave Direction

Fig. 3.14

WAVE REDUCTION/AMPLIFICATION NEAR THE BREAKWATER MODEL

TEST NO. 212:

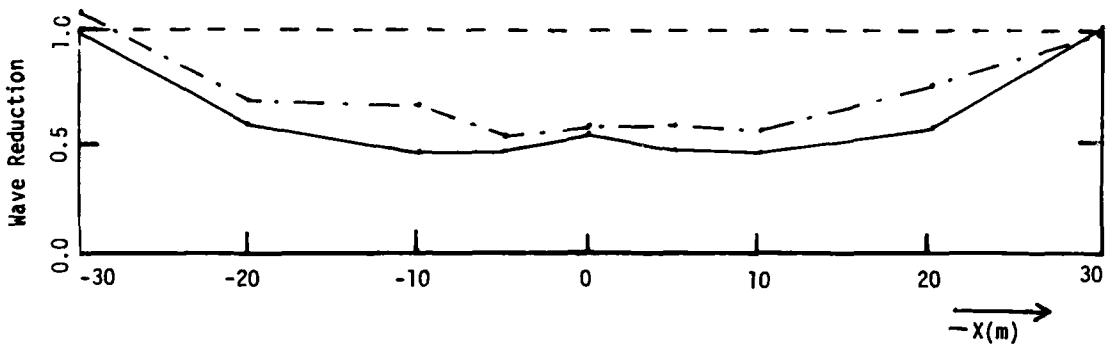
$T_p = 3.2\text{s}$ $H_s = 0.75\text{m}$ $\Gamma_m = 3.3$ Long-crested

Fendered Model

$$\frac{H_{mo} \text{ with model}}{H_{mo} \text{ without model}}$$

$$\frac{H_{max} \text{ with model}}{H_{max} \text{ without model}}$$

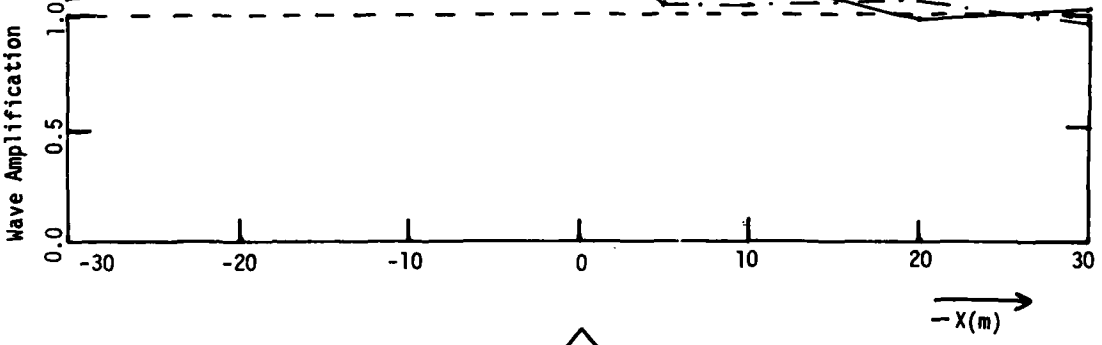
10 M BEHIND:



y
↑

BREAKWATER MODEL

20 M IN FRONT:



↑
Mean Wave Direction

Fig. 3.15

WAVE REDUCTION, Fendered Model

Input: JONSWAP $T_p = 3.2s$ $H_s = 0.75m$ $Gam = 3.3$

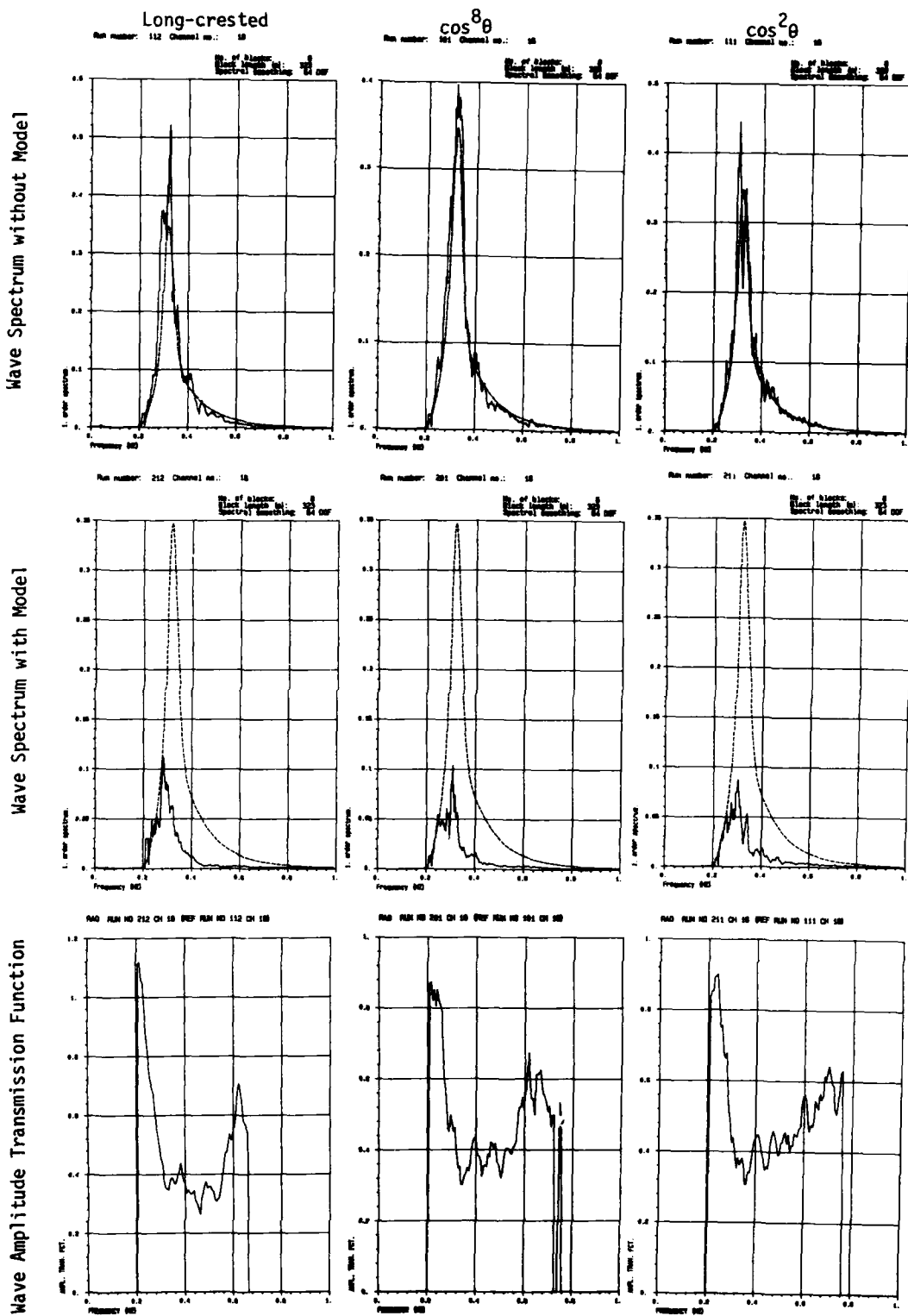


Fig. 3.16

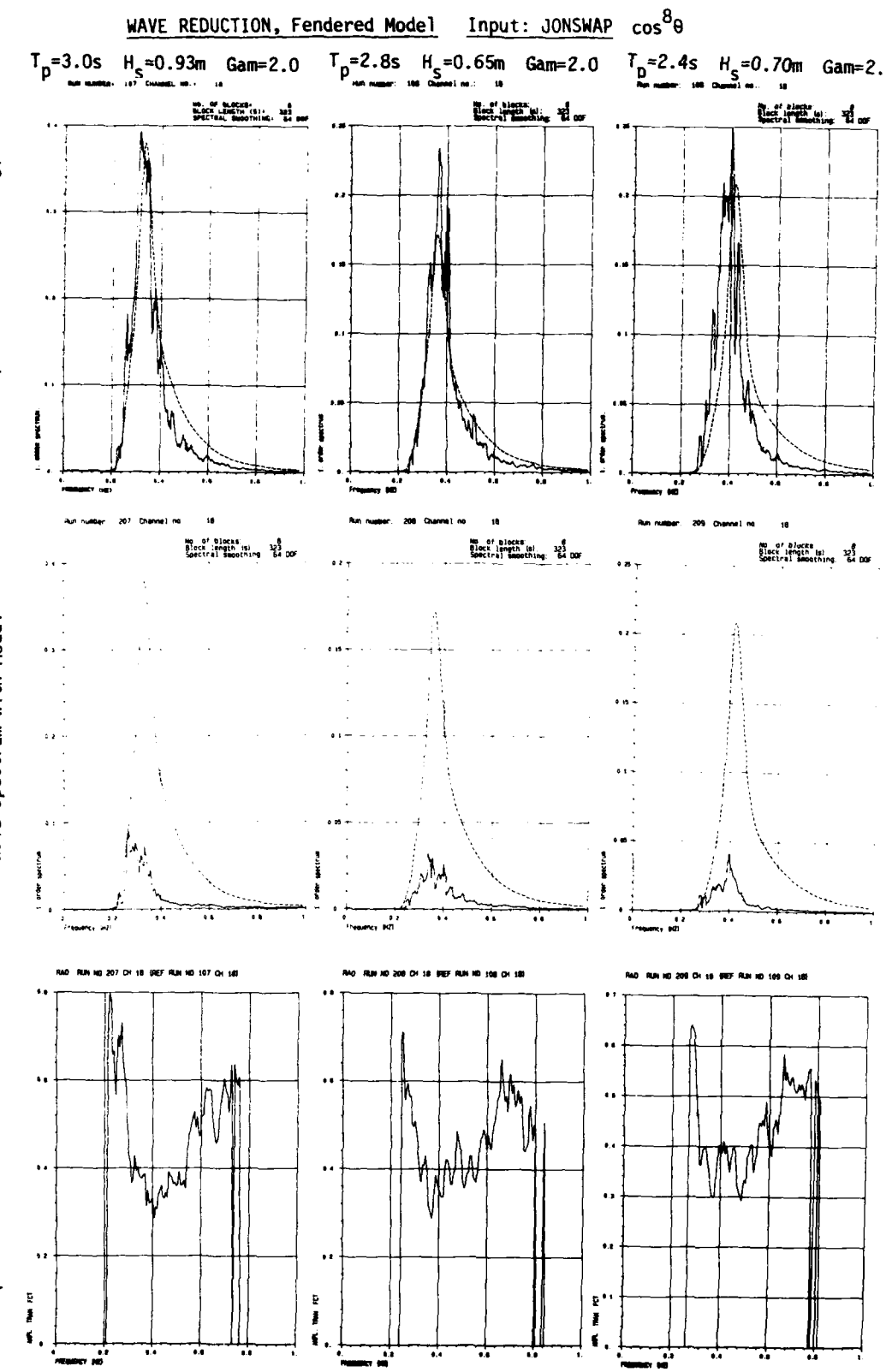


Fig. 3.17

WAVE REDUCTION, Fendered Model

$T_p = 4.3\text{s}$ $H_s = 1.0\text{m}$ $\text{Gam} = 3.3$

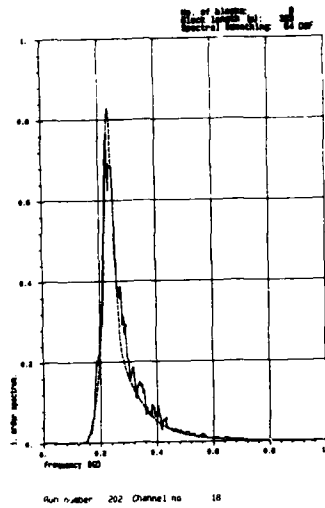
Run number: 102 Channel no.: 18

Input: JONSWAP $\cos^8 \theta$

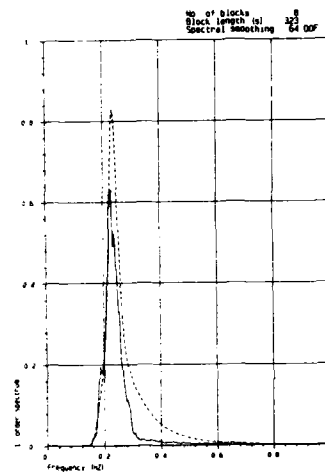
$T_p = 5.0\text{s}$ $H_s = 1.5\text{m}$ $\text{Gam} = 3.3$

Run number: 103 Channel no.: 18

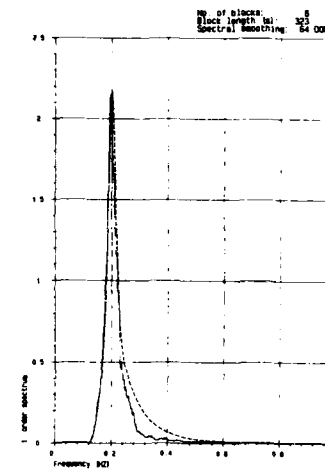
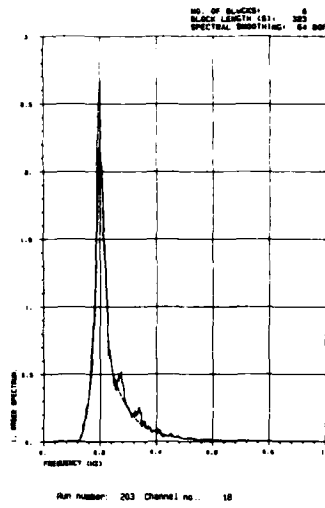
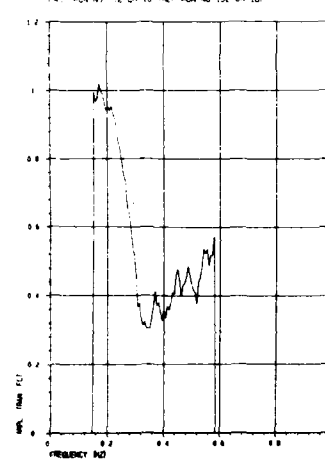
Wave Spectrum without Model



Wave Spectrum with Model



Wave Amplitude Transmission Function



TA - RUN NO. 2 CH 18 / REF RUN NO. 12 CH 18

RA - RUN NO. 203 CH 18 (REF RUN NO. 103 CH 18)

Fig. 3.18

WAVES IN FRONT, Fendered Model Input: JONSWAP $T_p = 3.2\text{s}$ $H_s = 0.75\text{m}$ $\text{Gam} = 3.3$

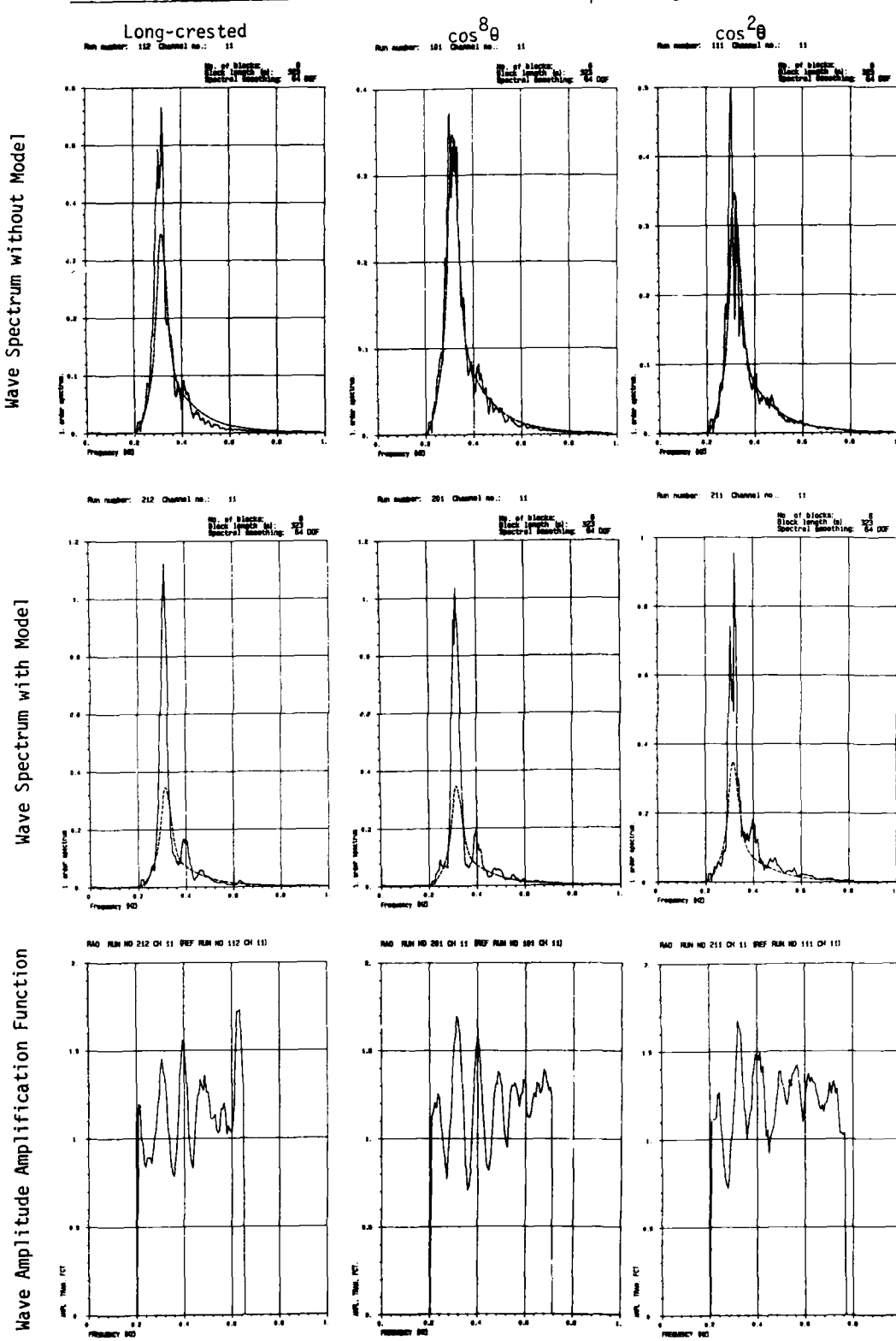


Fig. 3.19

WAVES IN FRONT, Fendered Model Input: JONSWAP $\cos^8 \theta$

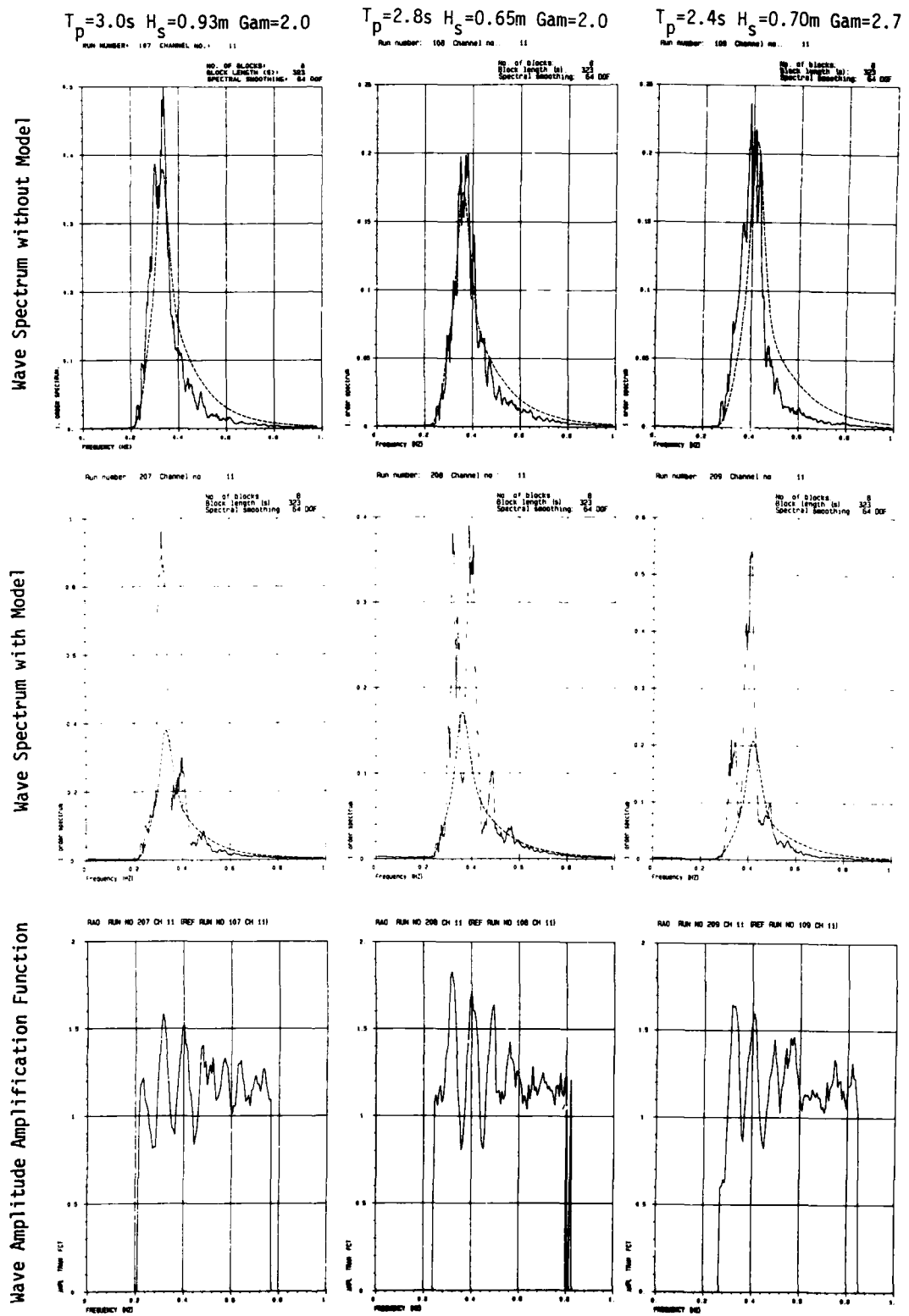


Fig. 3.20

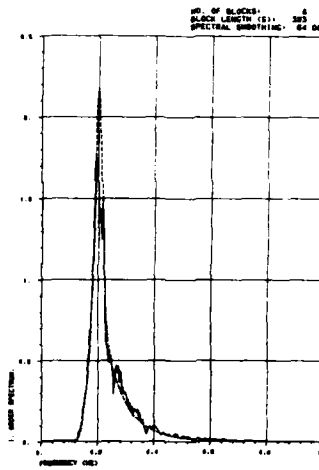
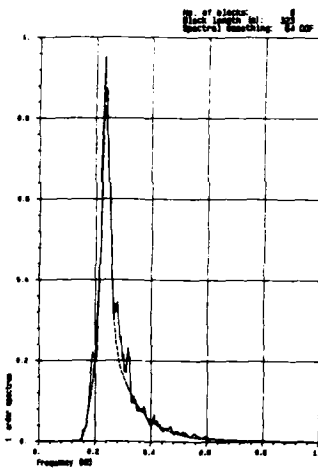
WAVES IN FRONT, Fendered Model

$T_p = 4.3\text{s}$ $H_s = 1.0\text{m}$ $\text{Gam} = 3.3$
Run number: 102 Channel no.: 11

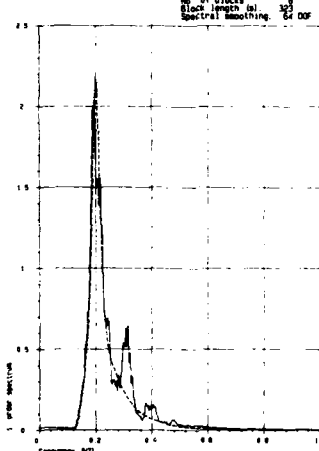
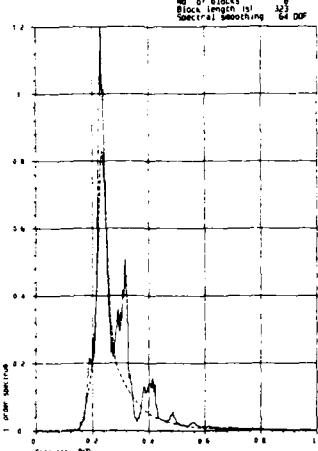
Input: JONSWAP $\cos^8 \theta$

$T_p = 5.0\text{s}$ $H_s = 1.5\text{m}$ $\text{Gam} = 3.3$
Run number: 103 Channel no.: 11

Wave Spectrum without Model



Wave Spectrum with Model



Wave Amplitude Amplification Function

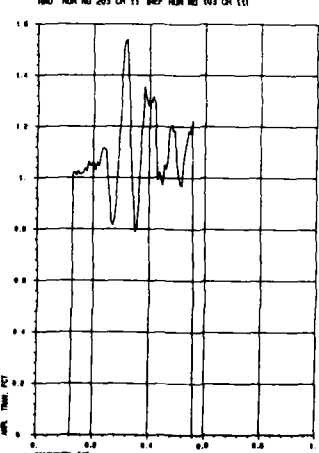
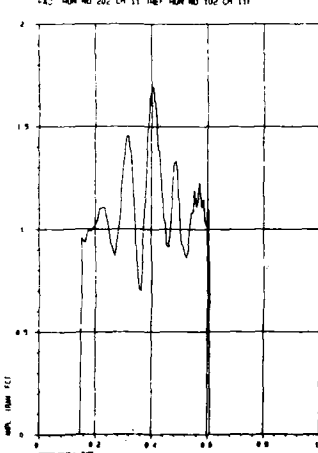


Fig. 3.21

WAVE STATISTICS BEHIND FENDERED MODEL Input: JONSWAP $T_p = 3.2s$ $H_s = 0.75m$ $\Gamma_m = 3.3$

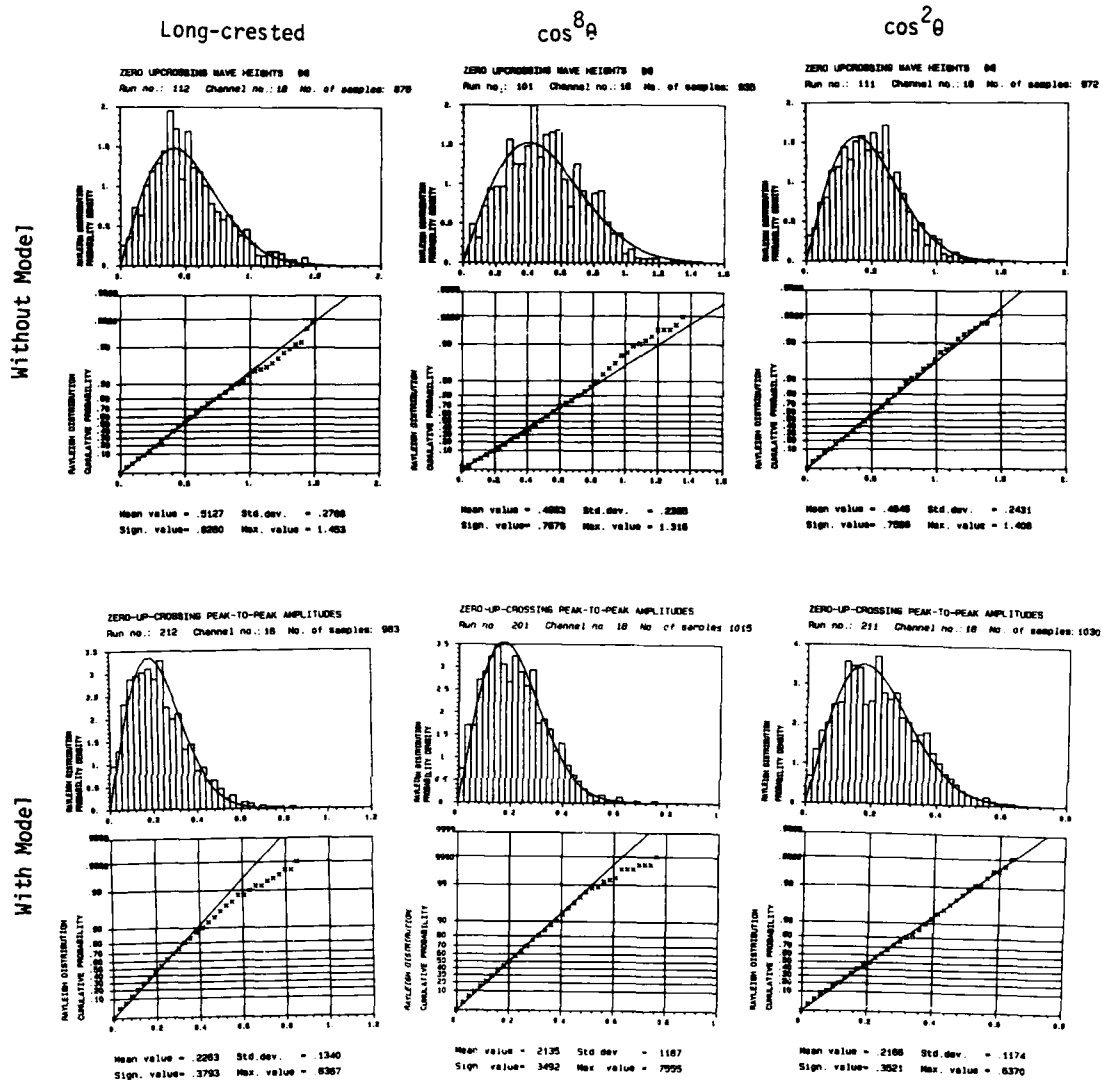


Fig. 3.22

WAVE STATISTICS BEHIND FENDERED MODEL Input: JONSWAP $\cos^8 \theta$

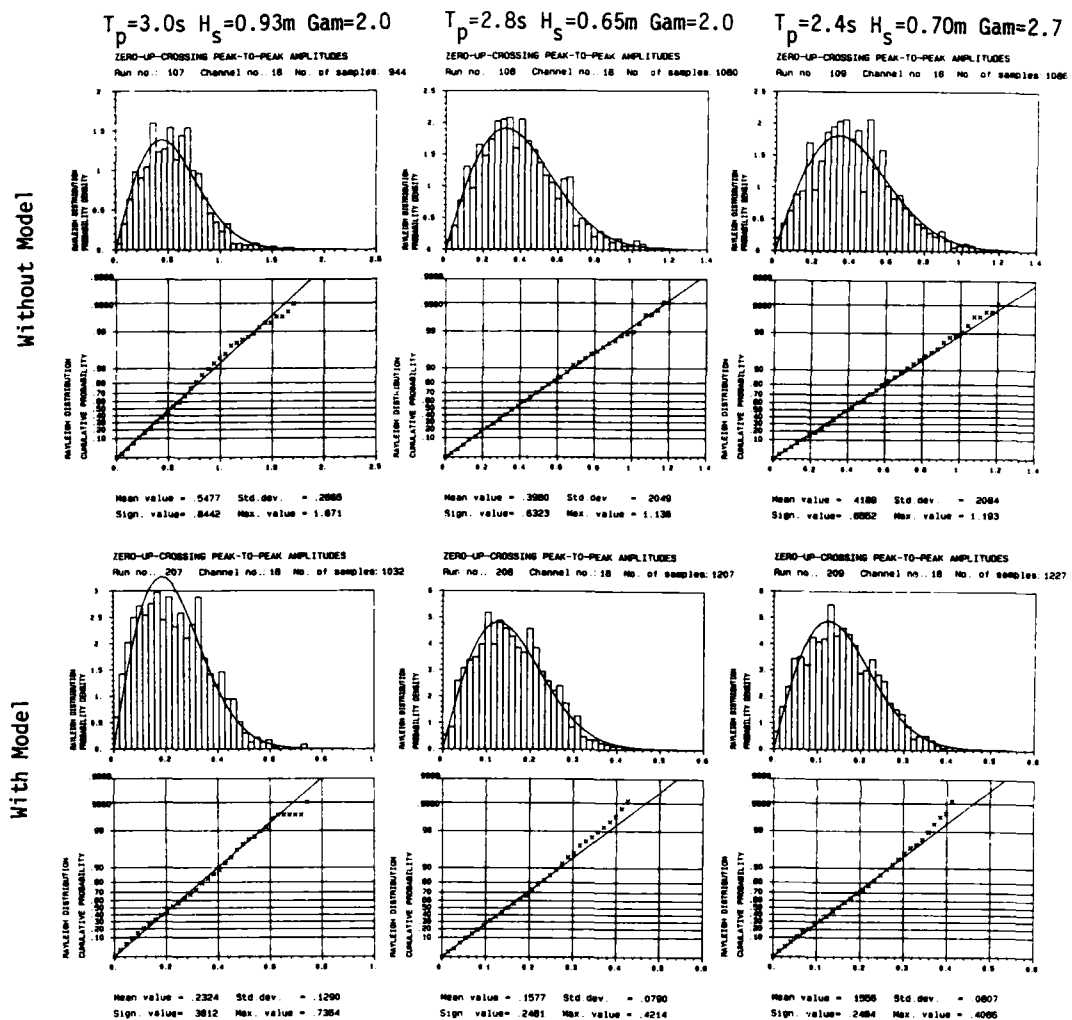
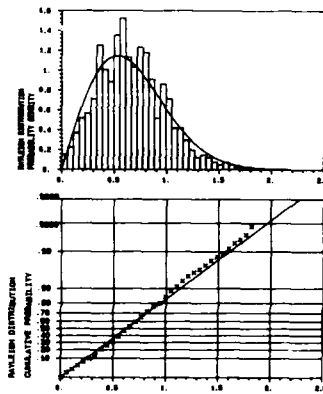


Fig. 3.23

WAVE STATISTICS BEHIND FENDERED MODEL Input: JONSWAP $\cos^8\theta$

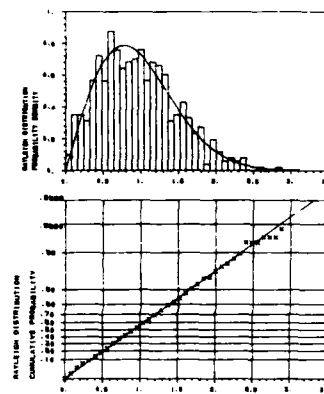
$T_p = 4.3\text{s}$ $H_s = 1.0\text{m}$ $\text{Gam} = 3.3$

ZERO UP-CROSSING WAVE HEIGHTS (m)
Run no.: 102 Channel no.: 18 No. of samples: 739



$T_p = 5.0\text{s}$ $H_s = 1.5\text{m}$ $\text{Gam} = 3.3$

ZERO UP-CROSSING WAVE HEIGHTS (m)
Run no.: 183 Channel no.: 18 No. of samples: 641



Without Model

With Model

Fig. 3.24

WAVE STATISTICS in front of Fendered Model Input: JONSWAP $T_p = 3.2\text{s}$ $H_s = 0.75\text{m}$ $\Gamma_m = 3.3$

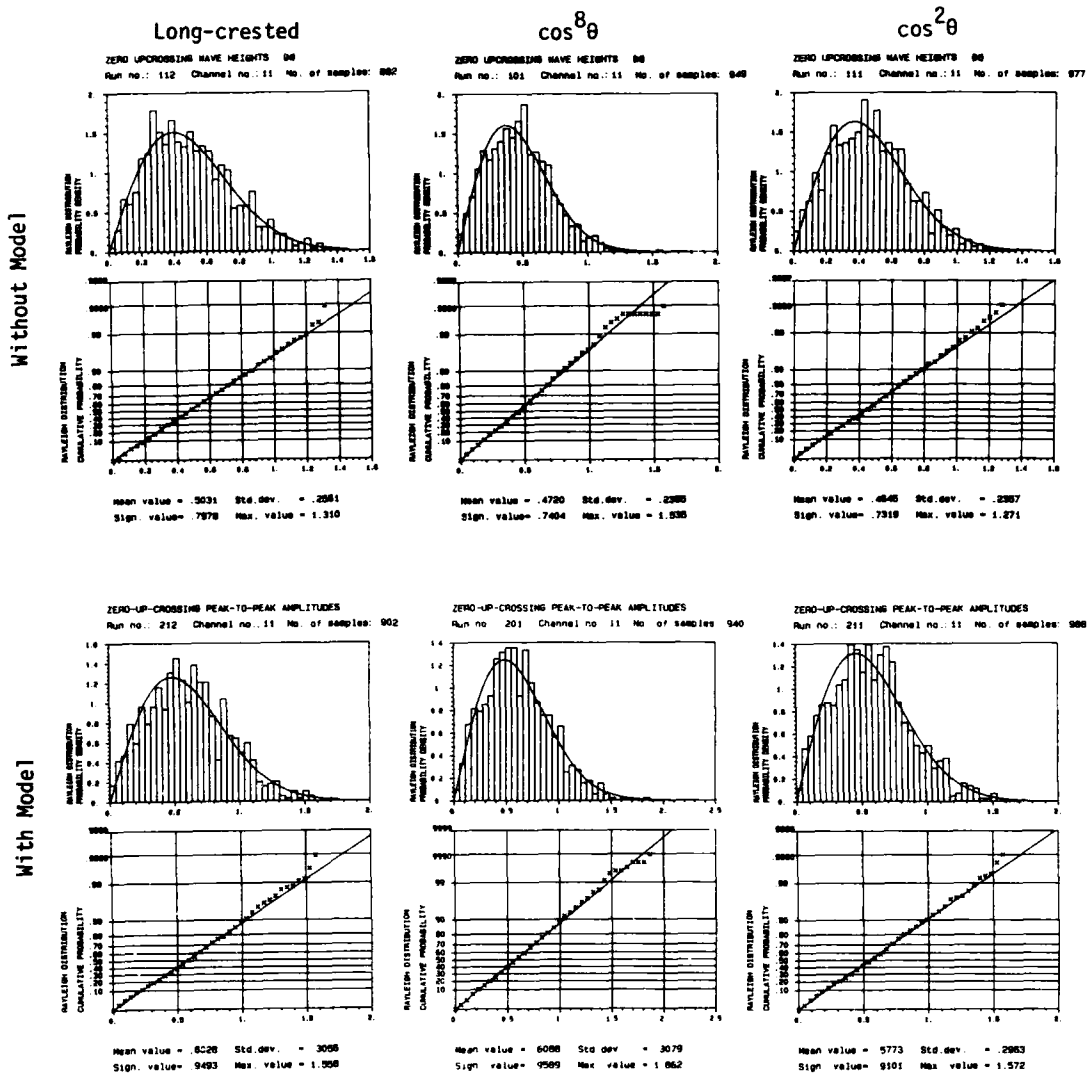


Fig. 3.25

WAVE STATISTICS in front of Fendered Model Input: JONSWAP $\cos^8 \theta$

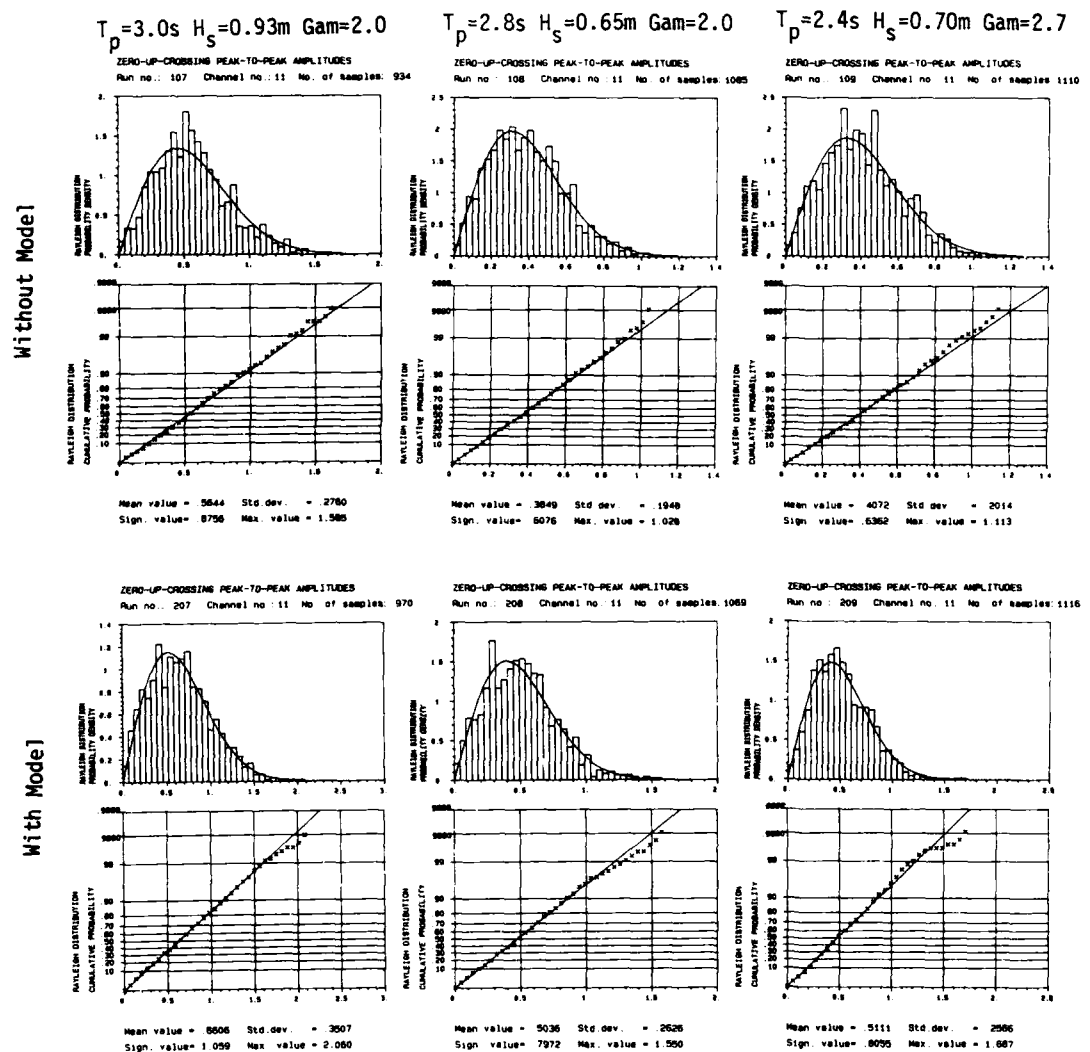


Fig. 3.26

WAVE STATISTICS in front of Fendered Model

Input: JONSWAP $\cos^8 \theta$

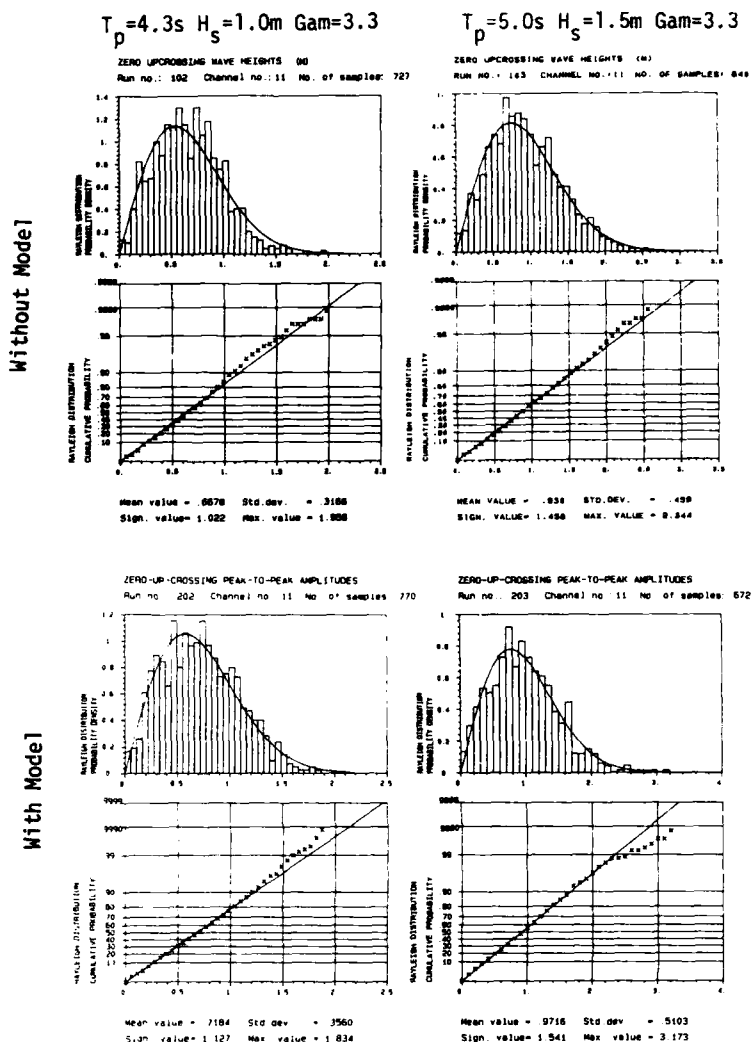


Fig. 3.27

WAVE GROUP SPECTRA behind Fendered Model Input: JONSWAP $T_p = 3.2\text{ s}$ $H_s = 0.75\text{ m}$ $\text{Gam} = 3.3$

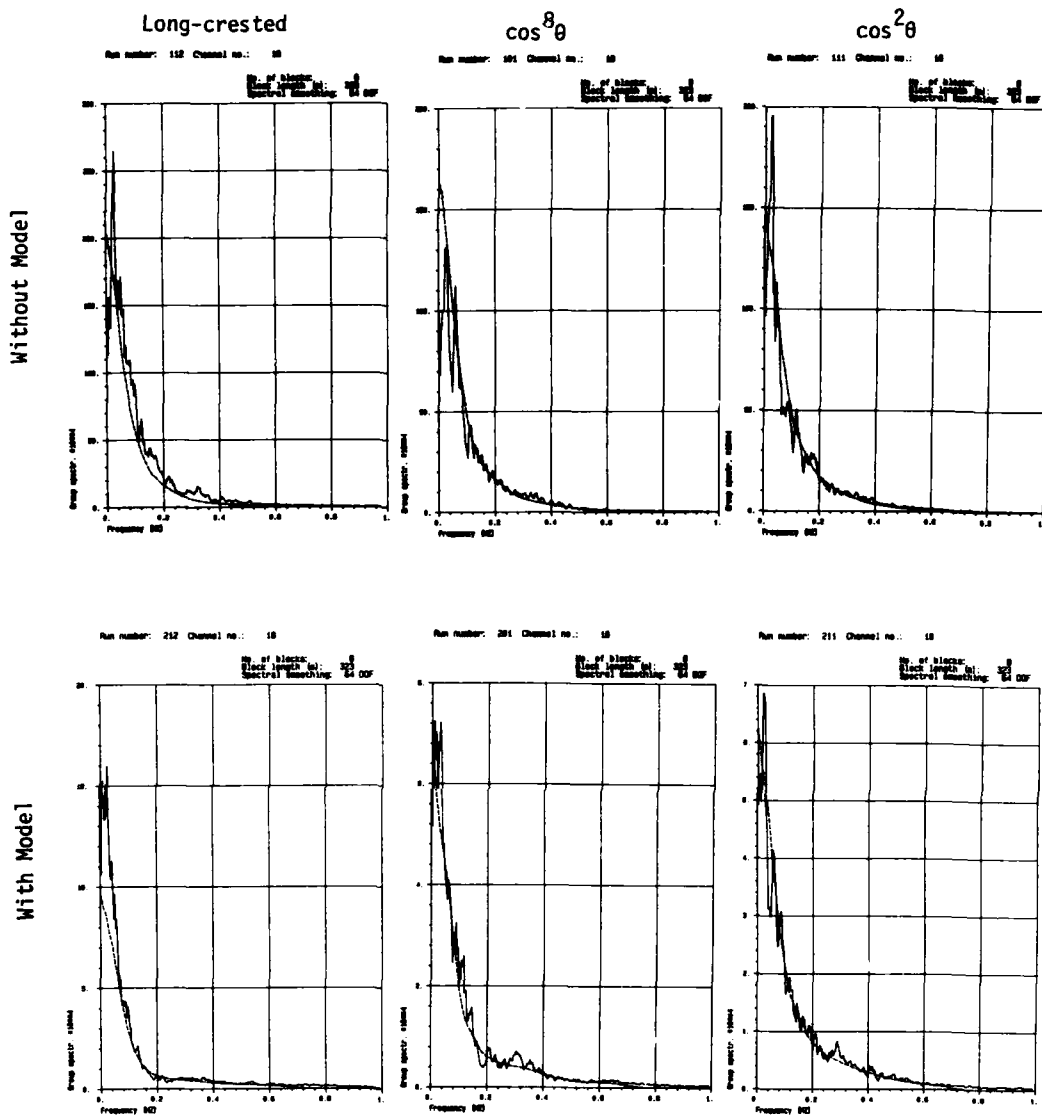


Fig. 3.28

WAVE GROUP SPECTRA behind Fendered Model Input: JONSWAP $\cos^8 \theta$

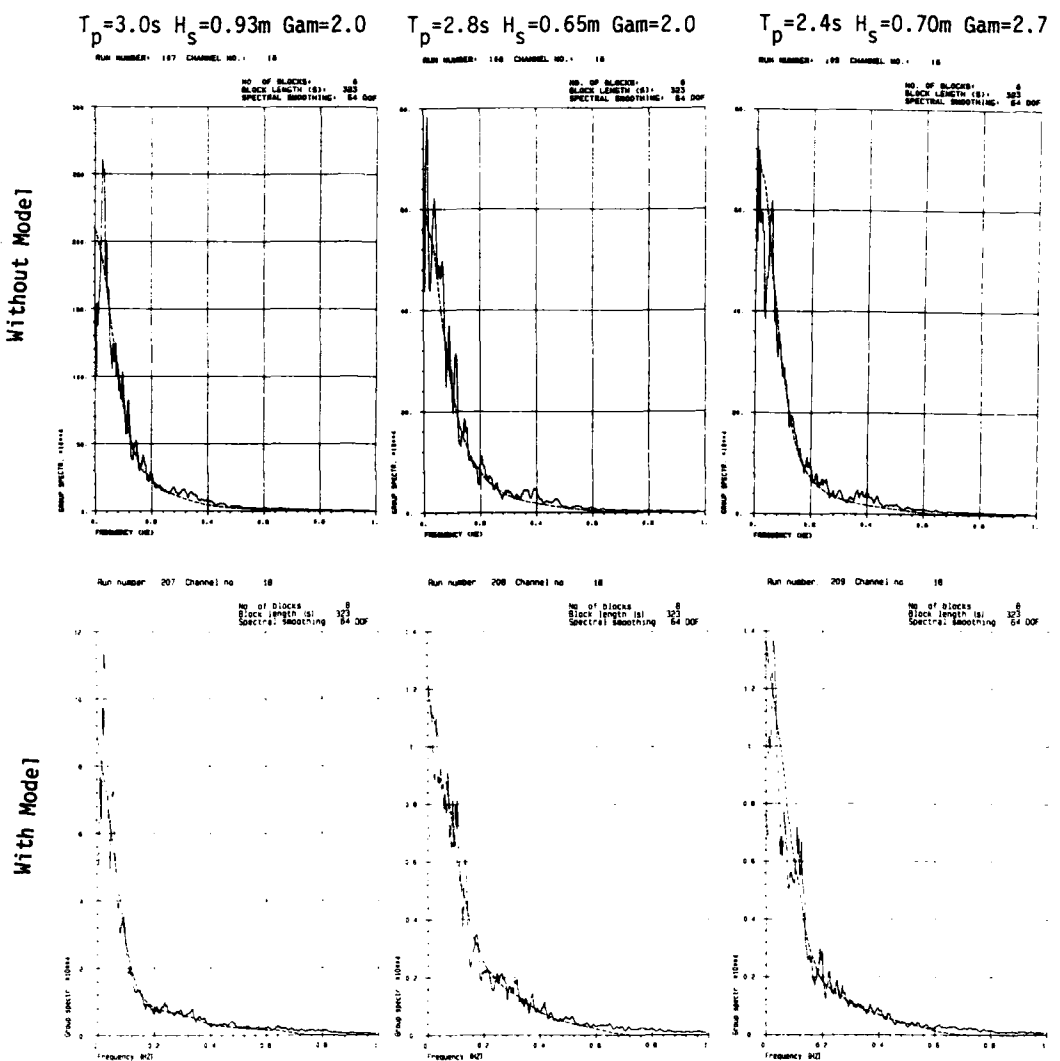
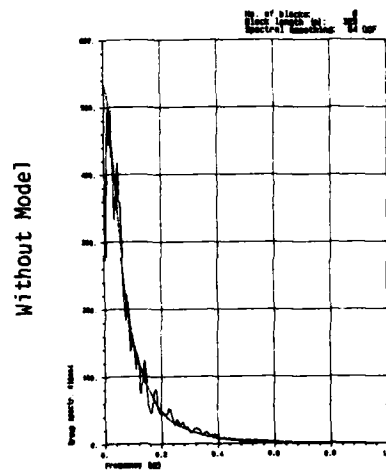


Fig. 3.29

WAVE GROUP SPECTRA behind Fendered Model

Input: JONSWAP $\cos^8 \theta$

$T_p = 4.3s$ $H_s = 1.0m$ $Gam = 3.3$
Run number: 102 Channel no.: 10



$T_p = 5.0s$ $H_s = 1.5m$ $Gam = 3.3$
Run number: 103 Channel no.: 10

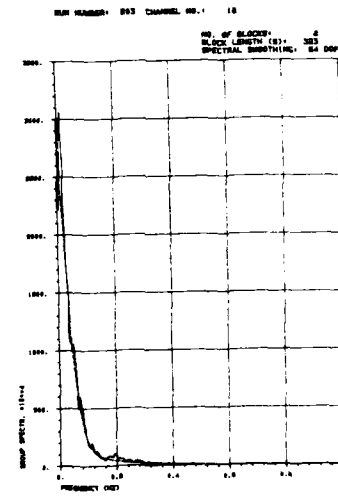
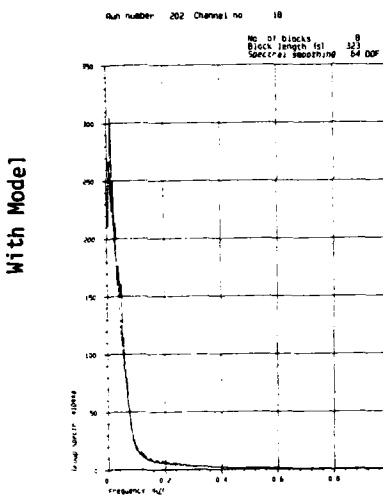
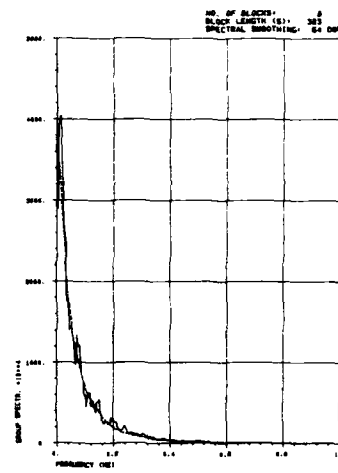


Fig. 3.30

WAVE GROUP SPECTRA in front of Fendered Model Input: JONSWAP $T_p=3.2s$ $H_s=0.75m$ $\text{Gam}=3.3$

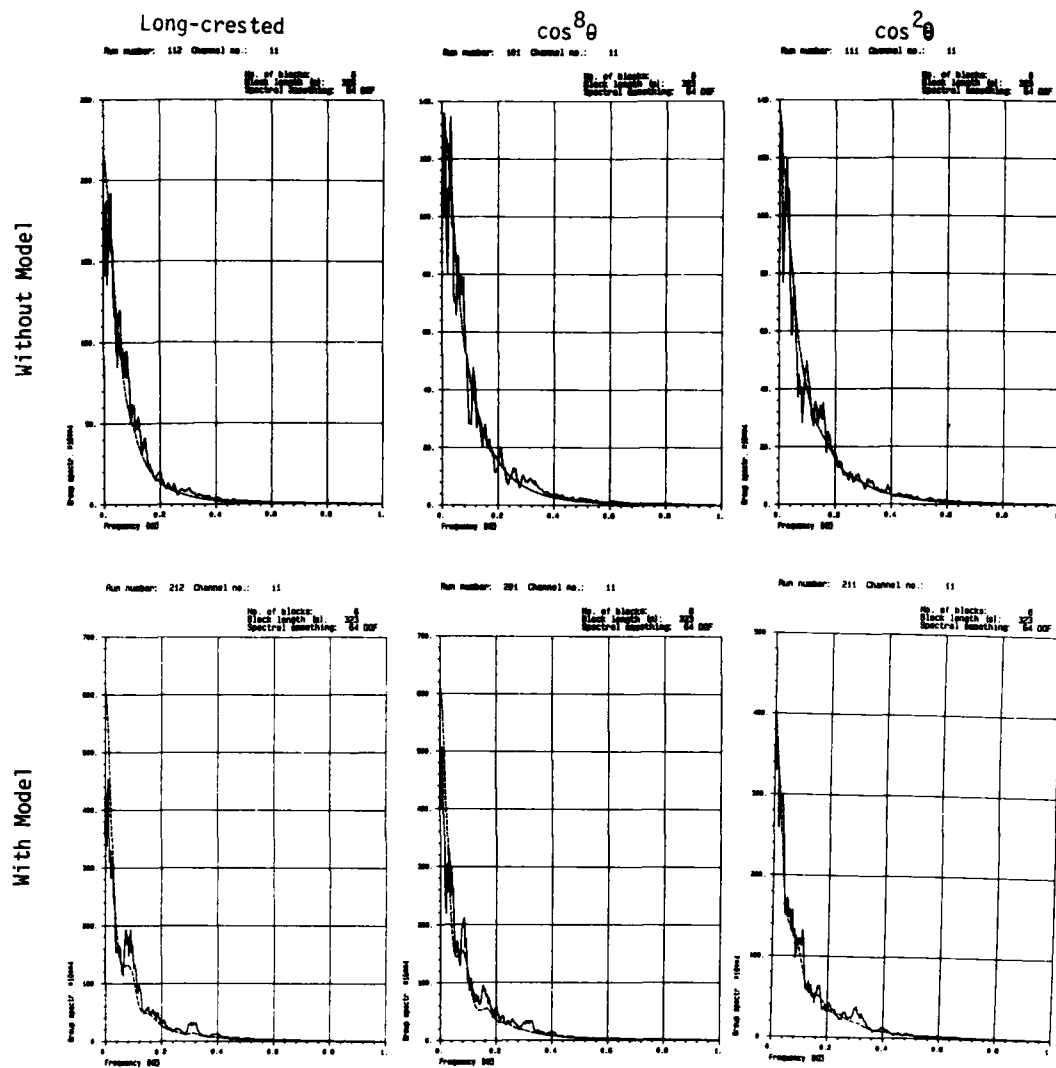


Fig. 3.31

WAVE GROUP SPECTRA in front of Fendered Model Input: JONSWAP $\cos^8 \theta$

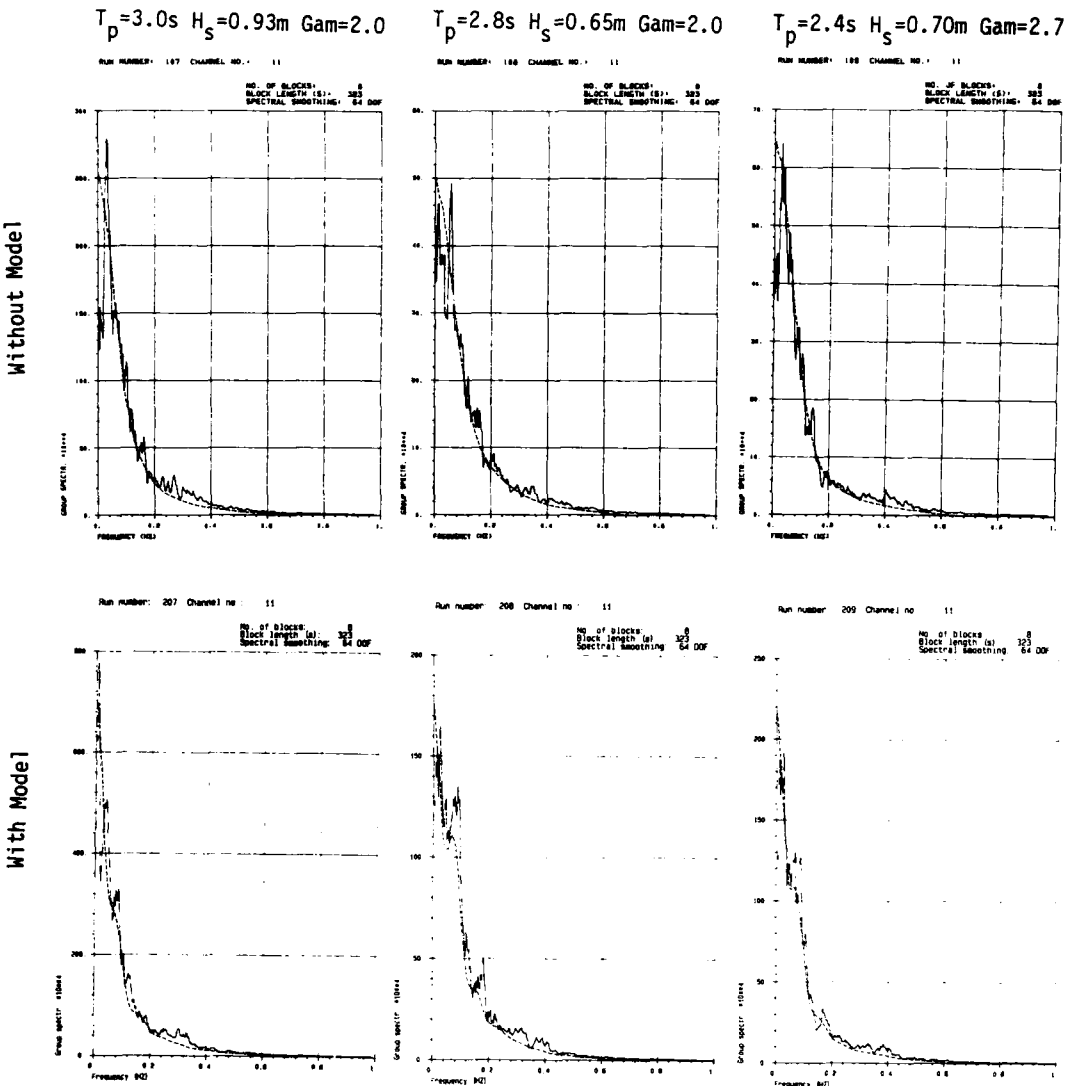


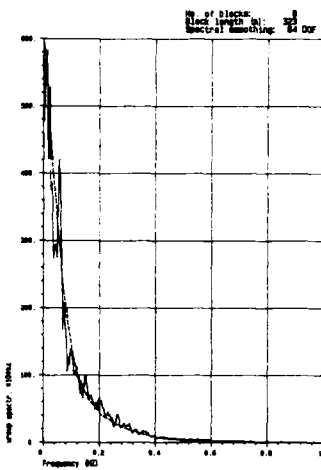
Fig. 3.32

WAVE GROUP SPECTRA in front of Fendered Model

Input: JONSWAP $\cos^8 \theta$

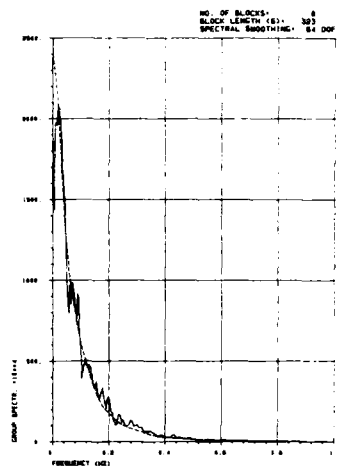
$T_p = 4.3\text{s}$ $H_s = 1.0\text{m}$ $\text{Gam} = 3.3$

Run number: 102 Channel no.: 11



$T_p = 5.0\text{s}$ $H_s = 1.5\text{m}$ $\text{Gam} = 3.3$

Run number: 103 Channel no.: 11



Without Model

With Model

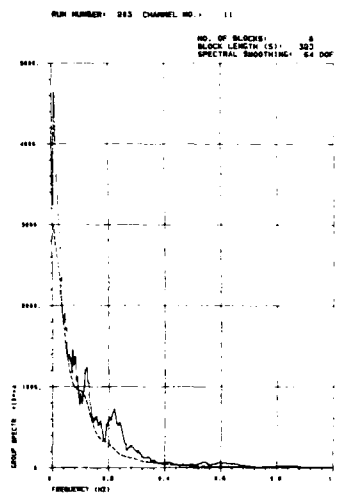
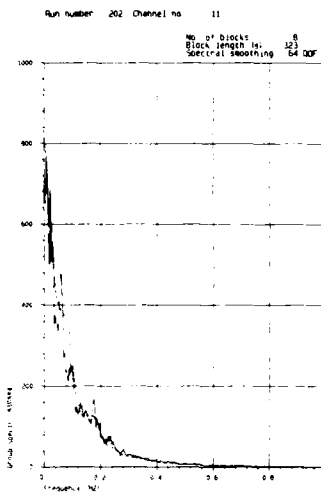


Fig. 3.33

3.1.3 Mooring line forces

Results are shown for force sensor no. 10, 11 and 12 (channel 33, 34 and 35), see fig. 2.18. These sensors measure tension forces in mooring lines going from the pontoons and in front of the breakwater. By simple reasoning one realizes that these forces are likely to be larger than the forces in the lines going behind the breakwater, due to expected non-linear offset in the sway motion (y-position). This assumption is verified by the experiments, except from the case with very long regular waves, (6.3s period) where the forces in the opposite lines were slightly larger (see the Data Reports).

The first 3 plots (figs. 3.34 - 3.36) show the maximum force and RMS value (square root of (square mean + variance)) for each of the 3 sensors, as a function of the input (calibrated) significant wave height $H_{mo,o}$. The next 3 plots (figs. 3.37 - 3.39) show the maximum force deviation from the static force value, and the RMS deviation from the static value, normalized by $H_{mo,o}$, as a function of the input peak wave period T_p . Plots of force spectra, linear transfer functions (RAO) and coherence/phase functions, for each of the 8 irregular sea states, and each of the 3 sensors, follow next (figs. 3.40 - 3.48). Wave staff 11 in front of the model is used as a reference (see section 2.5). Figs. 3.49 - 3.51 present statistics of force maxima in each test run (actually: force minima, since the force sensor gave negative signals with reversed sign), compared to Rayleigh curves. Finally, figs. 3.52 - 3.54 illustrate the coupling between the 3 force sensors, and between forces and selected motions (sway-heave-roll) by coherence/phase analysis.

Note that "mean amplitude" in the statistics diagrams means "mean amplitude of the deviation from the mean force". Thus the "mean force" is the starting left point of the Rayleigh curve.

The absolute maximum force measured with this model was 102 kN (test run no. 203, force sensor 9). It occurred simultaneously with 75 kN in force sensor 10. These two sensors were connected in a y-connection (see chapter 2). thus the maximum force in their common line (from the y-connection to the bottom) was more than 150 kN.

MAXIMUM AND RMS VALUES vs INPUT SIGNIFICANT WAVE HEIGHT
 ANCHOR LINE FORCE NO. 10 FENDERED MODEL

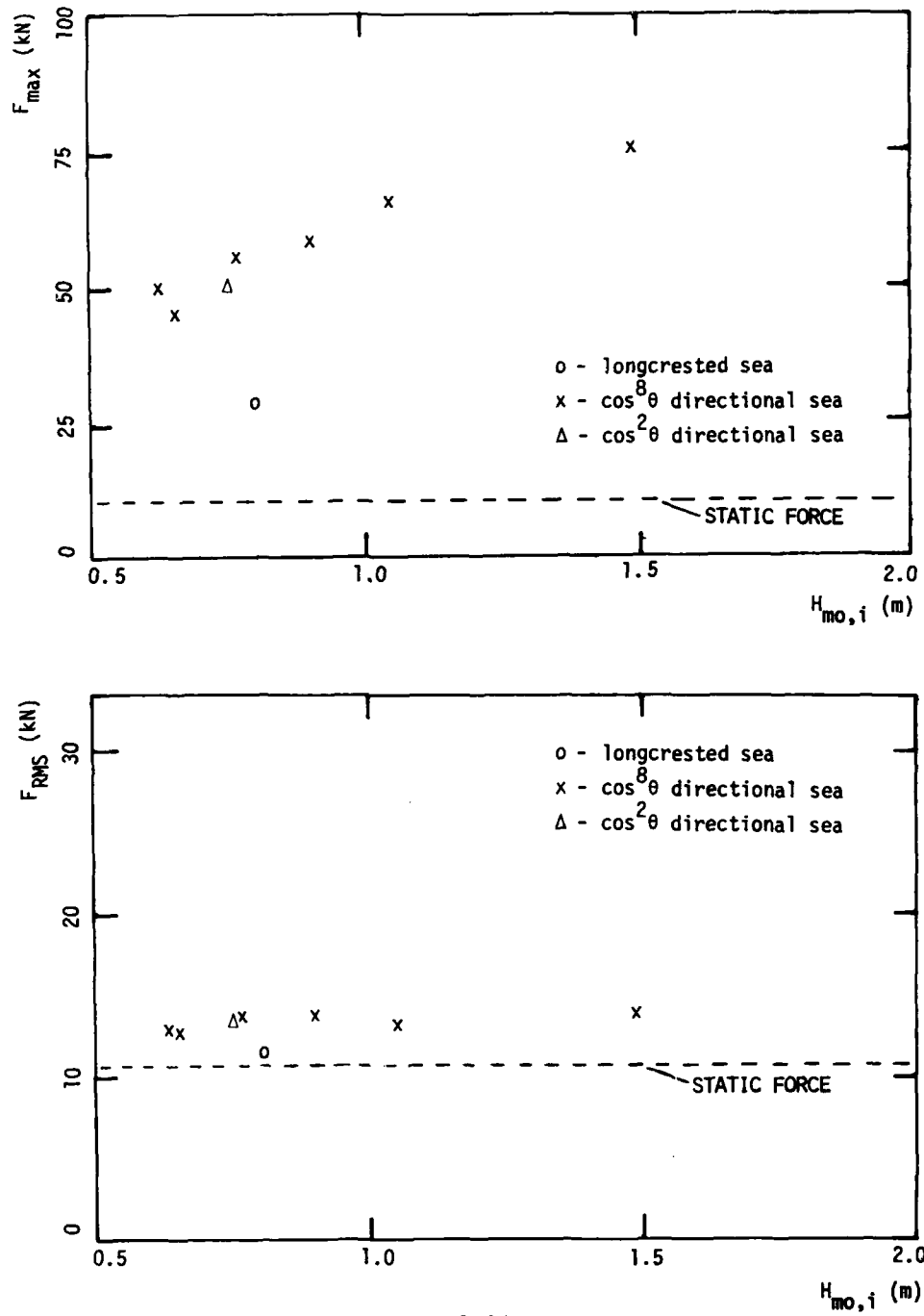


Fig. 3.34

MAXIMUM AND RMS VALUES VS INPUT SIGNIFICANT WAVE HEIGHT
ANCHOR LINE FORCE NO. 11 FENDERED MODEL

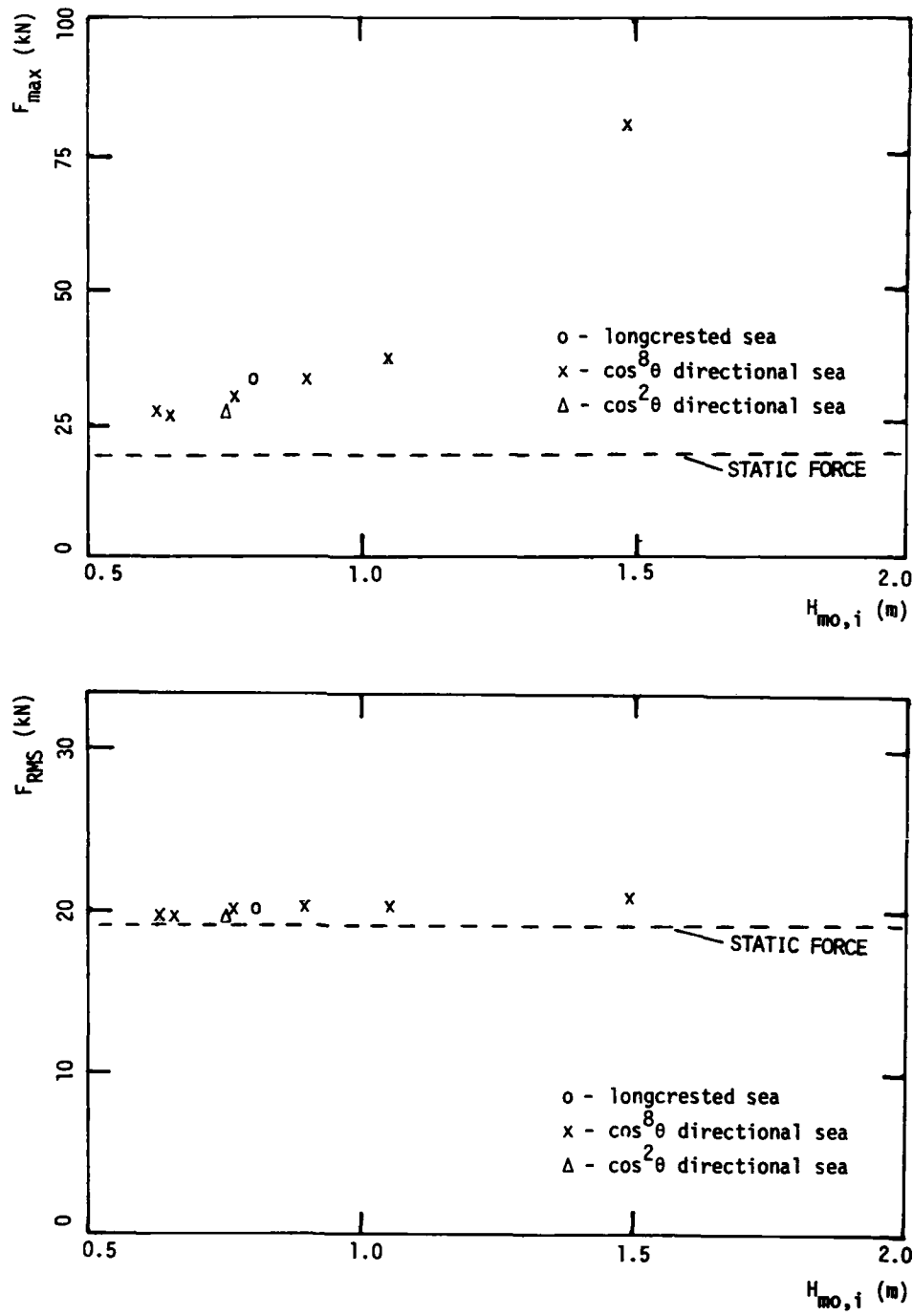


Fig. 3.35

MAXIMUM AND RMS VALUES VS INPUT SIGNIFICANT WAVE HEIGHT
ANCHOR LINE FORCE NO. 12 FENDERED MODEL

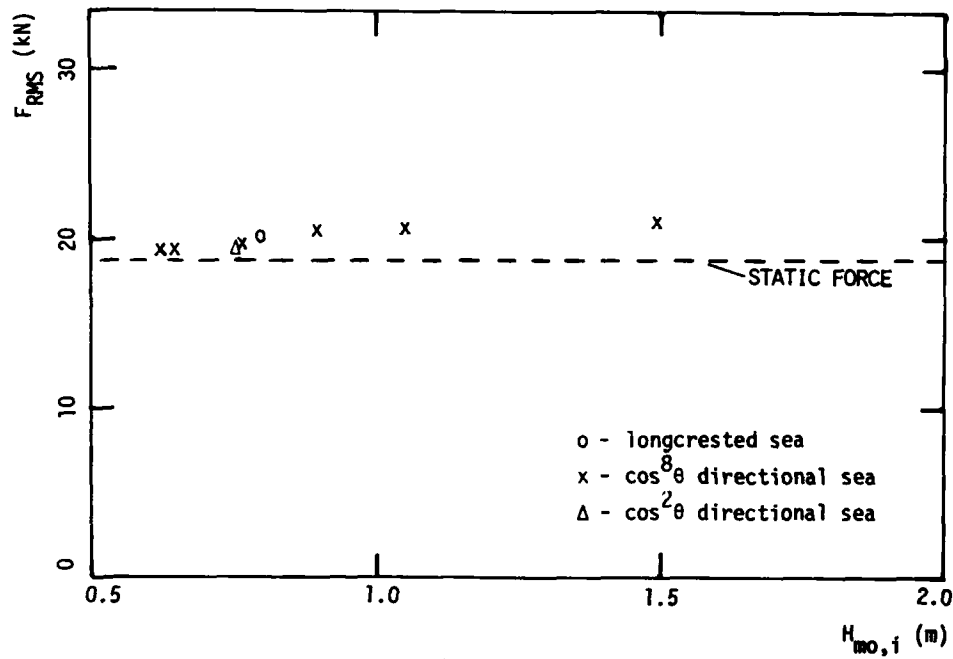
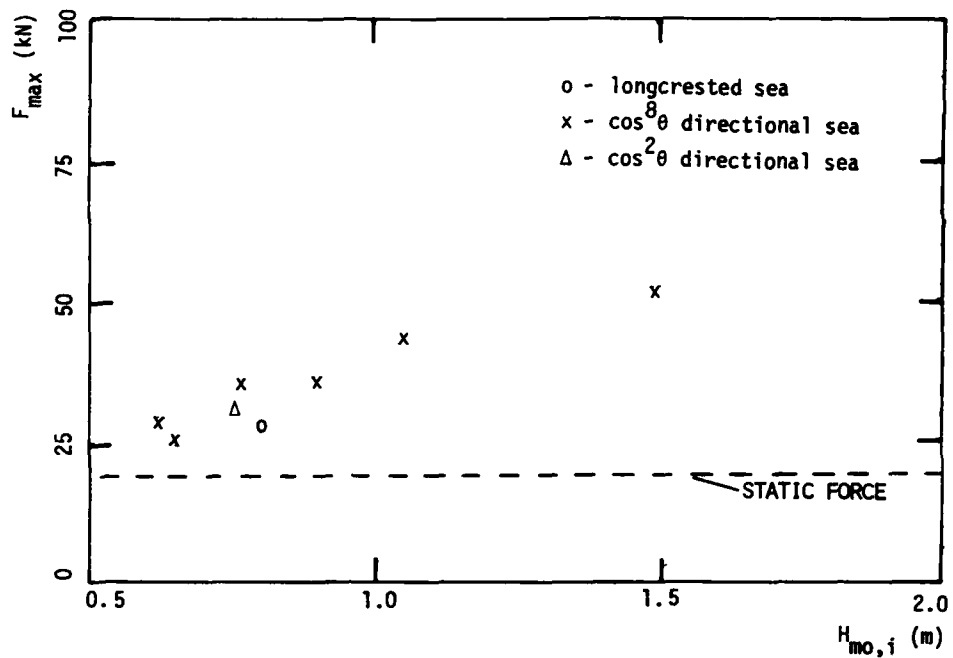


Fig. 3.36

NORMALIZED MAXIMUM AND RMS VALUES VS PEAK PERIOD OF INPUT WAVE
 ANCHOR LINE FORCE NO. 10 FENDERED MODEL
 STATIC FORCE HAS BEEN SUBTRACTED FROM SIGNAL

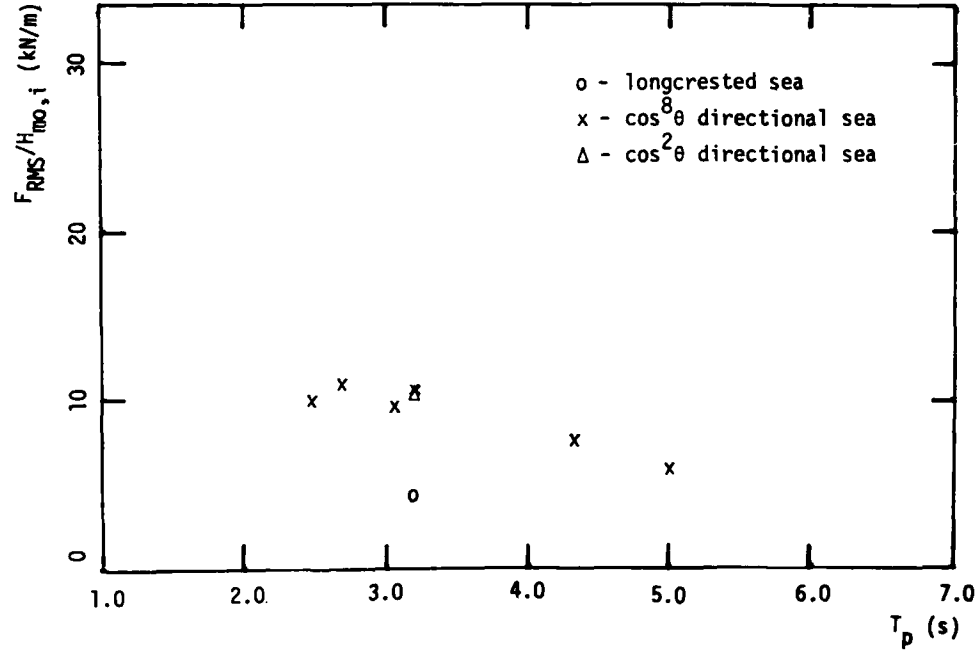
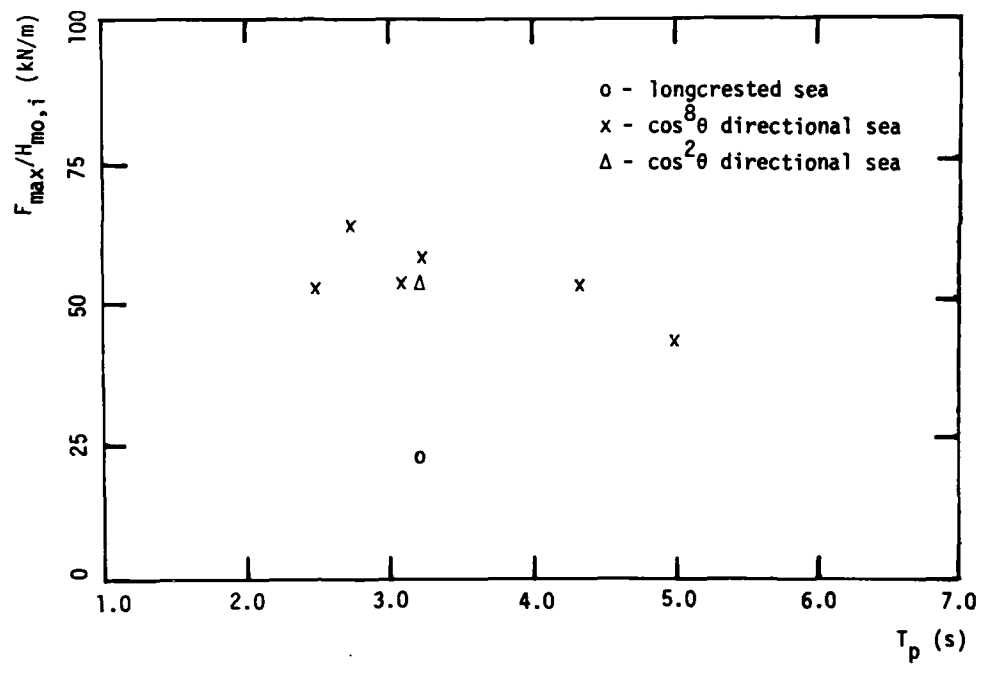


Fig. 3.37

NORMALIZED MAXIMUM AND RMS VALUES vs PEAK PERIOD OF INPUT WAVE

ANCHOR LINE FORCE NO. 11 FENDERED MODEL

STATIC FORCE HAS BEEN SUBTRACTED FROM SIGNAL

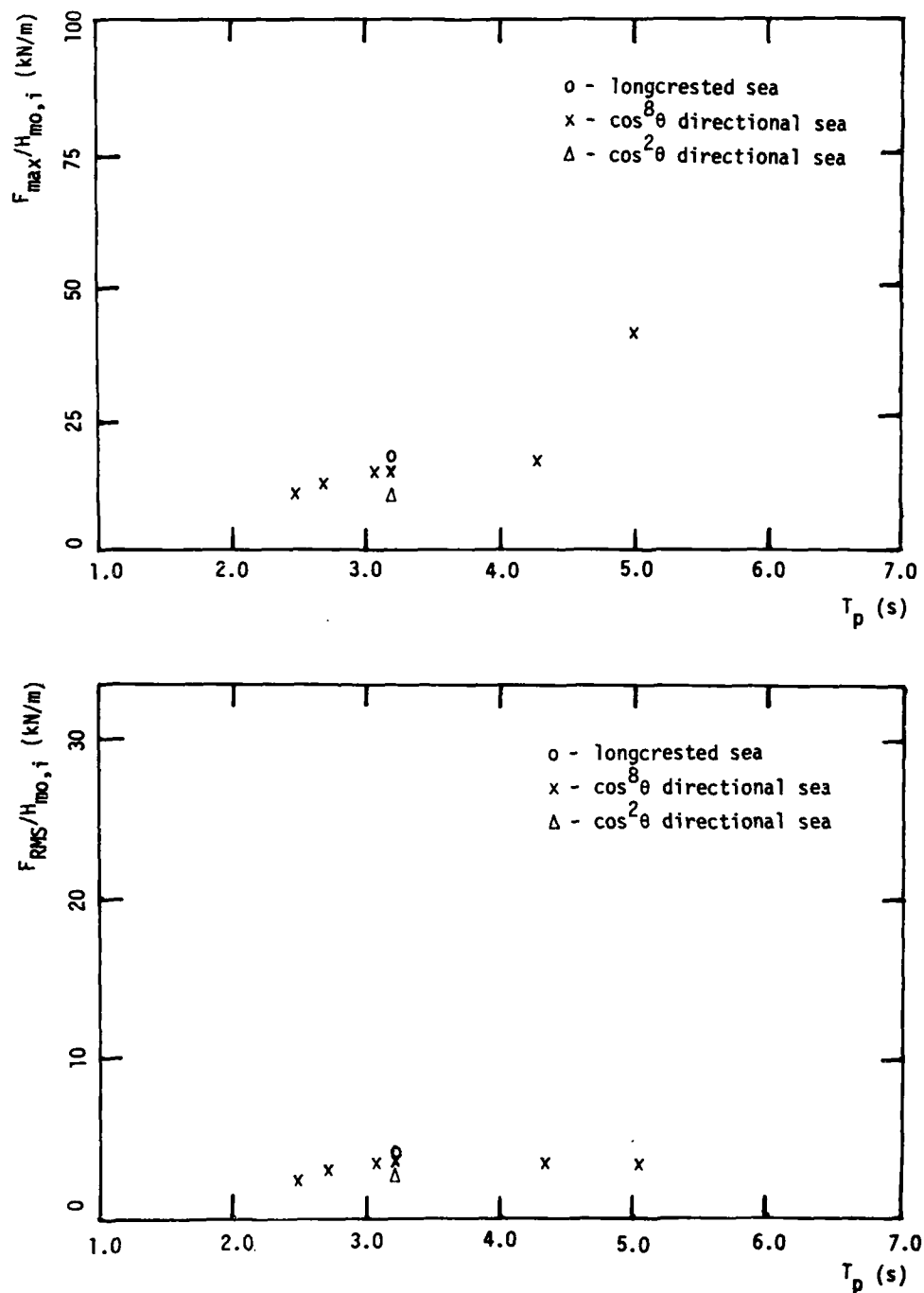


Fig. 3.38

NORMALIZED MAXIMUM AND RMS VALUES VS PEAK PERIOD OF INPUT WAVE

ANCHOR LINE FORCE NO. 12 FENDERED MODEL

STATIC FORCE HAS BEEN SUBTRACTED FROM SIGNAL

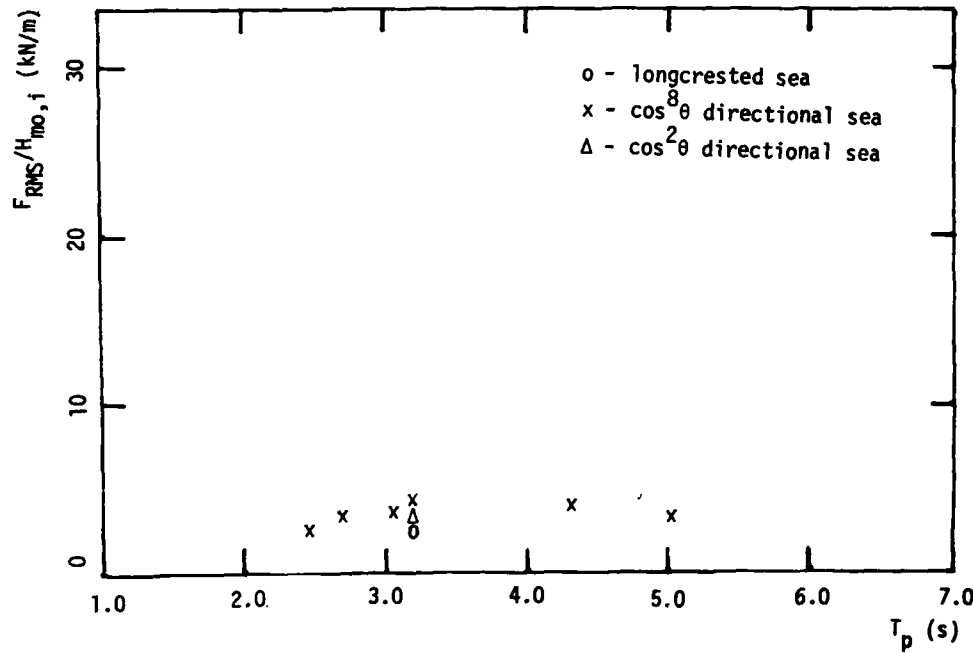
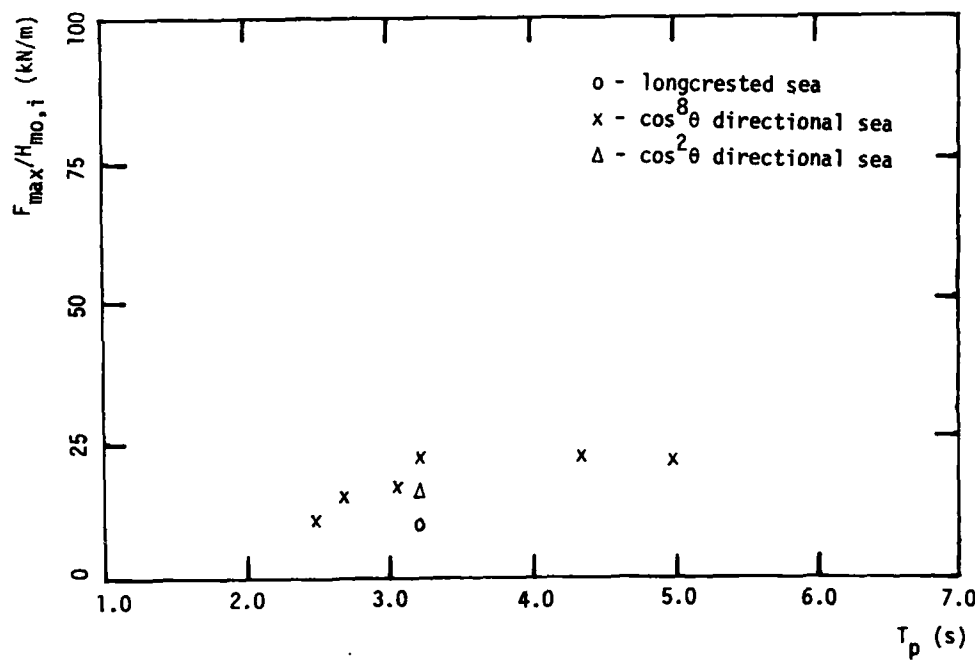


Fig. 3.39

SPECTRAL ANALYSIS FORCE NO. 10 Fendered Model Input: JONSWAP $T_p = 3.2$ s $H_s = 0.75$ m $\text{Gam} = 3.3$

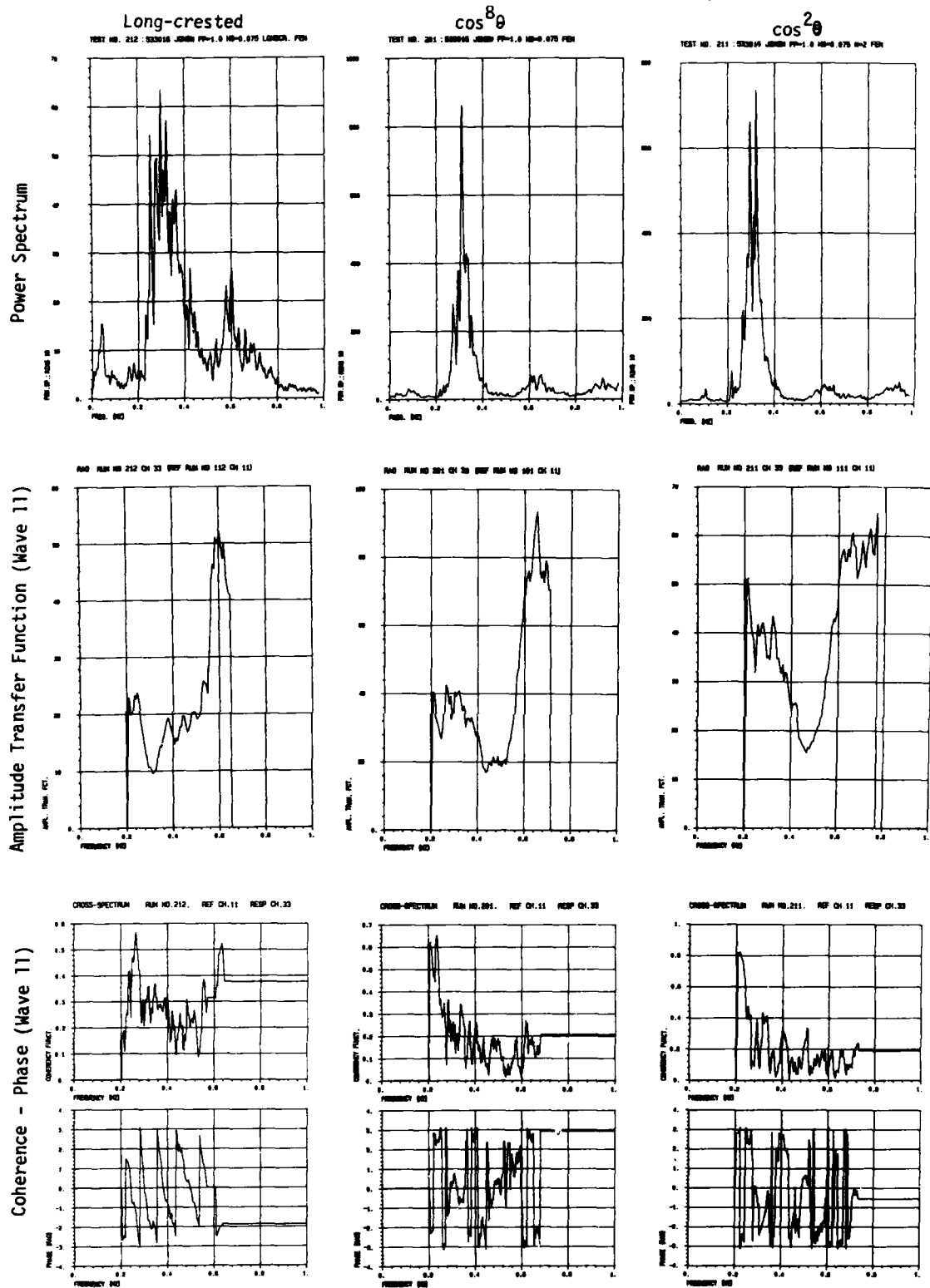


Fig. 3.40

SPECTRAL ANALYSIS FORCE NO. 10 Fendered Model Input: JONSWAP $\cos^8\theta$

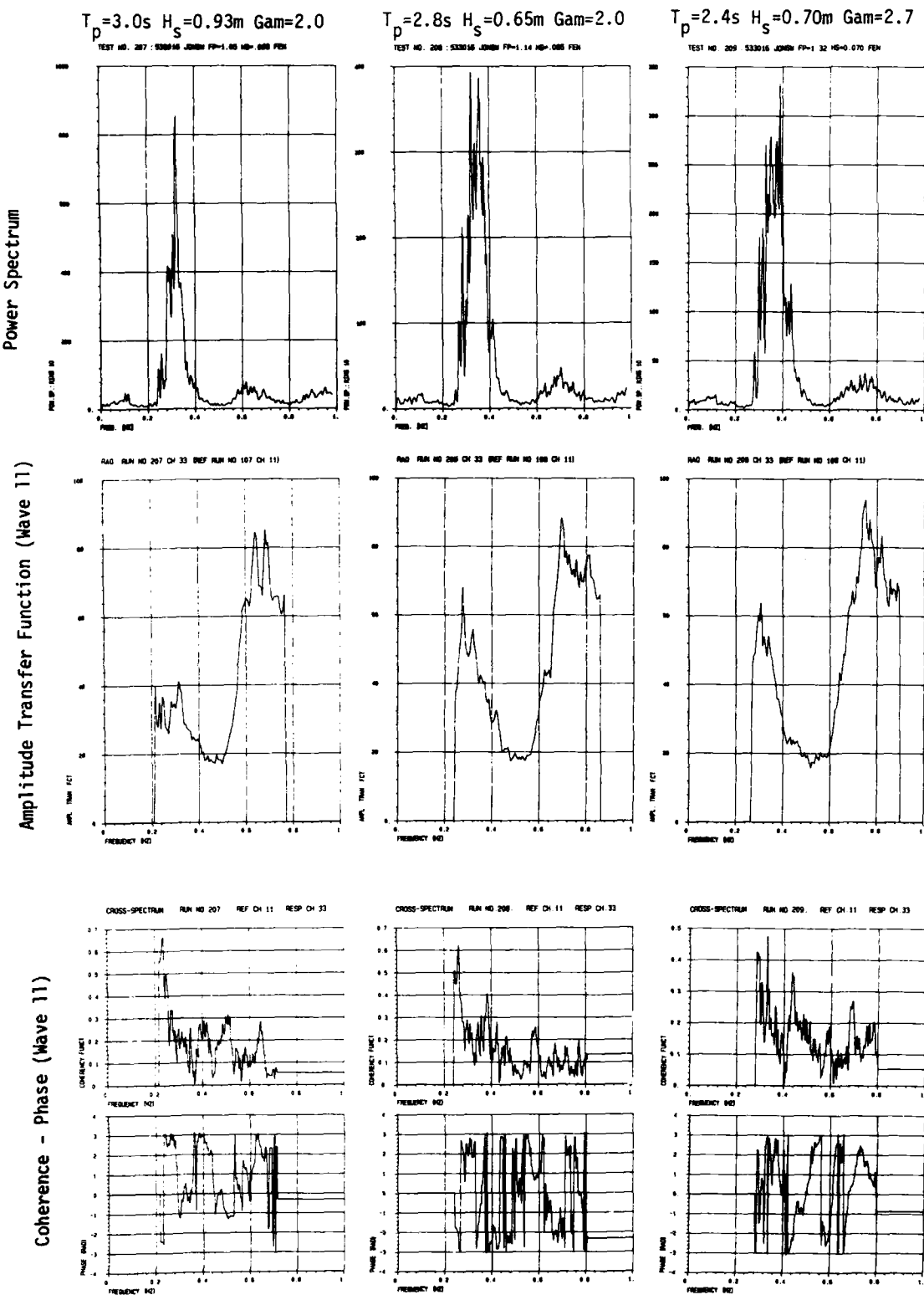


Fig. 3.41

SPECTRAL ANALYSIS FORCE NO. 10 Fendered Model

Input: JONSWAP $\cos^8 \theta$

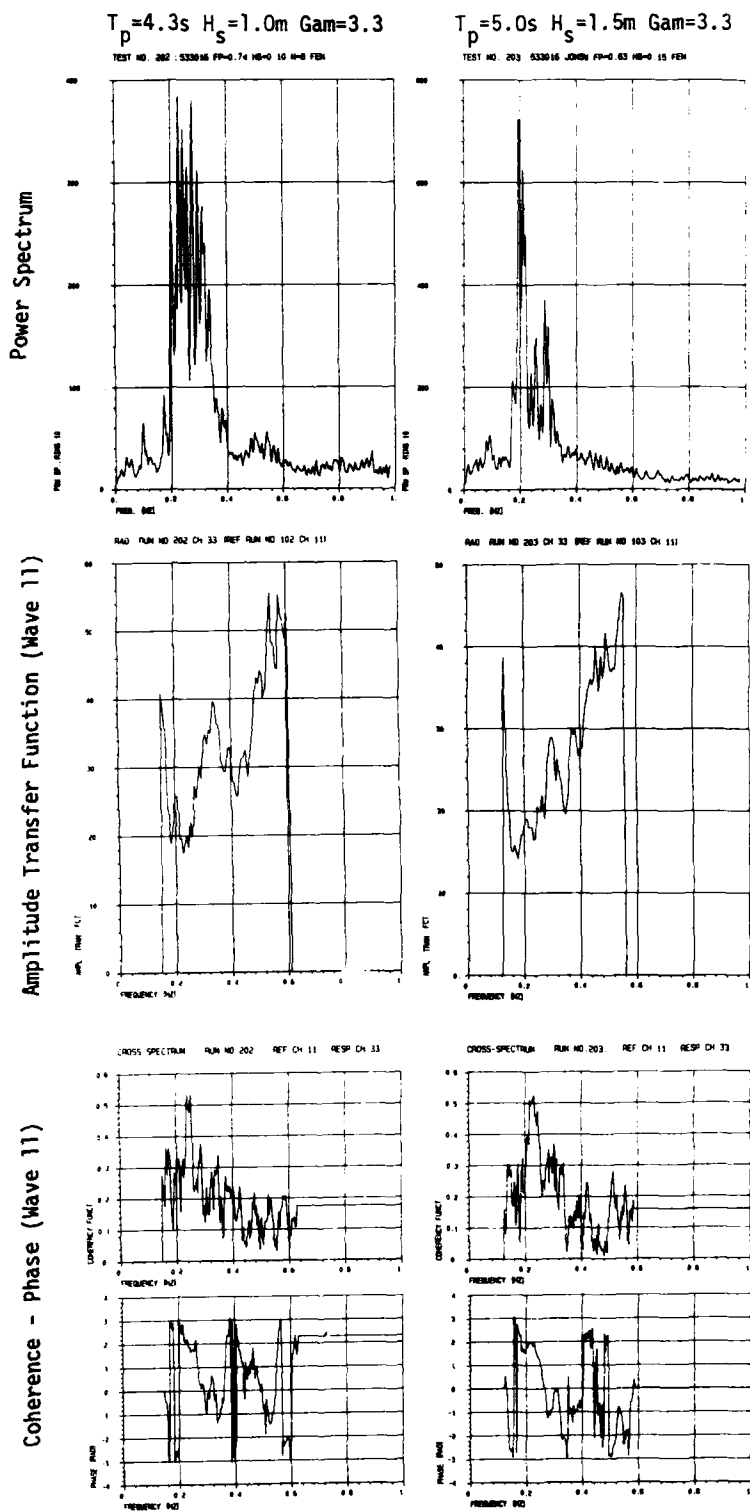


Fig. 3.42

SPECTRAL ANALYSIS FORCE NO. 11 Fendered Model Input: JONSWAP $T_p = 3.2\text{s}$ $H_s = 0.75\text{m}$ $\text{Gam} = 3.3$

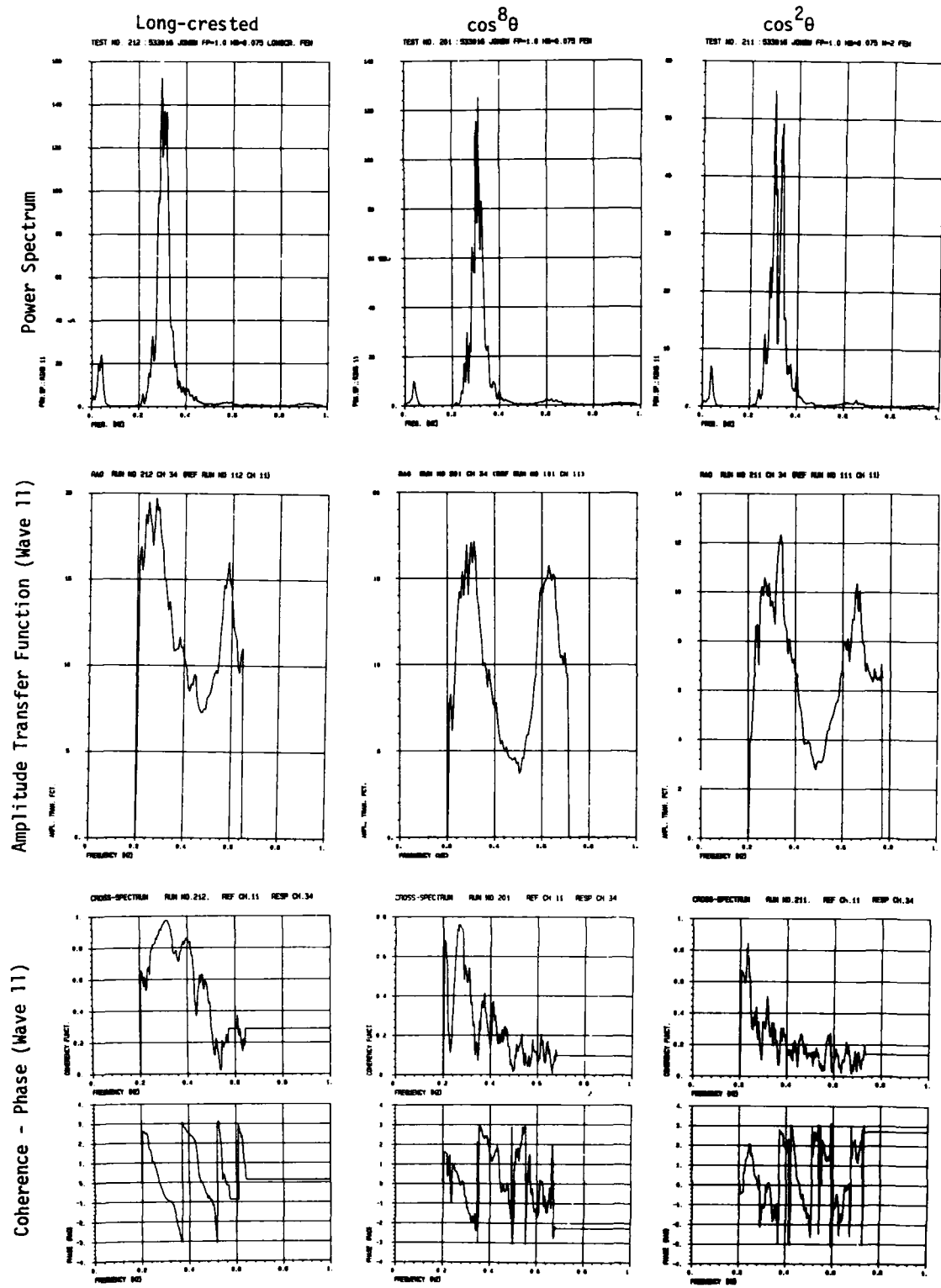


Fig. 3.43

SPECTRAL ANALYSIS FORCE NO. 11 Fendered Model Input: JONSWAP $\cos^8 \theta$

$T_p = 3.0\text{s}$ $H_s = 0.93\text{m}$ $\text{Gam} = 2.0$
TEST NO. 207 : 533816 JONSWP FP=1.05 Hs=0.93 Pds

$T_p = 2.8\text{s}$ $H_s = 0.65\text{m}$ $\text{Gam} = 2.0$
TEST NO. 208 : 533818 JONSWP FP=1.14 Hs=0.65 Pds

$T_p = 2.4\text{s}$ $H_s = 0.70\text{m}$ $\text{Gam} = 2.7$
TEST NO. 209 : 533819 JONSWP FP=1.32 Hs=0.70 Pds

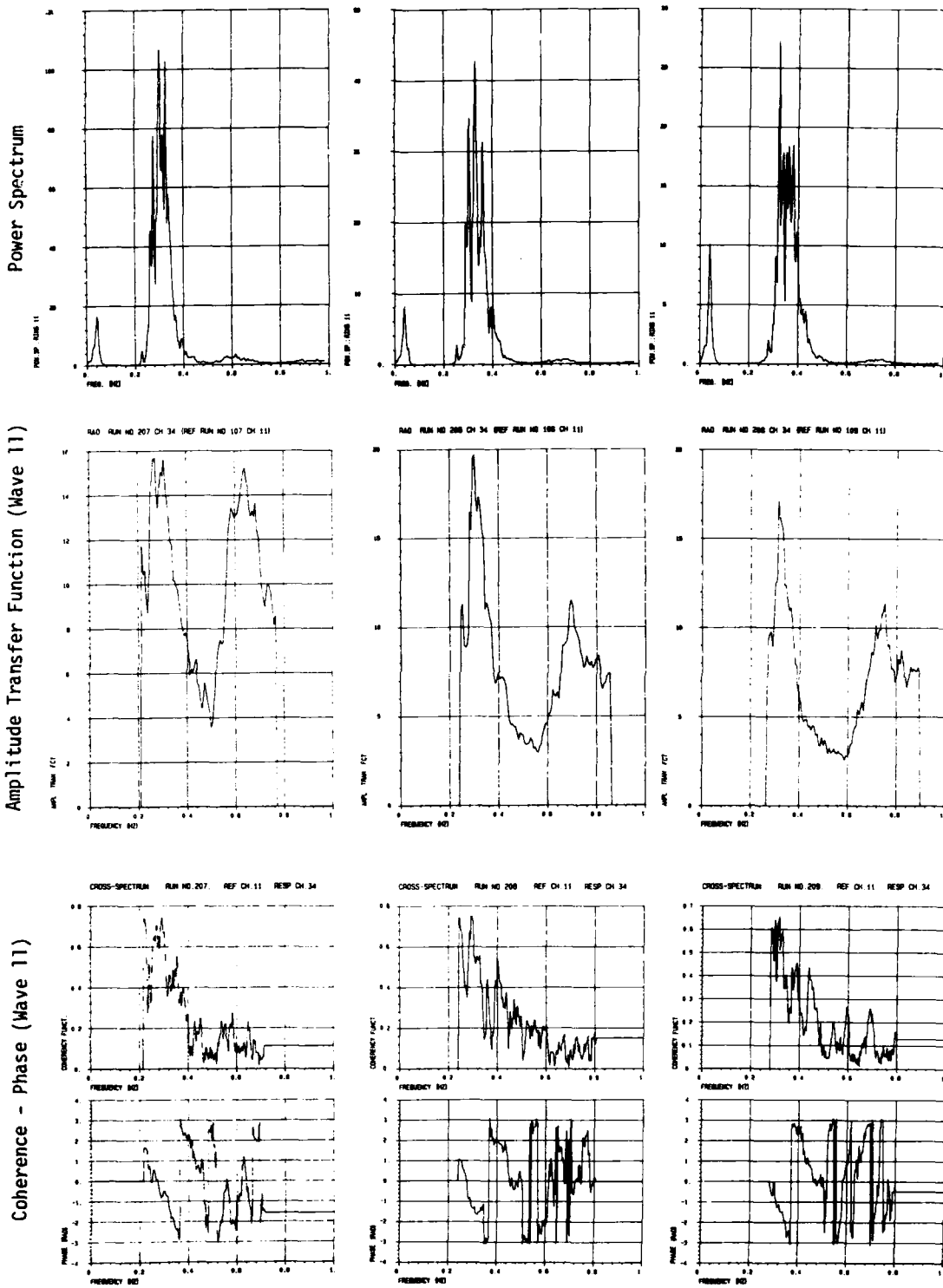
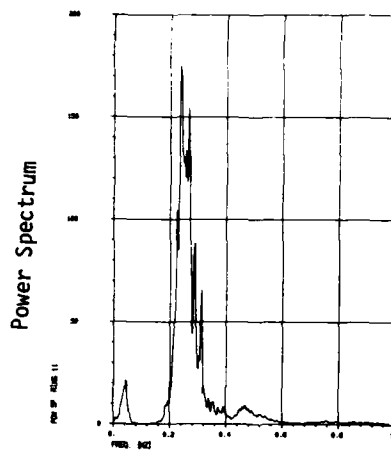


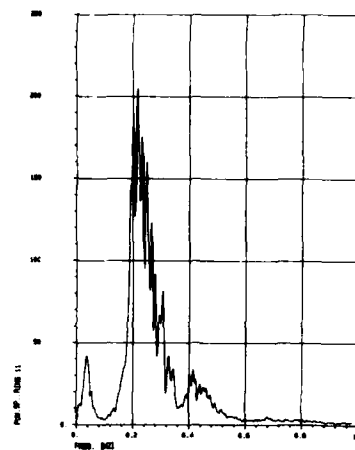
Fig. 3.44

SPECTRAL ANALYSIS FORCE NO. 11 Fendered Model Input: JONSWAP $\cos^8 \theta$

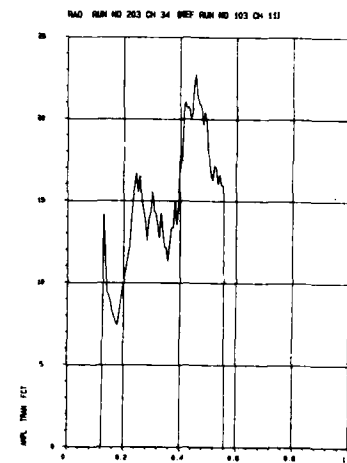
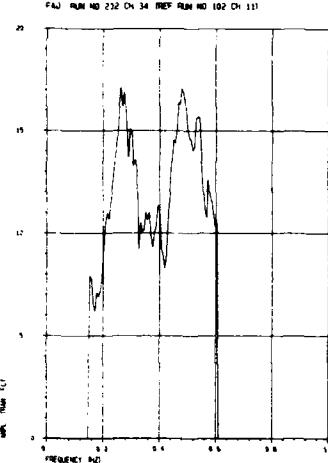
$T_p = 4.3\text{s}$ $H_s = 1.0\text{m}$ $\Gamma = 3.3$
TEST NO. 202 S33016 FM=0 74 HS=0 10 RM=0 FEM



$T_p = 5.0\text{s}$ $H_s = 1.5\text{m}$ $\Gamma = 3.3$
TEST NO. 203 S33016 FM=0 63 HS=0 15 RM=0 FEM



Amplitude Transfer Function (Wave 11)



Coherence - Phase (Wave 11)

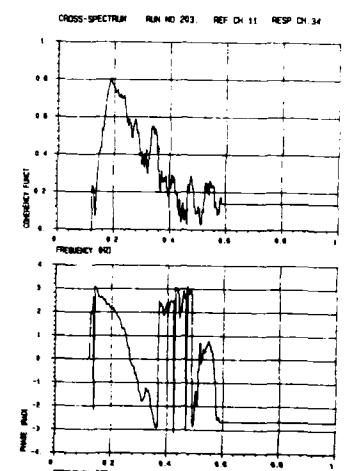
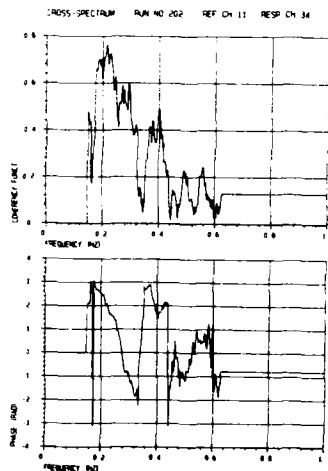


Fig. 3.45

SPECTRAL ANALYSIS FORCE NO. 12 Fendered Model Input: JONSWAP $T_p = 3.2\text{ s}$ $H_s = 0.75\text{ m}$ $\text{Gam} = 3.3$

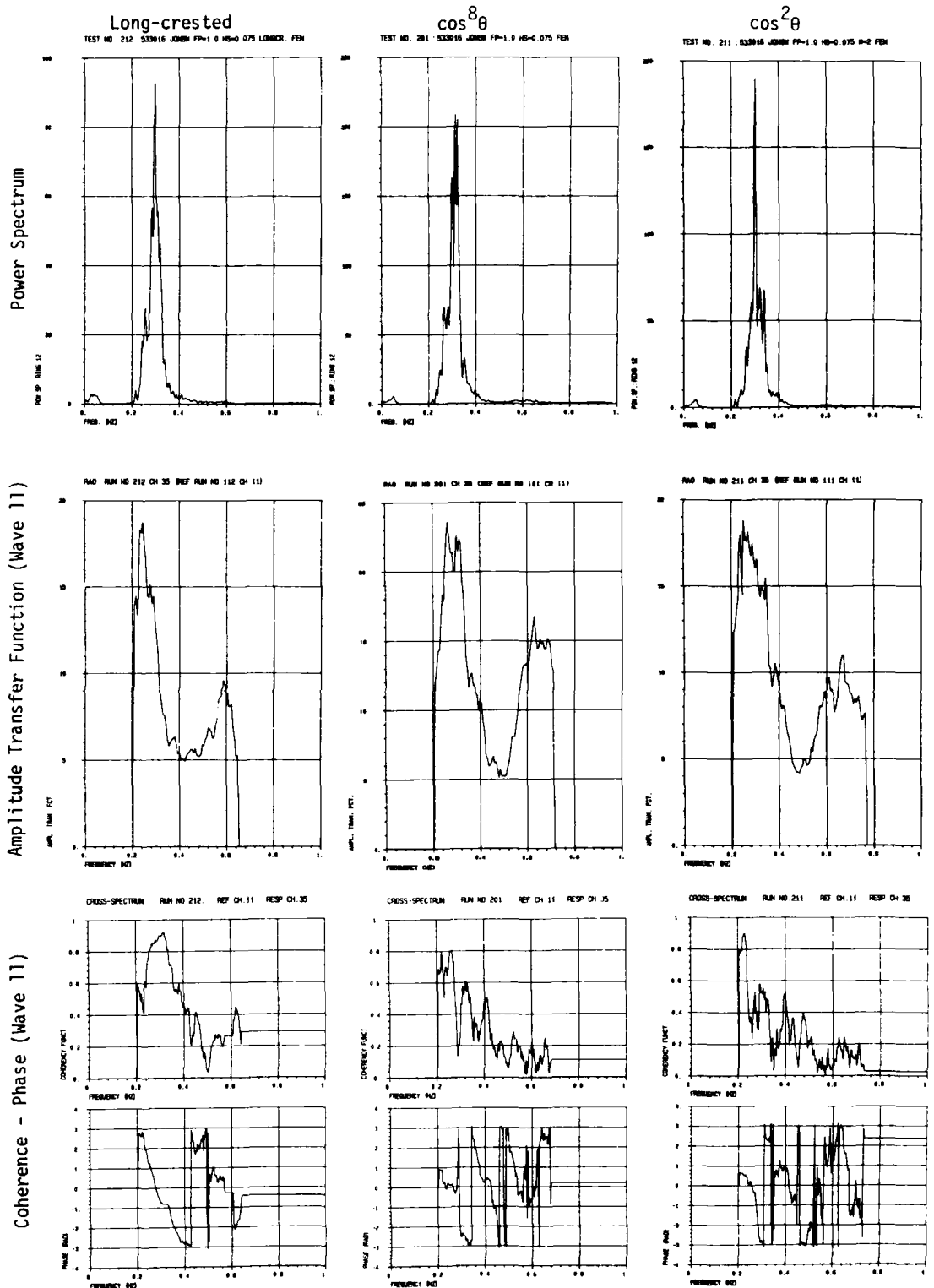


Fig. 3.46

SPECTRAL ANALYSIS FORCE NO. 12 Fendered Model Input: JONSWAP $\cos^8 \theta$

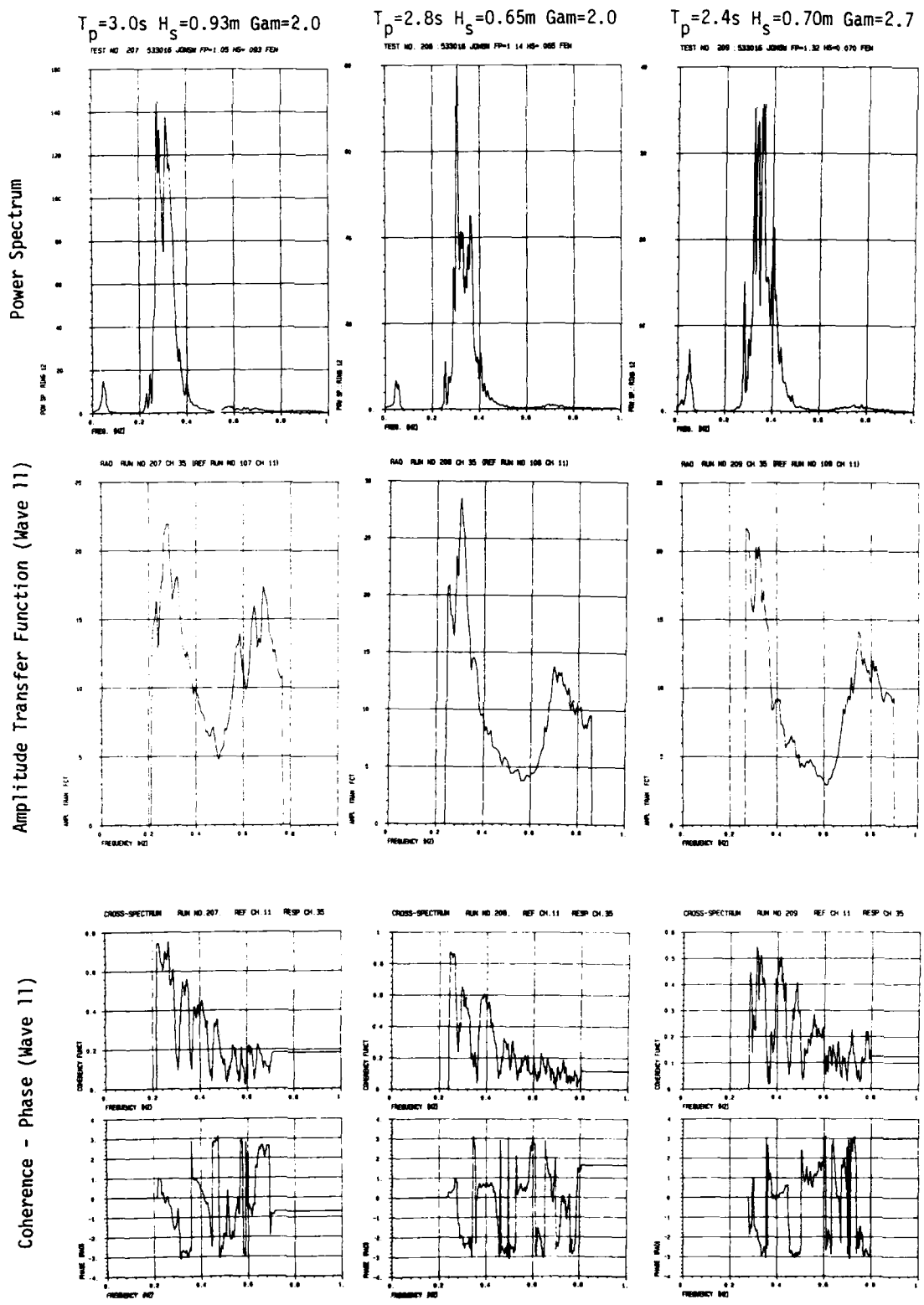
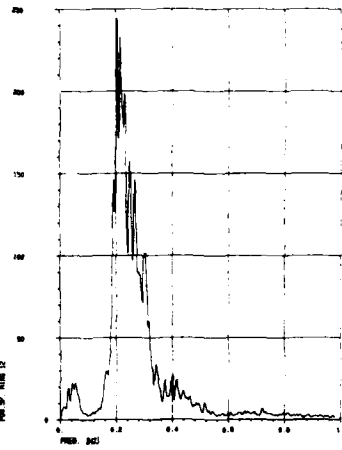
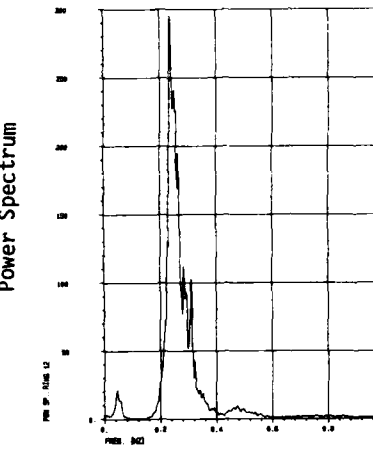


Fig. 3.47

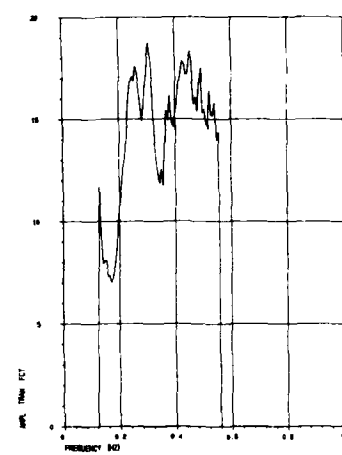
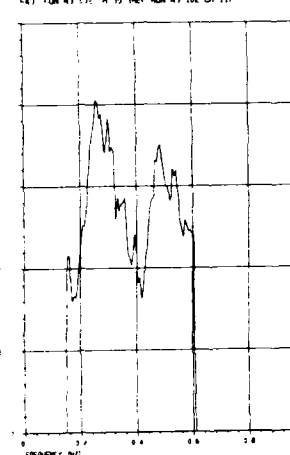
SPECTRAL ANALYSIS FORCE NO. 12 Fendered Model Input: JONSWAP $\cos^8 \theta$

$T_p = 4.3\text{s}$ $H_s = 1.0\text{m}$ $\Gamma = 3.3$
TEST NO. 202 533015 FP=0 74 HS=0 10 MMF FEN

$T_p = 5.0\text{s}$ $H_s = 1.5\text{m}$ $\Gamma = 3.3$
TEST NO. 203 533016 JONSWAP FP=0 63 HS=0 15 FEN



Amplitude Transfer Function (Wave 11)



Coherence - Phase (Wave 11)

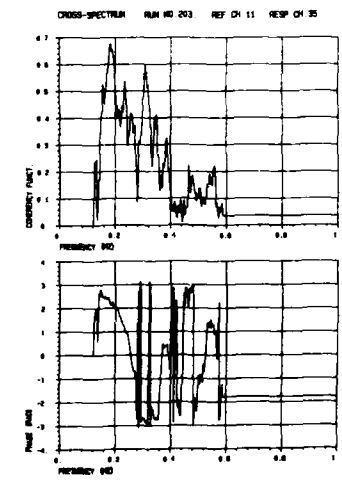
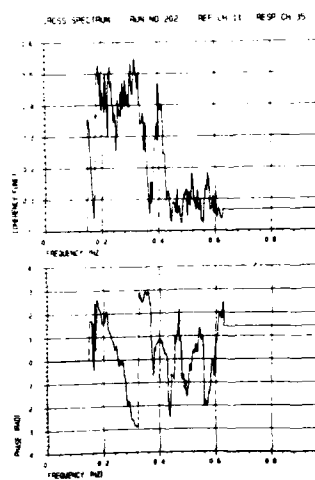


Fig. 3.48

AMPLITUDE STATISTICS FORCE Fendered Model Input: JONSWAP $T_p=3.2s$ $H_s=0.75m$ $\Gamma_m=3.3$

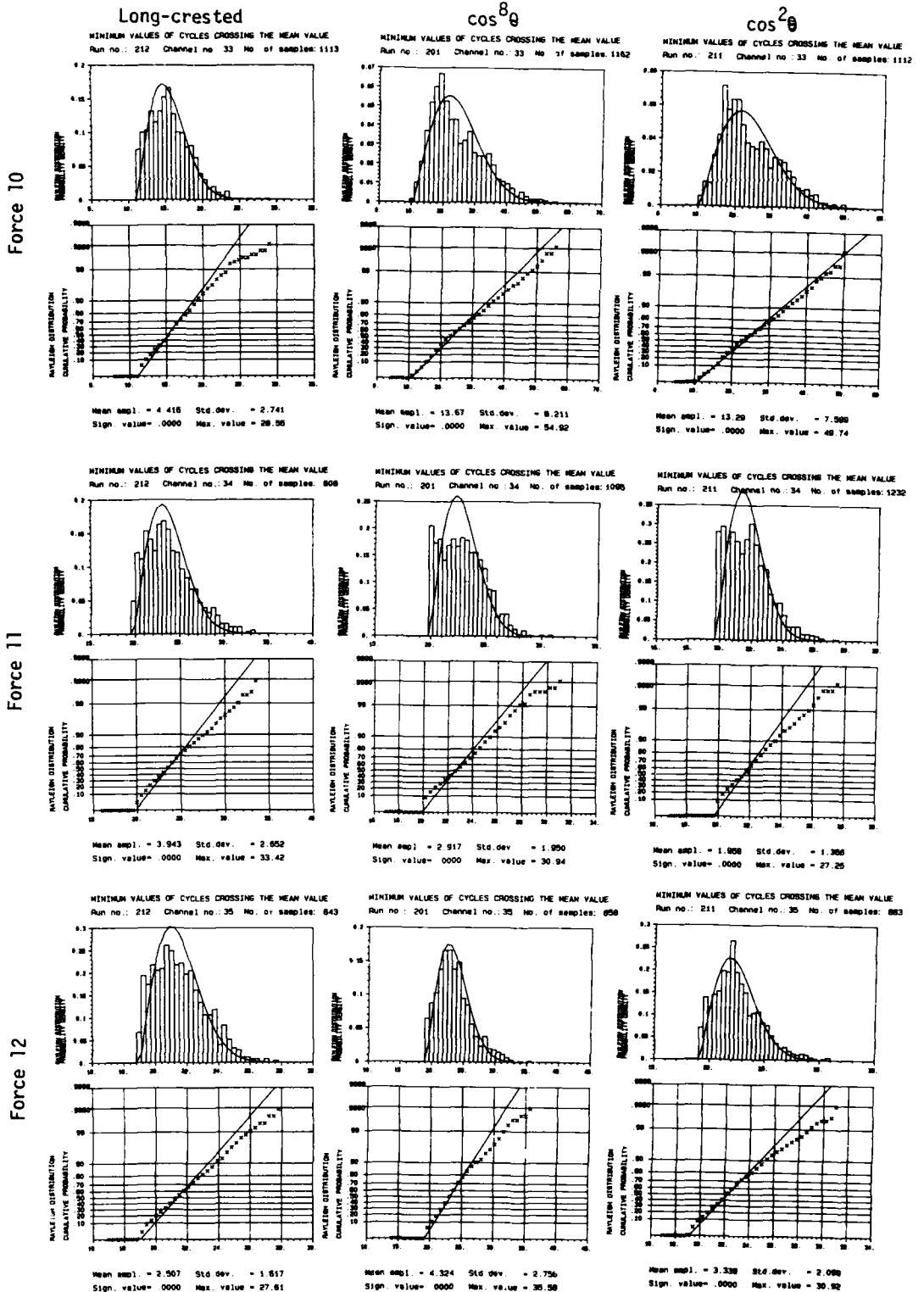


Fig. 3.49

AMPLITUDE STATISTICS FORCE Fendered Model

Input: JONSWAP $\cos^8 \theta$

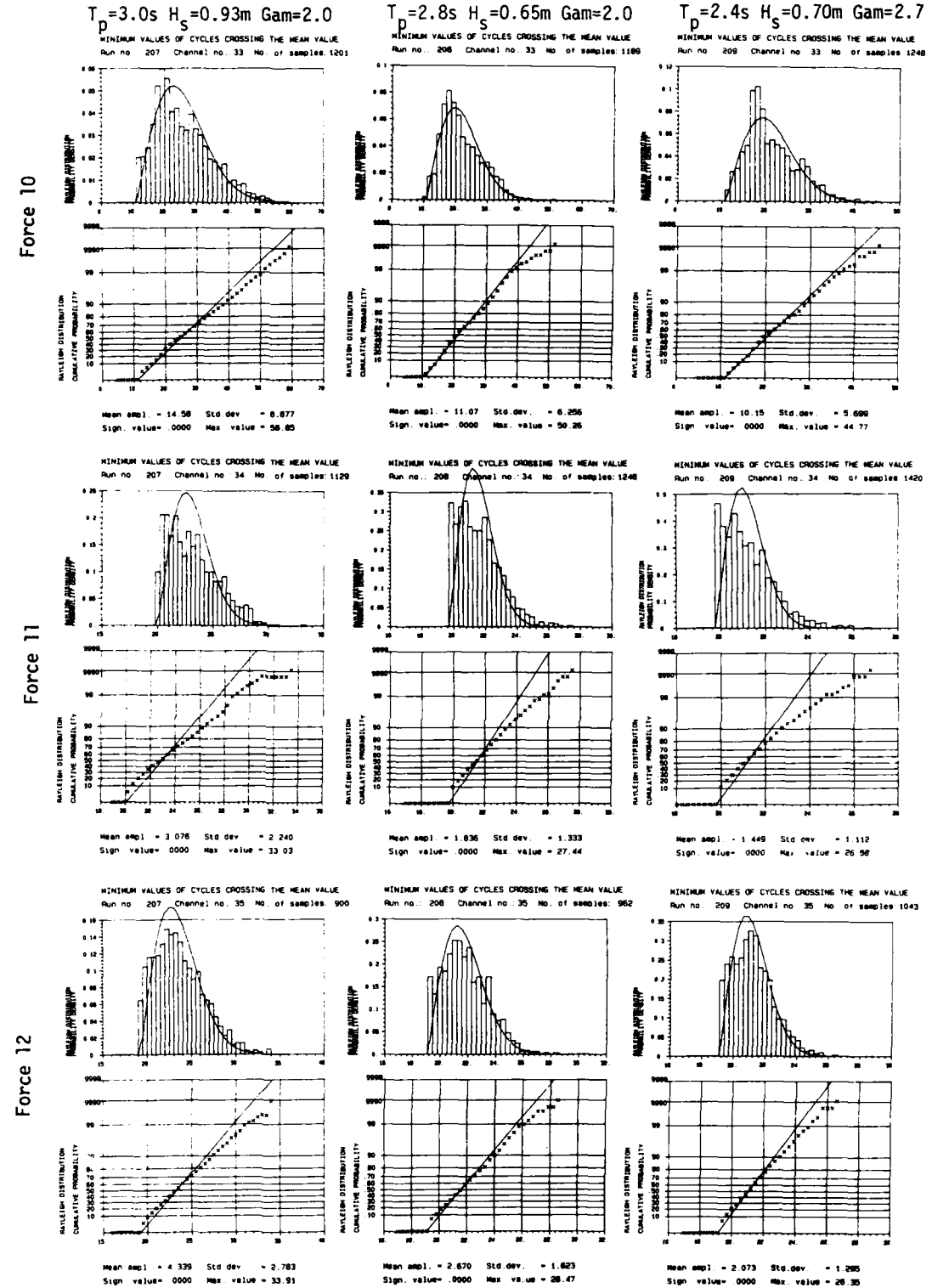


Fig. 3.50

AMPLITUDE STATISTICS FORCE Fendered Model Input: JONSWAP $\cos^8 \theta$

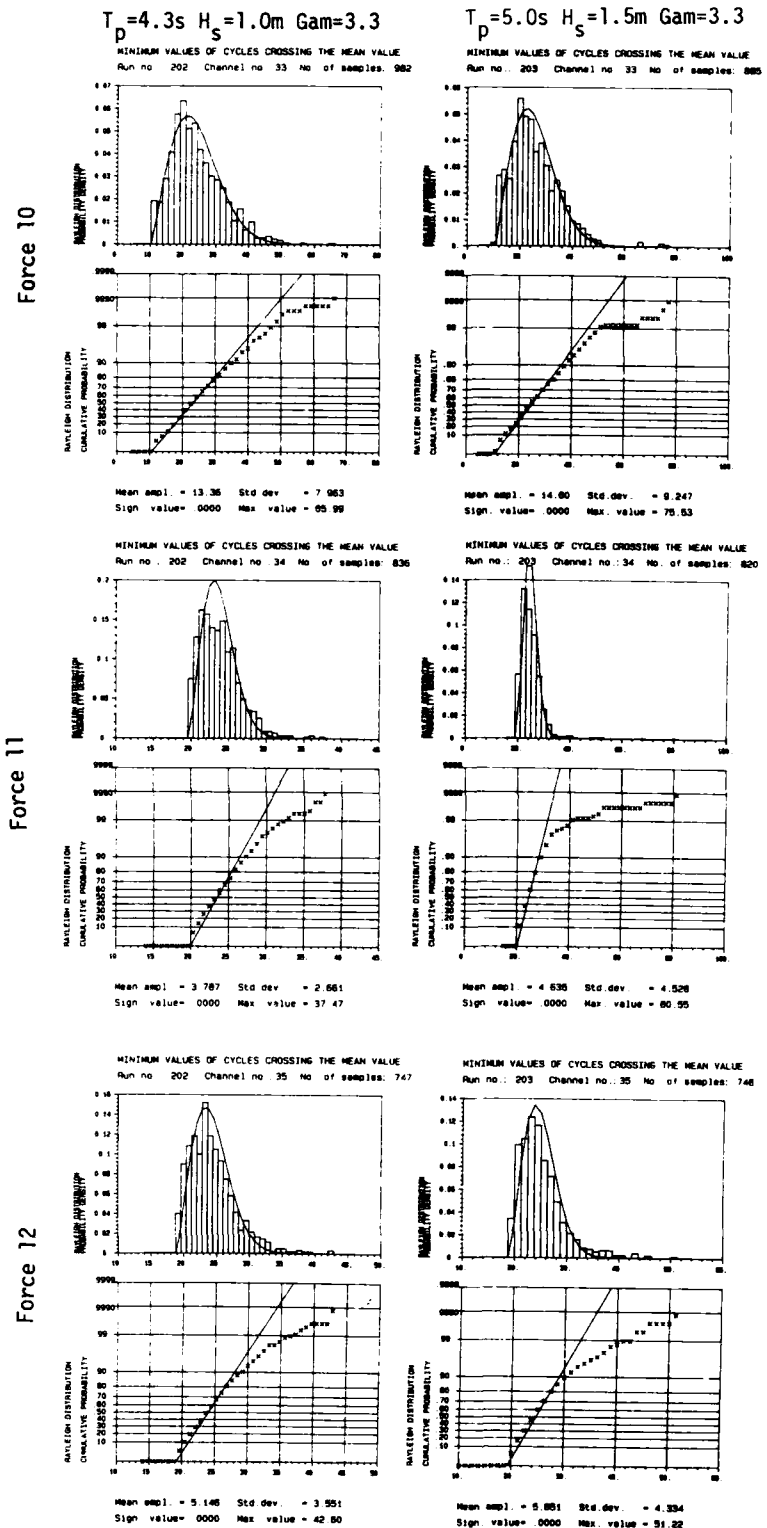


Fig. 3.51

COHERENCE-PHASE ANALYSIS FORCE - FORCE Fendered Model Input: JONSWAP $T_p = 3.2s$ $H_s = 0.75m$ $\text{Gam} = 3.$

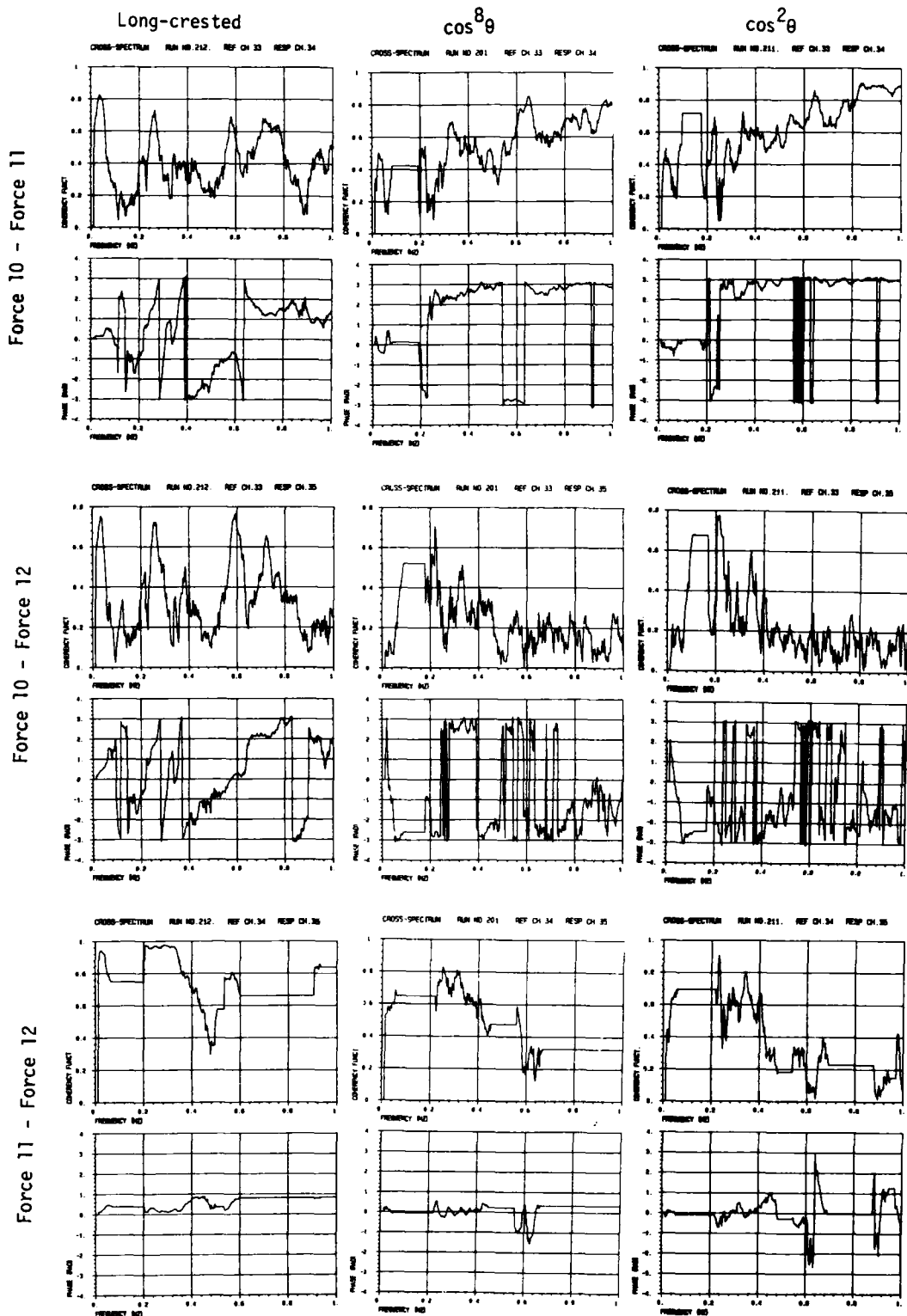
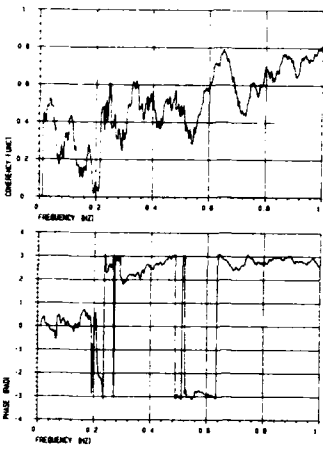


Fig. 3.52

COHERENCE-PHASE ANALYSIS FORCE - FORCE Fendered Model Input: JONSWAP $\cos^8 \theta$

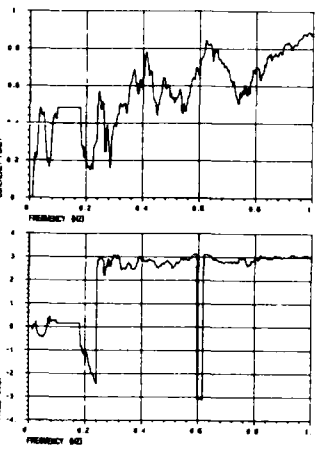
$T_p = 3.0\text{s}$ $H_s = 0.93\text{m}$ $\text{Gam} = 2.0$

CROSS-SPECTRUM RUN NO 207 REF CH 33 RESP CH 34



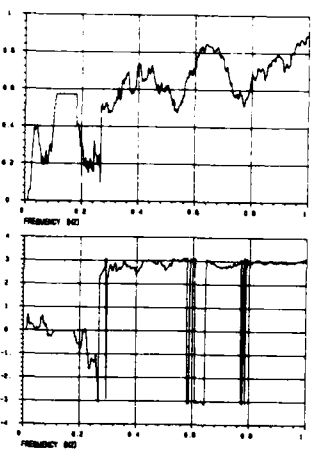
$T_p = 2.8\text{s}$ $H_s = 0.65\text{m}$ $\text{Gam} = 2.0$

CROSS-SPECTRUM RUN NO 208 REF CH 33 RESP CH 34



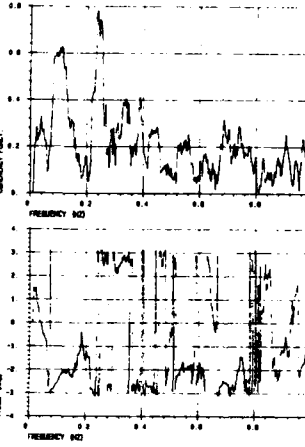
$T_p = 2.4\text{s}$ $H_s = 0.70\text{m}$ $\text{Gam} = 2.7$

CROSS-SPECTRUM RUN NO 209 REF CH 33 RESP CH 34

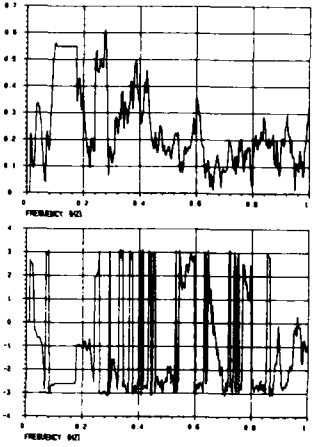


Force 10 - Force 11

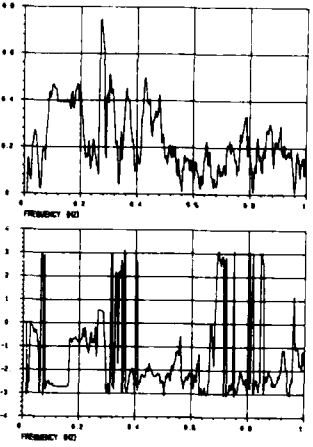
CROSS-SPECTRUM RUN NO 207 REF CH 33 RESP CH 35



CROSS-SPECTRUM RUN NO 208 REF CH 33 RESP CH 35

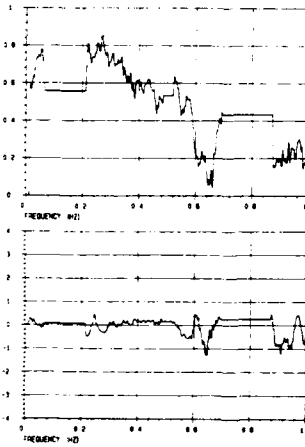


CROSS-SPECTRUM RUN NO 209 REF CH 33 RESP CH 35

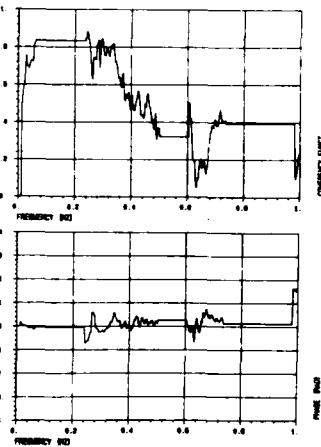


Force 10 - Force 12

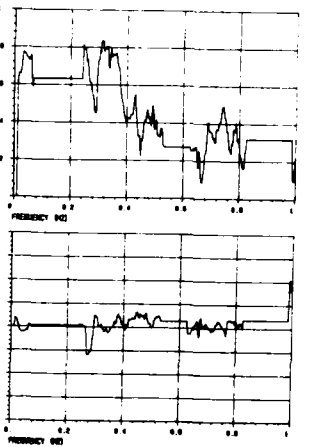
CROSS-SPECTRUM RUN NO 207 REF CH 34 RESP CH 35



CROSS-SPECTRUM RUN NO 208 REF CH 34 RESP CH 35



CROSS-SPECTRUM RUN NO 209 REF CH 34 RESP CH 35



Force 11 - Force 12

Fig. 3.53

COHERENCE-PHASE ANALYSIS FORCE - FORCE Fendered Model Input: JONSWAP $\cos^8\theta$

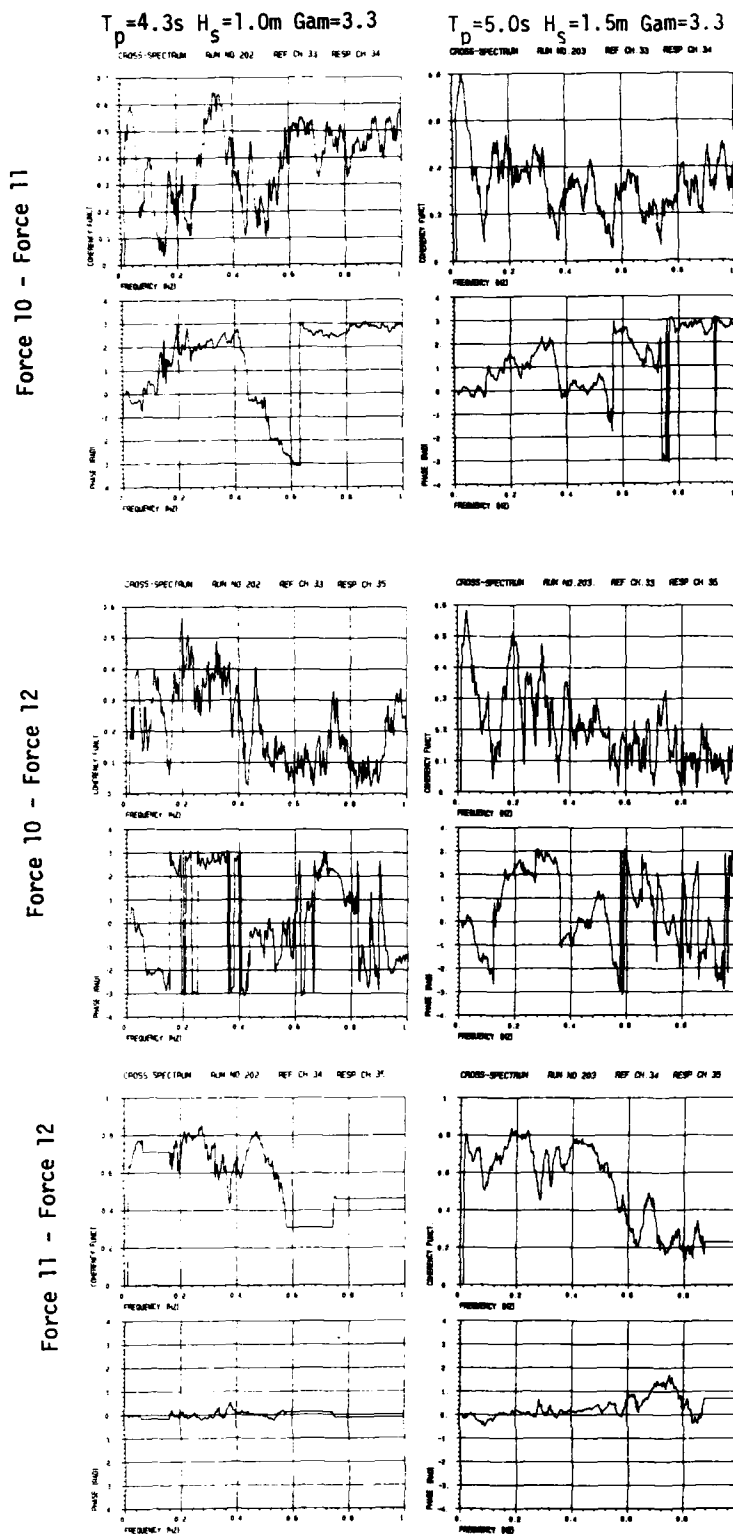


Fig. 3.54

COHERENCE-PHASE ANALYSIS FORCE - MOTION Fendered Model Input: JONSWAP $T_p=3.2s$ $H_s=0.75m$ $\text{Gam}=3.3$

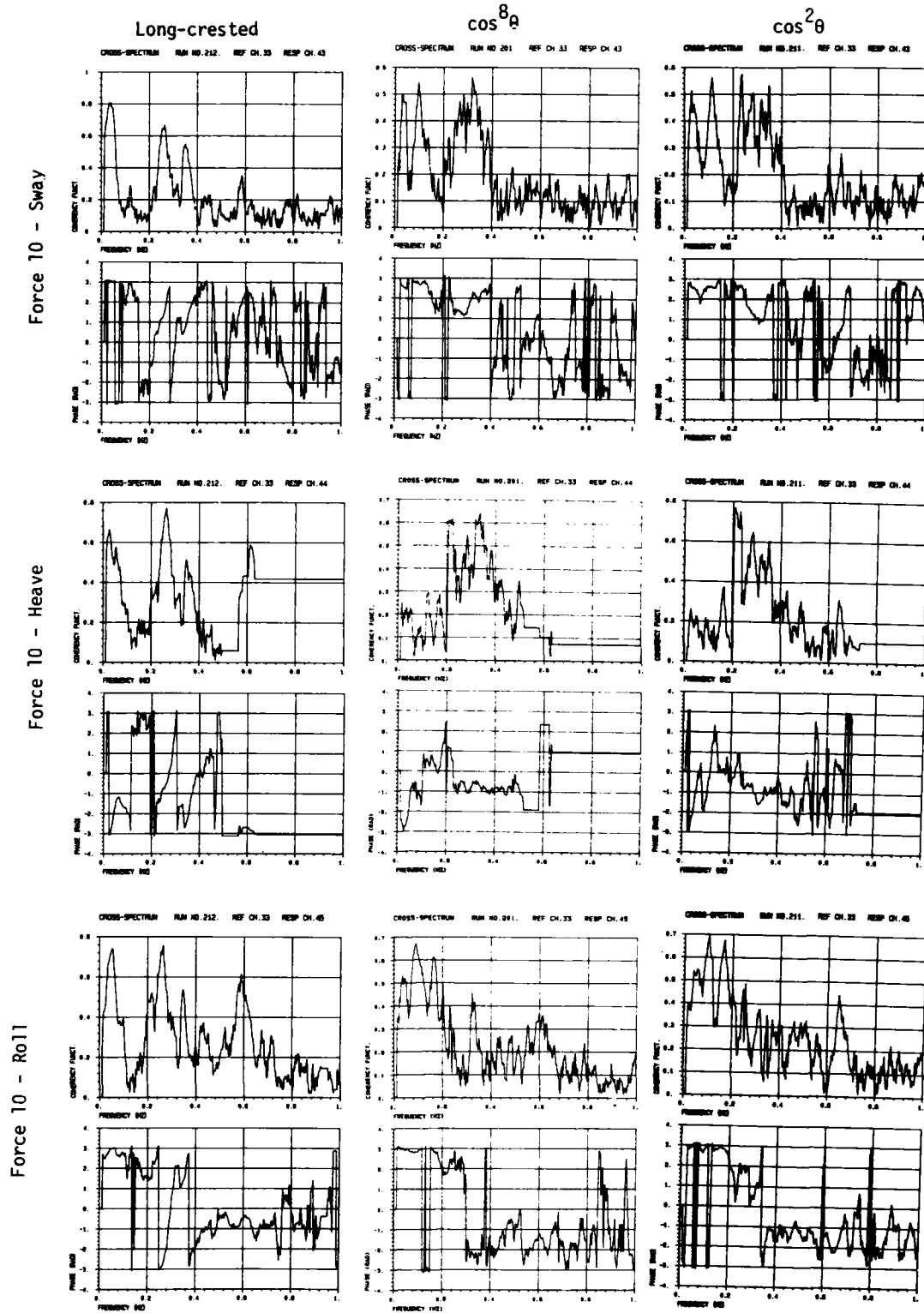


Fig. 3.55

COHERENCE-PHASE ANALYSIS FORCE - MOTION Fendered Model Input: JONSWAP $\cos^8 \theta$

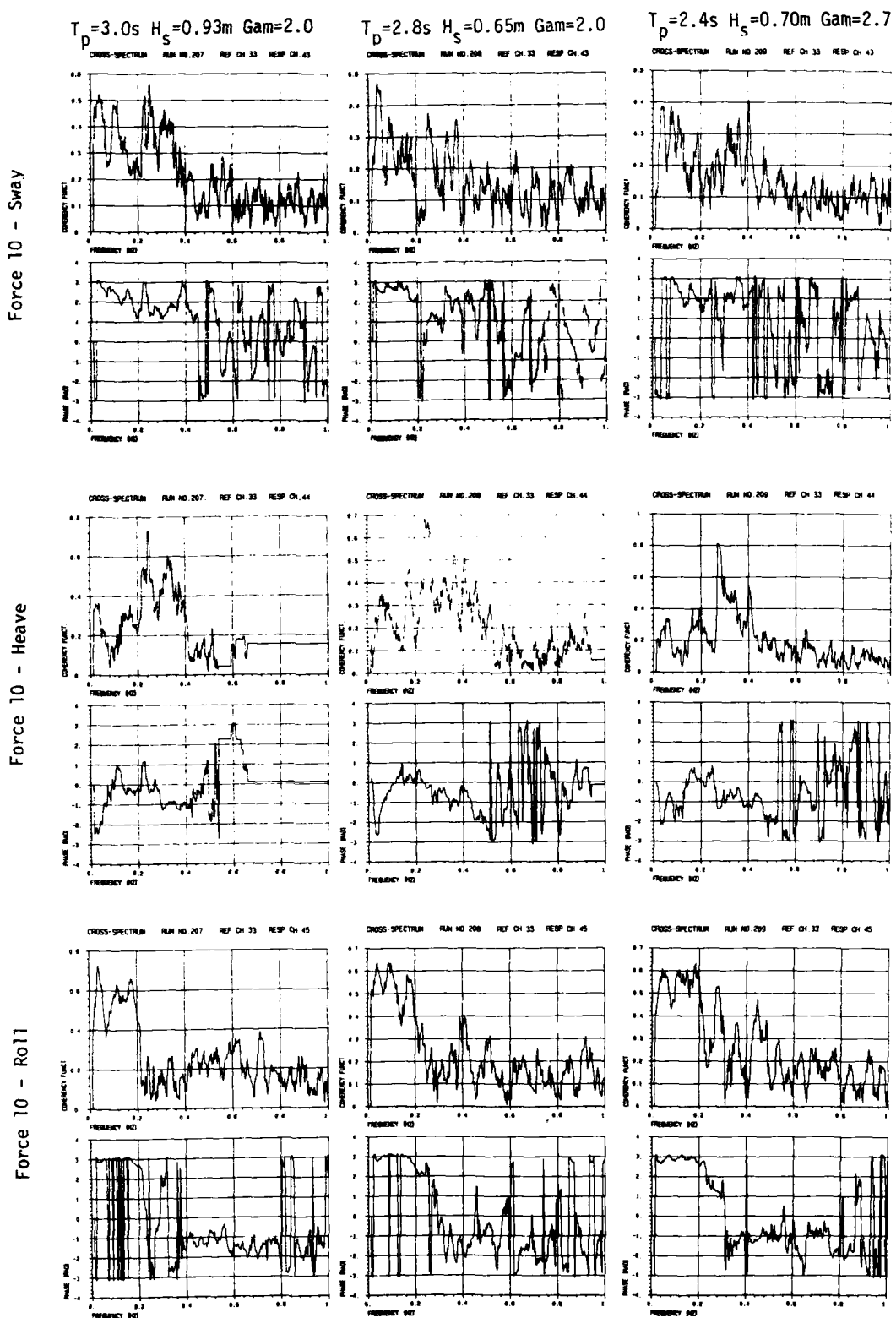


Fig. 3.56

COHERENCE-PHASE ANALYSIS FORCE - MOTION Fendered Model

Input: JONSWAP $\cos^8 \theta$

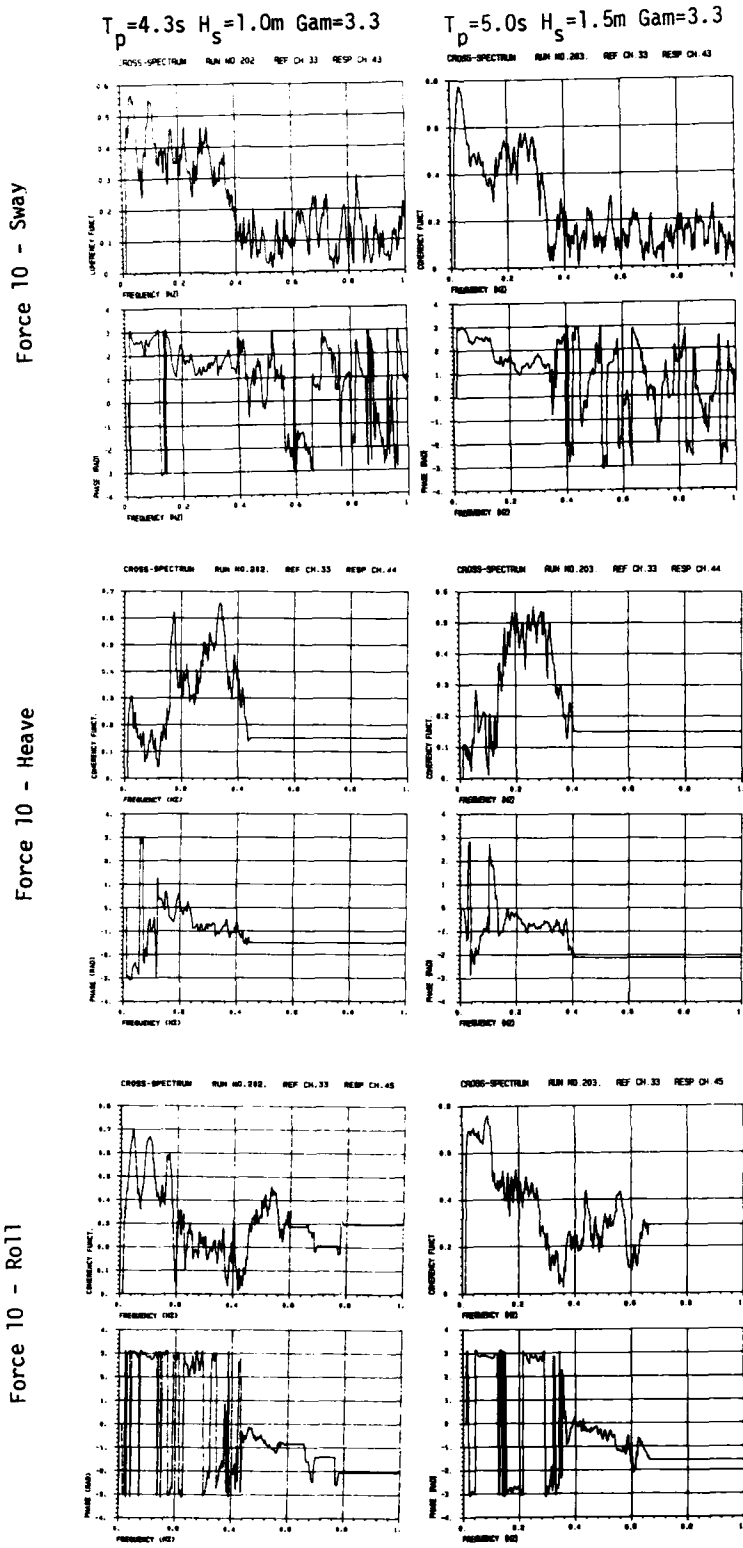


Fig. 3.57

COHERENCE-PHASE ANALYSIS FORCE - MOTION Fendered Model Input: JONSWAP $T_p = 3.2\text{s}$ $H_s = 0.75\text{m}$ $\text{Gam} = 3.3$

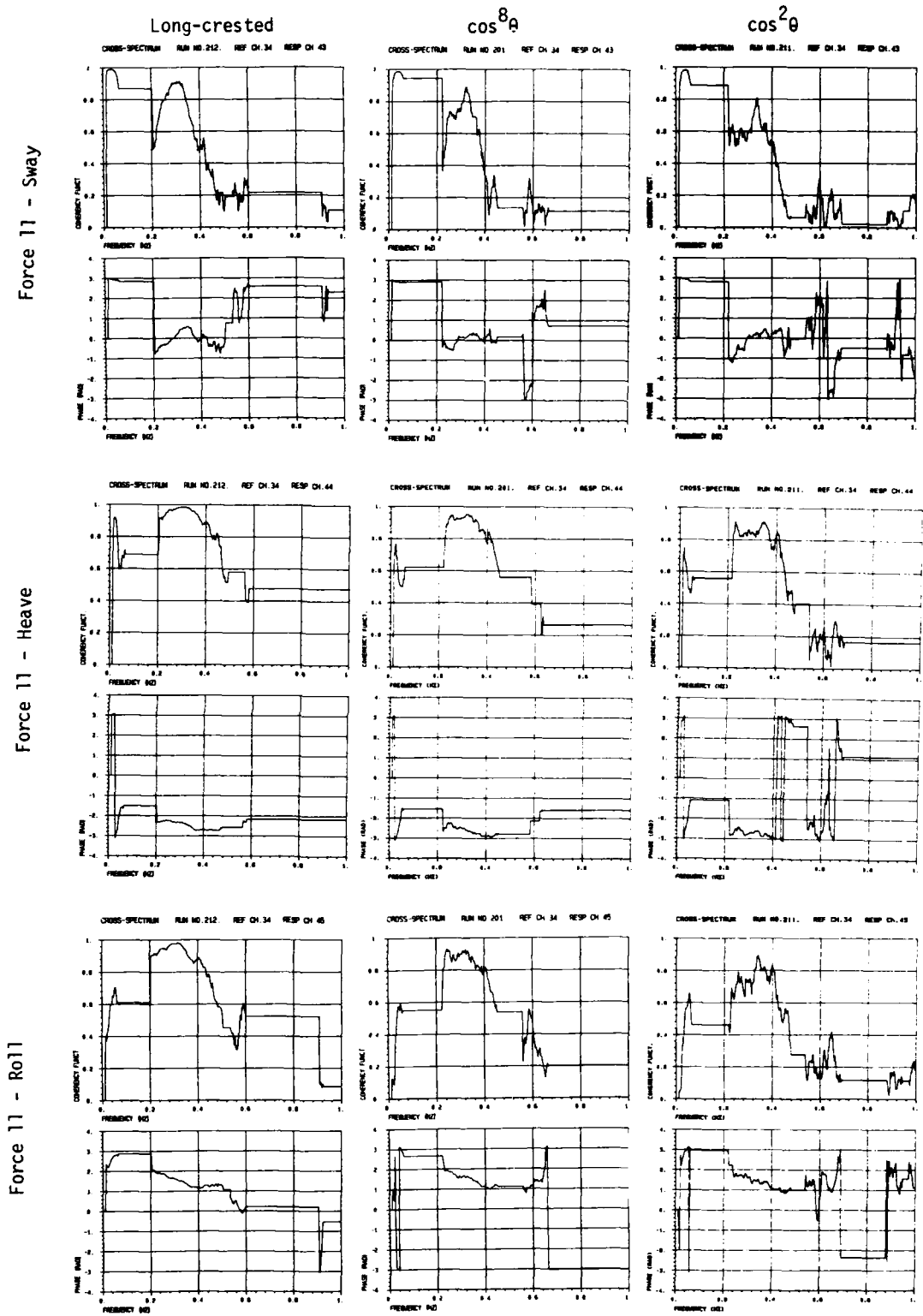


Fig. 3.58

COHERENCE-PHASE ANALYSIS FORCE - MOTION Fendered Model Input: JONSWAP $\cos^8 \theta$

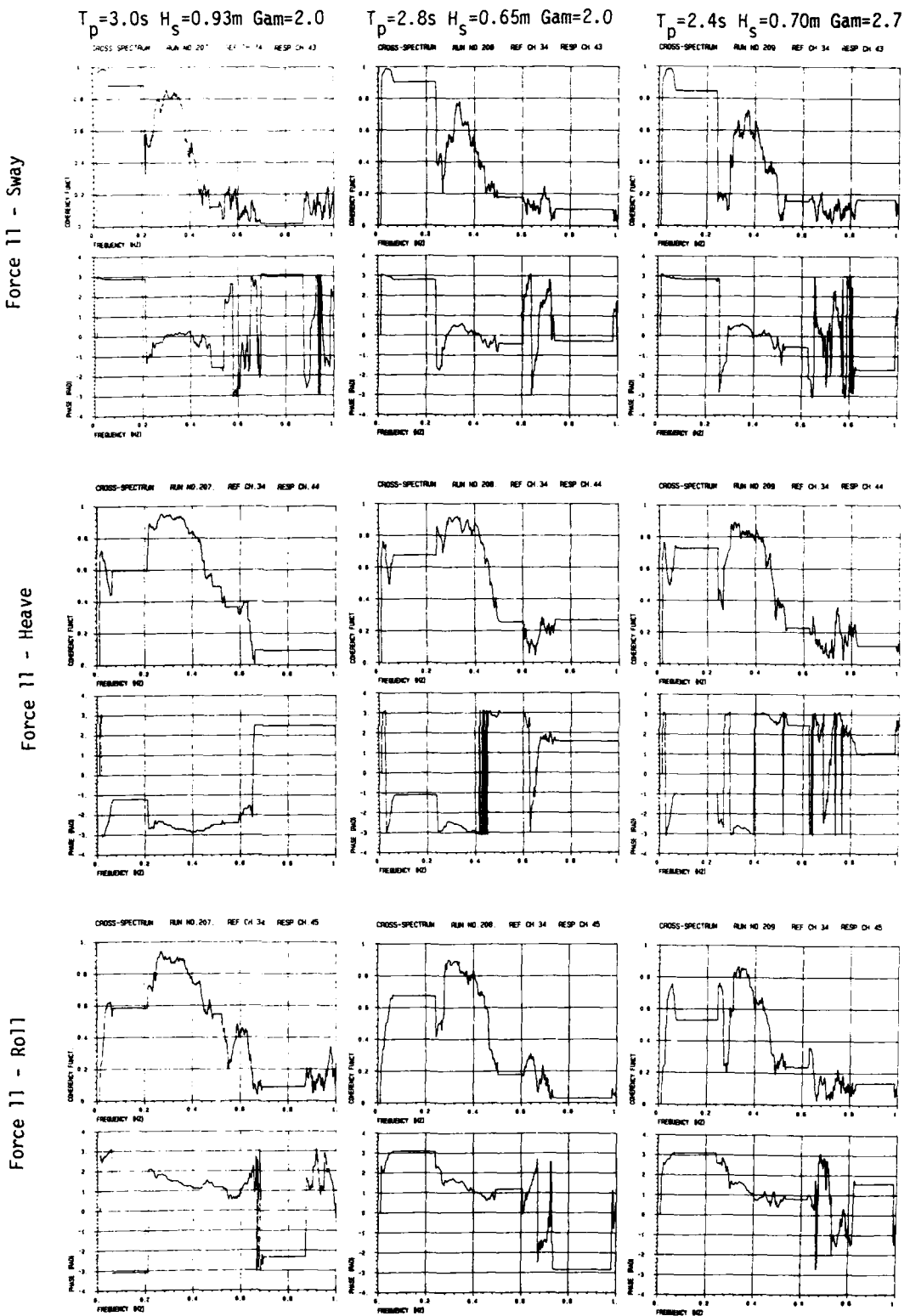


Fig. 3.59

COHERENCE-PHASE ANALYSIS FORCE - MOTION Fendered Model

Input: JONSWAP $\cos^8 \theta$

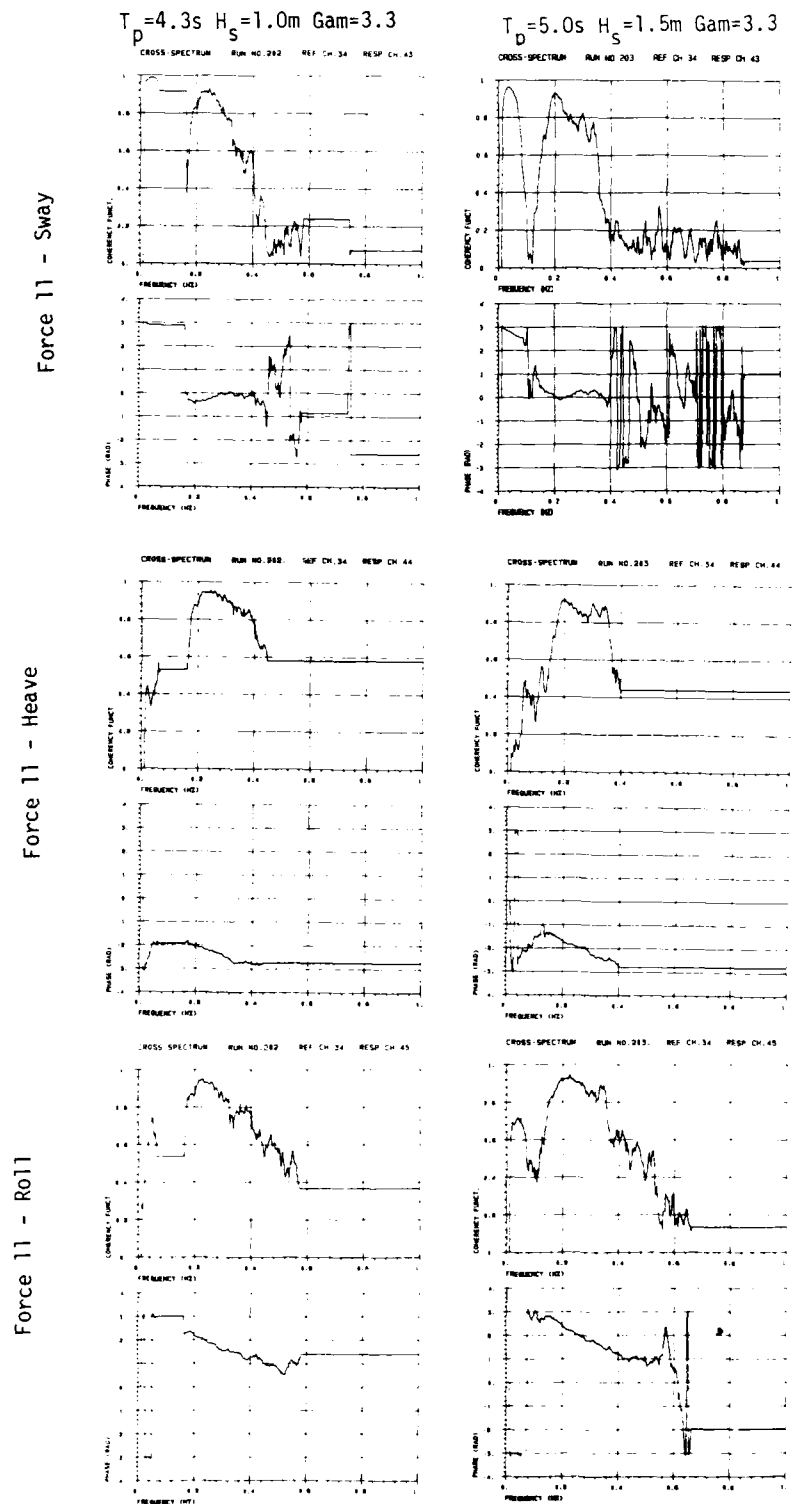


Fig. 3.60

COHERENCE-PHASE ANALYSIS FORCE - MOTION Fendered Model Input: JONSWAP $T_p = 3.2\text{ s}$ $H_s = 0.75\text{ m}$ $\Gamma_m = 3.3$

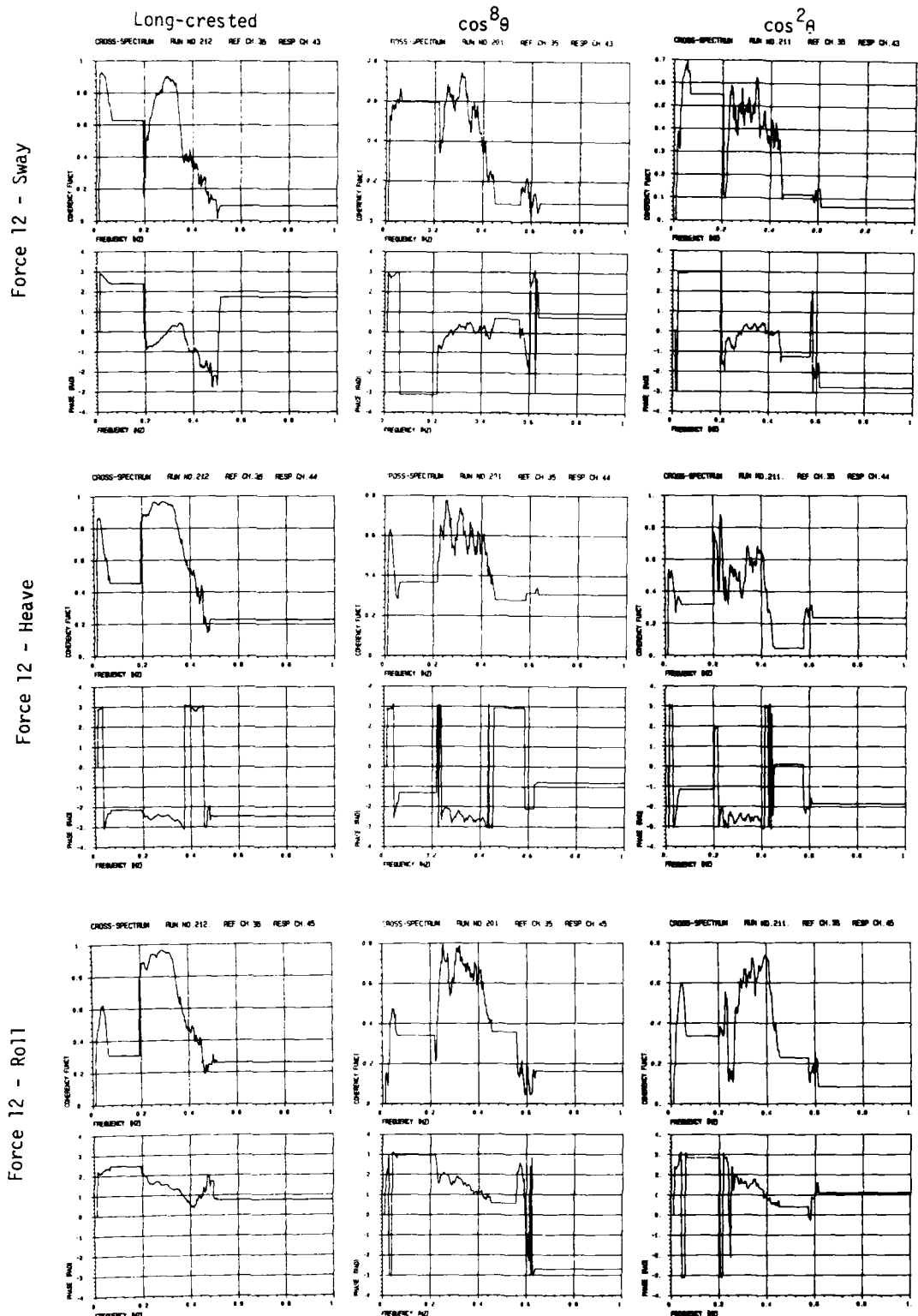


Fig. 3.61

COHERENCE-PHASE ANALYSIS FORCE - MOTION Fendered Model Input: JONSWAP $\cos^8 \theta$

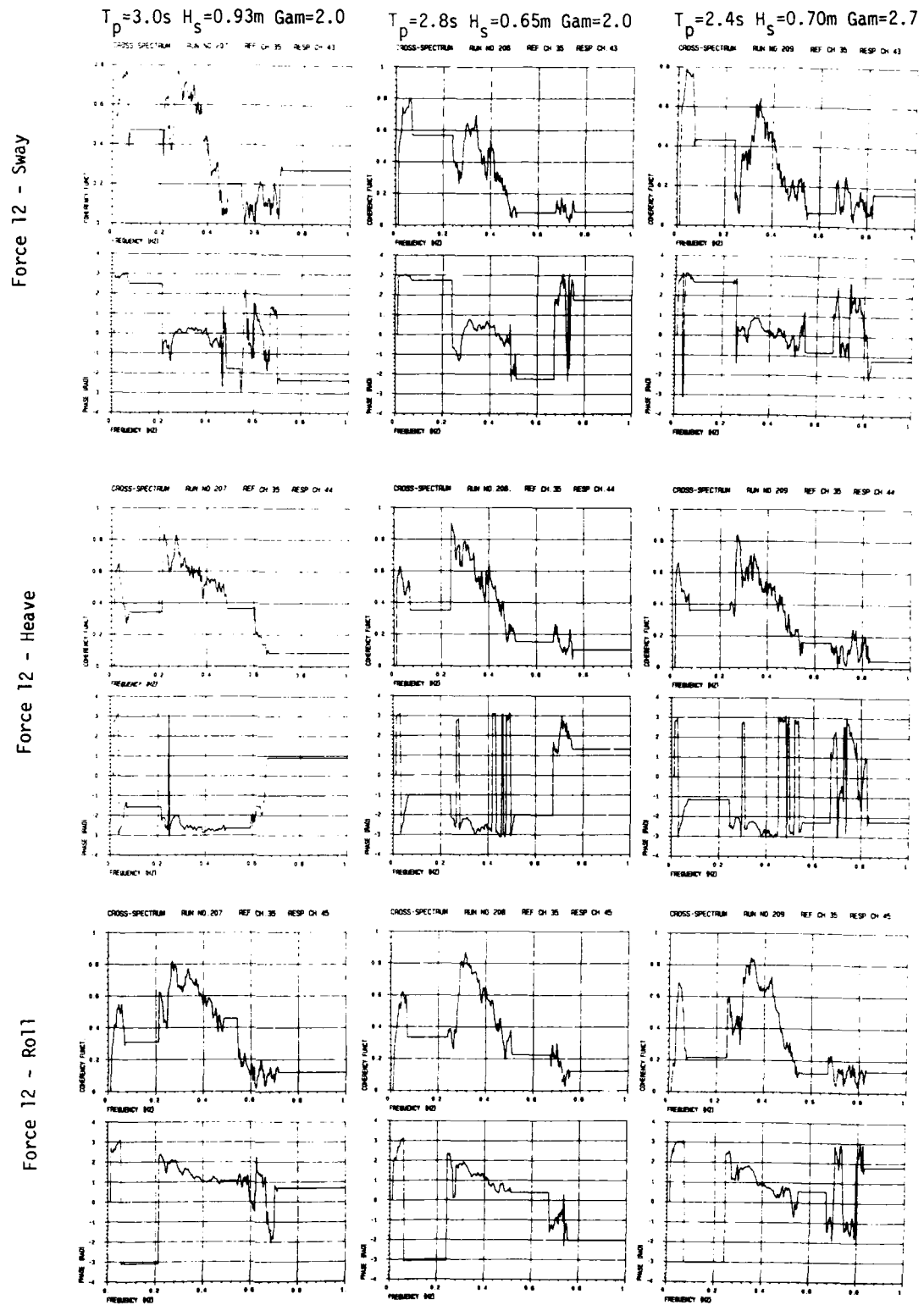


Fig. 3.62

COHERENCE-PHASE ANALYSIS FORCE - MOTION Fendered Model Input: JONSWAP $\cos^8 \theta$

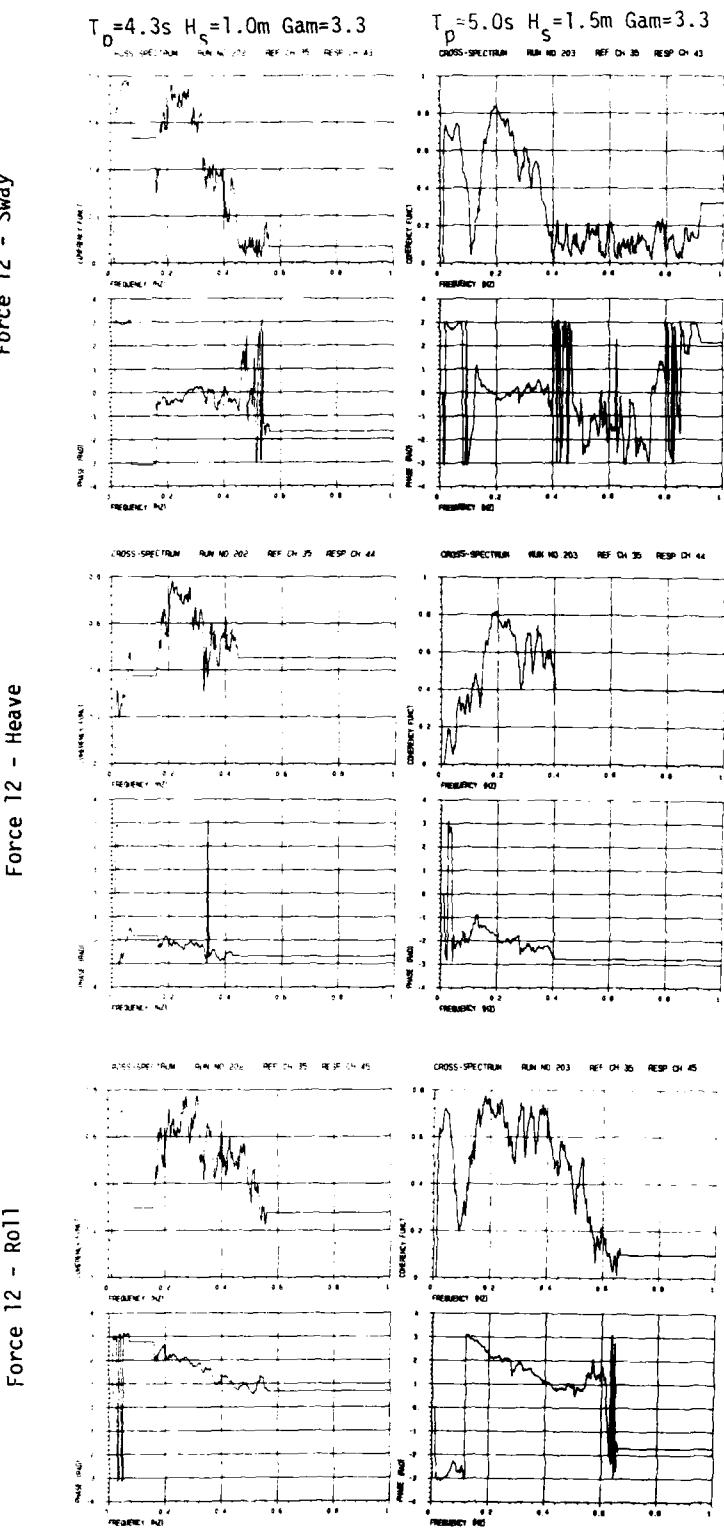


Fig. 3.63

3.1.4 Motions analysis

The following presentation of results for breakwater motions is quite similar to the previous presentation of force results.

First the 3 plots in figs. 3.64 - 3.66 show the maximum and RMS values for sway (y-position), heave (z-position) and roll motion, as a function of the input significant wave height $H_{mo,o}$. Next, 3 plots showing the maximum and RMS values, normalized by $H_{mo,o}$, as a function of the input peak wave period T_p , are presented (figs. 3.67 - 3.69). Then follow 9 pages (figs. 3.70 - 3.78) with plots of spectra, transfer functions and coherence/phase functions for sway, heave and roll, with wave staff 11 as a reference. Statistics of maxima (or in some cases: minima - see the coordinate system definition in fig. 2.18) of all 6 motions of pontoon 1 (surge-sway-heave-roll-pitch-yaw) are then presented and compared to Rayleigh curves (figs. 3.79 - 3.84). Coupling sway-heave, sway-roll and heave-roll is finally illustrated by coherence/phase plots in figs. 3.85 - 3.97.

MAXIMUM AND RMS VALUES vs INPUT SIGNIFICANT WAVE HEIGHT
 SWAY (Y-POSITION) PONTOON 1 FENDERED MODEL

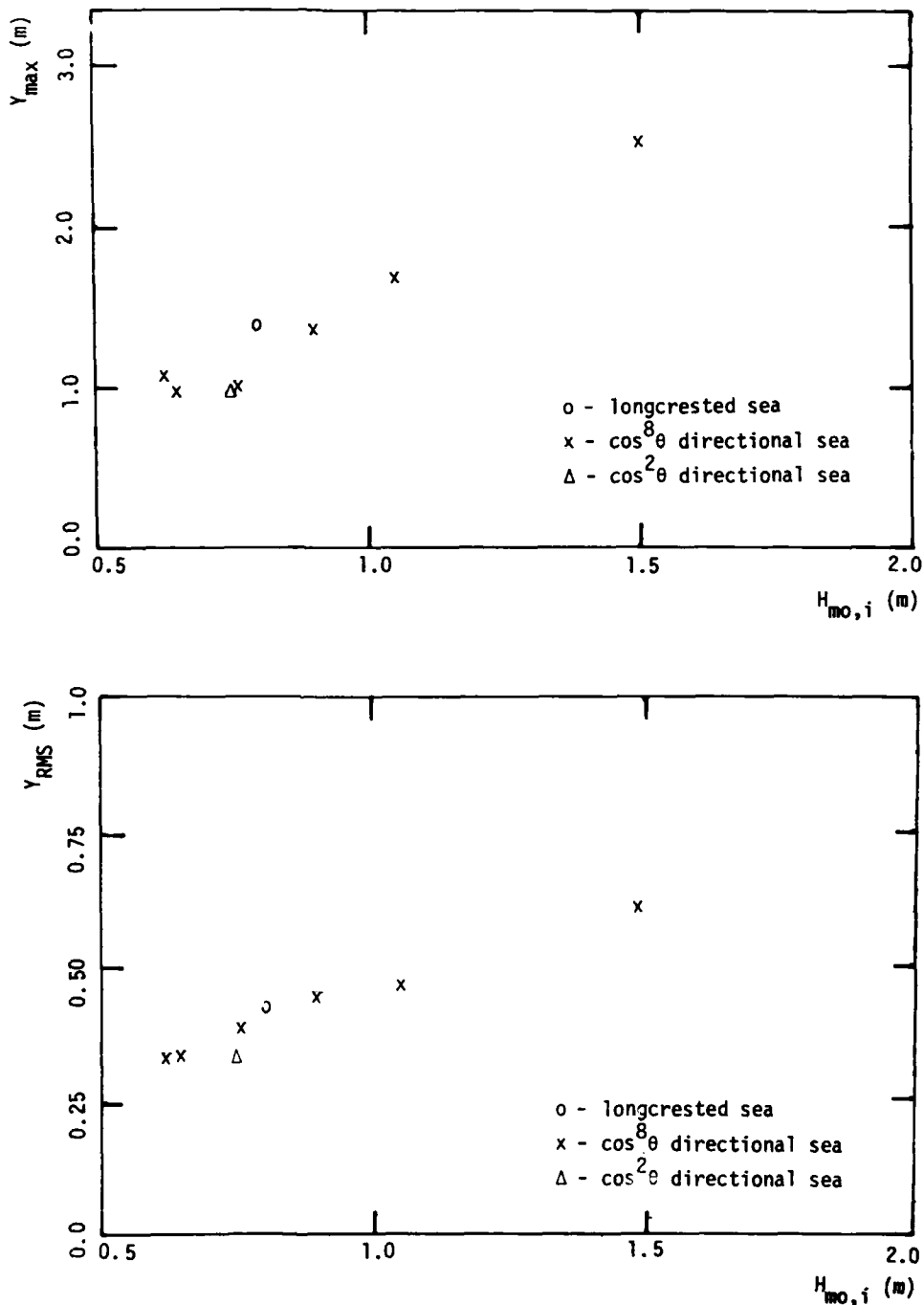


Fig. 3.64

MAXIMUM AND RMS VALUES vs INPUT SIGNIFICANT WAVE HEIGHT
 HEAVE (Z-POSITION) PONTOON 1 FENDERED MODEL

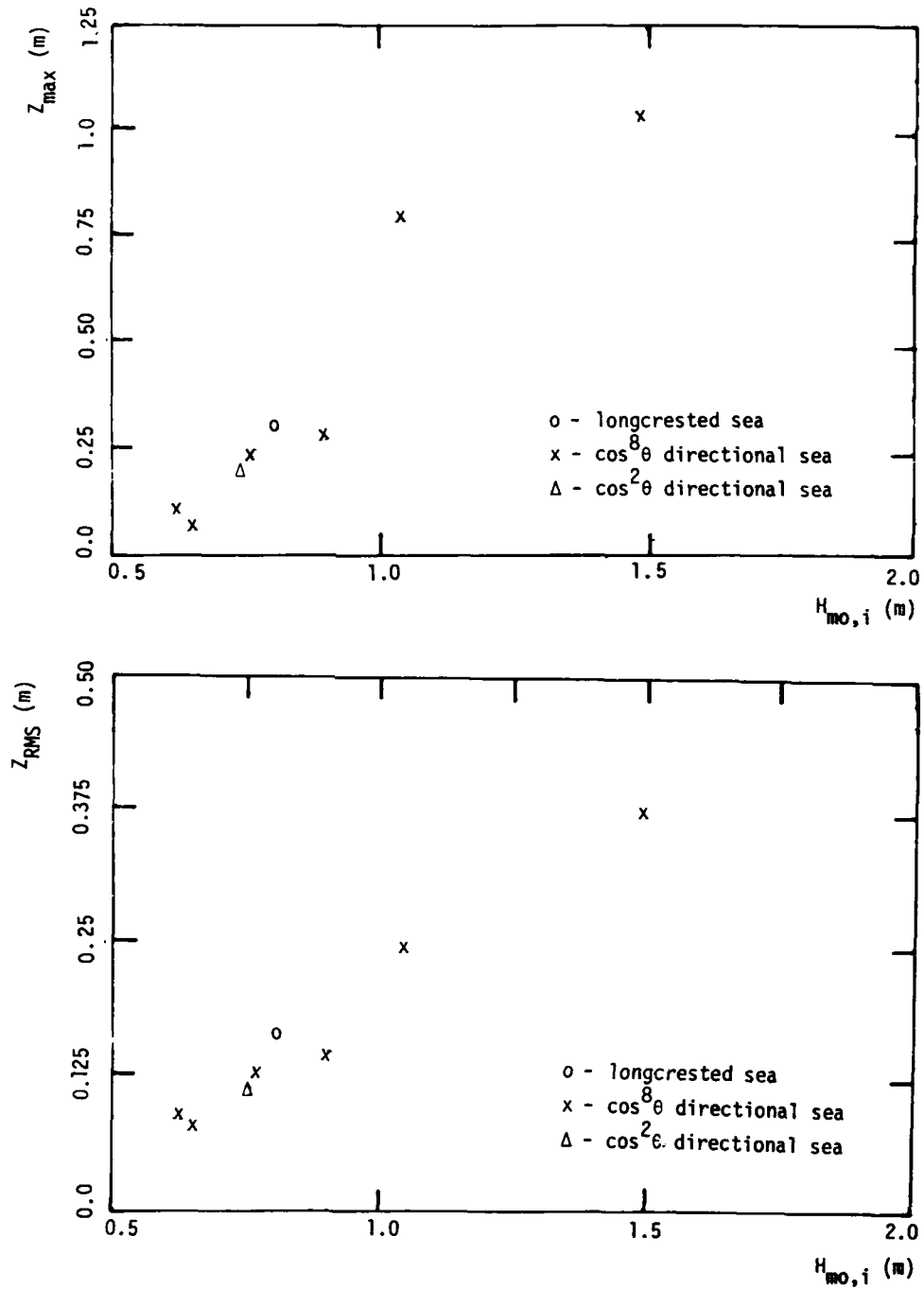


Fig. 3.65

MAXIMUM AND RMS VALUES VS INPUT SIGNIFICANT WAVE HEIGHT
 ROLL PONTOON 1 FENDERED MODEL

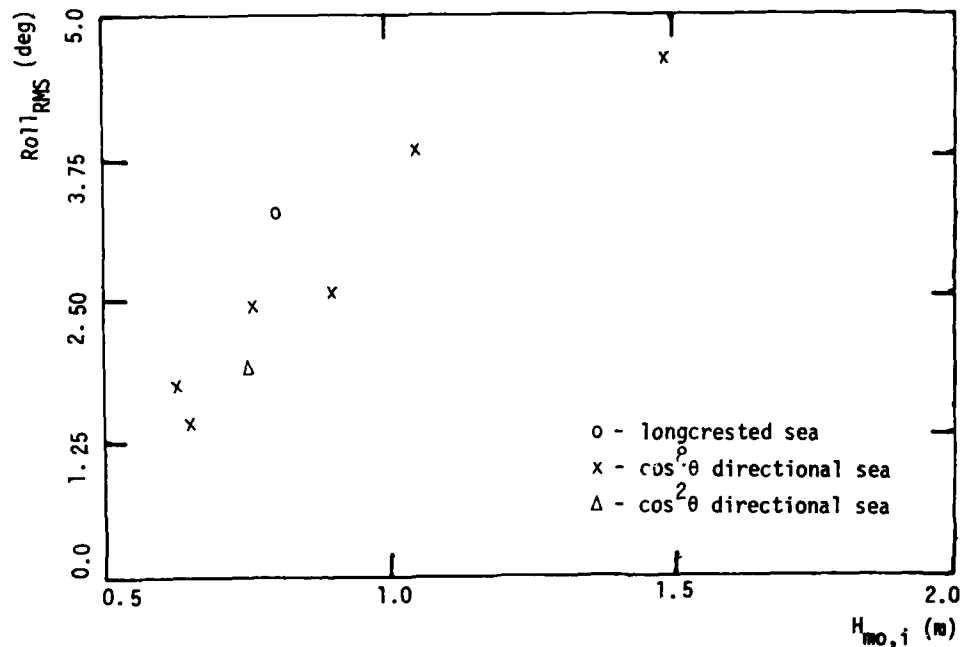
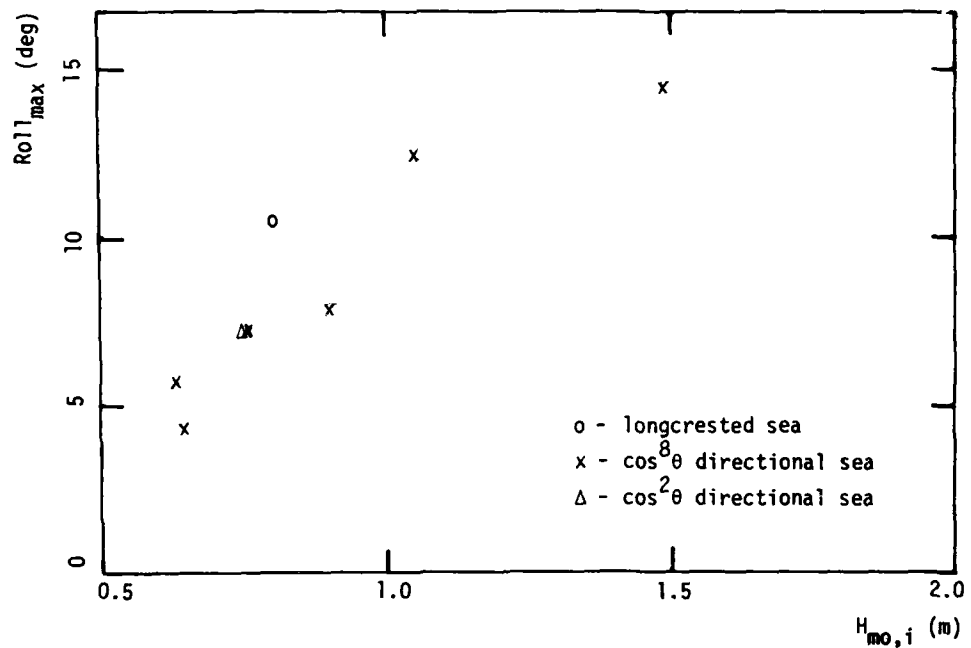


Fig. 3.66

NORMALIZED MAXIMUM AND RMS VALUES vs PEAK PERIOD OF INPUT WAVE
 SWAY (Y-POSITION) PONTOON 1 FENDERED MODEL

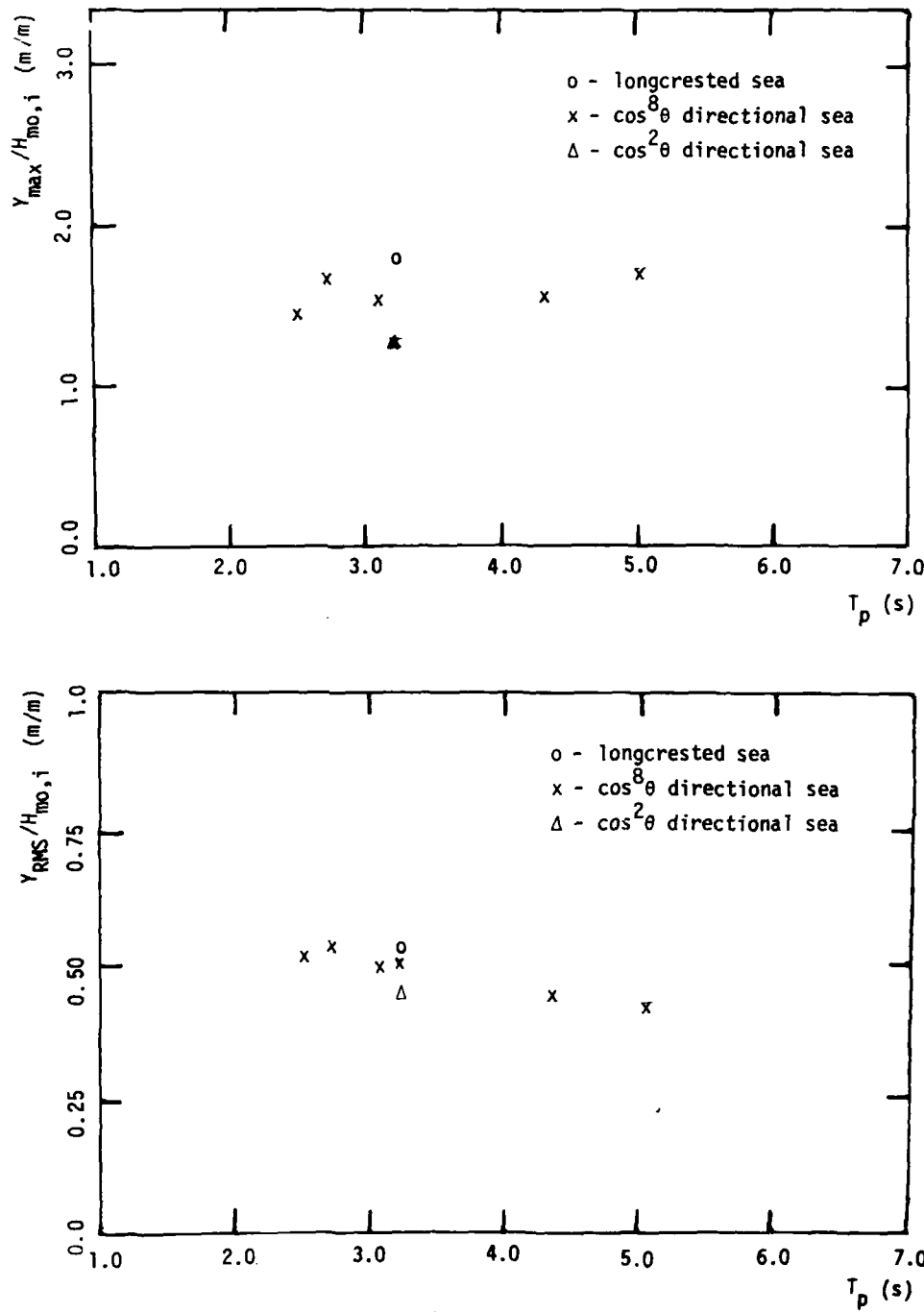


Fig. 3.67

NORMALIZED MAXIMUM AND RMS VALUES VS PEAK PERIOD OF INPUT WAVE
 HEAVE (Z-POSITION) PONTOON 1 FENDERED MODEL

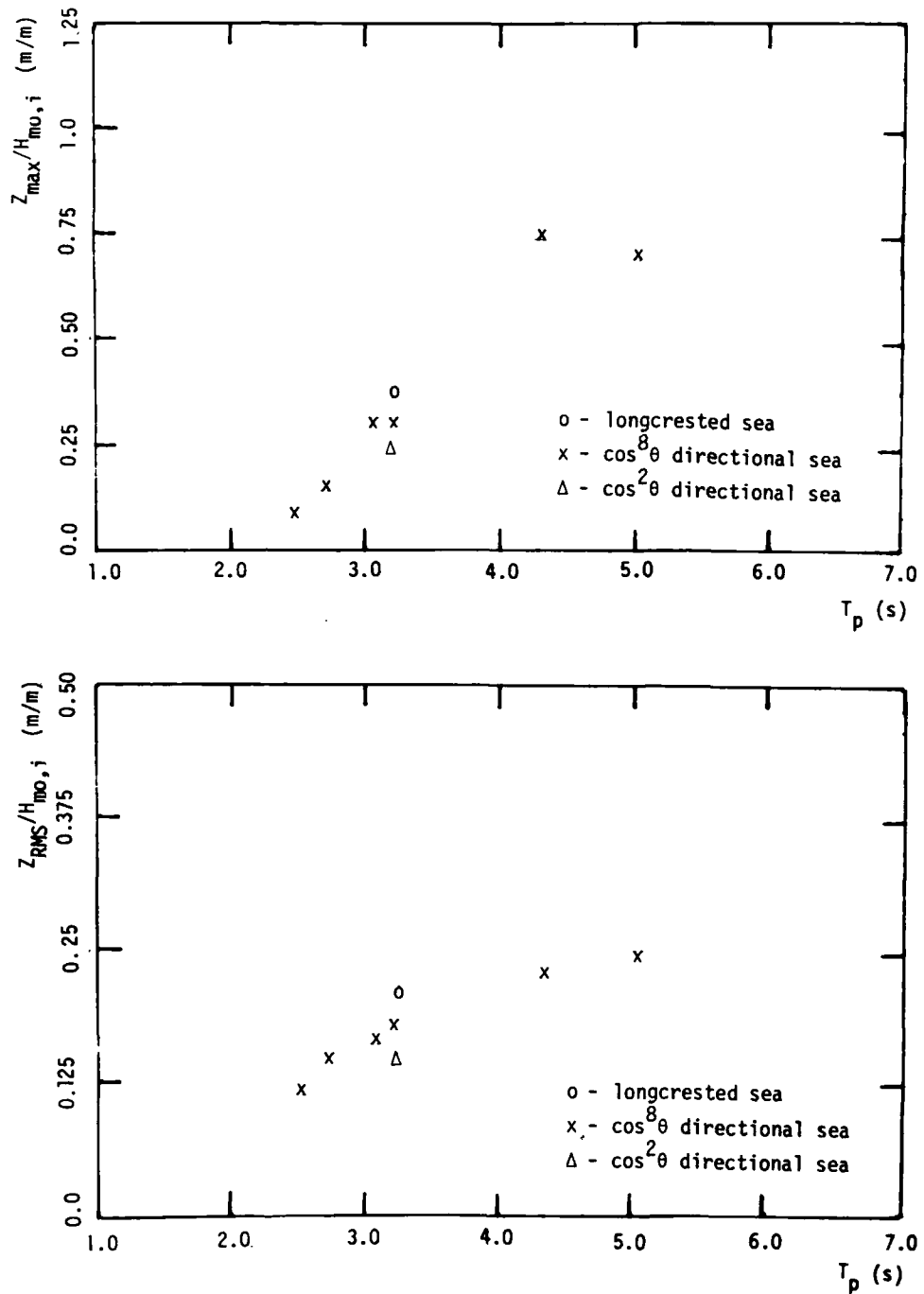


Fig. 3.68

NORMALIZED MAXIMUM AND RMS VALUES VS PEAK PERIOD OF INPUT WAVE
 ROLL PONTOON 1 FENDERED MODEL

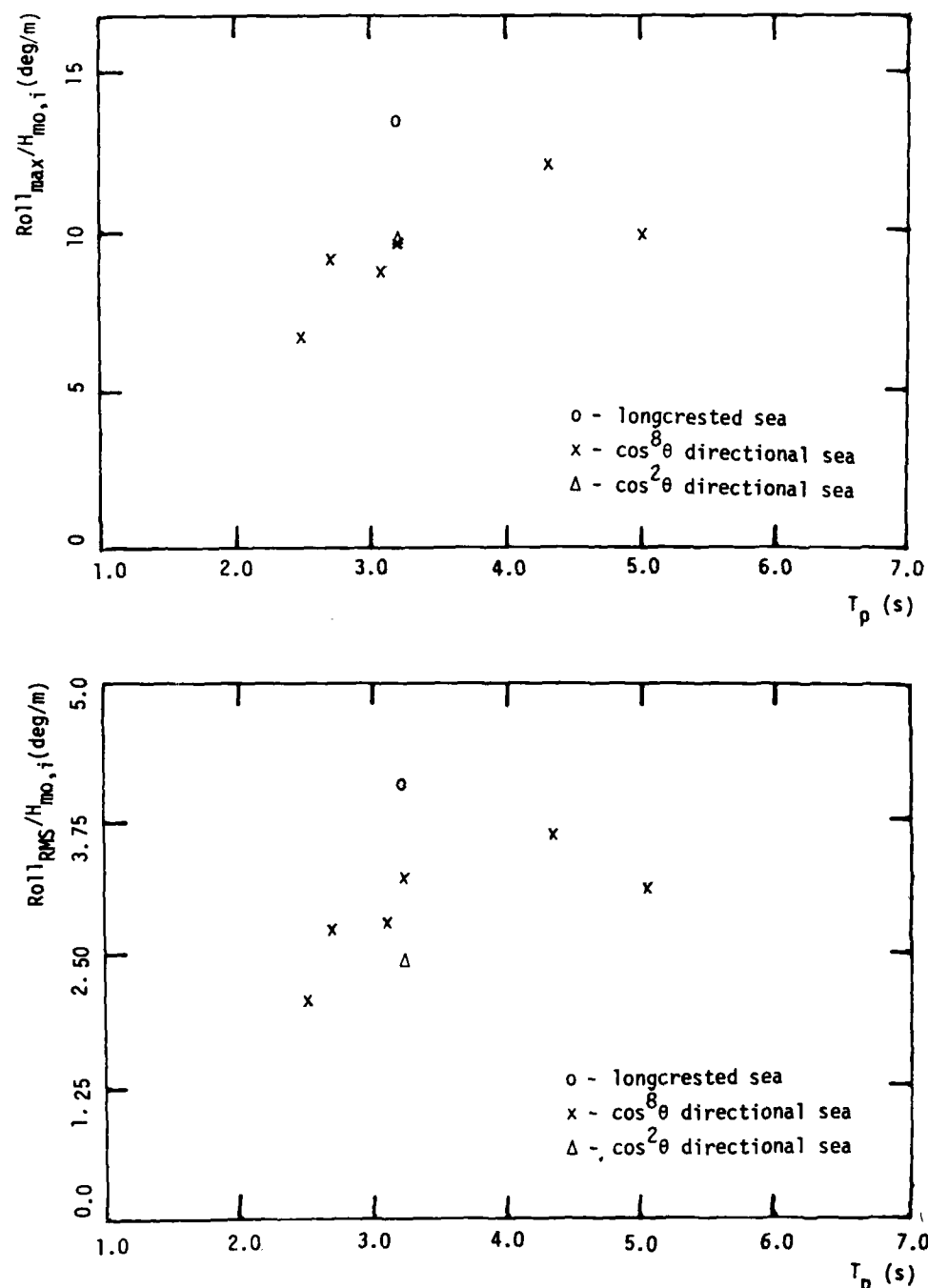


Fig. 3.69

SPECTRAL ANALYSIS SWAY (Y-POS) Fendered Model Pontoon 1 Input: JONSWAP $T_p = 3.2\text{s}$ $H_s = 0.75\text{m}$ $\text{Gam} = 3.$

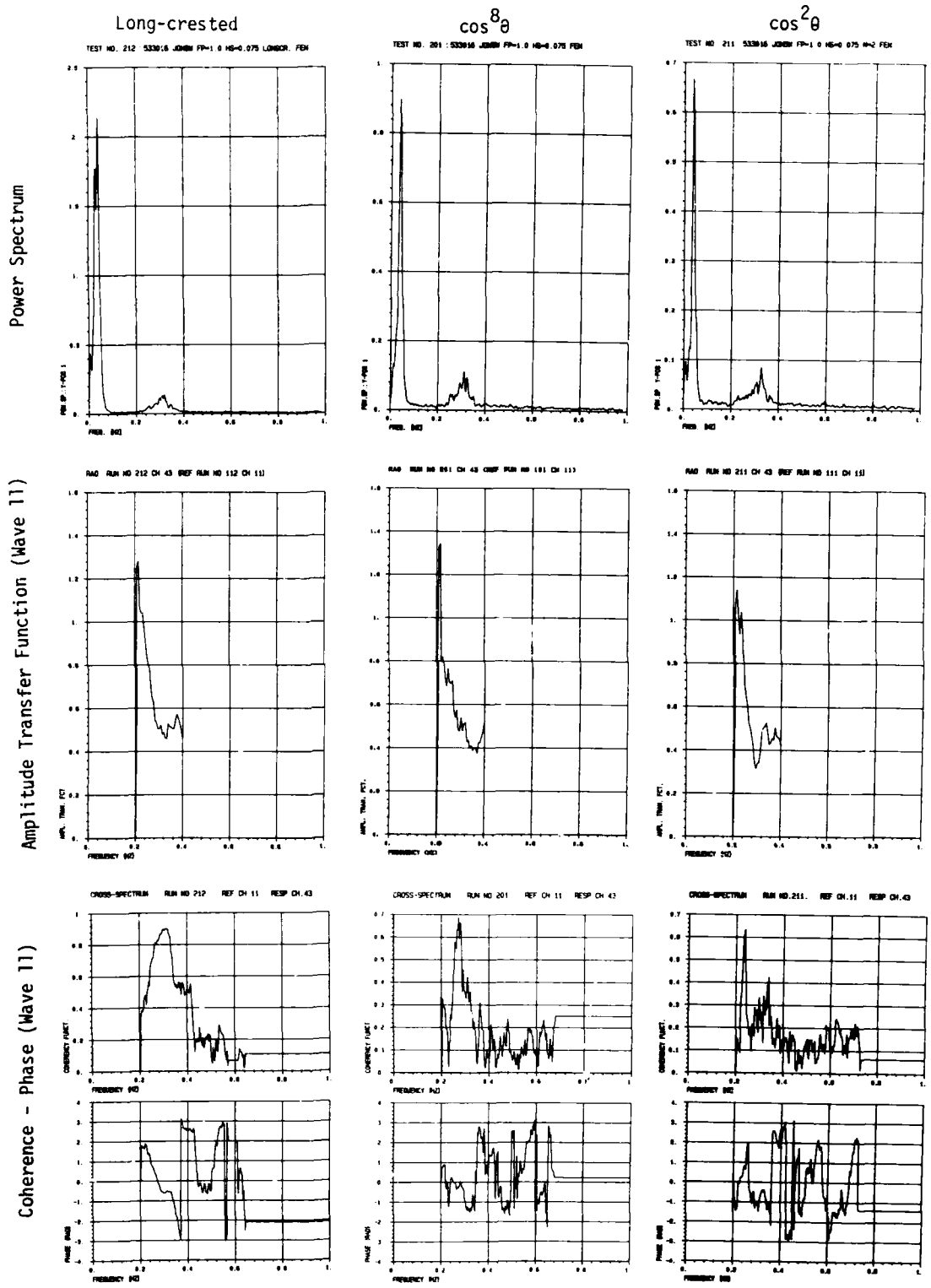


Fig. 3.70

SPECTRAL ANALYSIS SWAY (Y-POS) Fendered Model Pontoon 1 Input: JONSWAP $\cos^8 \theta$

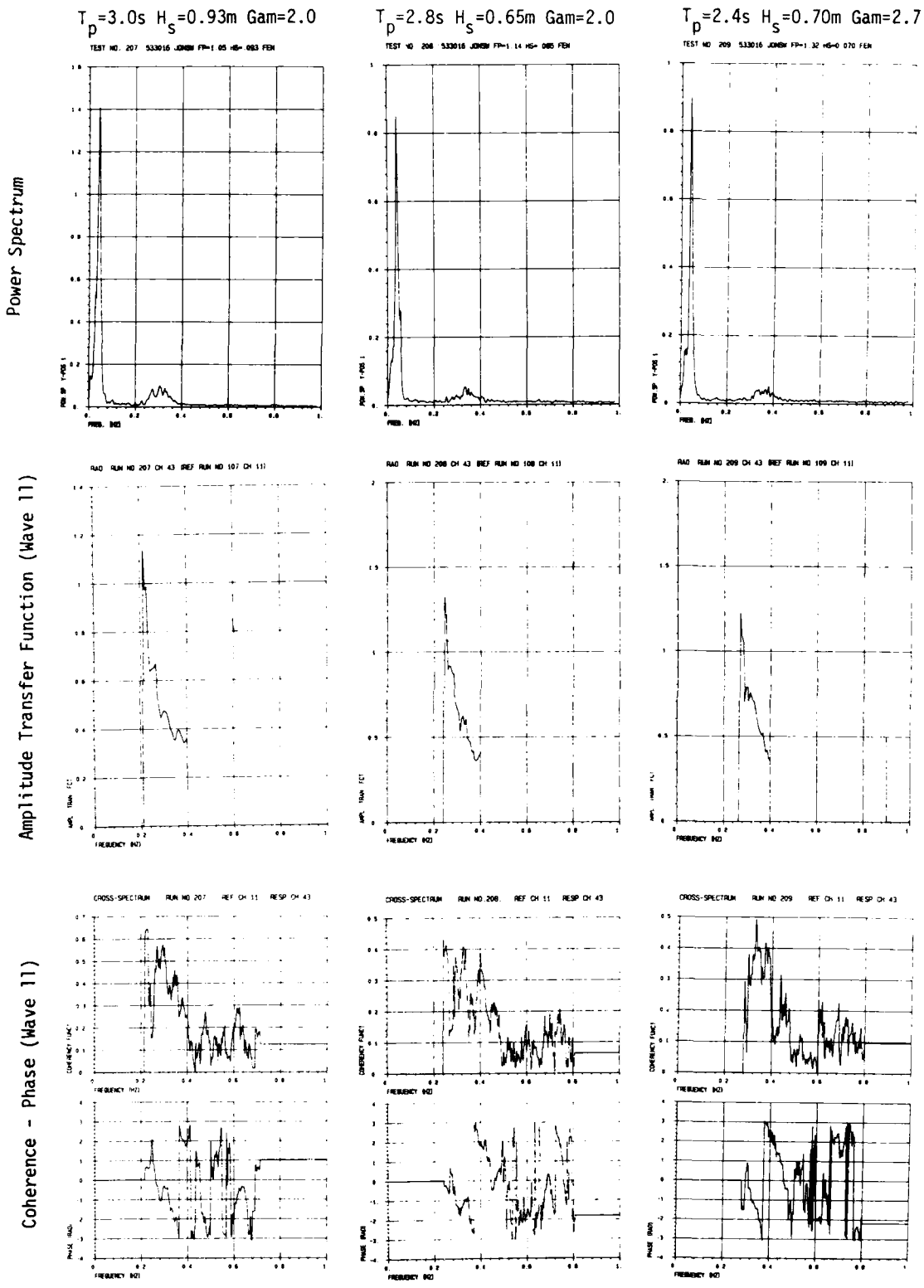


Fig. 3.71

SPECTRAL ANALYSIS SWAY (Y-POS) Fendered Model Pontoon 1 Input: JONSWAP $\cos^8 \theta$

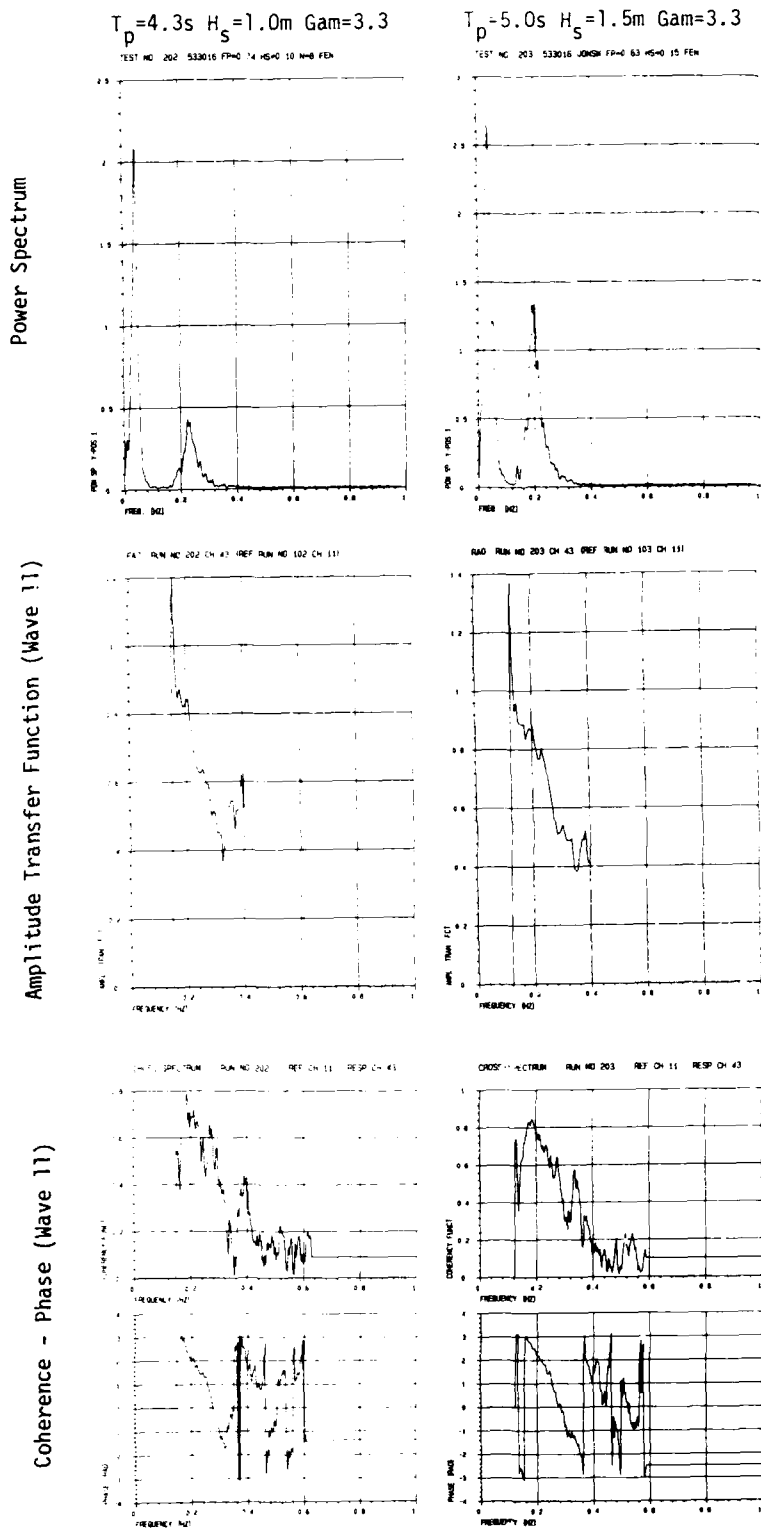


Fig. 3.72

45-4204 145

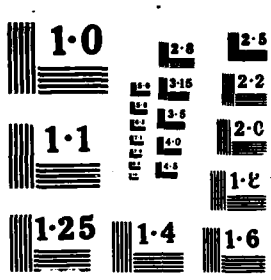
MODEL TESTS ON THE CERC FULL SCALE TEST FLOATING
BREAKWATER(U) MARINTEX TRONDHEIM (NORWAY)
A TORUM ET AL. JUN 87 DAJA45-86-C-0035

2/3

UNCLASSIFIED

F/G 13/2

MJ



SPECTRAL ANALYSIS HEAVE (Z-POS) Fendered Model Pontoon 1 Input: JONSWAP $T_p=3.2s$ $H_s=0.75m$ $Gam=3.0$

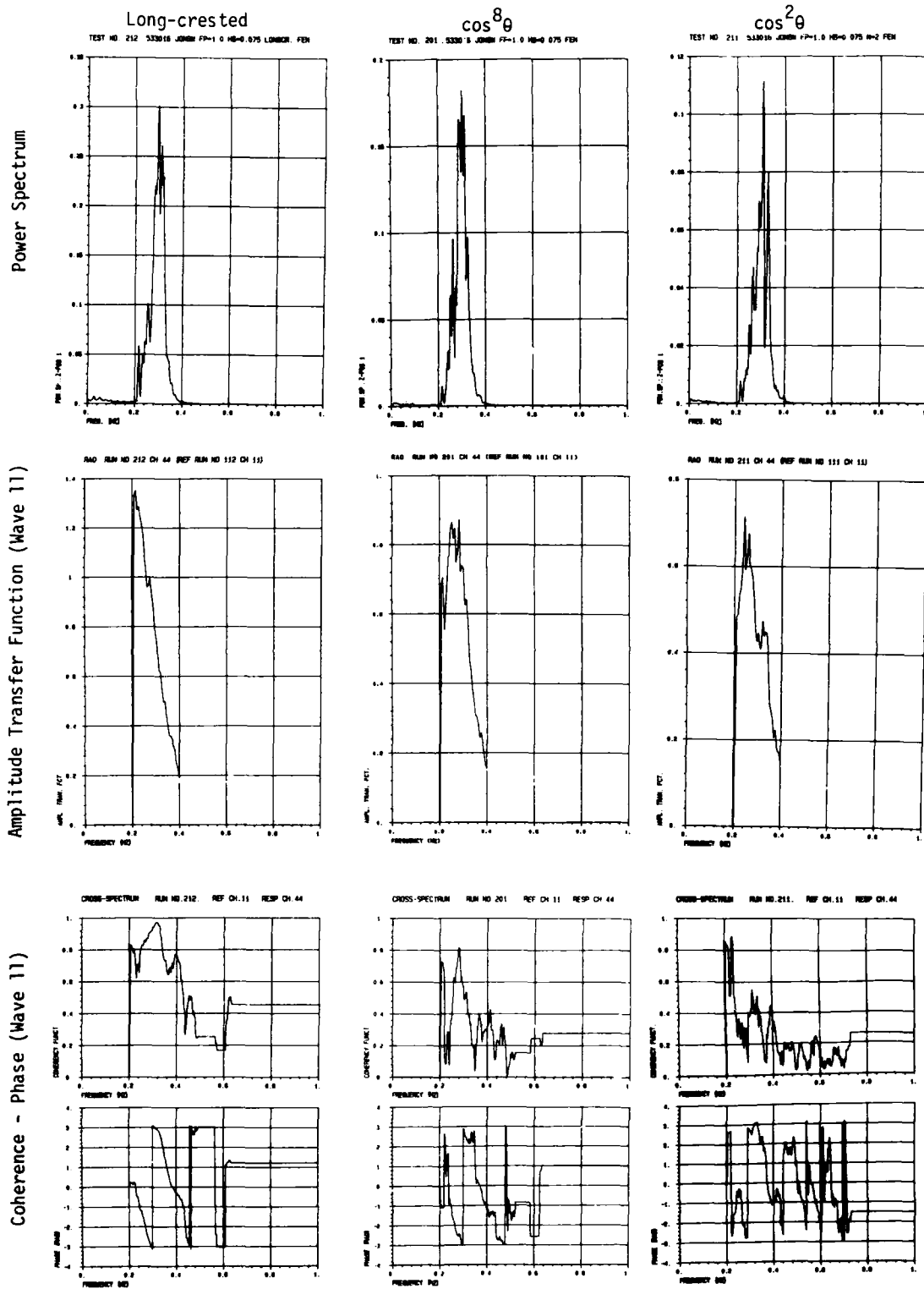
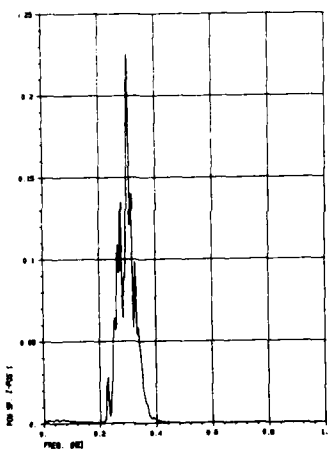


Fig. 3.73

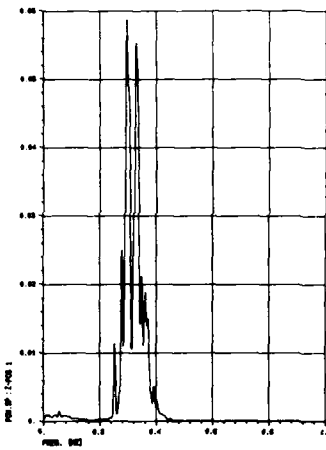
SPECTRAL ANALYSIS HEAVE (Z-POS) Fendered Model Pontoon 1

Input: JONSWAP $\cos^8 \theta$

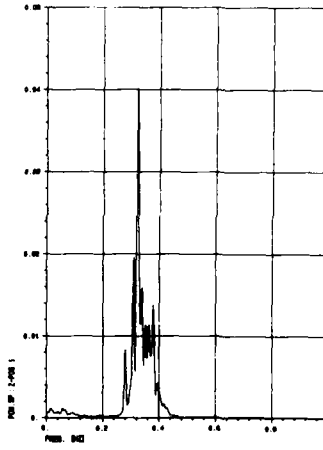
$T_p = 3.0\text{s}$ $H_s = 0.93\text{m}$ $\text{Gam} = 2.0$
TEST NO. 207 533016 JONSWP FP=1.05 HS=0.93 FDN



$T_p = 2.8\text{s}$ $H_s = 0.65\text{m}$ $\text{Gam} = 2.0$
TEST NO. 208 533016 JONSWP FP=1.14 HS=0.65 FDN



$T_p = 2.4\text{s}$ $H_s = 0.70\text{m}$ $\text{Gam} = 2.7$
TEST NO. 209 533016 JONSWP FP=1.32 HS=0.70 FDN



Power Spectrum

Amplitude Transfer Function (Wave 11)

Coherence - Phase (Wave 11)

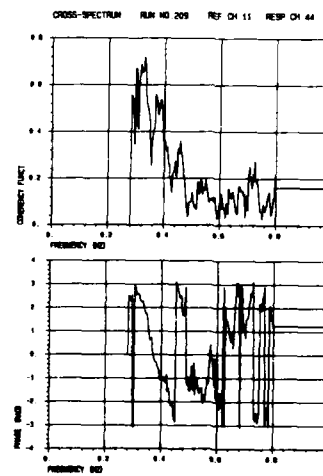
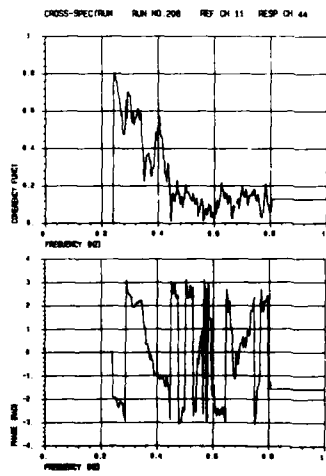
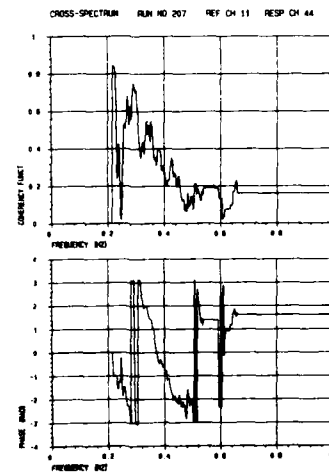
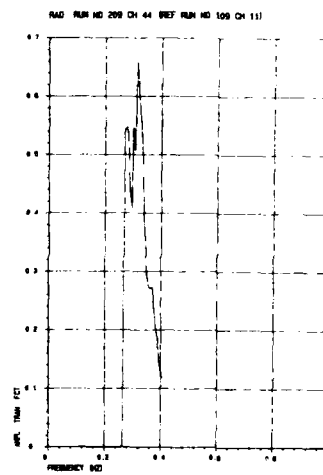
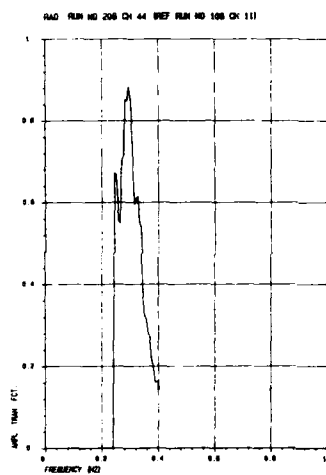
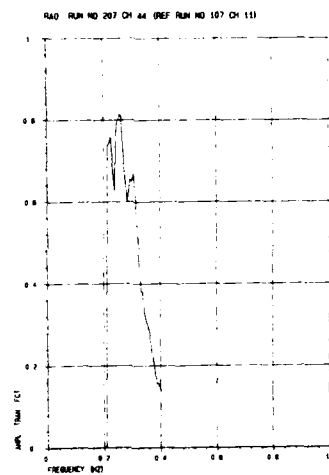
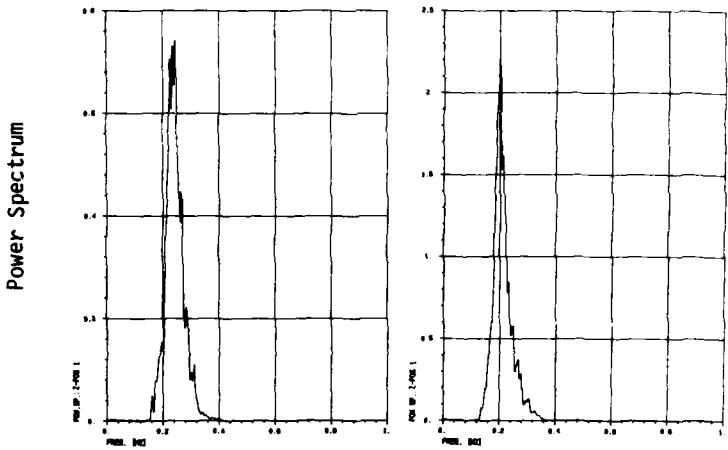


Fig. 3.74

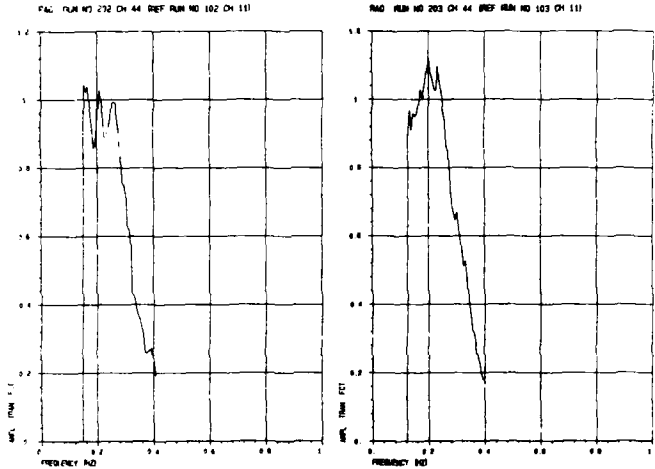
SPECTRAL ANALYSIS HEAVE (Z-POS) Fendered Model Pontoon 1 Input: JONSWAP $\cos^8 \theta$

$T_p = 4.3\text{s}$ $H_s = 1.0\text{m}$ $\text{Gam} = 3.3$
TEST NO. 202 533016 PWD 74 HS=0.10 MWS FEN

$T_p = 5.0\text{s}$ $H_s = 1.5\text{m}$ $\text{Gam} = 3.3$
TEST NO. 203 533016 JONSW HS=0.15 MWS FEN



Amplitude Transfer Function (Wave 11)



Coherence - Phase (Wave 11)

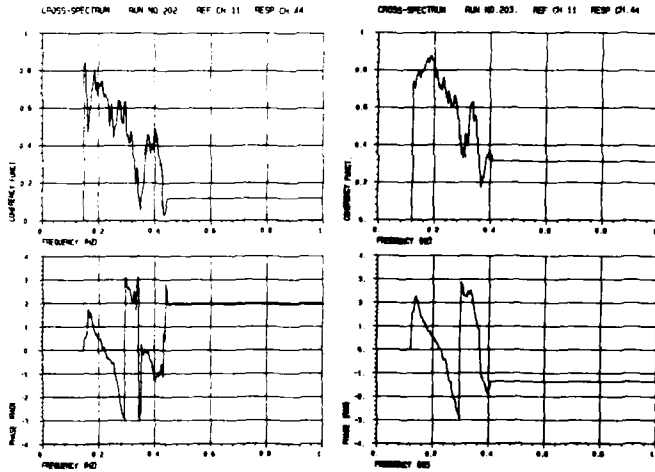


Fig. 3.75

SPECTRAL ANALYSIS ROLL Fendered Model Pontoon 1 Input: JONSWAP $T_p = 3.2\text{s}$ $H_s = 0.75\text{m}$ $\text{Gam} = 3.3$

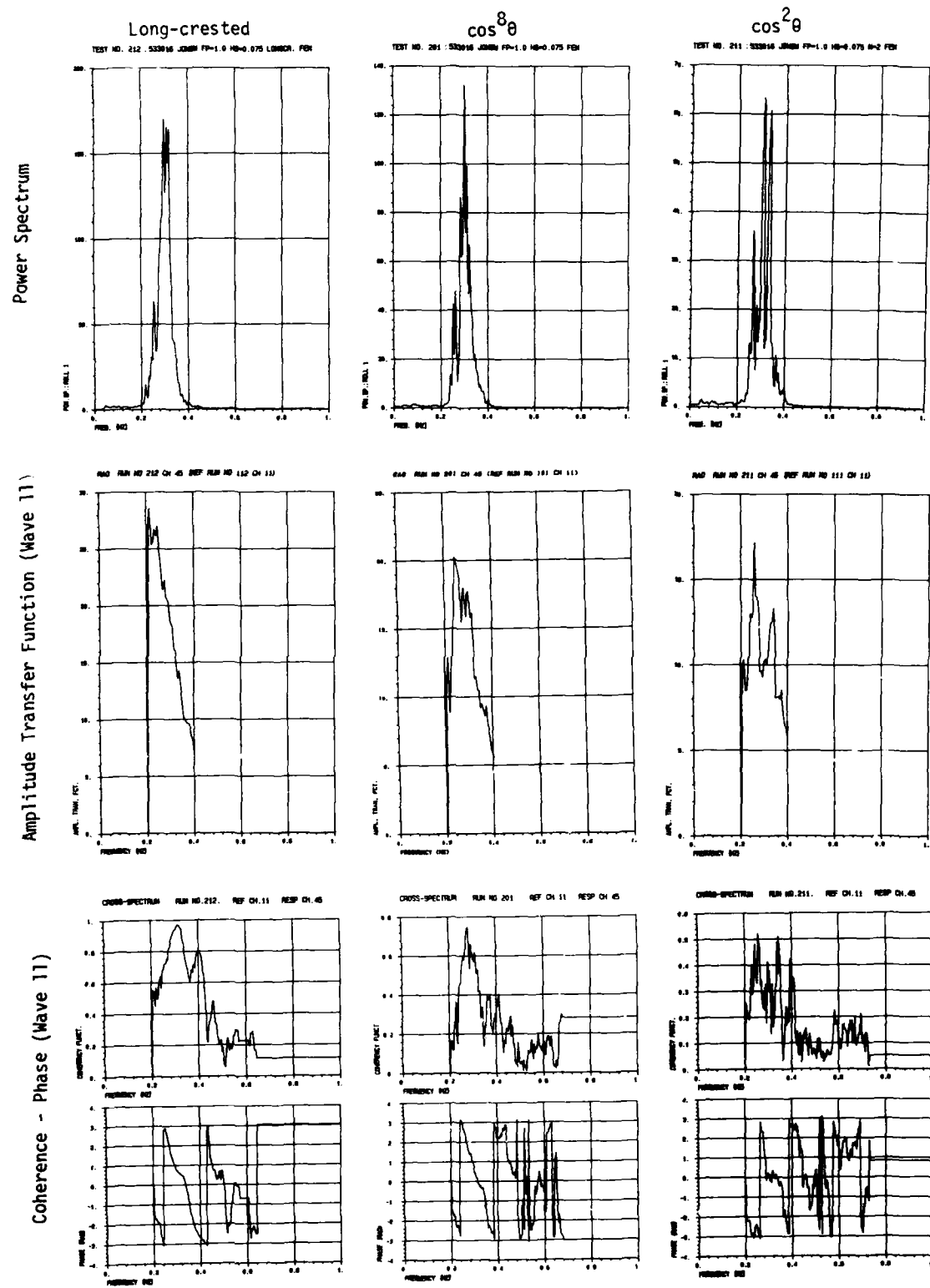


Fig. 3.76

SPECTRAL ANALYSIS ROLL Fendered Model Pontoon 1 Input: JONSWAP $\cos^8 \theta$

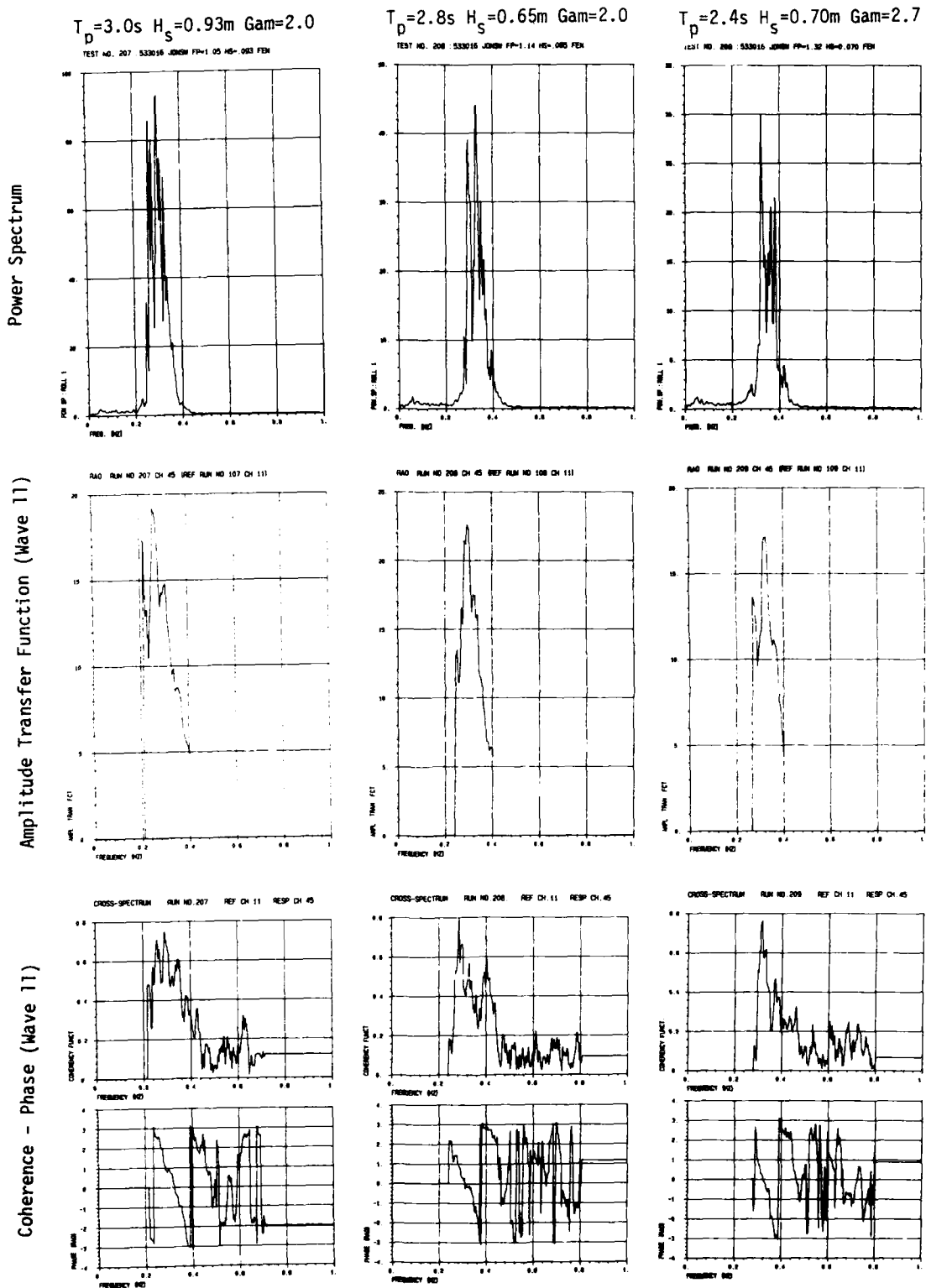


Fig. 3.77

SPECTRAL ANALYSIS ROLL Fendered Model Pontoon 1 Input: JONSWAP $\cos^8 \theta$

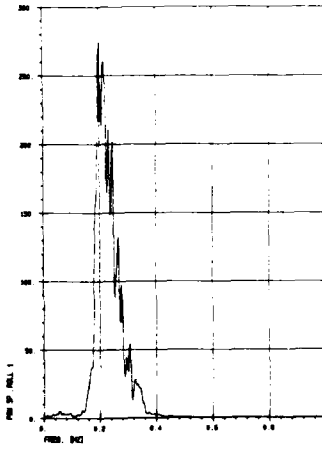
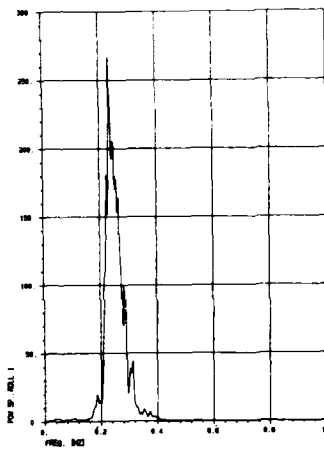
$T_p = 4.3\text{s}$ $H_s = 1.0\text{m}$ $\text{Gam} = 3.3$

TEST NO. 202 533016 FP=0.74 HS=0.10 MMF FEN

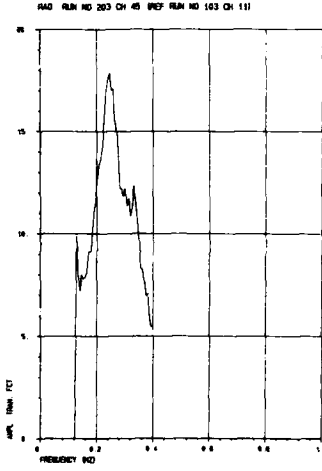
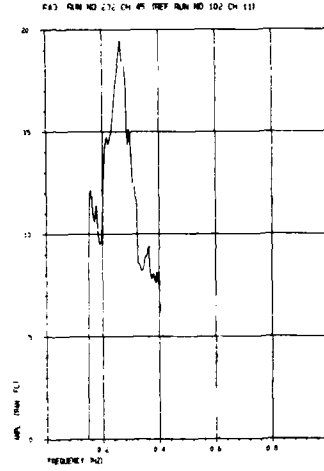
$T_p = 5.0\text{s}$ $H_s = 1.5\text{m}$ $\text{Gam} = 3.3$

TEST NO. 203 533016 JONSWP FP=0.63 HS=0.15 MMF

Power Spectrum



Amplitude Transfer Function (Wave 11)



Coherence - Phase (Wave 11)

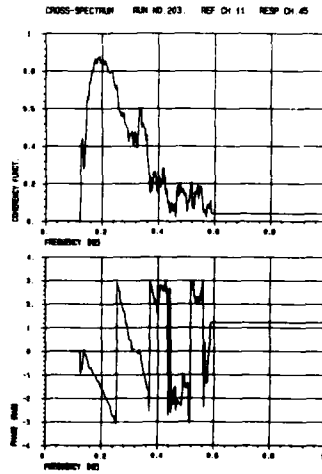
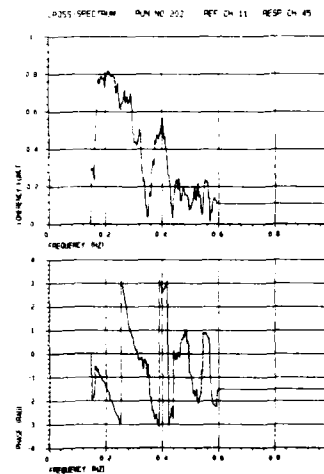


Fig. 3.78

AMPLITUDE STATISTICS MOTION Fendered Model Pontoon 1 Input: JONSWAP $T_p = 3.2\text{s}$ $H_s = 0.75\text{m}$ $\text{Gam} = 3.3$

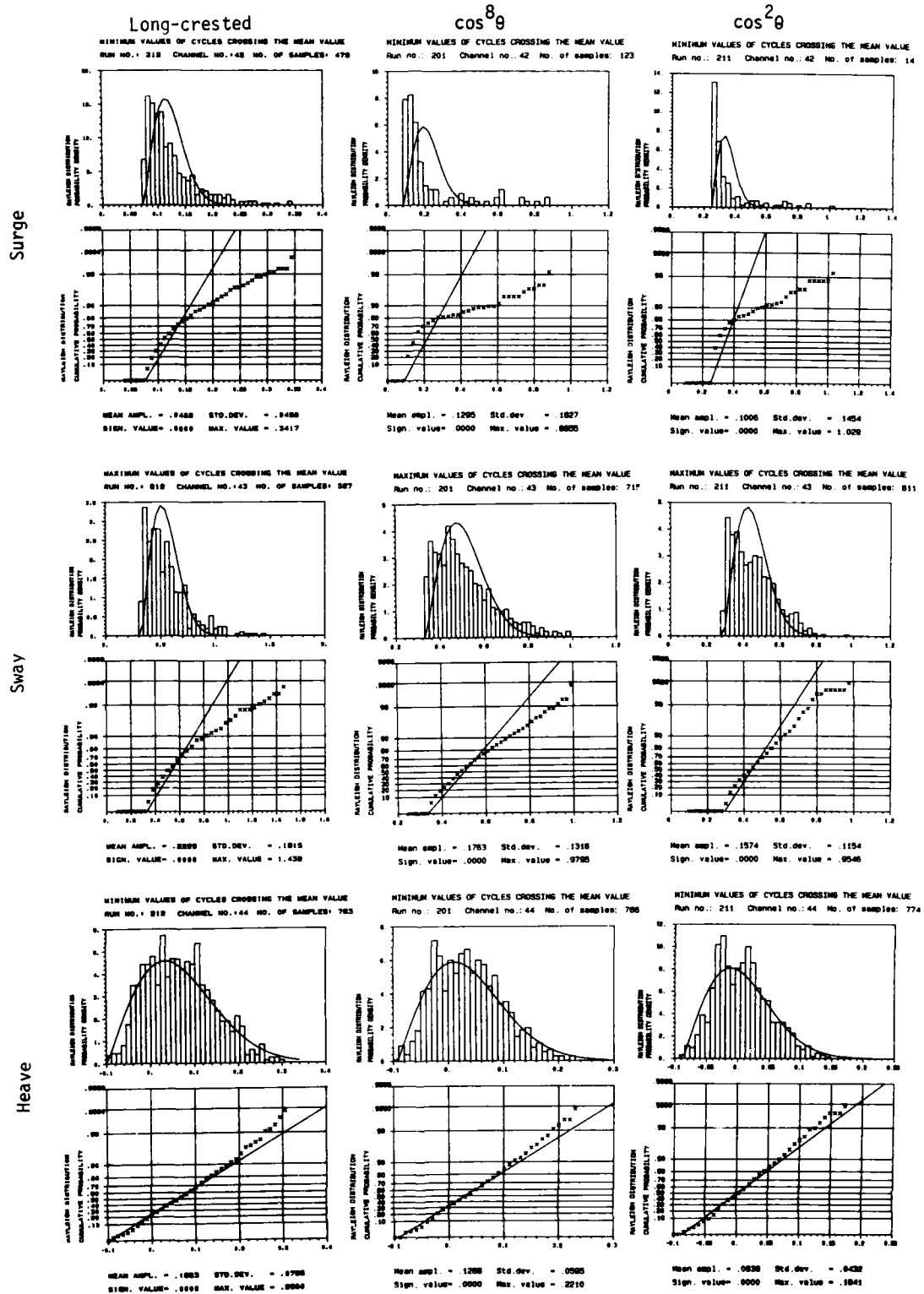


Fig. 3.79

AMPLITUDE STATISTICS MOTION Fendered Model Pontoon 1 Input: JONSWAP $\cos^8 \theta$

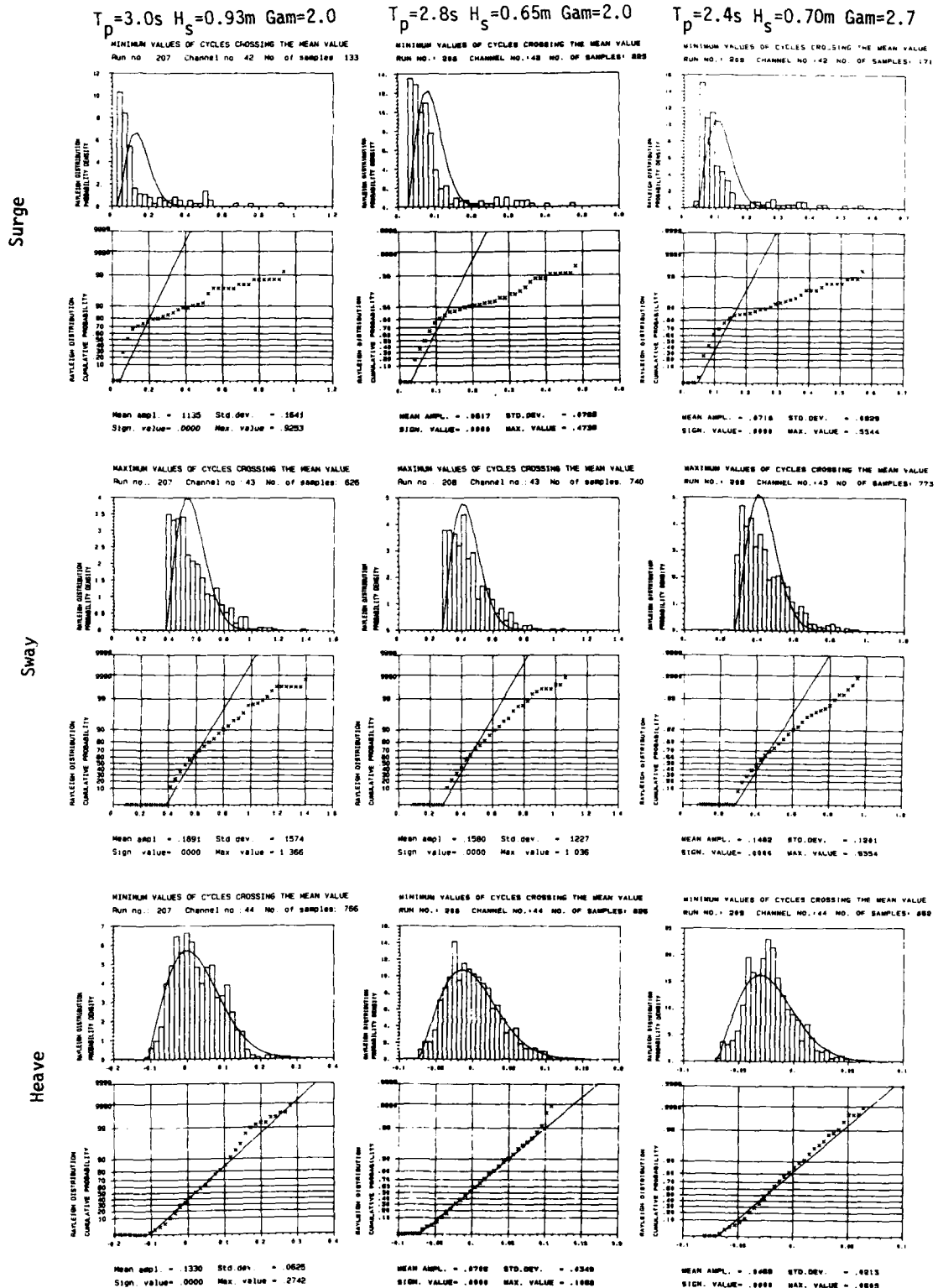


Fig. 3.80

AMPLITUDE STATISTICS MOTION Fendered Model Pontoon 1 Input: JONSWAP $\cos \theta$

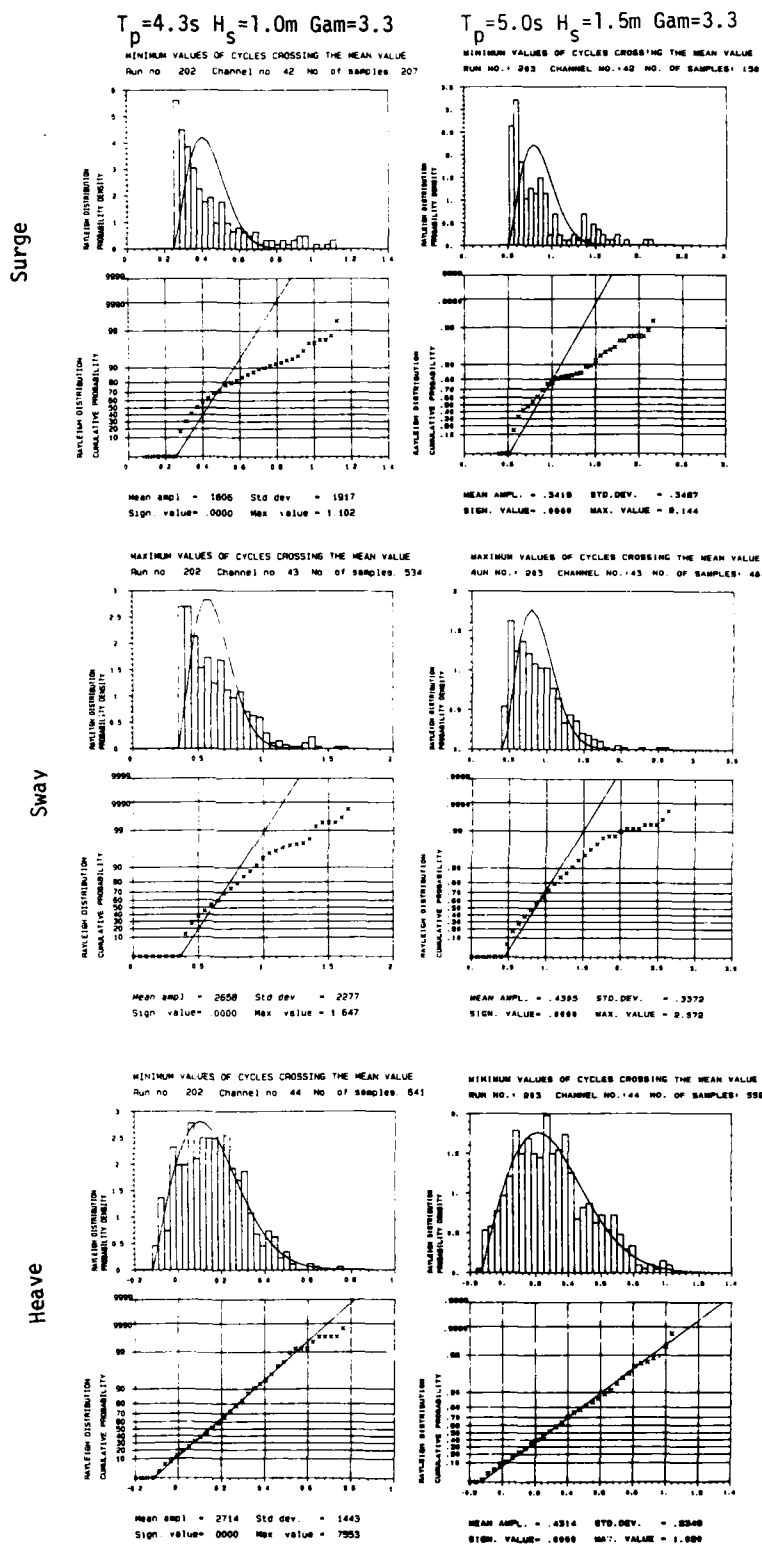


Fig. 3.81

AMPLITUDE STATISTICS MOTION Fendered Model Pontoon 1 Input: JONSWAP $T_p = 3.2\text{ s}$ $H_s = 0.75\text{ m}$ $\text{Gam} = 3.3$

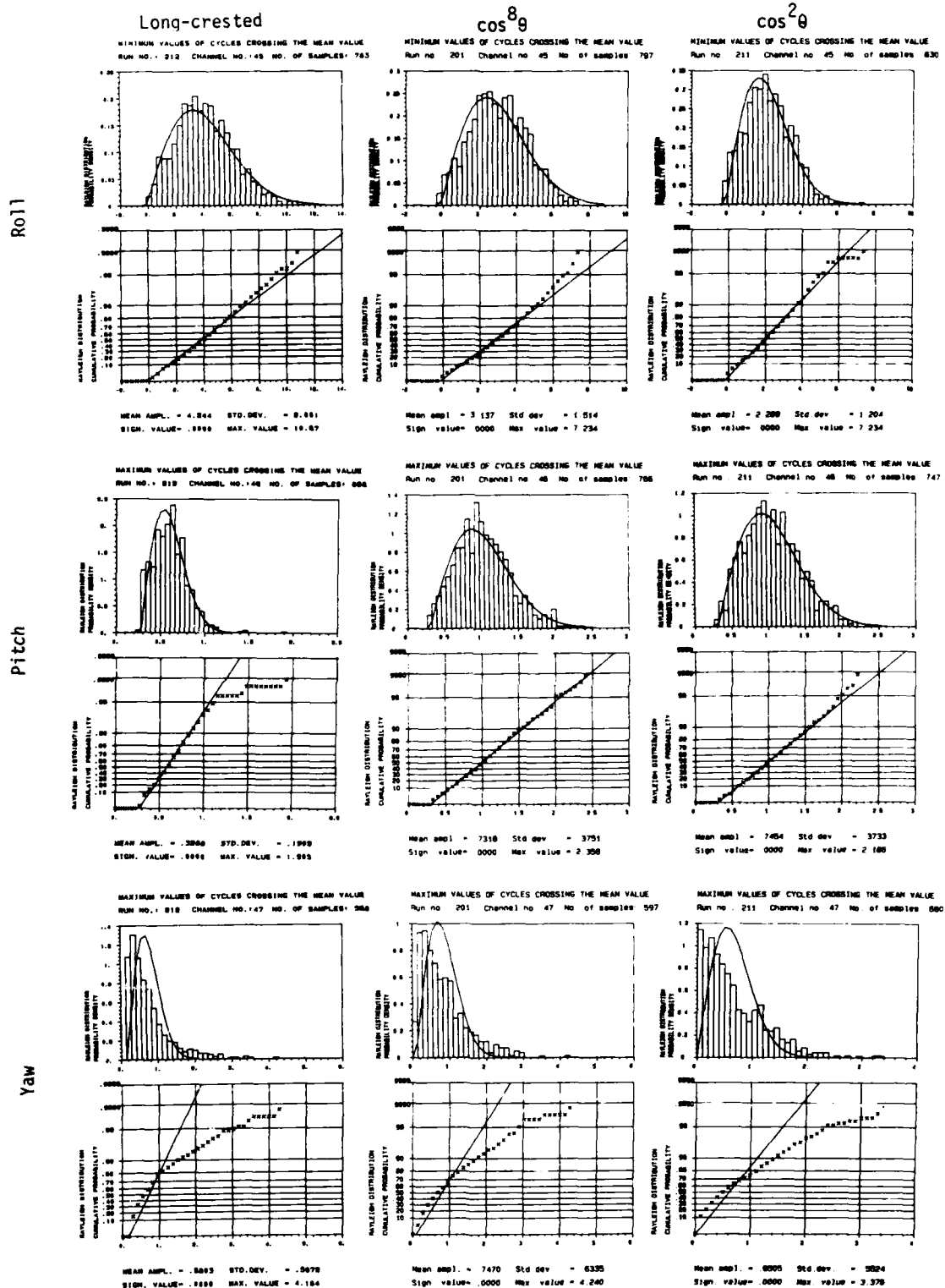


Fig. 3.82

AMPLITUDE STATISTICS MOTION Fendered Model Pontoon 1 Input: JONSWAP $\cos^8 \theta$

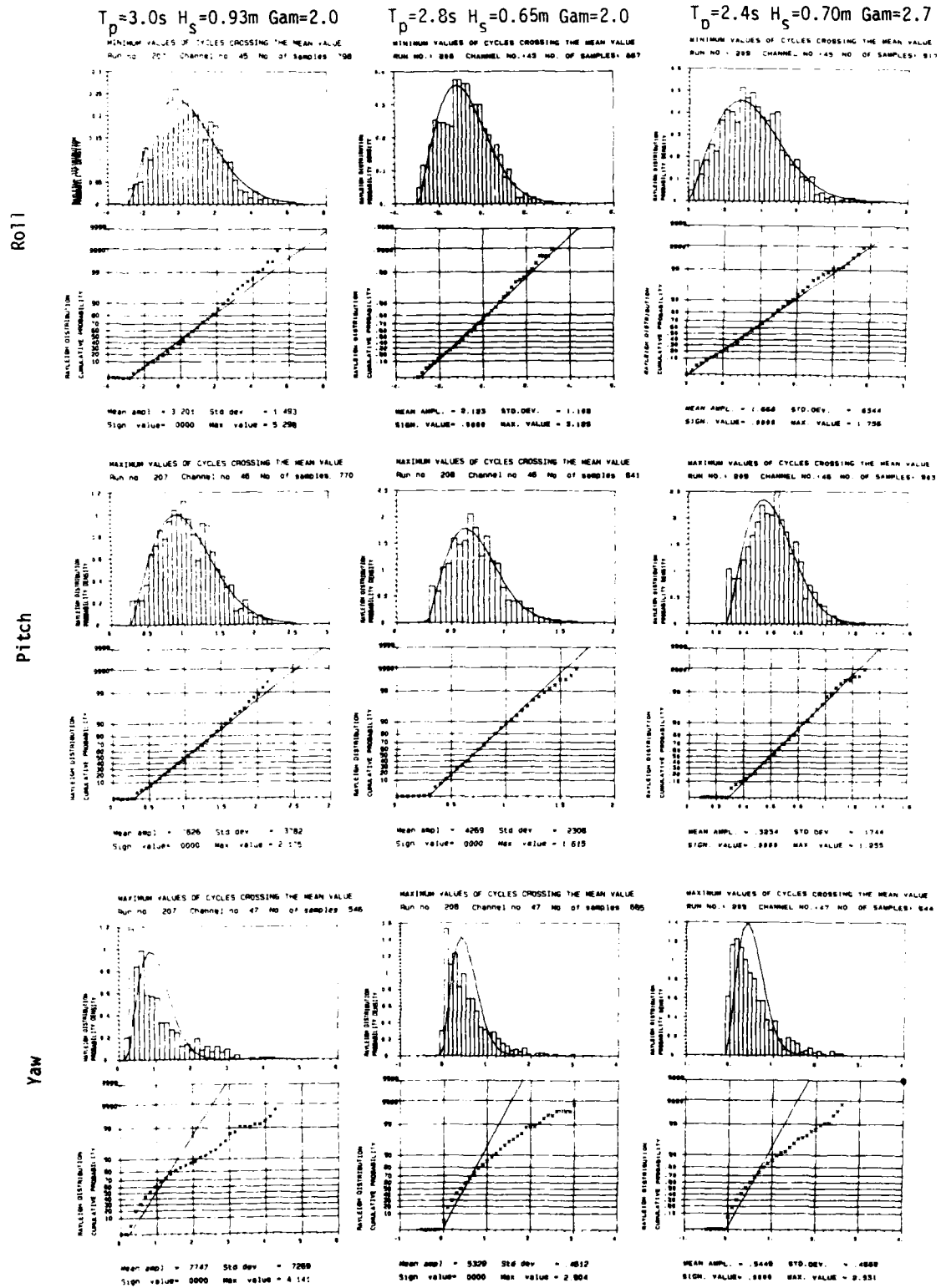


Fig. 3.83

AMPLITUDE STATISTICS MOTION Fendered Model Pontoon 1 Input: JONSWAP $\cos^8 \theta$

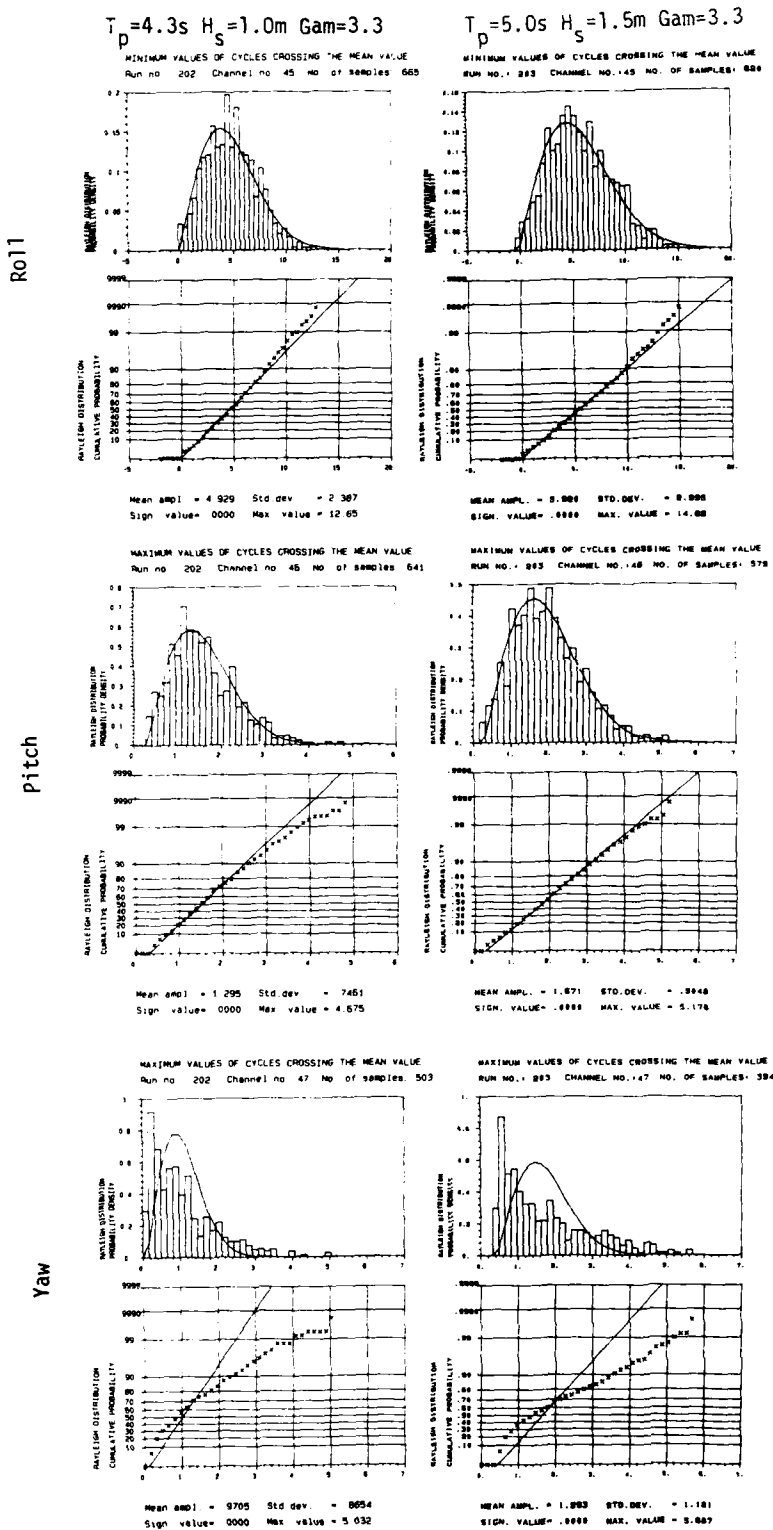


Fig. 3.84

COHERENCE-PHASE ANALYSIS MOTION-MOTION Fendered Model Input: JONSWAP $T_p = 3.2s$ $H_s = 0.75m$ $\text{Gam} = 3..$

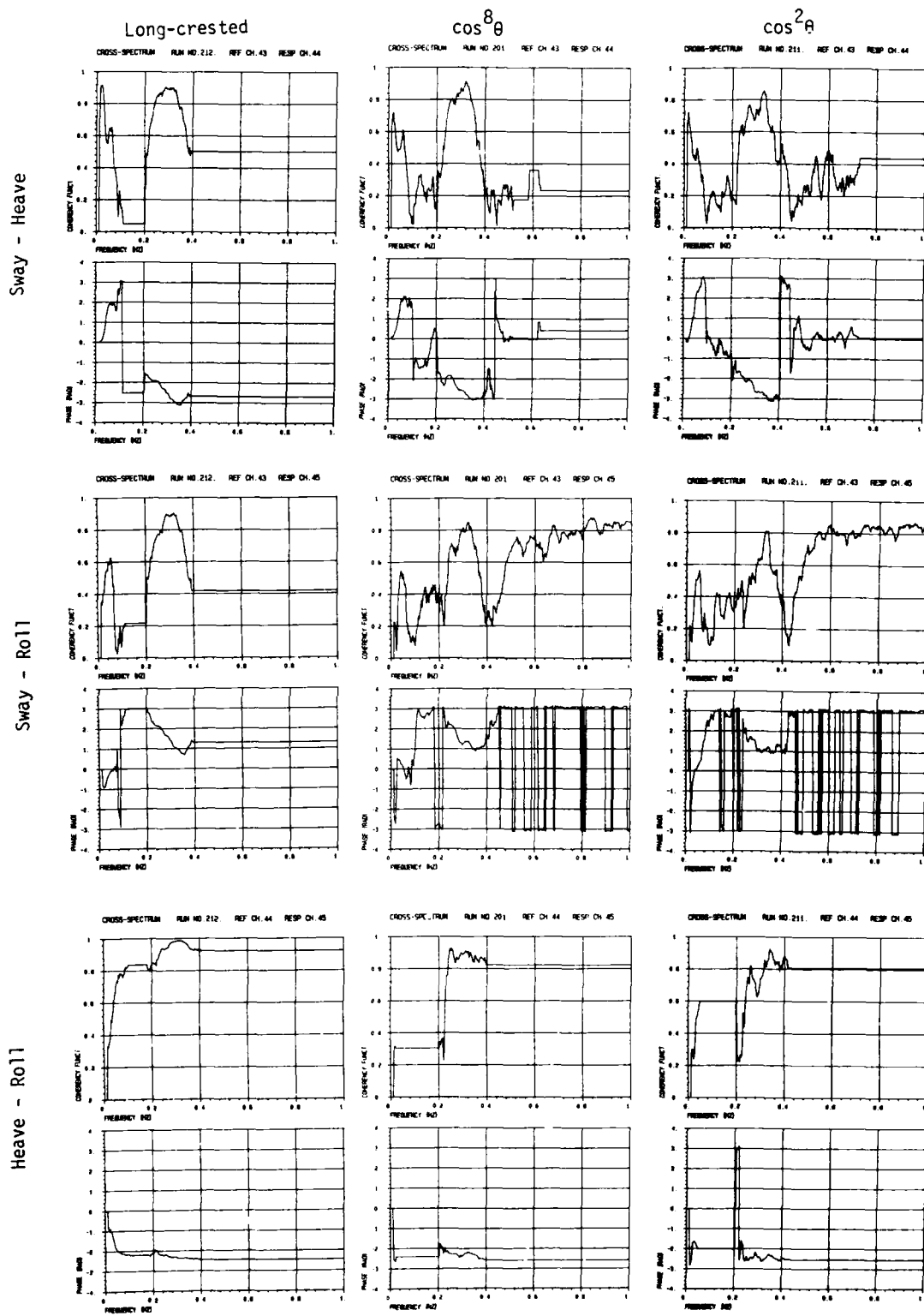


Fig. 3.85

COHERENCE - PHASE ANALYSIS MOTION - MOTION Fendered Model Input: JONSWAP $\cos^8 \theta$

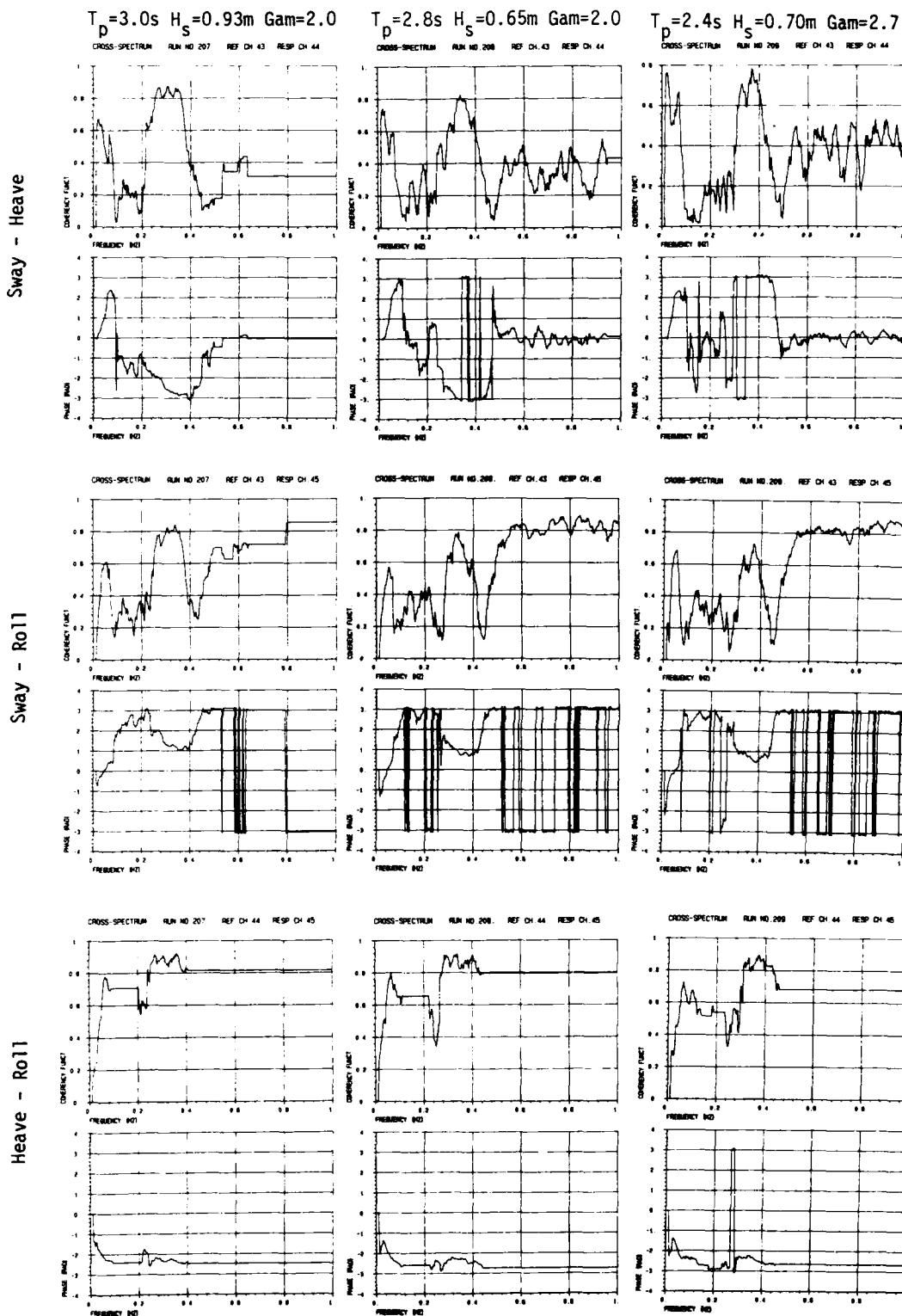


Fig. 3.86

COHERENCE - PHASE ANALYSIS MOTION - MOTION Fendered Model Input: JONSWAP $\cos^8 \theta$

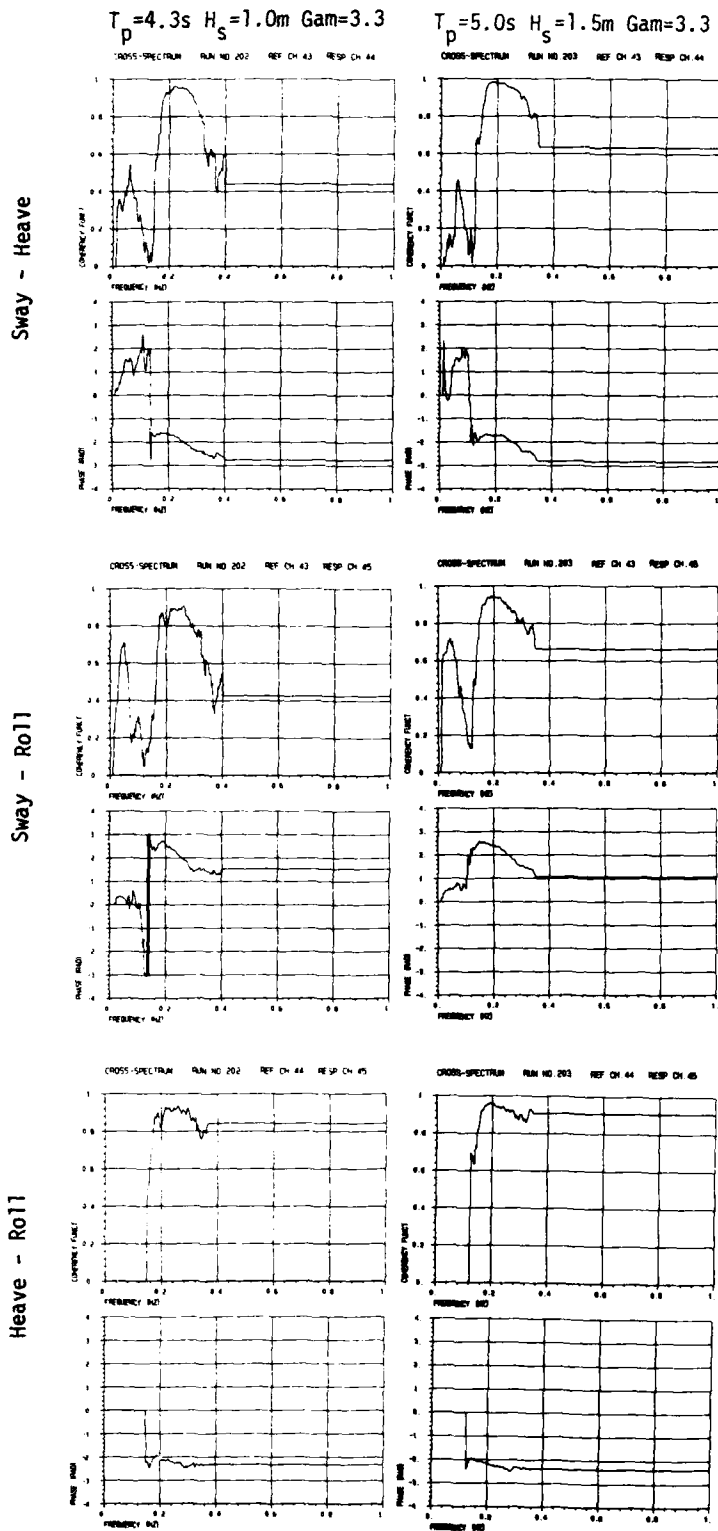


Fig. 3.87

3.2 Results for stiff model

3.2.1 Photographs of stiff breakwater model in irregular waves



Fig. 3.88
Run no. 357.

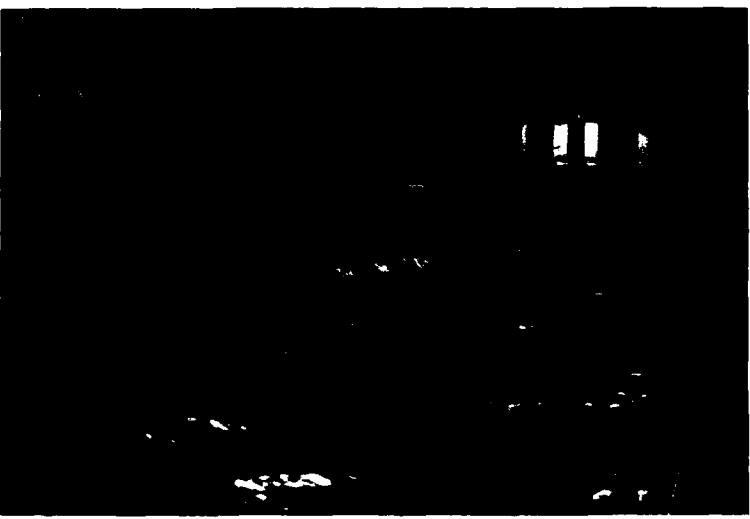


Fig. 3.89
Run no. 357.

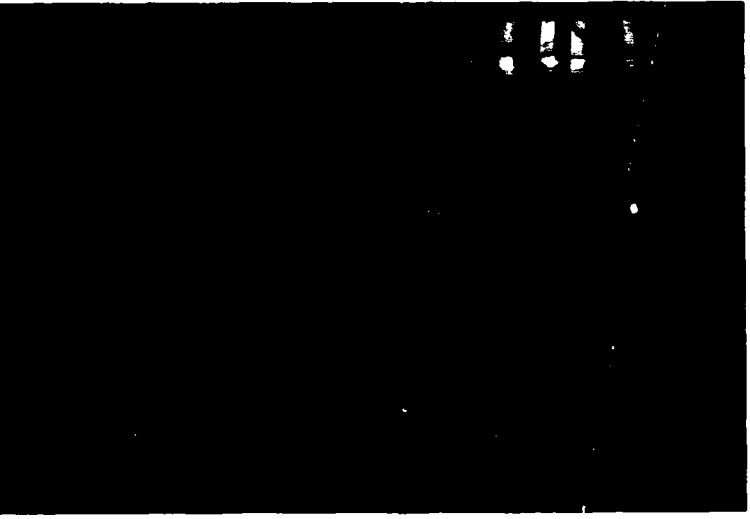


Fig. 3.90
Run no. 352.

3.2.2 Wave reduction/amplification around stiff breakwater model

The first plot (fig. 3.91) shows the normalized maximum wave height $H_{max,n} = H_{max}/H_{max,o}$ and normalized significant wave height $H_{mo,n} = H_{mo}/H_{mo,o}$ behind the model (wave staff 18, see fig. 2.19) as a function of the input peak wave period T_p . $H_{max,o}$ and $H_{mo,o}$ are wave height values obtained from calibration without model. Next, figs. 3.92 - 3.99 show plots of the distribution of $H_{max,n}$ and $H_{mo,n}$ 1m behind(wave staffs 1-9), and 2m in front of(wave staffs 13-21), the breakwater, for each of the 8 irregular sea states. Figs. 3.100 - 3.105 show wave spectra for wave staff 18 (1m behind) and 11 (1m in front) with and without model compared to theoretical input values, together with resulting amplitude transmission/amplification functions. Wave height statistics (compared to the Rayleigh distribution) and wave group spectra (compared to theoretical "Pinkster" curve /5, 6/), with and without model, are finally presented in figs. 3.106 - 3.117. Wave group spectra are calculated as the spectra of the square Hilbert envelope of the wave elevation /5/.

WAVE REDUCTION VS PEAK PERIOD OF INPUT WAVE

WAVE STAFF NO. 18

STIFF MODEL

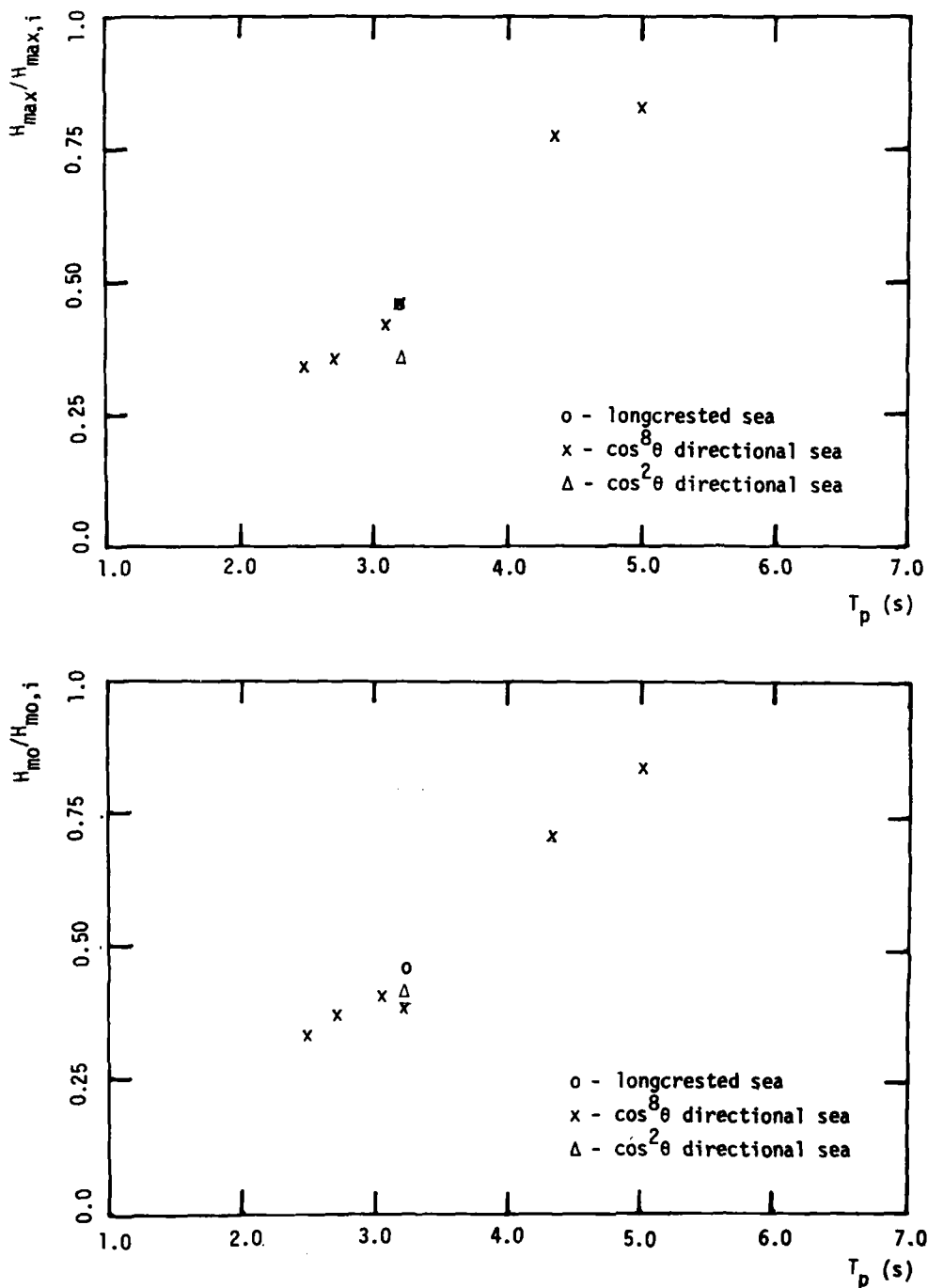


Fig. 3.91

WAVE REDUCTION/AMPLIFICATION NEAR THE BREAKWATER MODEL

TEST NO. 351:

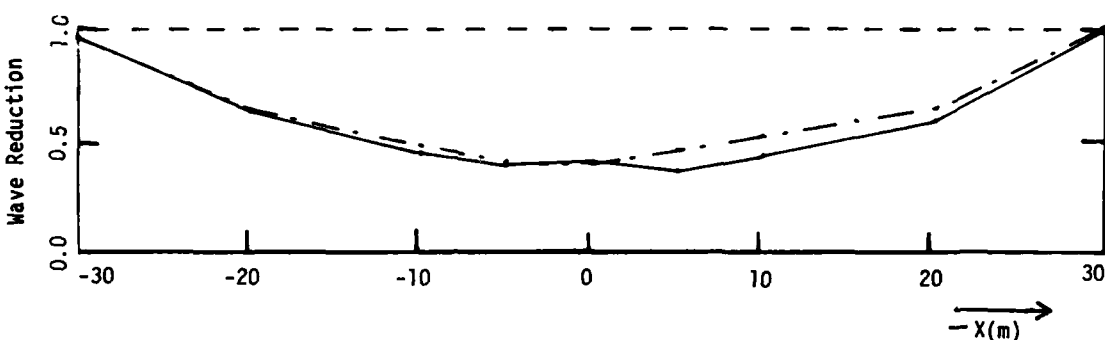
$T_p = 3.2\text{ s}$ $H_s = 0.75\text{ m}$ $\Gamma_m = 3.3 \cos^8 \theta$

Stiff Model

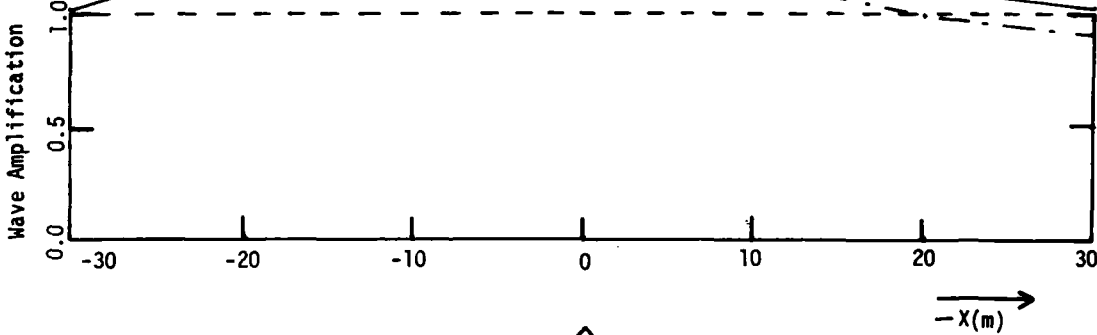
$\frac{H_{mo}}{H_{mo}}$ with model
 $\frac{H_{mo}}{H_{mo}}$ without model

$\frac{H_{max}}{H_{max}}$ with model
 $\frac{H_{max}}{H_{max}}$ without model

10 M BEHIND:



20 M IN FRONT:



Mean Wave Direction

Fig. 3.92

WAVE REDUCTION/AMPLIFICATION NEAR THE BREAKWATER MODEL

TEST NO. 352:

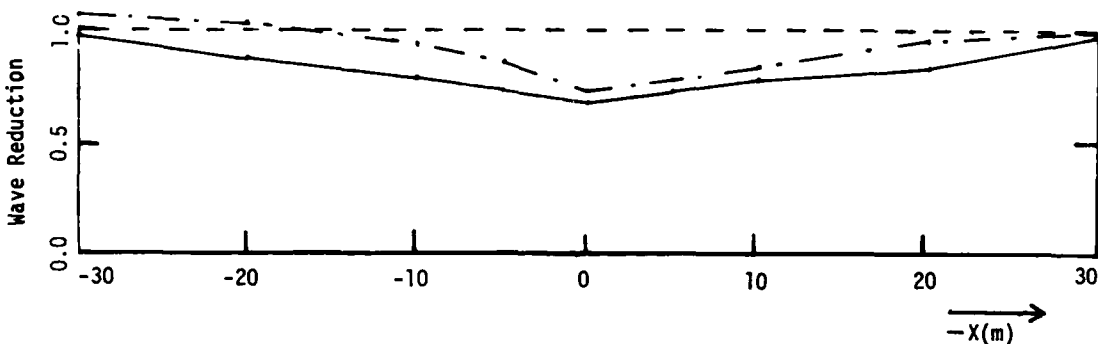
$$T_p = 4.3\text{s} \quad H_s = 1.0\text{m} \quad \text{Gam} = 3.3 \quad \cos^8 \theta$$

Stiff Model

$$\frac{H_{mo}}{H_{mo} \text{ without model}}$$

$$\frac{H_{max}}{H_{max} \text{ without model}}$$

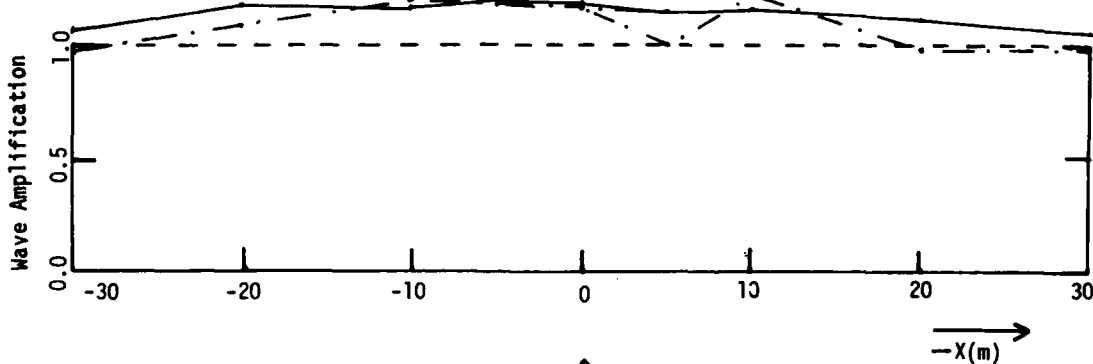
10 M BEHIND:



Y ↑

BREAKWATER MODEL

20 M IN FRONT:



↑

Mean Wave Direction

Fig. 3.93

WAVE REDUCTION/AMPLIFICATION NEAR THE BREAKWATER MODEL

TEST NO. 353:

$T_p = 5.0\text{s}$ $H_s = 1.5\text{m}$ $\text{Gam} = 3.3 \cos^8 \theta$

Stiff Model

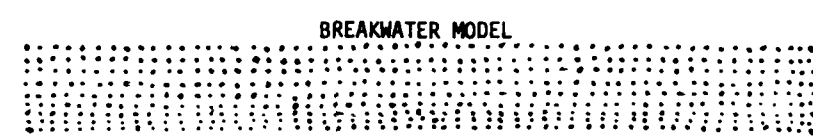
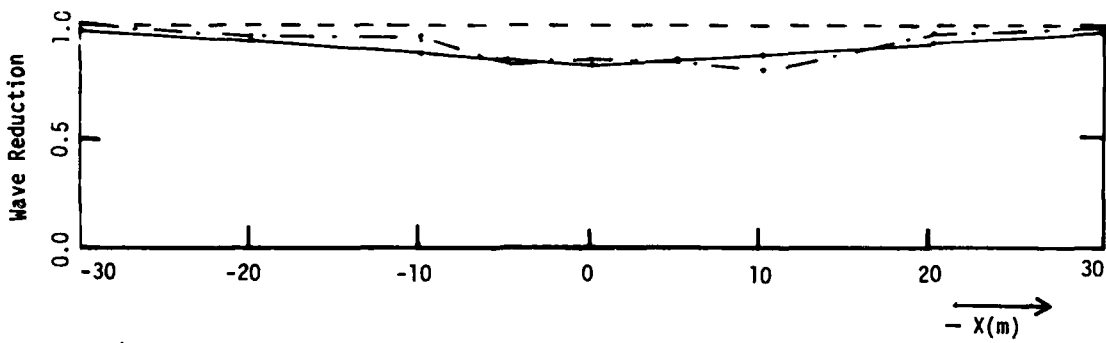
$\frac{H_{mo}}{H_{mo}}$ with model

$\frac{H_{mo}}{H_{mo}}$ without model

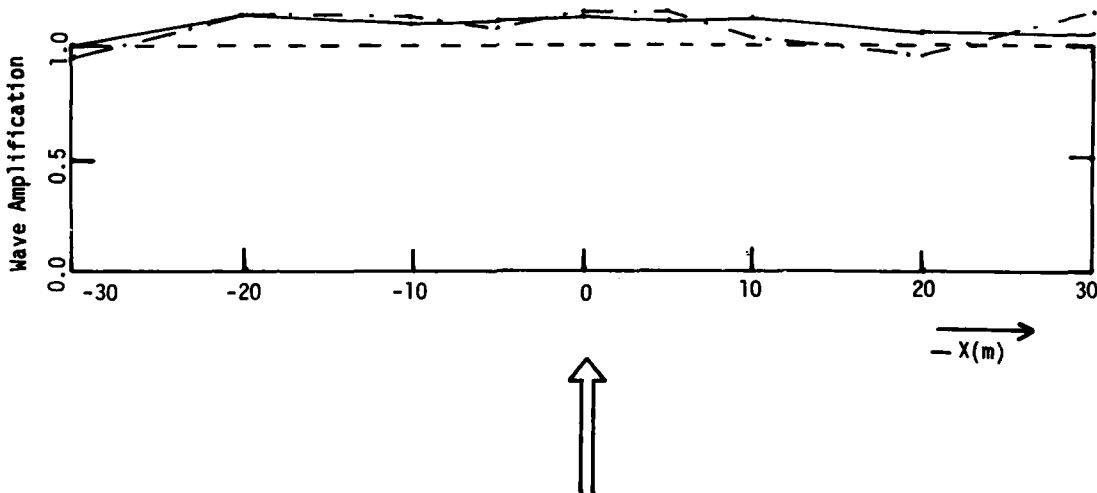
$\frac{H_{max}}{H_{max}}$ with model

$\frac{H_{max}}{H_{max}}$ without model

10 M BEHIND:



20 M IN FRONT:



Mean Wave Direction

Fig. 3.94

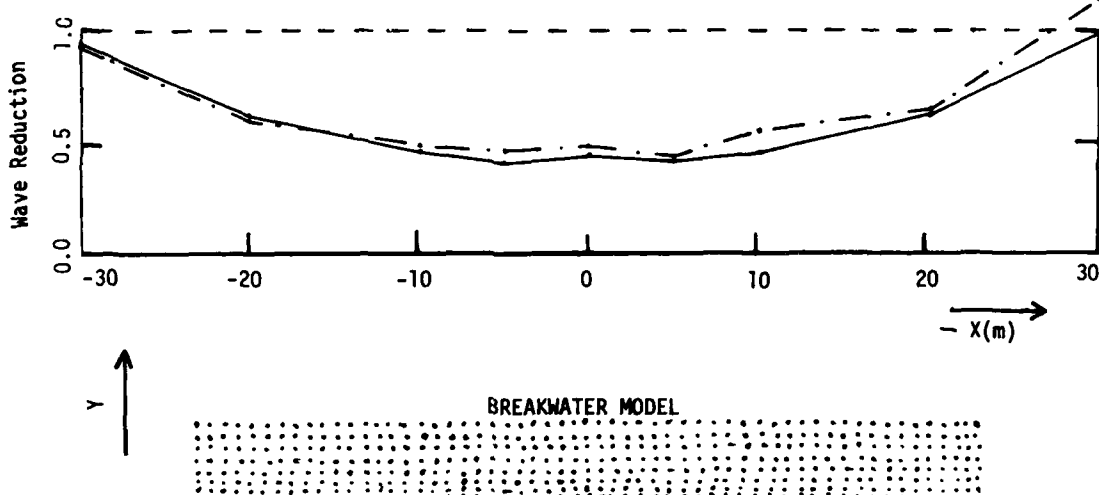
WAVE REDUCTION/AMPLIFICATION NEAR THE BREAKWATER MODEL

TEST NO. 357:

$$T_p = 3.0 \text{ s} \quad H_s = 0.93 \text{ m} \quad \Gamma_m = 2.0 \cos^8 \theta$$

Stiff Model

10 M BEHIND:



20 M-IN FRONT:

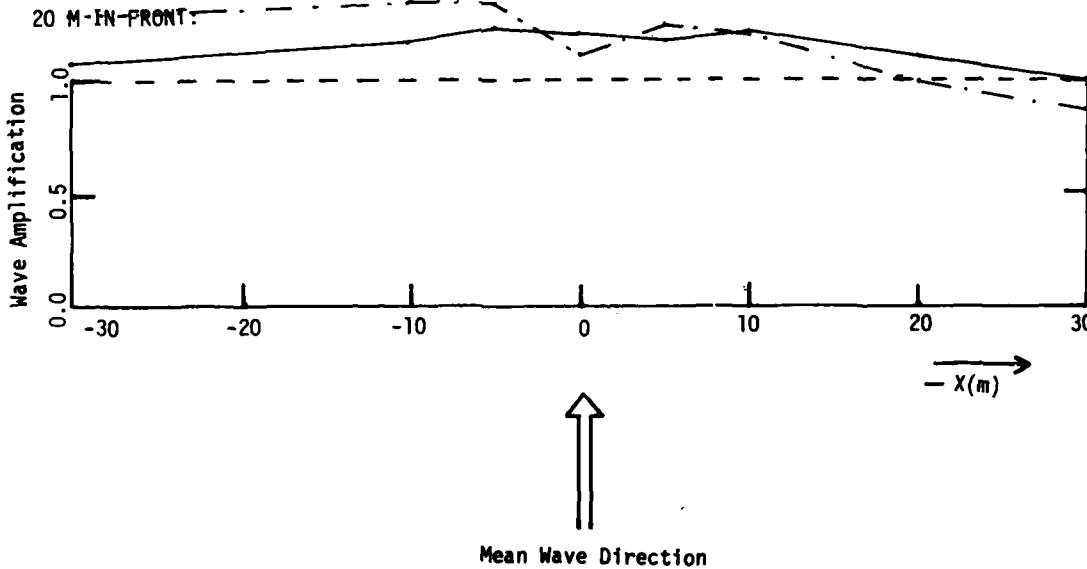


Fig. 3.95

WAVE REDUCTION/AMPLIFICATION NEAR THE BREAKWATER MODEL

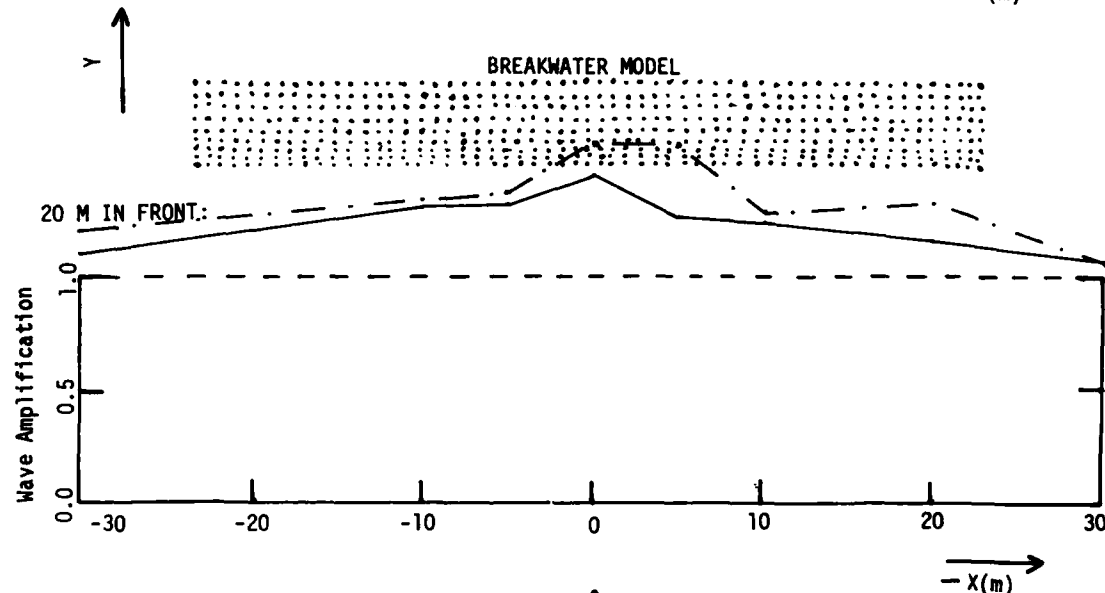
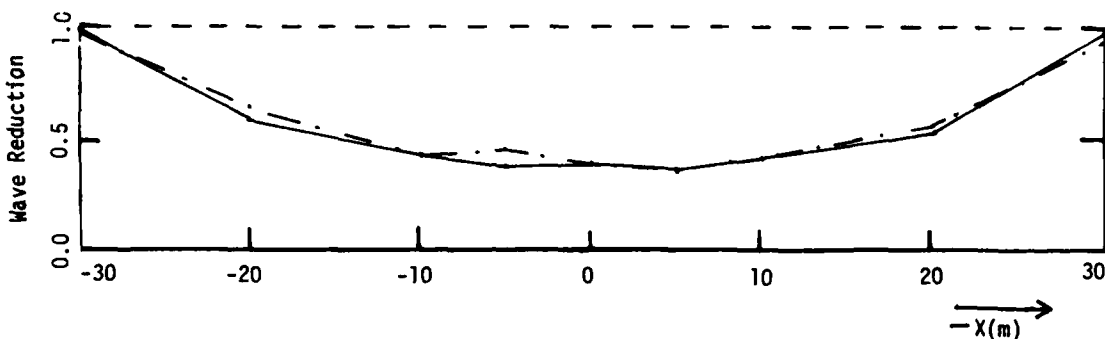
TEST NO. 358:

$T_p = 2.8\text{s}$ $H_s = 0.65\text{m}$ $\text{Gam} = 2.0 \cos^8 \theta$
Stiff Model

$\frac{H_{mo} \text{ with model}}{H_{mo} \text{ without model}}$

10 M BEHIND:

$\frac{H_{max} \text{ with model}}{H_{max} \text{ without model}}$



Mean Wave Direction

Fig. 3.96

WAVE REDUCTION/AMPLIFICATION NEAR THE BREAKWATER MODEL

TEST NO. 359:

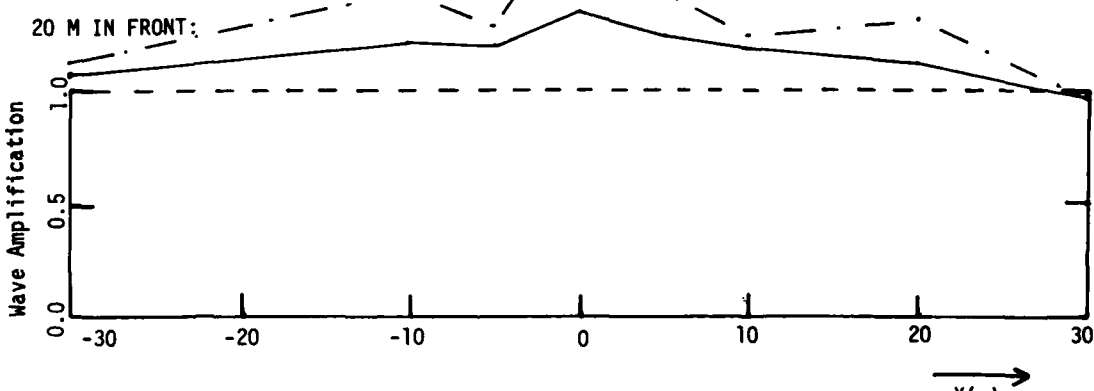
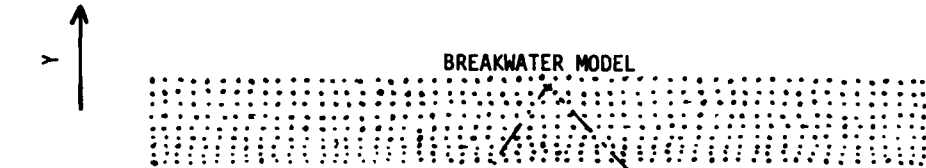
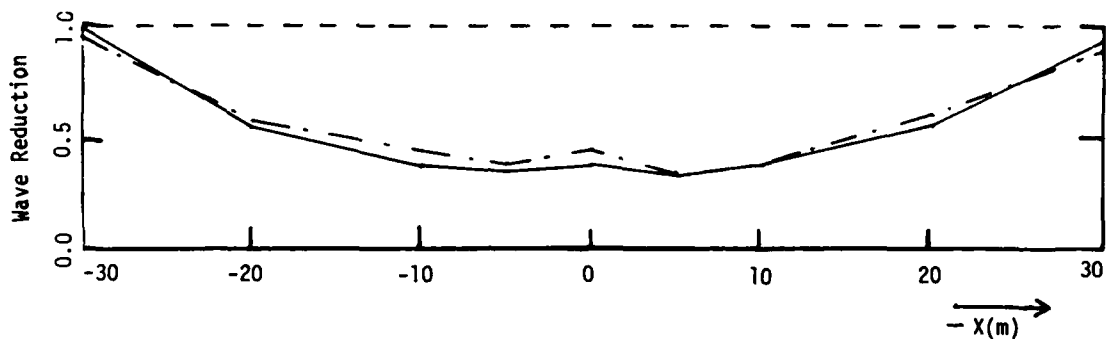
$$T_p = 2.4 \text{ s} \quad H_s = 0.70 \text{ m} \quad \text{Gam} = 2.7 \cos^8 \theta$$

Stiff Model

$$\frac{H_{mo} \text{ with model}}{H_{mo} \text{ without model}}$$

10 M BEHIND:

$$\frac{H_{max} \text{ with model}}{H_{max} \text{ without model}}$$



Mean Wave Direction

Fig. 3.97

WAVE REDUCTION/AMPLIFICATION NEAR THE BREAKWATER MODEL

TEST NO. 361:

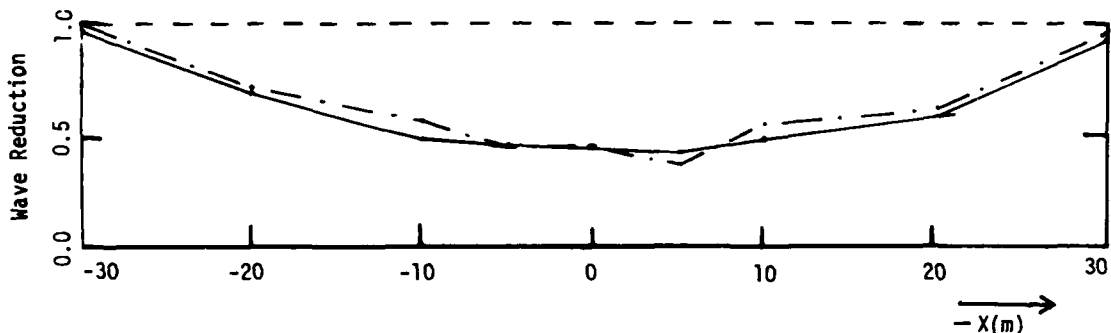
$$T_p = 3.2 \text{ s} \quad H_s = 0.75 \text{ m} \quad \text{Gam} = 3.3 \quad \cos^2 \theta$$

Stiff Model

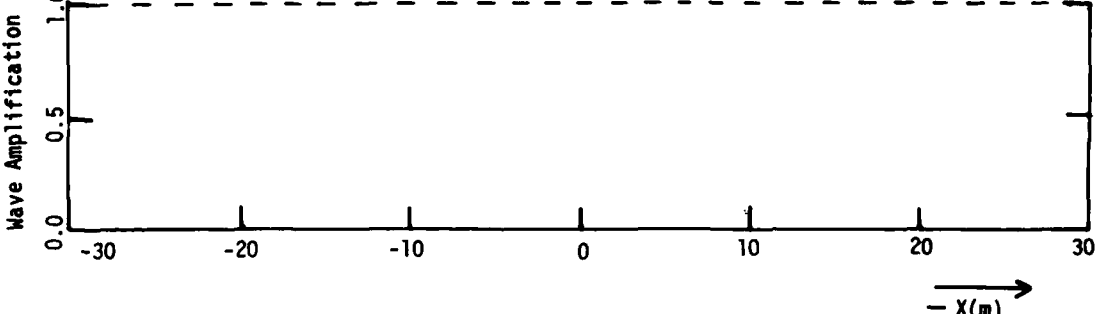
$$\frac{H_{mo} \text{ with model}}{H_{mo} \text{ without model}}$$

10 M BEHIND:

$$\frac{H_{max} \text{ with model}}{H_{max} \text{ without model}}$$



20 M IN FRONT:



Mean Wave Direction

Fig. 3.98

WAVE REDUCTION/AMPLIFICATION NEAR THE BREAKWATER MODEL

TEST NO. 362:

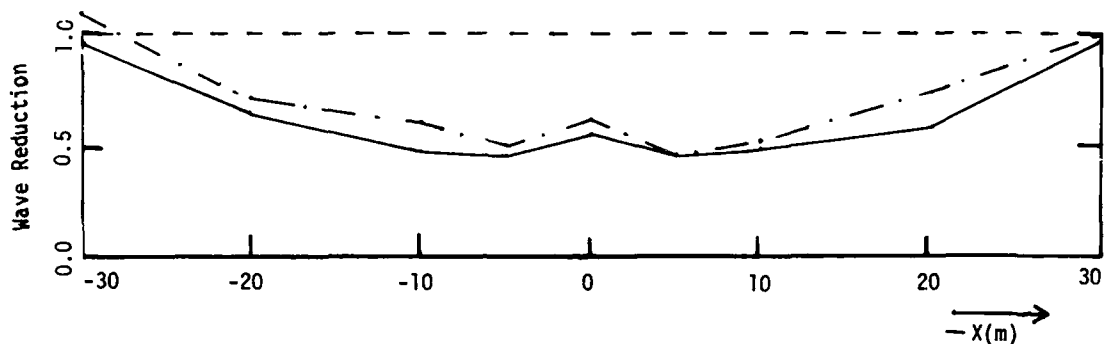
$T_p = 3.2\text{ s}$ $H_s = 0.75\text{ m}$ $\text{Gam} = 3.3$ Long-crested

Stiff Model

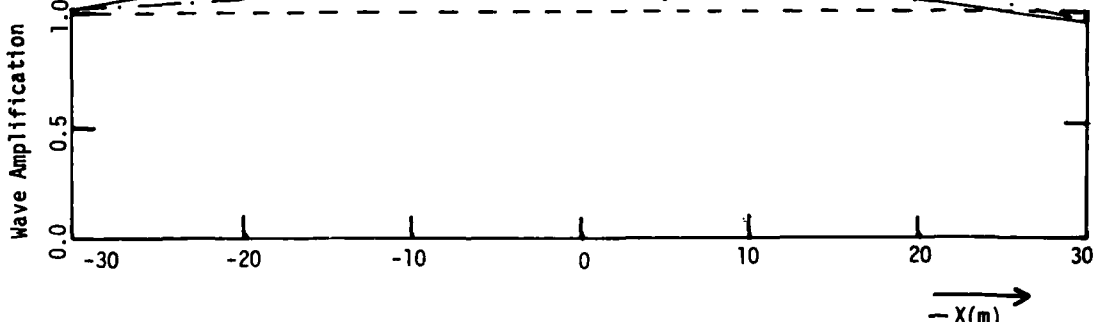
$\frac{H_{mo}}{H_{mo}}$ with model
 $\frac{H_{mo}}{H_{mo}}$ without model

$\frac{H_{max}}{H_{max}}$ with model
 $\frac{H_{max}}{H_{max}}$ without model

10 M BEHIND:



20 M IN FRONT:



BREAKWATER MODEL

Y



Mean Wave Direction

Fig. 3.99

WAVE REDUCTION, Stiff Model Input: JONSWAP $T_p = 3.2\text{s}$ $H_s = 0.75\text{m}$ $\text{Gam} = 3.3$

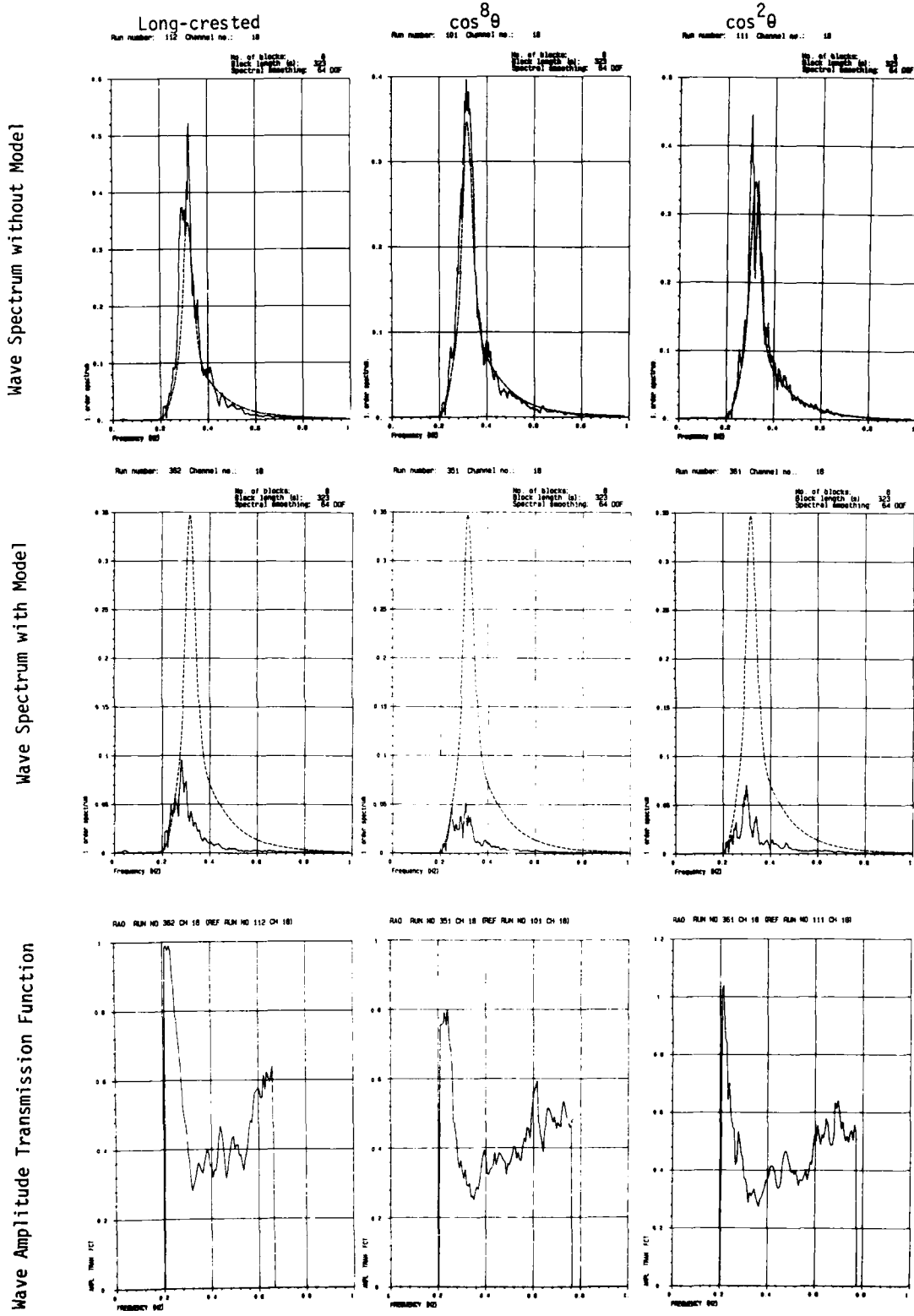


Fig. 3.100

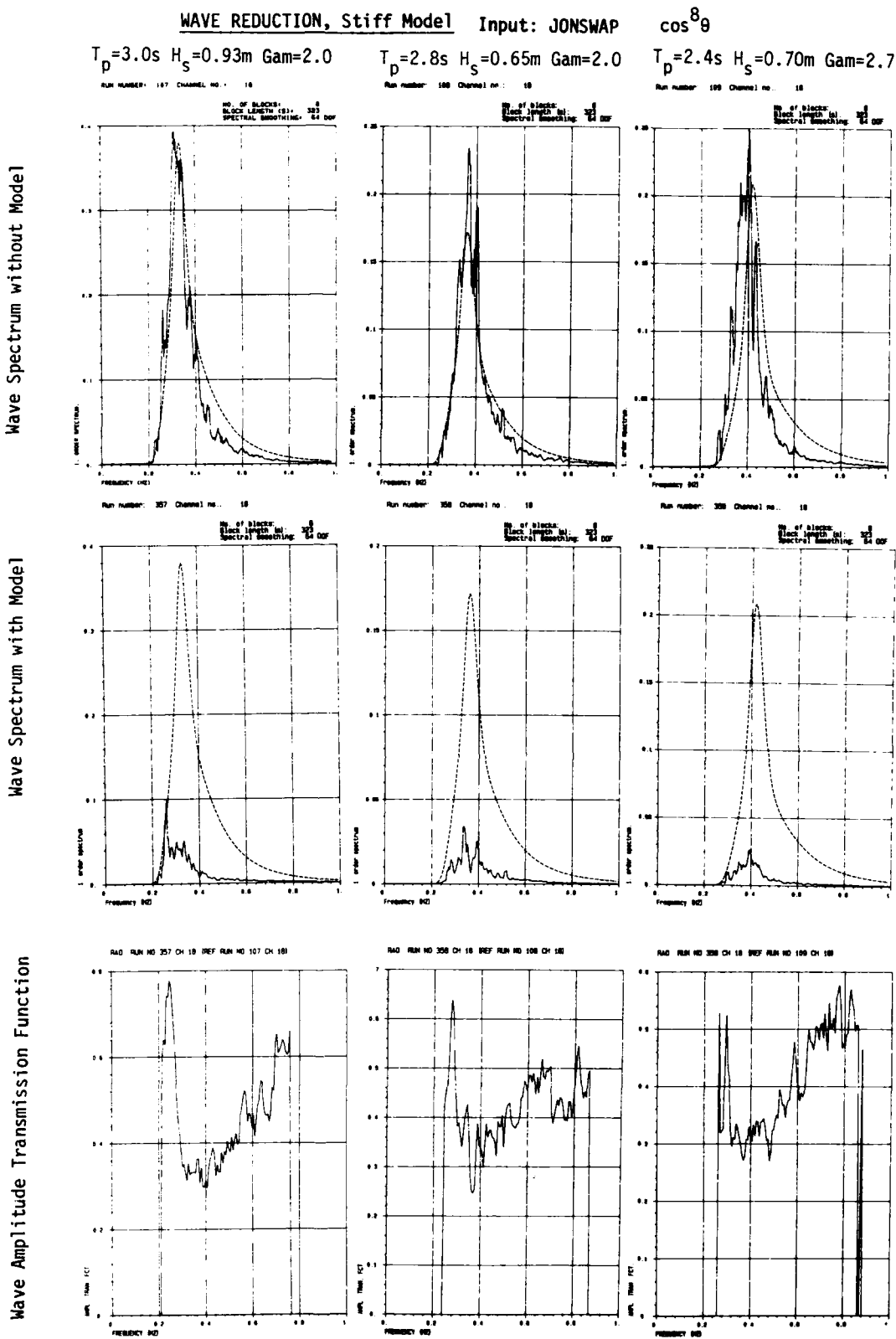
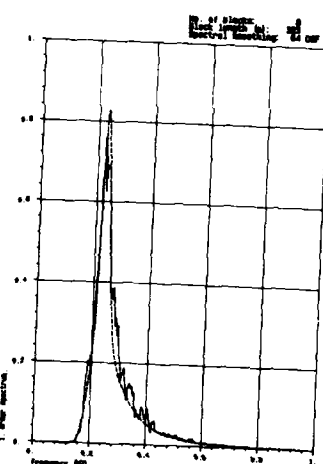


Fig. 3.101

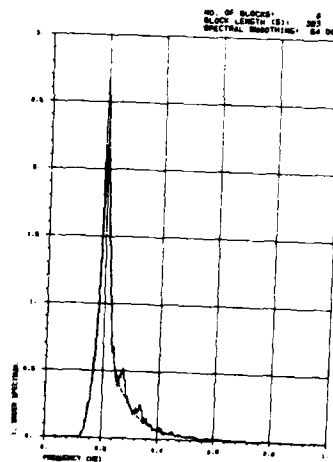
WAVE REDUCTION, Stiff Model

Input: JONSWAP $\cos^8 \theta$

$T_p = 4.3\text{s}$ $H_s = 1.0\text{m}$ $\text{Gam} = 3.3$
Run number: 352 Channel no.: 18

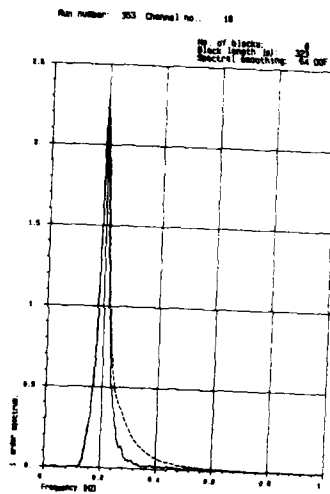
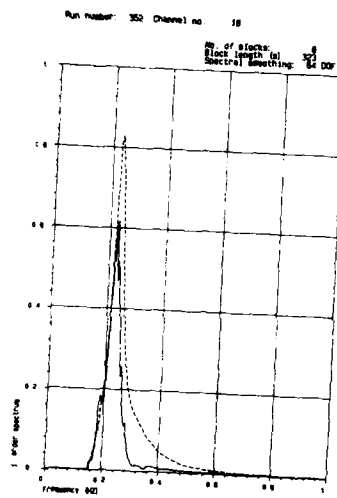


$T_p = 5.0\text{s}$ $H_s = 1.5\text{m}$ $\text{Gam} = 3.3$
Run number: 353 Channel no.: 18



Wave Spectrum without Model

Wave Spectrum with Model



Wave Amplitude Transmission Function

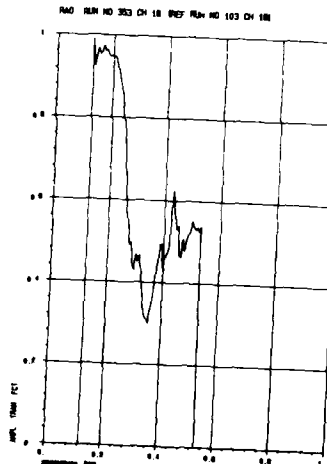
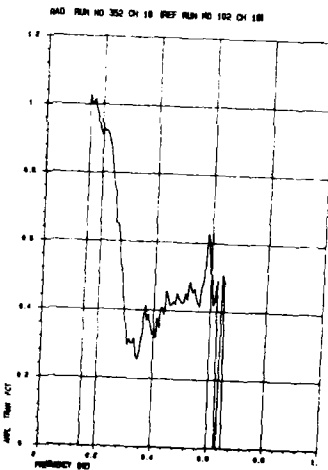


Fig. 3.102

WAVES IN FRONT, Stiff Model Input: JONSWAP $T_p = 3.2\text{s}$ $H_s = 0.75\text{m}$ $\text{Gam} = 3.3$

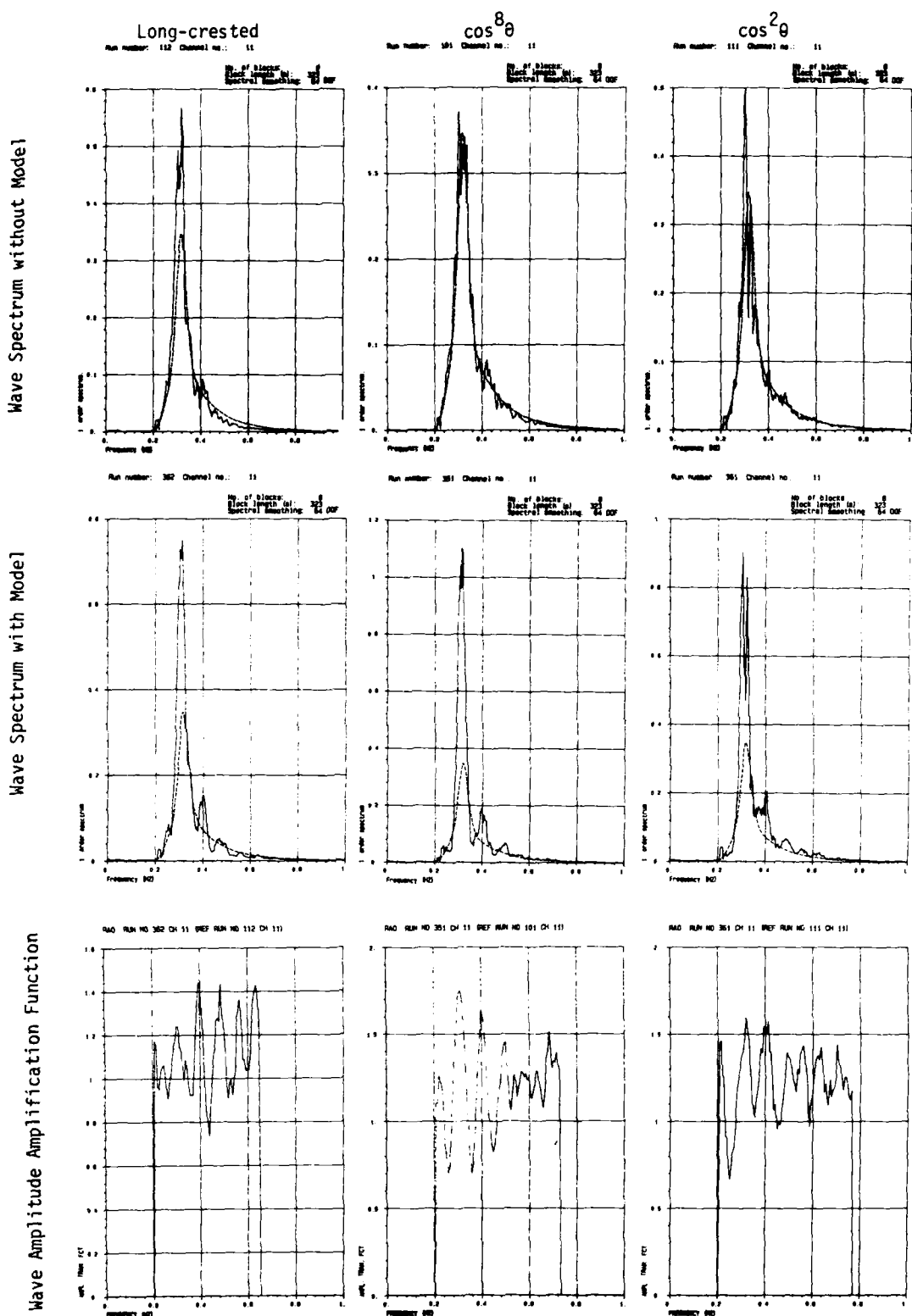


Fig. 3.103

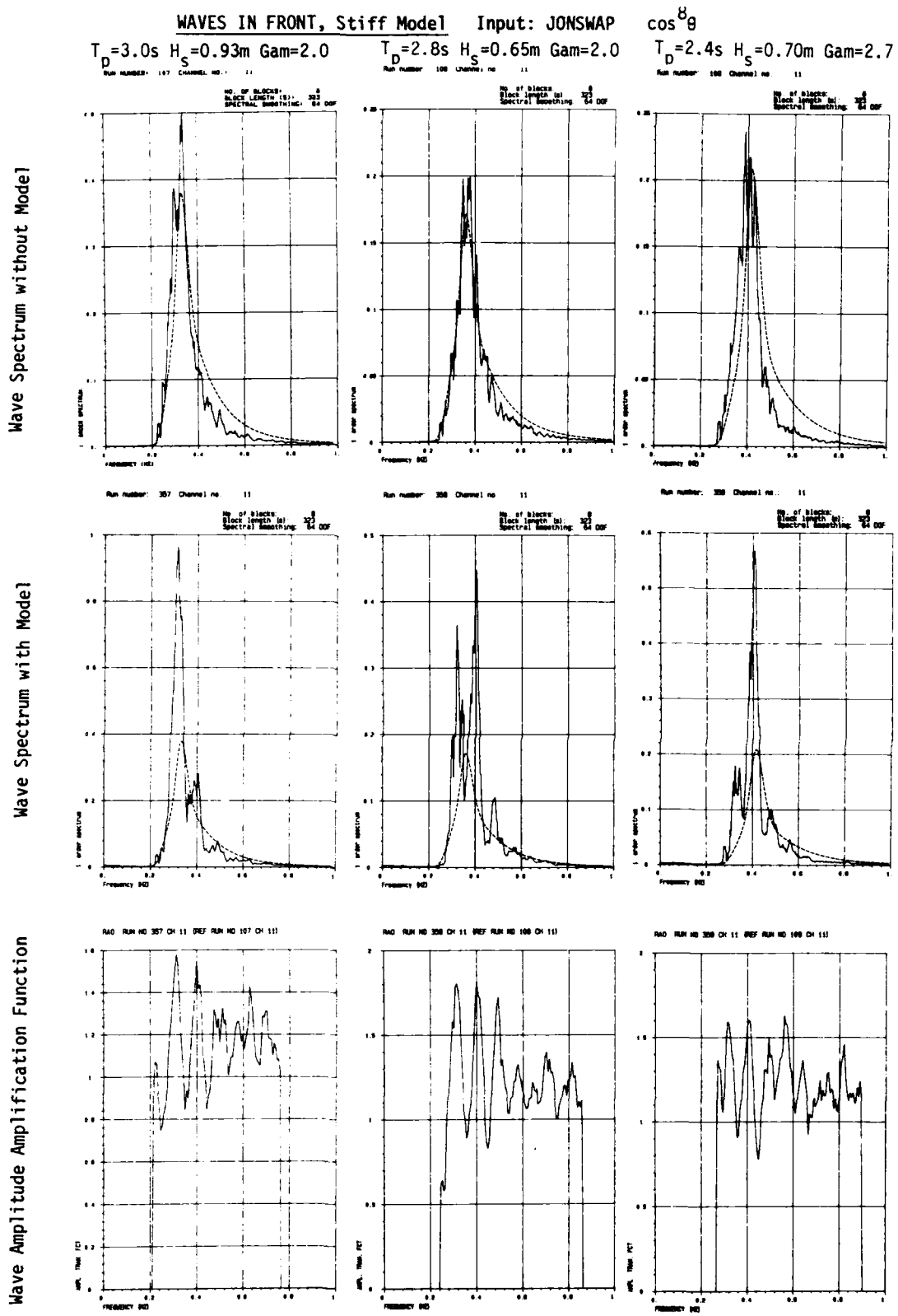
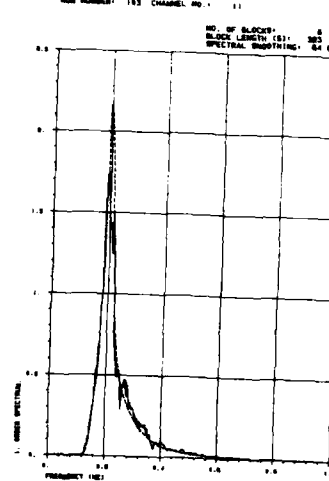
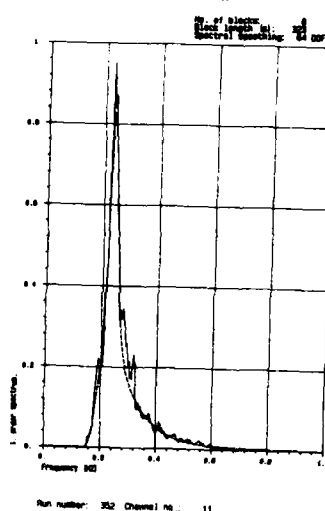


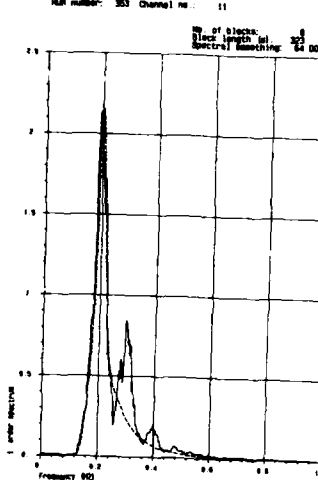
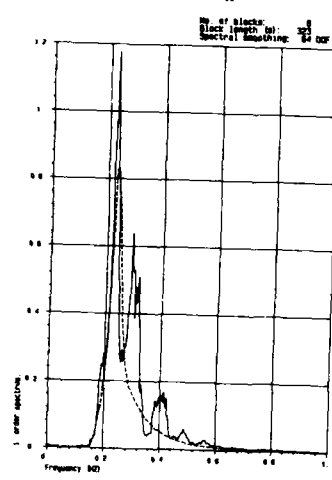
Fig. 3.104

WAVES IN FRONT, Stiff Model Input: JONSWAP $\cos^8 \theta$
 $T_d = 4.3\text{s}$ $H_s = 1.0\text{m}$ $\text{Gam} = 3.3$ $T_p = 5.0\text{s}$ $H_s = 1.5\text{m}$ $\text{Gam} = 3.3$
Run number: 352 Channel no.: 11 Run number: 353 Channel no.: 11

Wave Spectrum without Model



Wave Spectrum with Model



Wave Amplitude Amplification Function

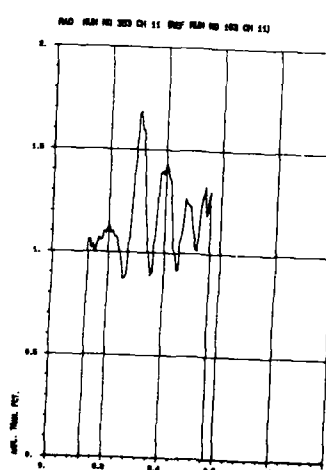
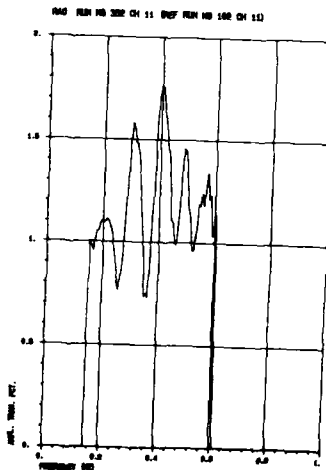


Fig. 3.105

WAVE STATISTICS behind Stiff Model Input: JONSWAP $T_p = 3.2\text{s}$ $H_s = 0.75\text{m}$ $\text{Gam} = 3.3$

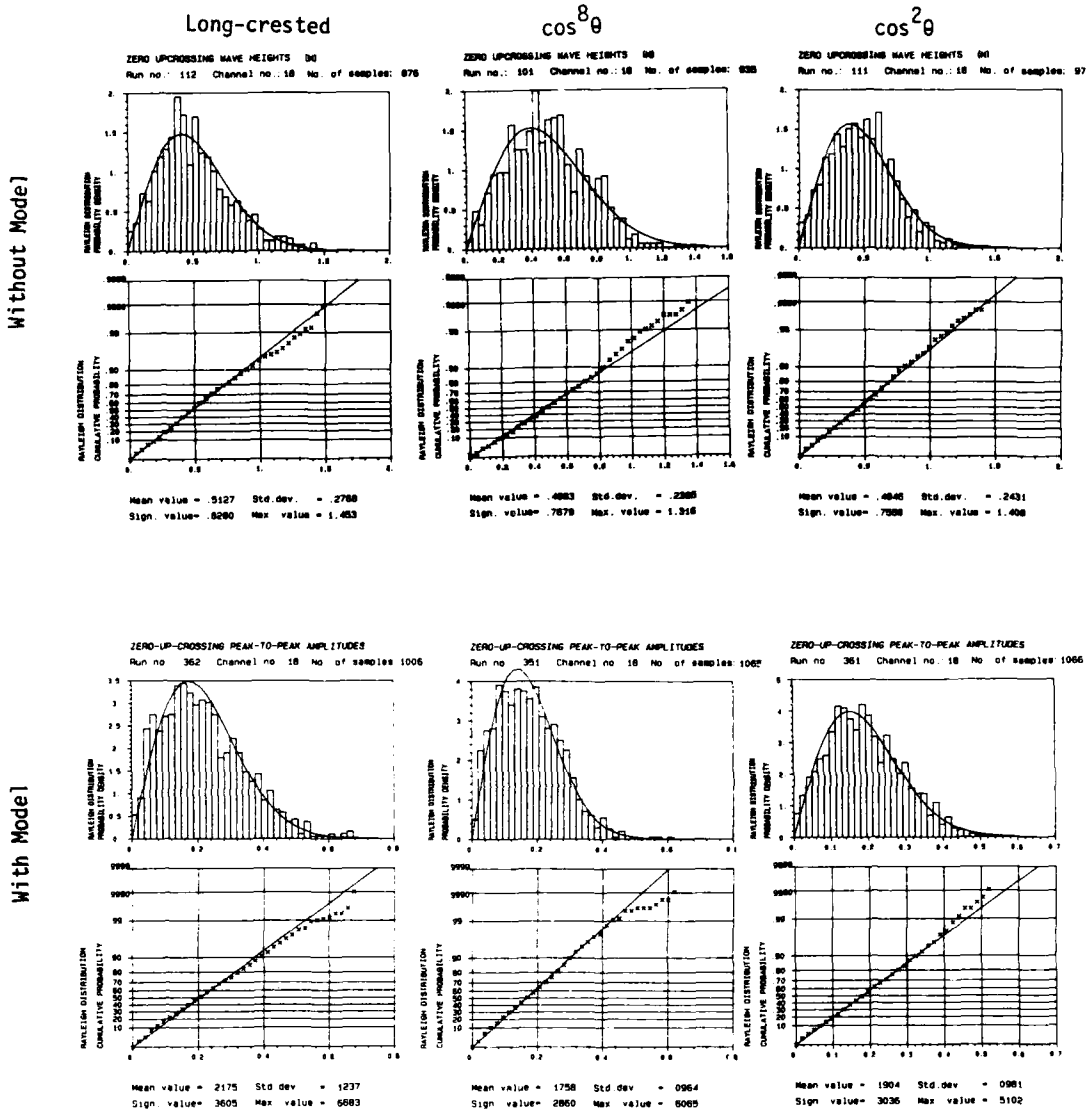


Fig. 3.106

WAVE STATISTICS behind Stiff Model Input: JONSWAP $\cos^8 \theta$

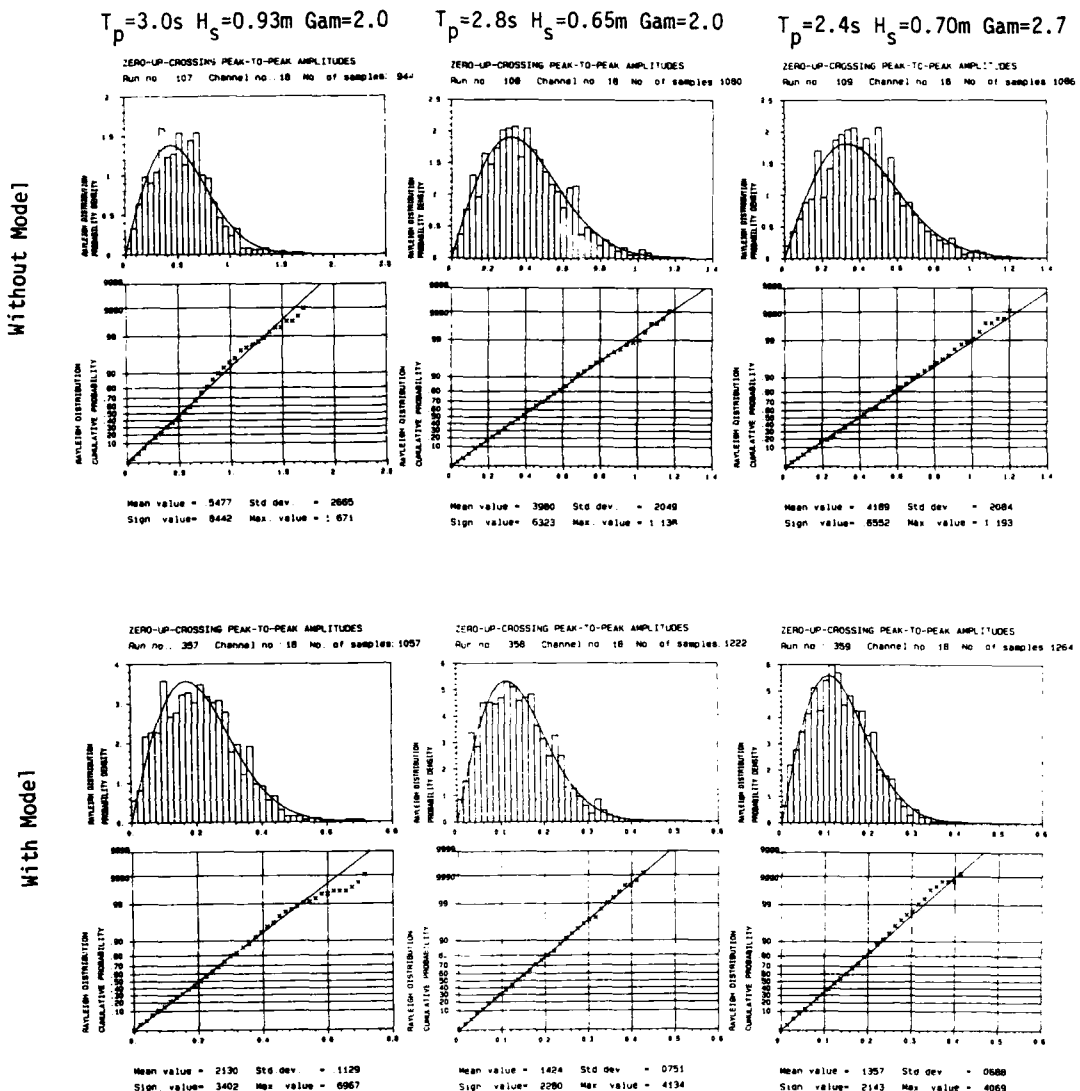


Fig. 3.107

WAVE STATISTICS behind Stiff Model

Input: JONSWAP $\cos^8 \theta$

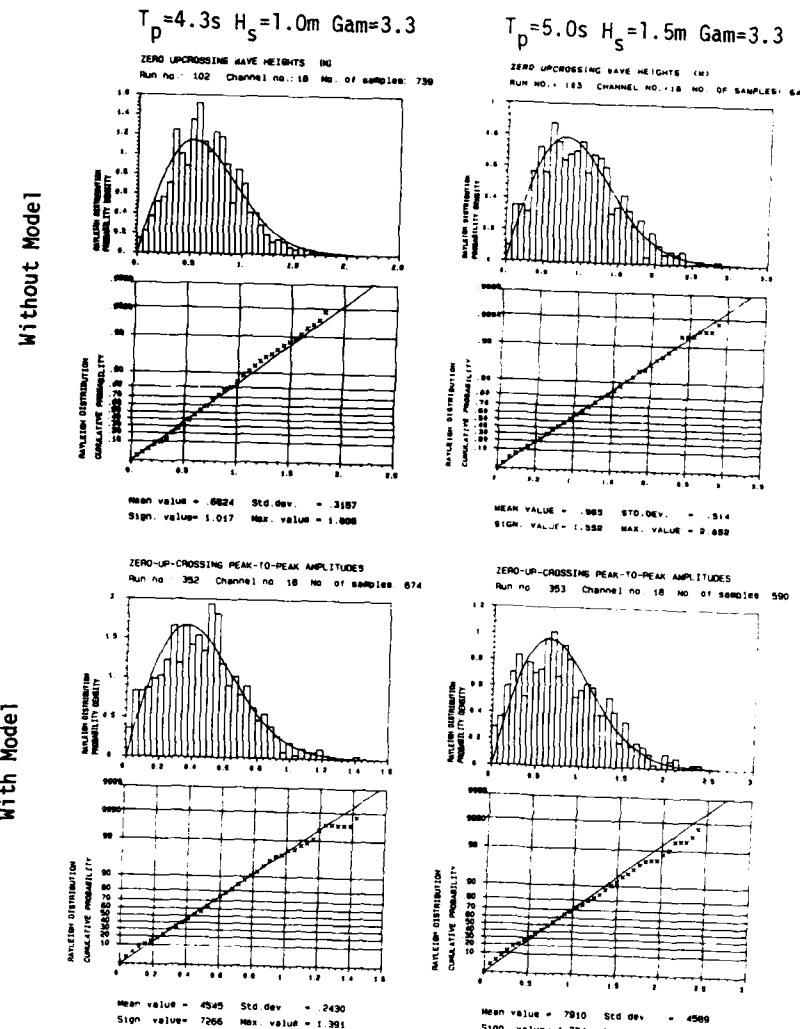


Fig. 3.108

WAVE STATISTICS in front of Stiff Model

Input: JONSWAP

$T_p = 3.2\text{s}$ $H_s = 0.75\text{m}$ $\Gamma_m = 3.3$

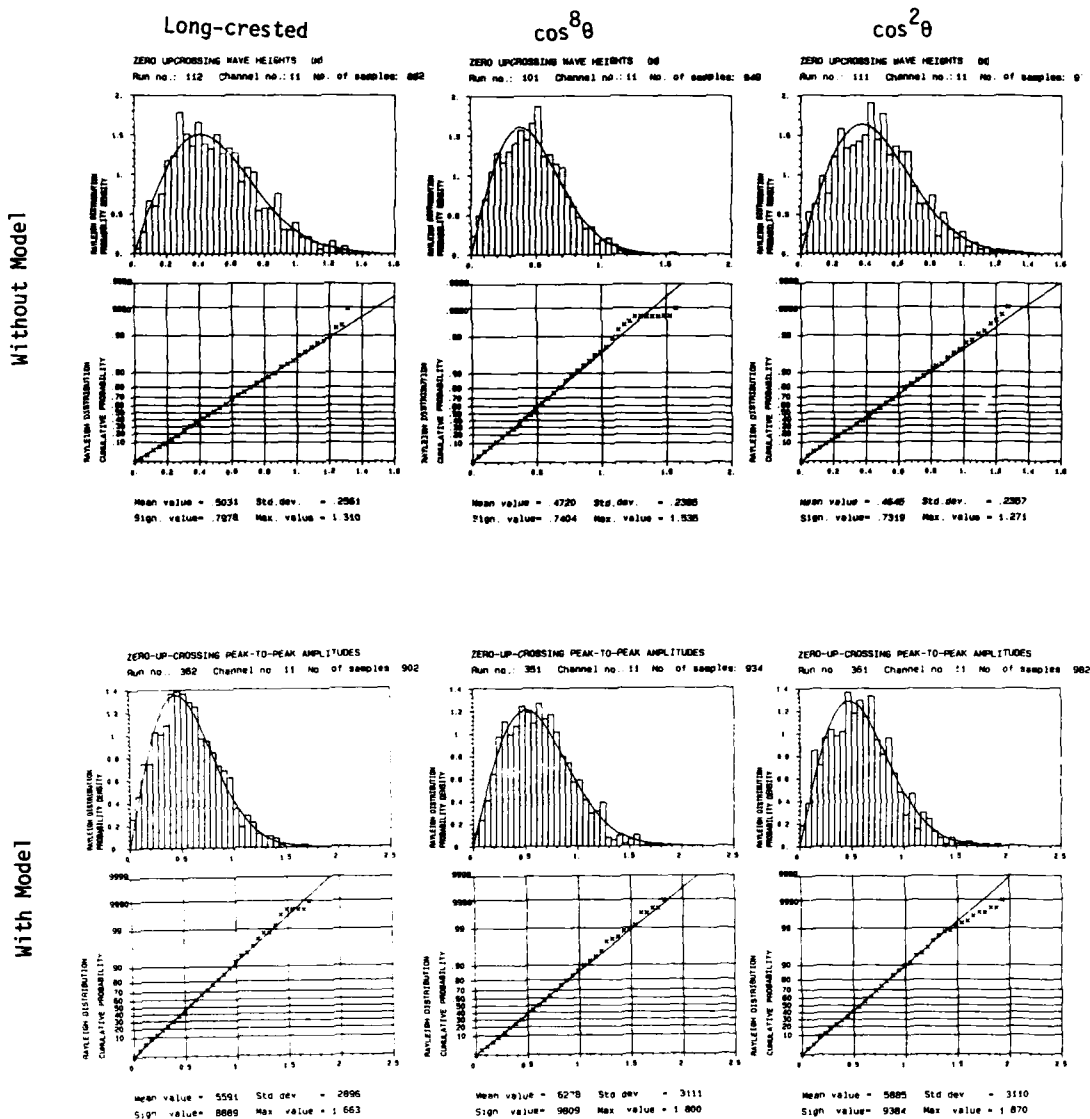


Fig. 3.109

WAVE STATISTICS in front of Stiff Model Input: JONSWAP $\cos^8 \theta$

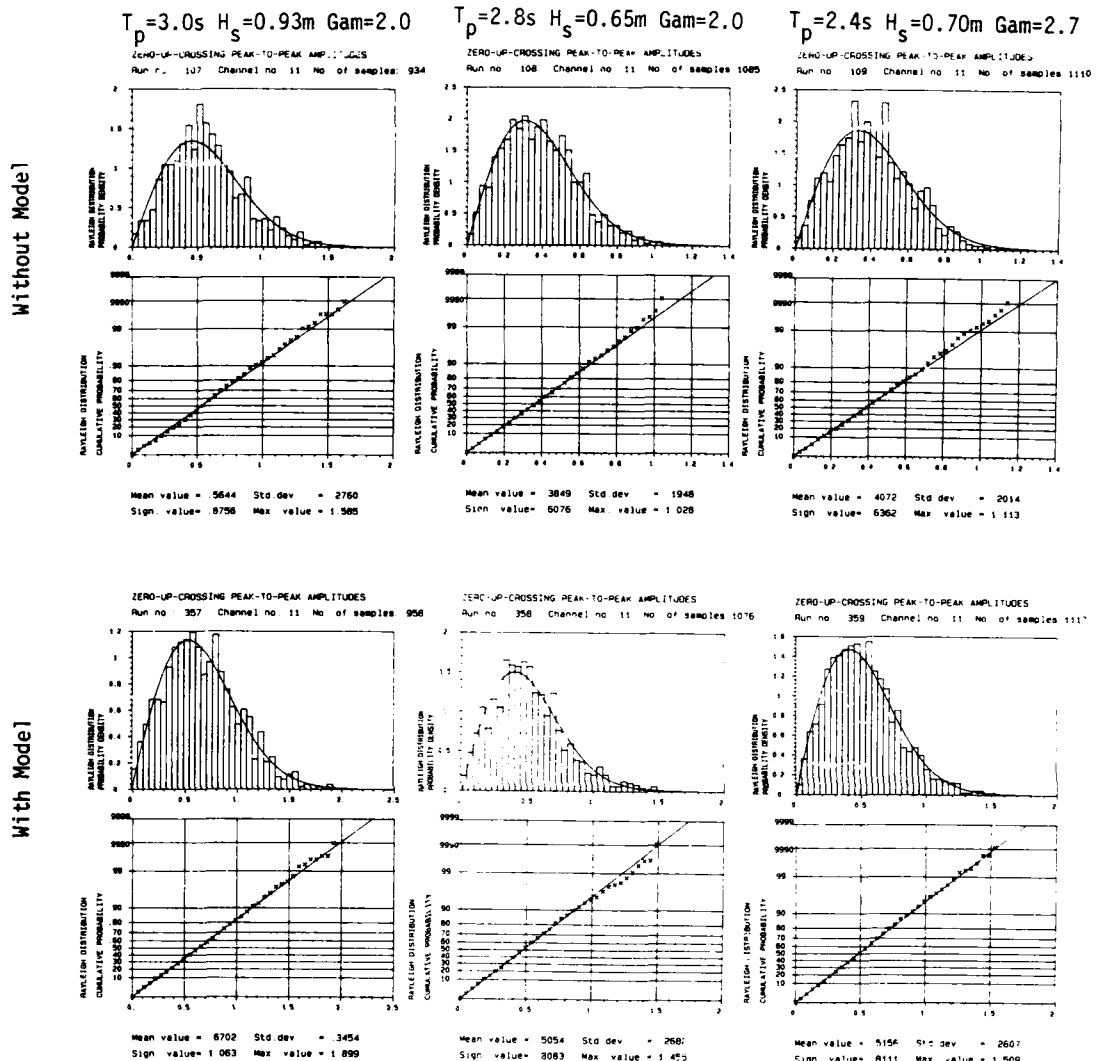


Fig. 3.110

WAVE STATISTICS in front of Stiff Model

Input: JONSWAP $\cos^8 \theta$

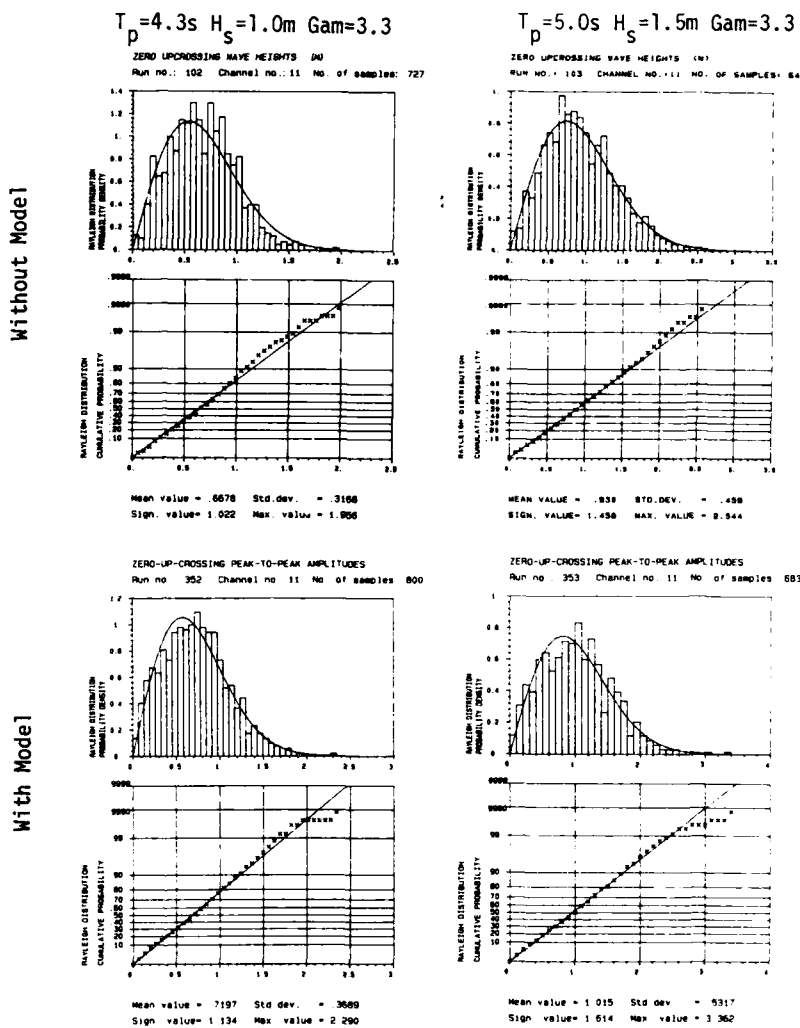


Fig. 3.111

WAVE GROUP SPECTRA behind Stiff Model

Input: JONSWAP $T_p = 3.2\text{ s}$ $H_s = 0.75\text{ m}$ $\text{Gam} = 3.3$

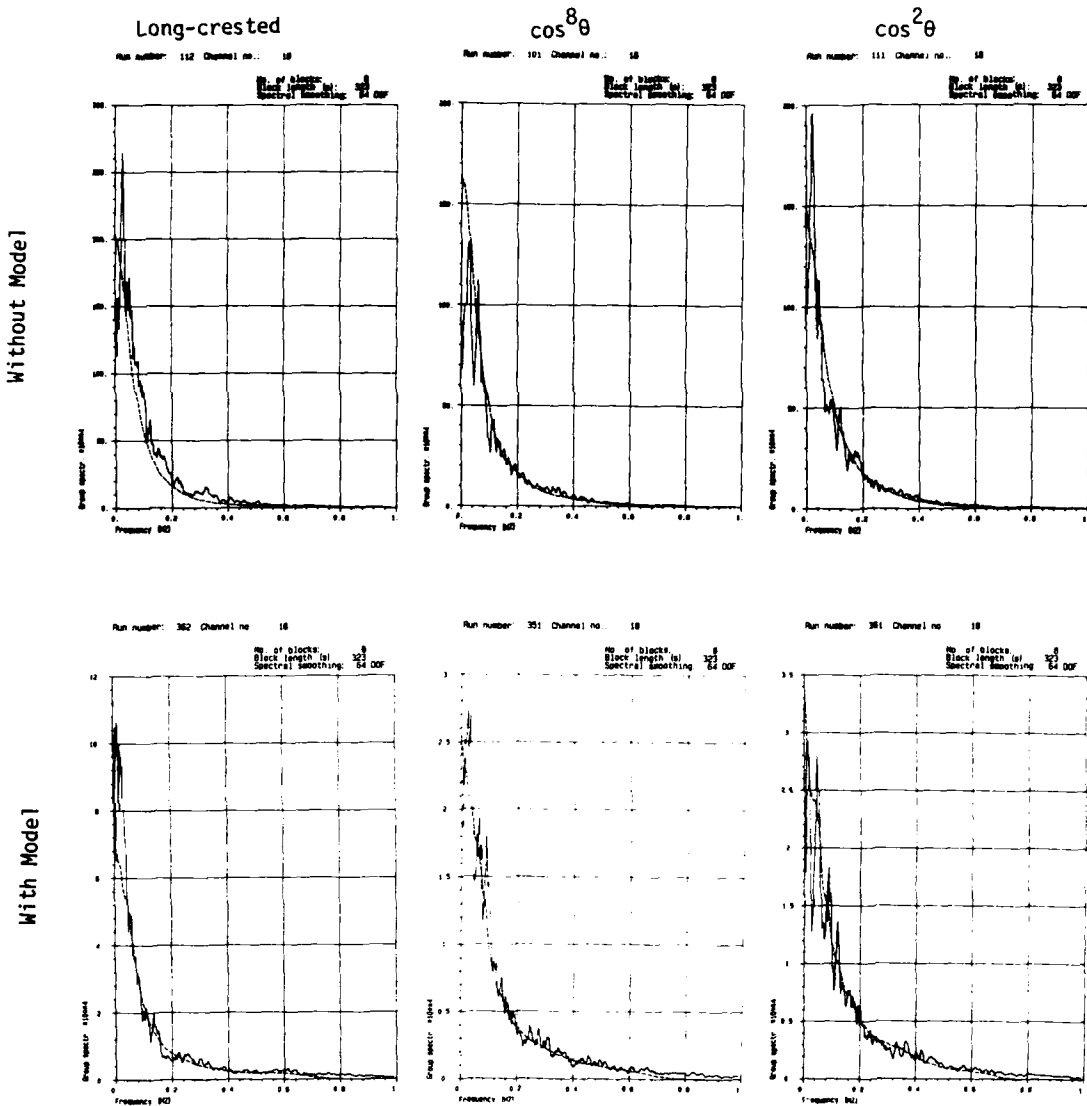


Fig. 3.112

WAVE GROUP SPECTRA behind Stiff Model

Input: JONSWAP $\cos^8 \theta$

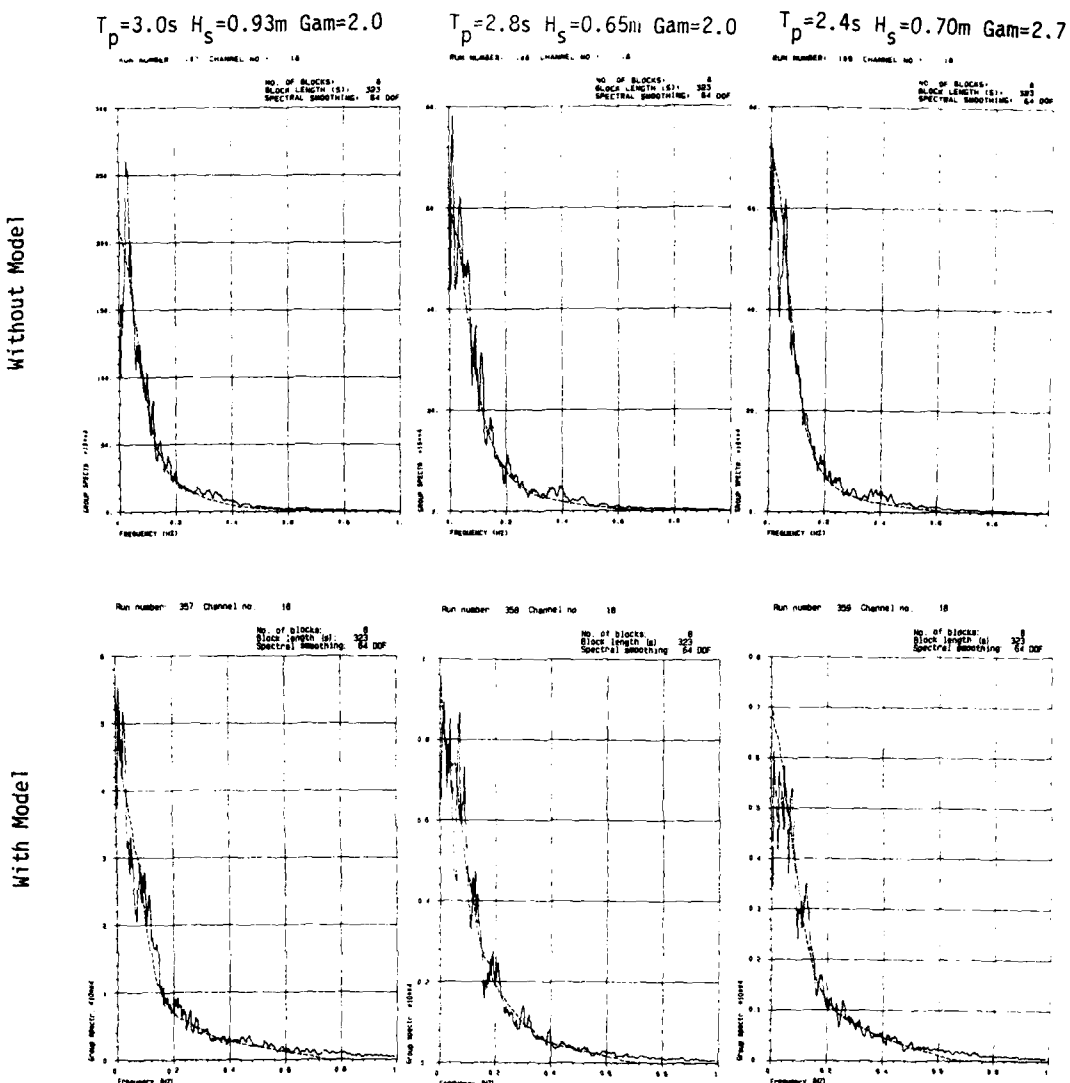


Fig. 3.113

WAVE GROUP SPECTRA behind Stiff Model Input: JONSWAP $\cos^8\theta$

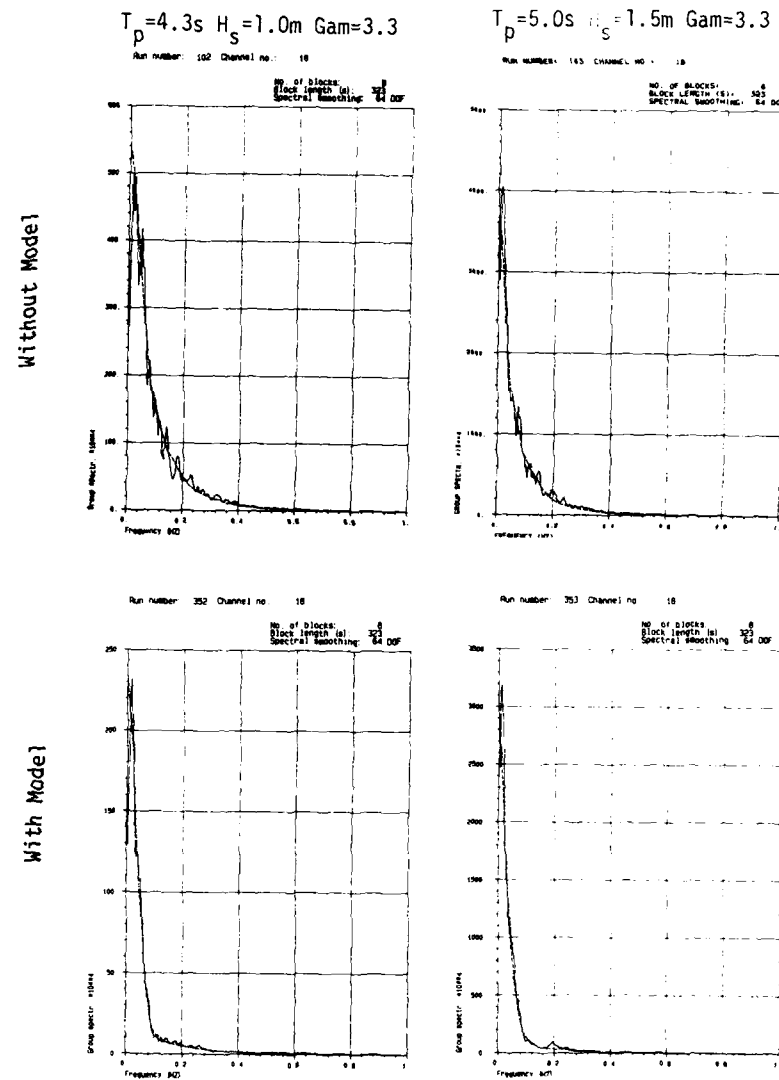


Fig. 3.114

WAVE GROUP SPECTRA in front of Stiff Model Input: JONSWAP $T_p = 3.2\text{ s}$ $H_s = 0.75\text{ m}$ $\text{Gam} = 3.3$

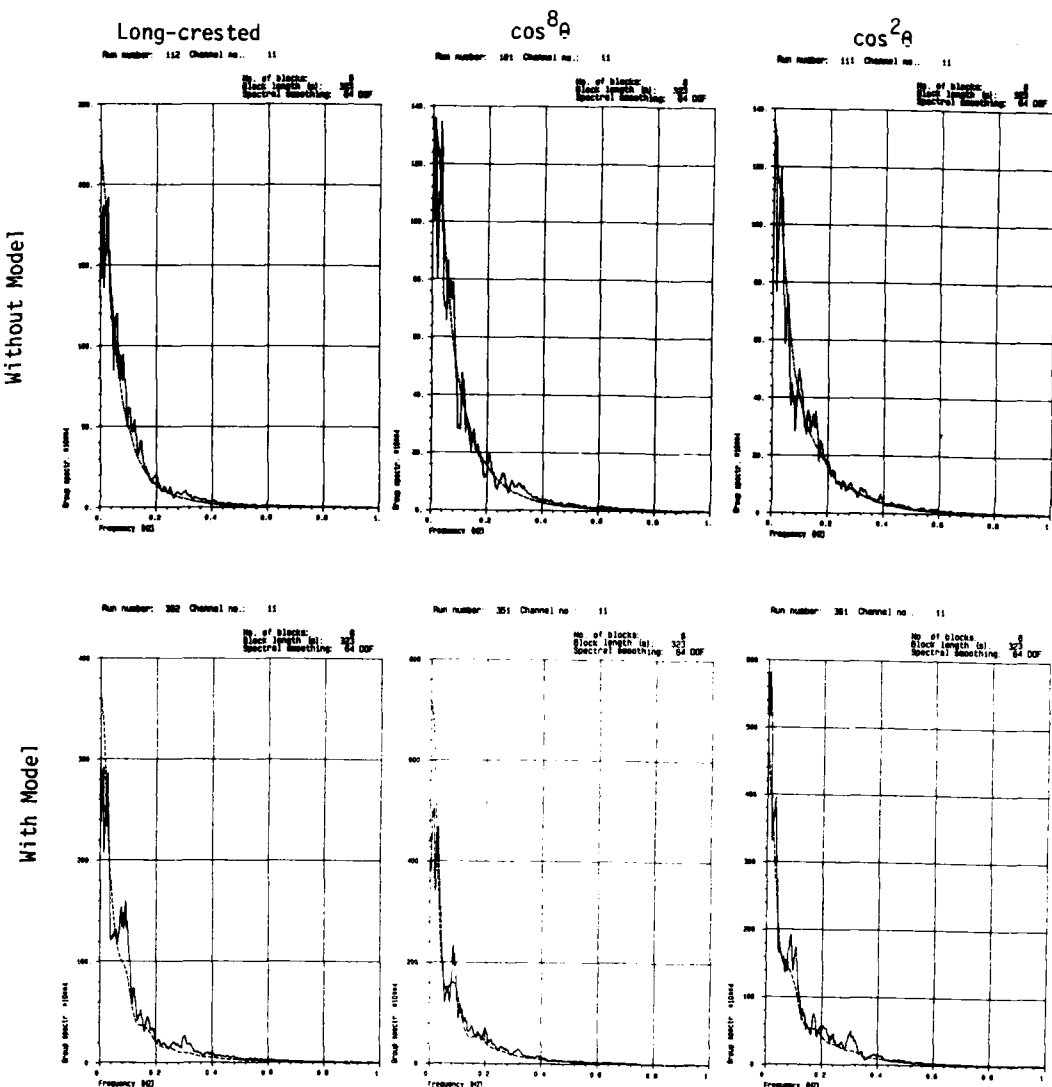


Fig. 3.115

WAVE GROUP SPECTRA in front of Stiff Model Input: JONSWAP $\cos^8 \theta$

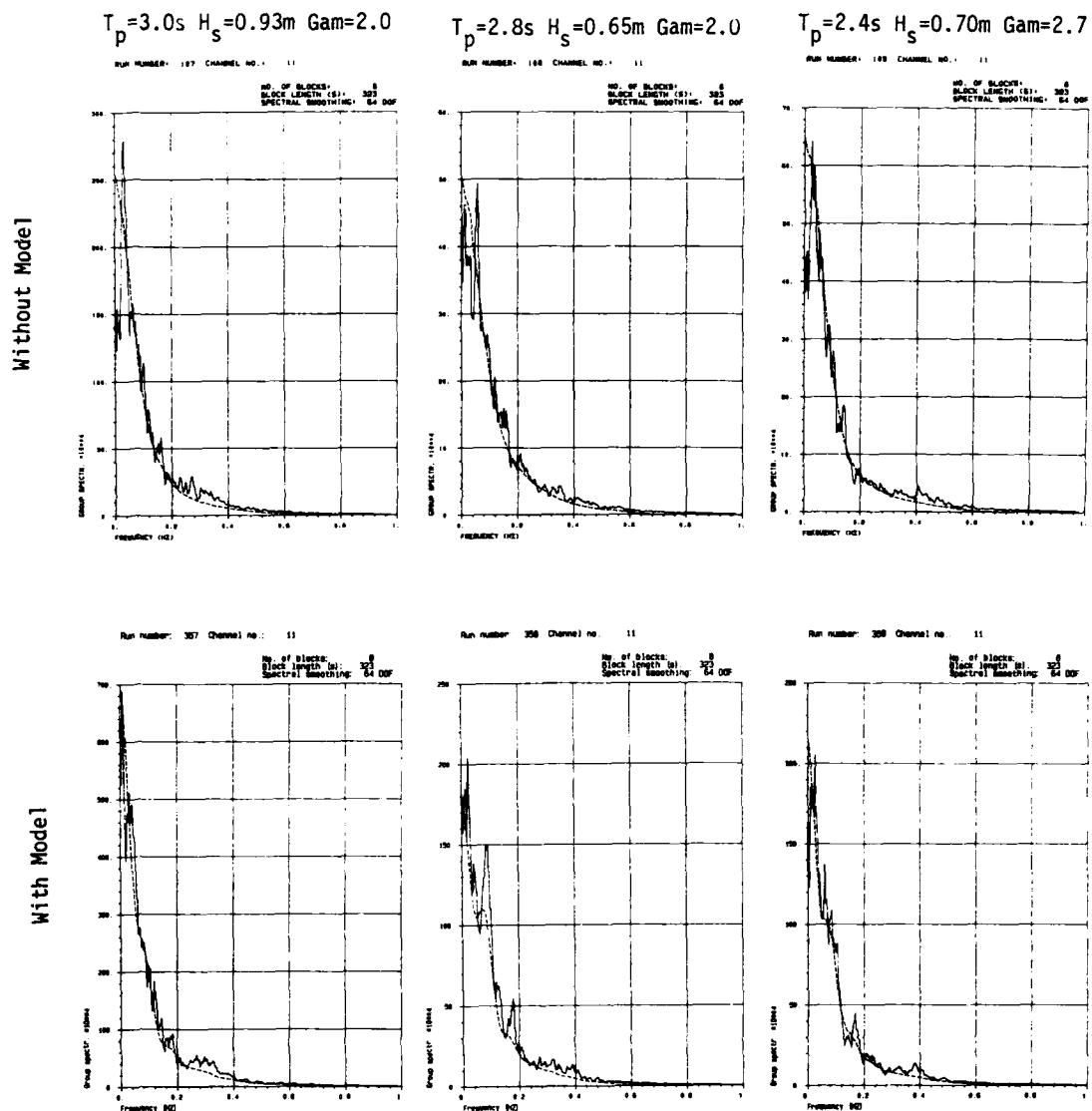
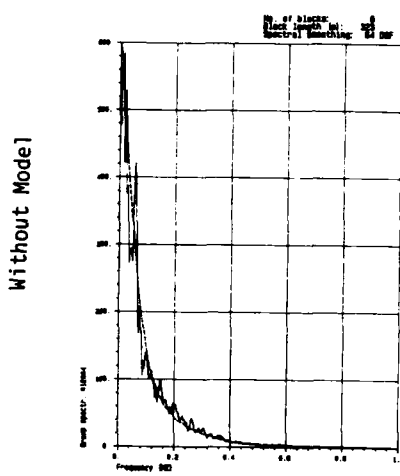


Fig. 3.116

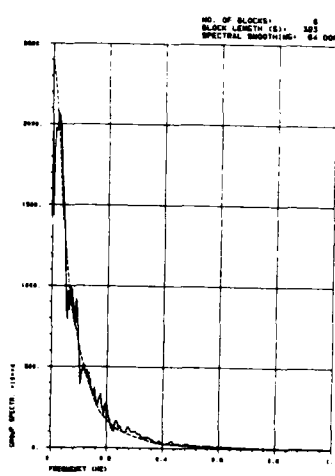
WAVE GROUP SPECTRA in front of Stiff Model

Input: JONSWAP $\cos^8 \theta$

$T_p = 4.3\text{s}$ $H_s = 1.0\text{m}$ $\text{Gam} = 3.3$
Run number: 162 Channel no.: 11



$T_p = 5.0\text{s}$ $H_s = 1.5\text{m}$ $\text{Gam} = 3.3$
Run number: 163 Channel no.: 11



[Without Model]

[With Model]

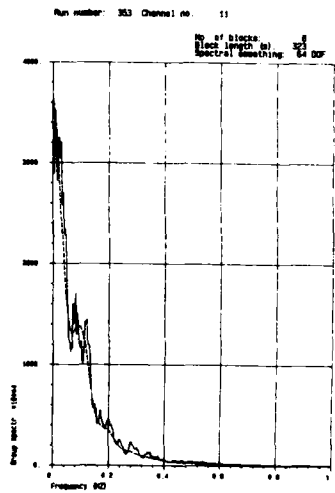
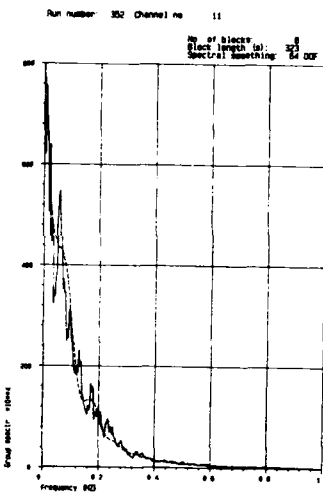


Fig. 3.117

3.2.3 Mooring line forces

Results are shown for force sensor no. 10, 11 and 12 (channel 33, 34 and 35), see fig. 2.18. These sensors measure tension forces in mooring lines going from the pontoons and in front of the breakwater. By simple reasoning one realizes that these forces (plus sensor no. 7, 8, 9) are likely to be larger than the forces in the lines going behind the breakwater (sensors 1-6), due to expected non-linear offset in the sway motion (y-position). This assumption is verified by the experiments, except from the case with very long regular waves (6.3s period), where the forces in the opposite lines were slightly larger (see the Data Reports).

The first 3 plots (figs. 3.118 - 3.120) show the maximum force and RMS value (square root of (square mean + variance)) for each of the 3 sensors, as a function of the input (calibrated) significant wave height $H_{mo,o}$. The next 3 plots (figs. 3.121 - 3.123) show the maximum force deviation from the static force value, and the RMS deviation, normalized by $H_{mo,o}$, as a function of the input peak wave period T_p . Plots of force spectra, linear transfer functions and coherence/phase functions, for each of the 3 sensors, follow next (figs. 3.124 - 3.132). Wave staff 11 in front of the model is used as a reference (see section 2.5). Figs. 3.133 - 3.135 present statistics of force maxima in each test run (actually: force minima, since the force sensor gave negative signals with reversed sign), compared to Rayleigh curves. Finally, figs. 3.136 - 3.147 illustrate the coupling between the 3 force sensors, and between forces and selected motions (sway-heave-roll) by coherence/phase analysis.

Note that "mean amplitude" in the statistics diagrams means "mean amplitude of the deviation from the mean force". Thus the "mean force" is the starting left point of the Rayleigh curve.

The absolute maximum force measured with this model was 98 kN (test run no. 353, force sensor no. 7).

MAXIMUM AND RMS VALUES vs INPUT SIGNIFICANT WAVE HEIGHT
 ANCHOR LINE FORCE NO. 10 STIFF MODEL

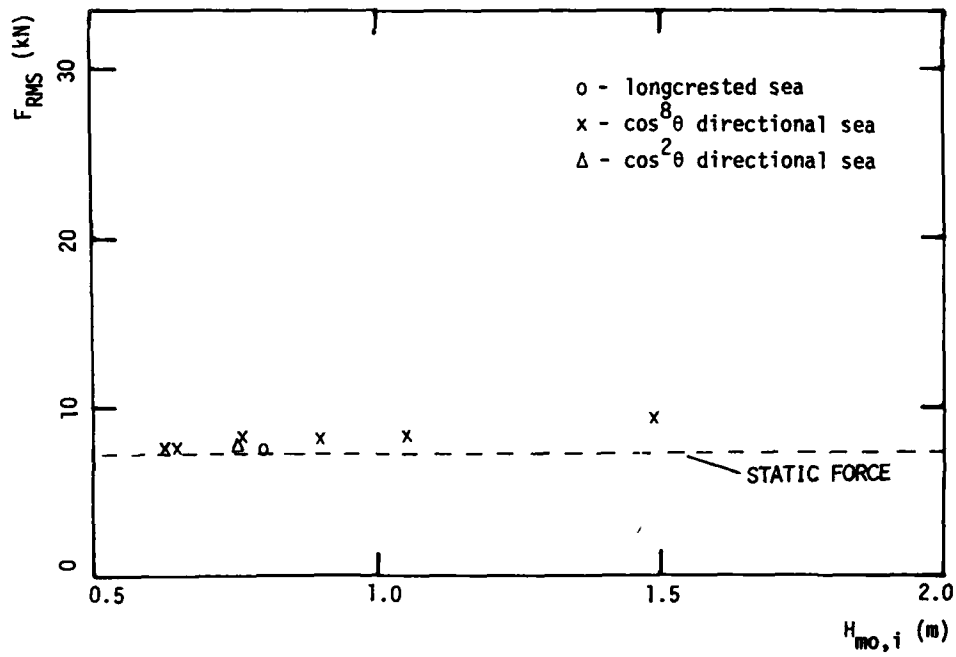
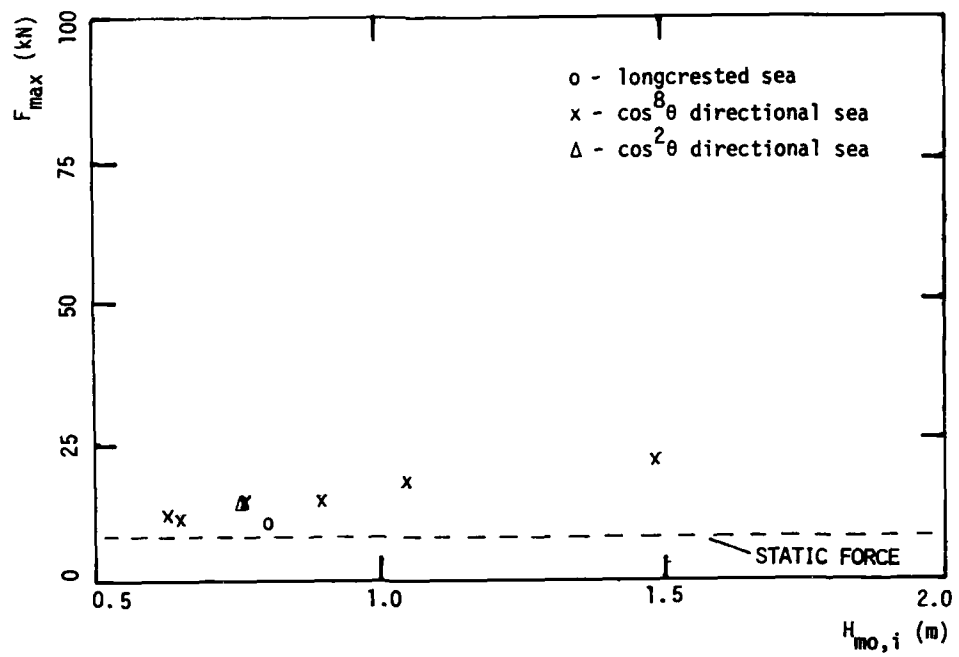


Fig. 3.118

MAXIMUM AND RMS VALUES vs INPUT SIGNIFICANT WAVE HEIGHT
 ANCHOR LINE FORCE NO. 11 STIFF MODEL

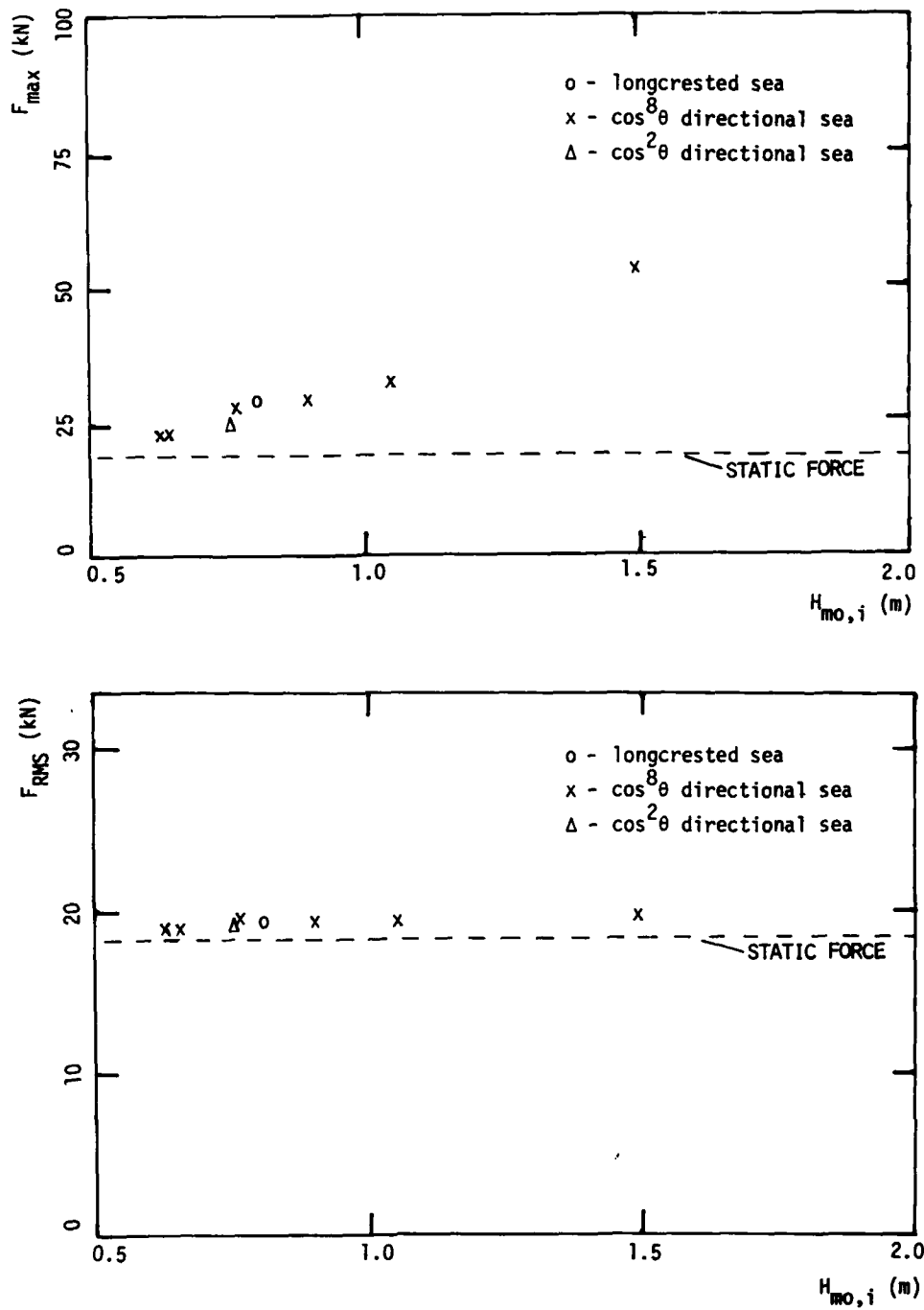


Fig. 3.119

MAXIMUM AND RMS VALUES VS INPUT SIGNIFICANT WAVE HEIGHT
 ANCHOR LINE FORCE NO. 12 STIFF MODEL

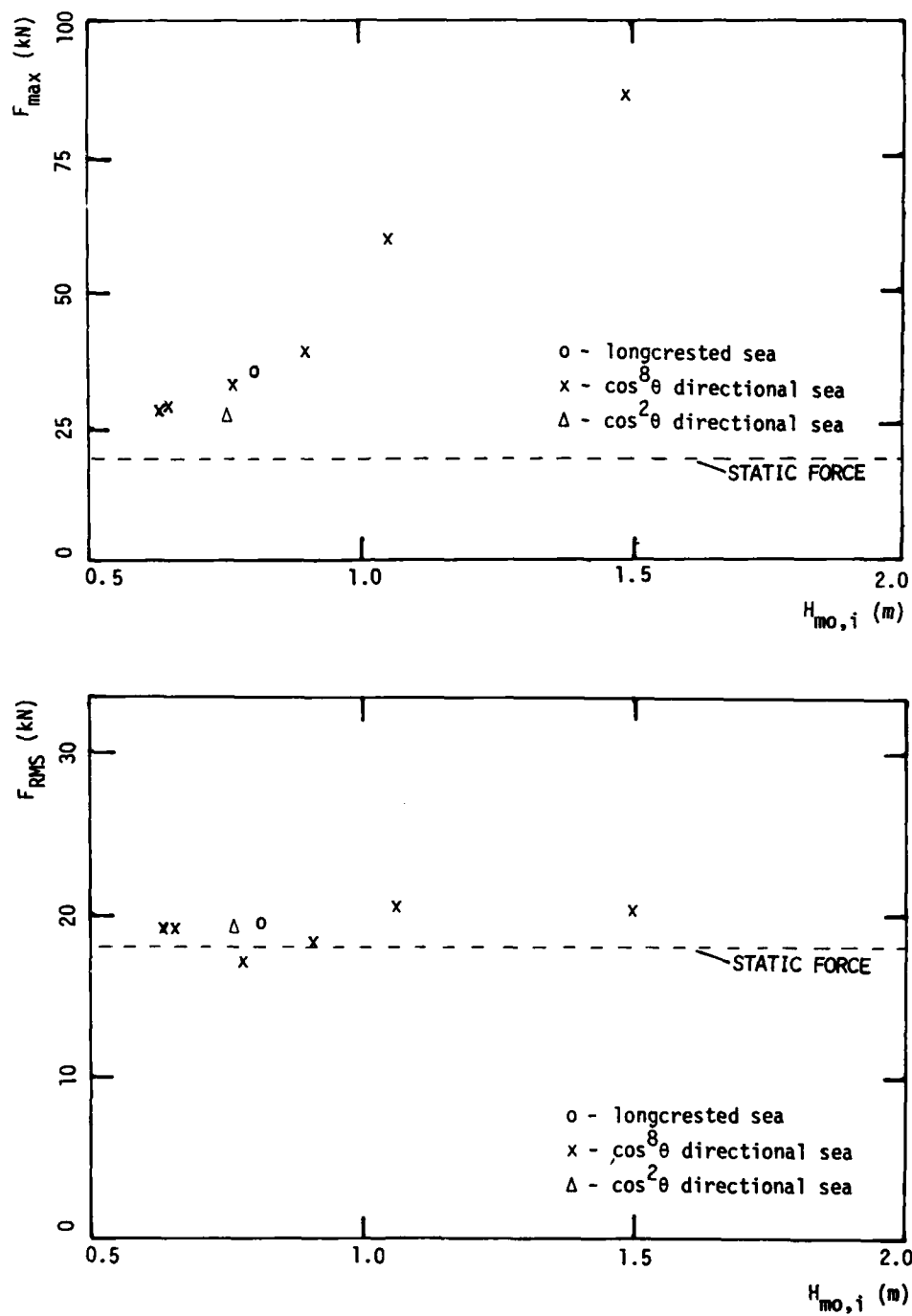


Fig. 3.120

NORMALIZED MAXIMUM AND RMS VALUES VS PEAK PERIOD OF INPUT WAVE

ANCHOR LINE FORCE NO. 10 STIFF MODEL

STATIC FORCE HAS BEEN SUBTRACTED FROM SIGNAL

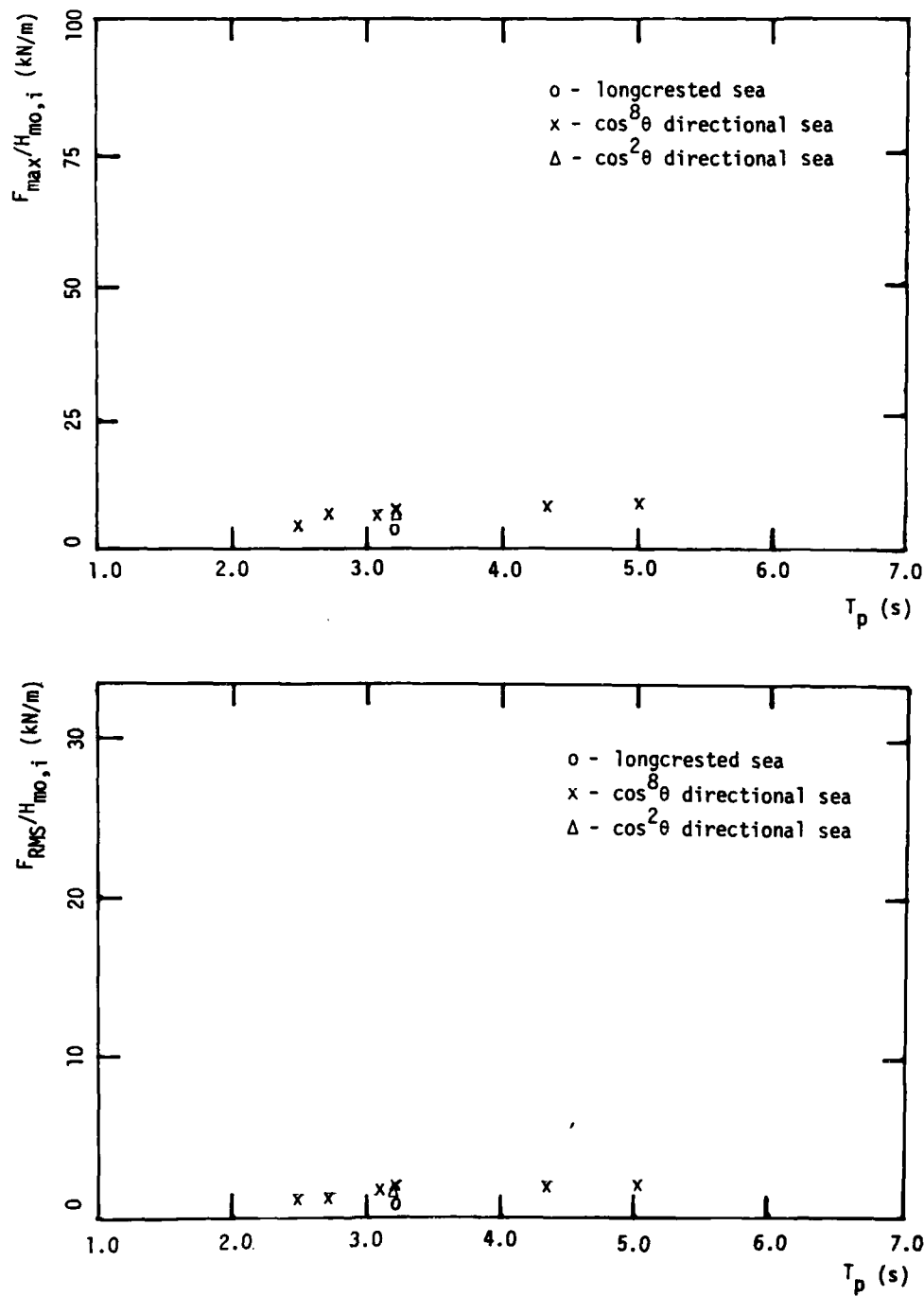


Fig. 3.121

NORMALIZED MAXIMUM AND RMS VALUES VS PEAK PERIOD OF INPUT WAVE

ANCHOR LINE FORCE NO. 11 STIFF MODEL

STATIC FORCE HAS BEEN SUBTRACTED FROM SIGNAL

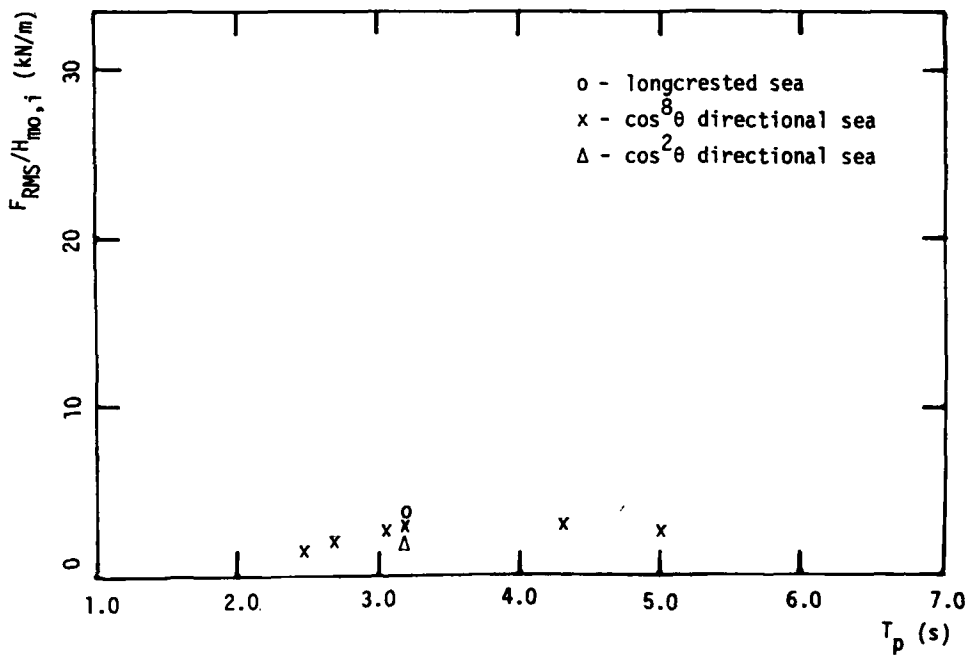
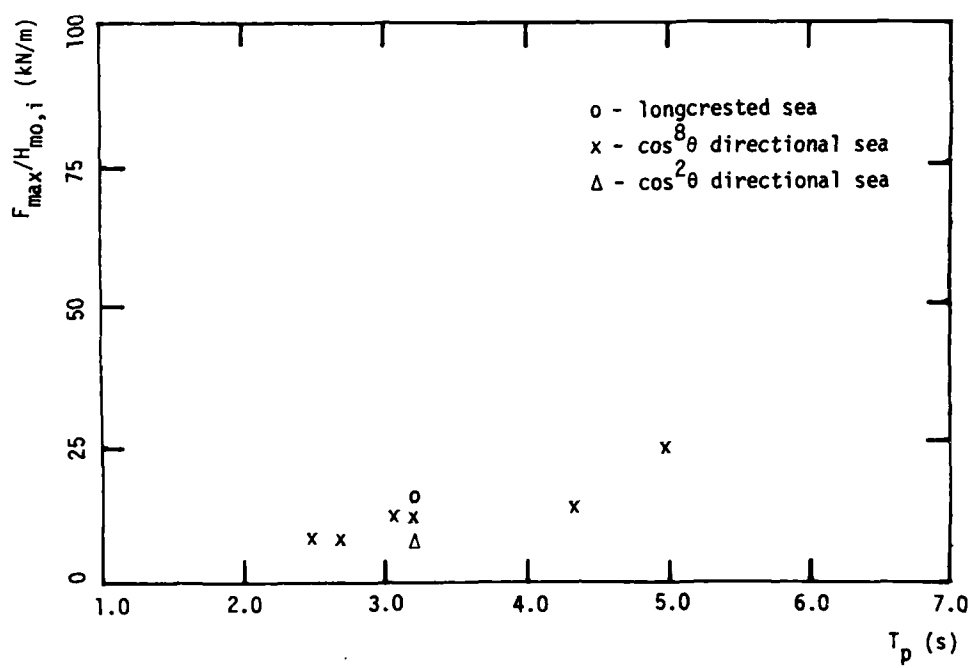


Fig. 3.122

NORMALIZED MAXIMUM AND RMS VALUES VS PEAK PERIOD OF INPUT WAVE

ANCHOR LINE FORCE NO. 12 STIFF MODEL

STATIC FORCE HAS BEEN SUBTRACTED FROM SIGNAL

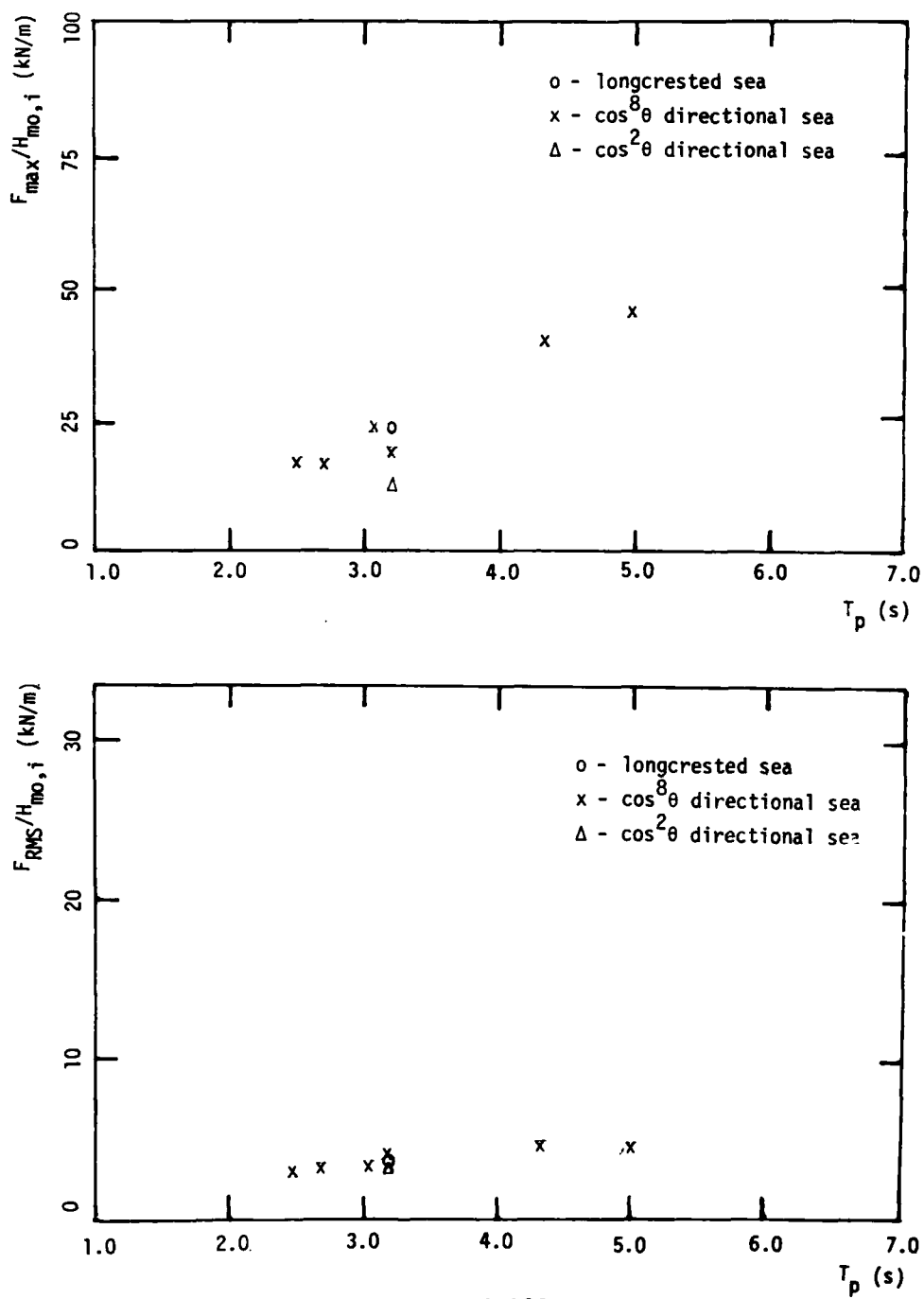


Fig. 3.123

SPECTRAL ANALYSIS FORCE NO.10 Stiff Model Input: JONSWAP $T_p = 3.2s$ $H_s = 0.75m$ $\Gamma_m = 3.3$

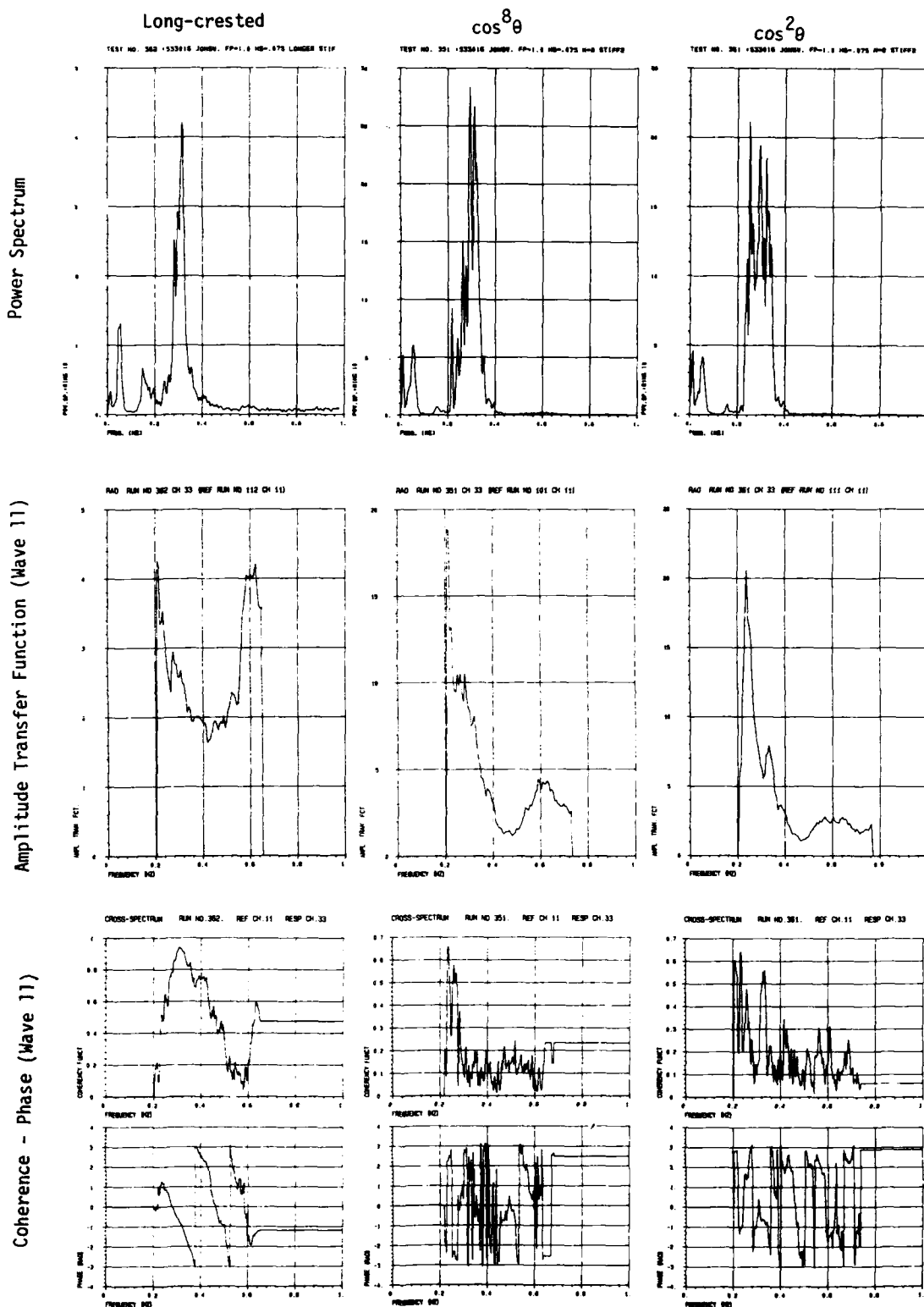


Fig. 3.124

SPECTRAL ANALYSIS FORCE NO.10 Stiff Model Input: JONSWAP $\cos^8 \theta$

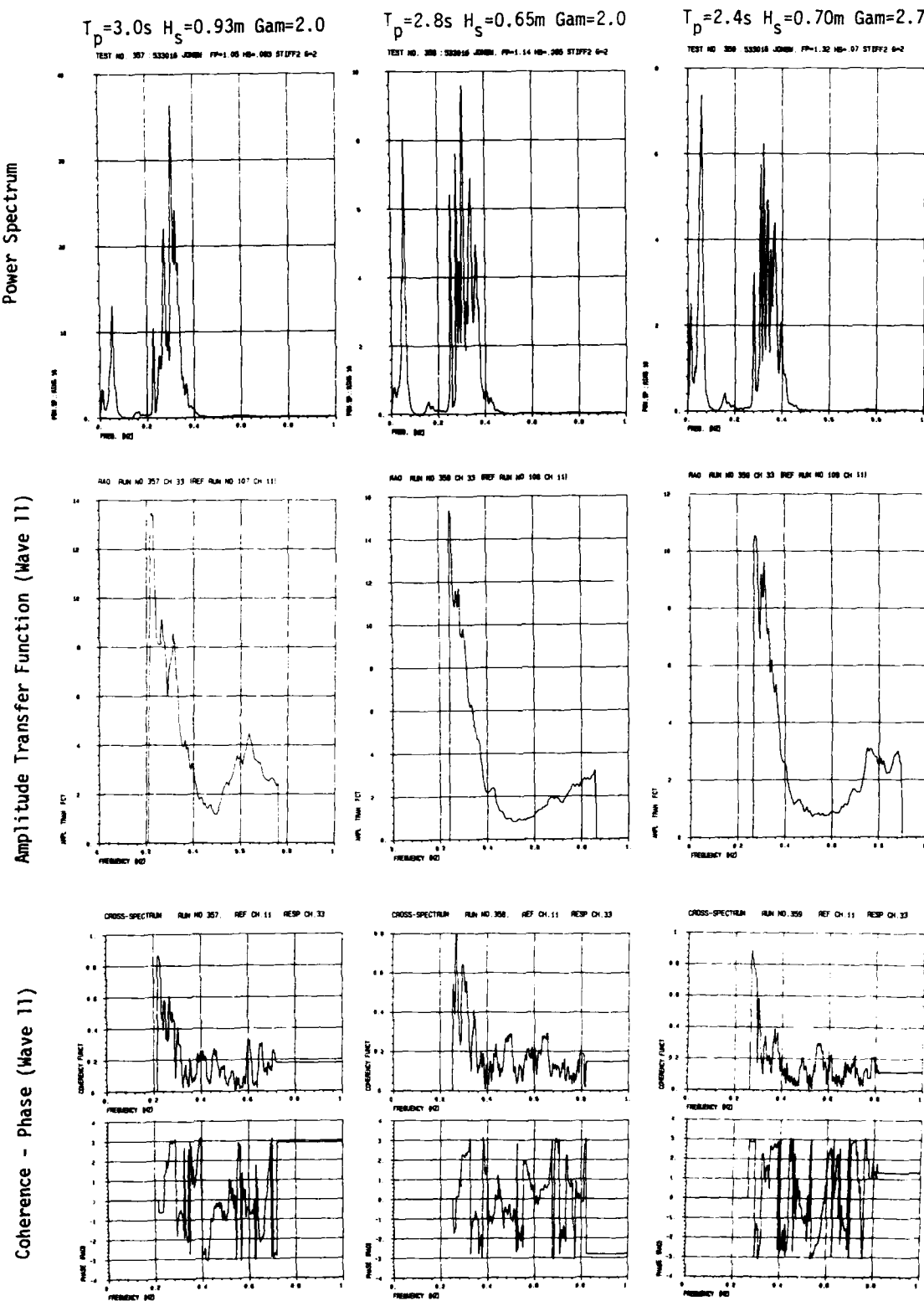


Fig. 3.125

SPECTRAL ANALYSIS FORCE NO.10 Stiff Model Input: JONSWAP $\cos^8 \theta$

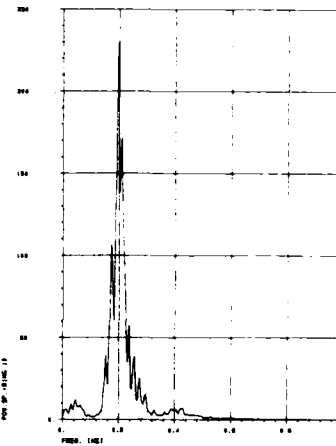
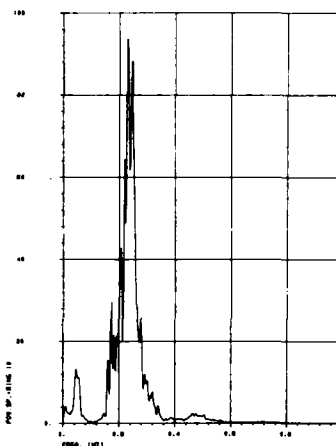
$T_p = 4.3\text{s}$ $H_s = 1.0\text{m}$ $\Gamma_{\text{am}} = 3.3$

TEST NO. 352 - 533816 JONSWP FP=74 H=1.0 H=0 STIFF2

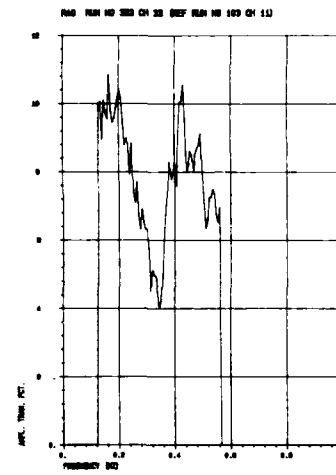
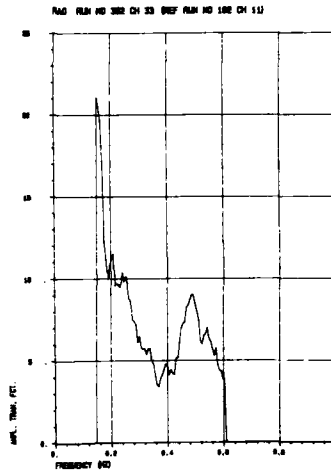
$T_p = 5.0\text{s}$ $H_s = 1.5\text{m}$ $\Gamma_{\text{am}} = 3.3$

TEST NO. 353 - 533816 JONSWP FP=65 H=1.5 H=0 STIFF2

Power Spectrum



Amplitude Transfer Function (Wave 11)



Coherence - Phase (Wave 11)

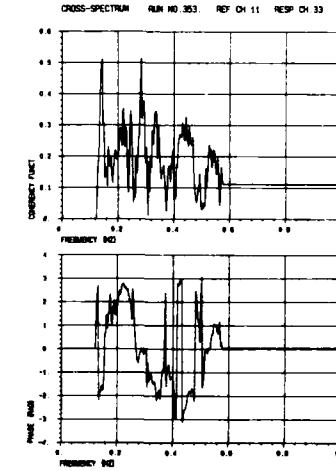
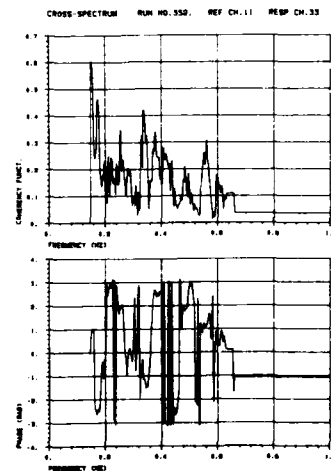


Fig. 3.126

SPECTRAL ANALYSIS FORCE NO.11 Stiff Model Input: JONSWAP $T_p = 3.2s$ $H_s = 0.75m$ $Gam = 3.3$

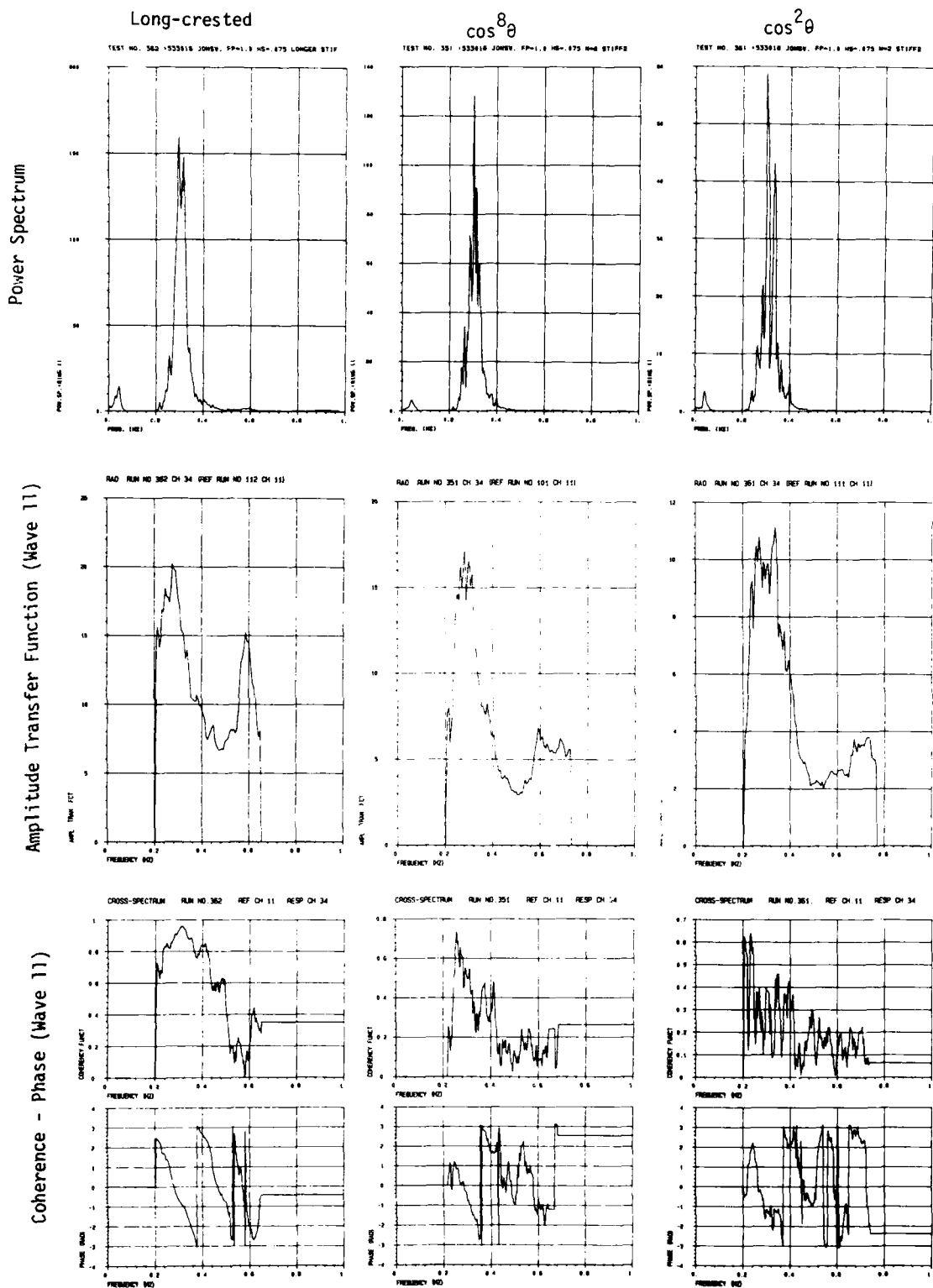


Fig. 3.127

SPECTRAL ANALYSIS FORCE NO.11 Stiff Model Input: JONSWAP $\cos^8 \theta$

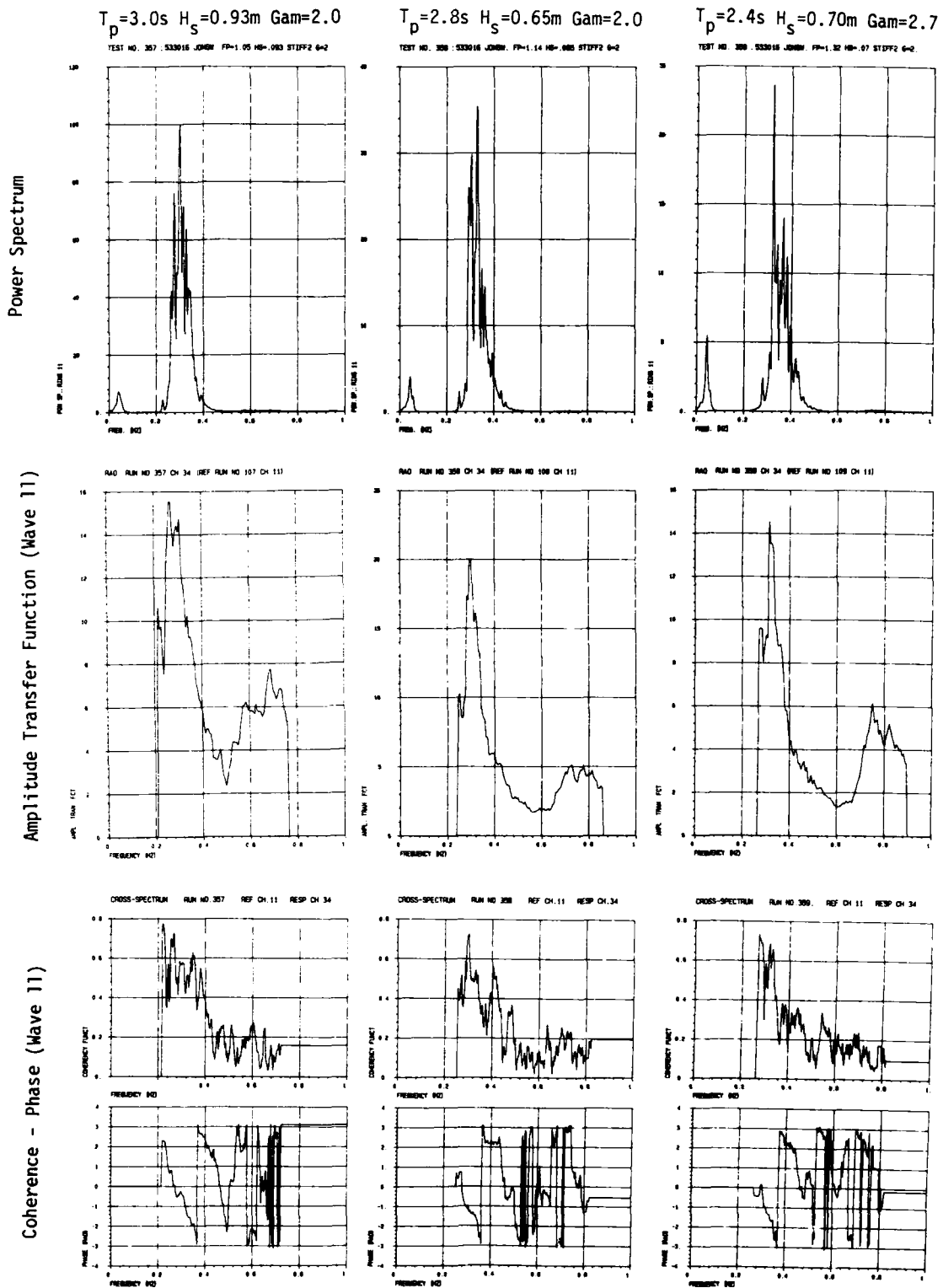


Fig. 3.128

SPECTRAL ANALYSIS FORCE NO.11 Stiff Model Input: JONSWAP $\cos^8 \theta$

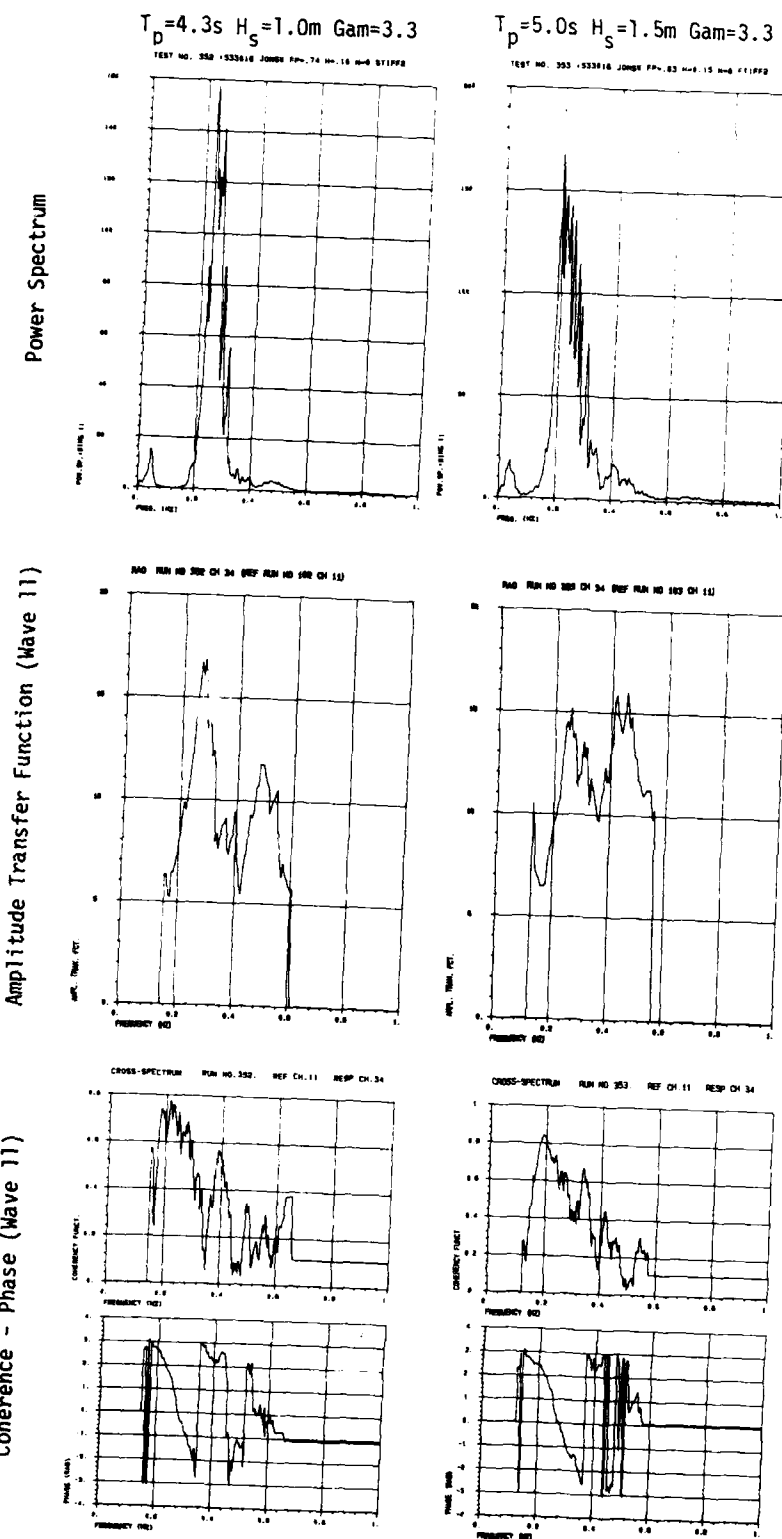


Fig. 3.129

SPECTRAL ANALYSIS FORCE NO.12 Stiff Model Input: JONSWAP

$T_p = 3.2\text{s}$ $H_s = 0.75\text{m}$ $\text{Gam} = 3.3$

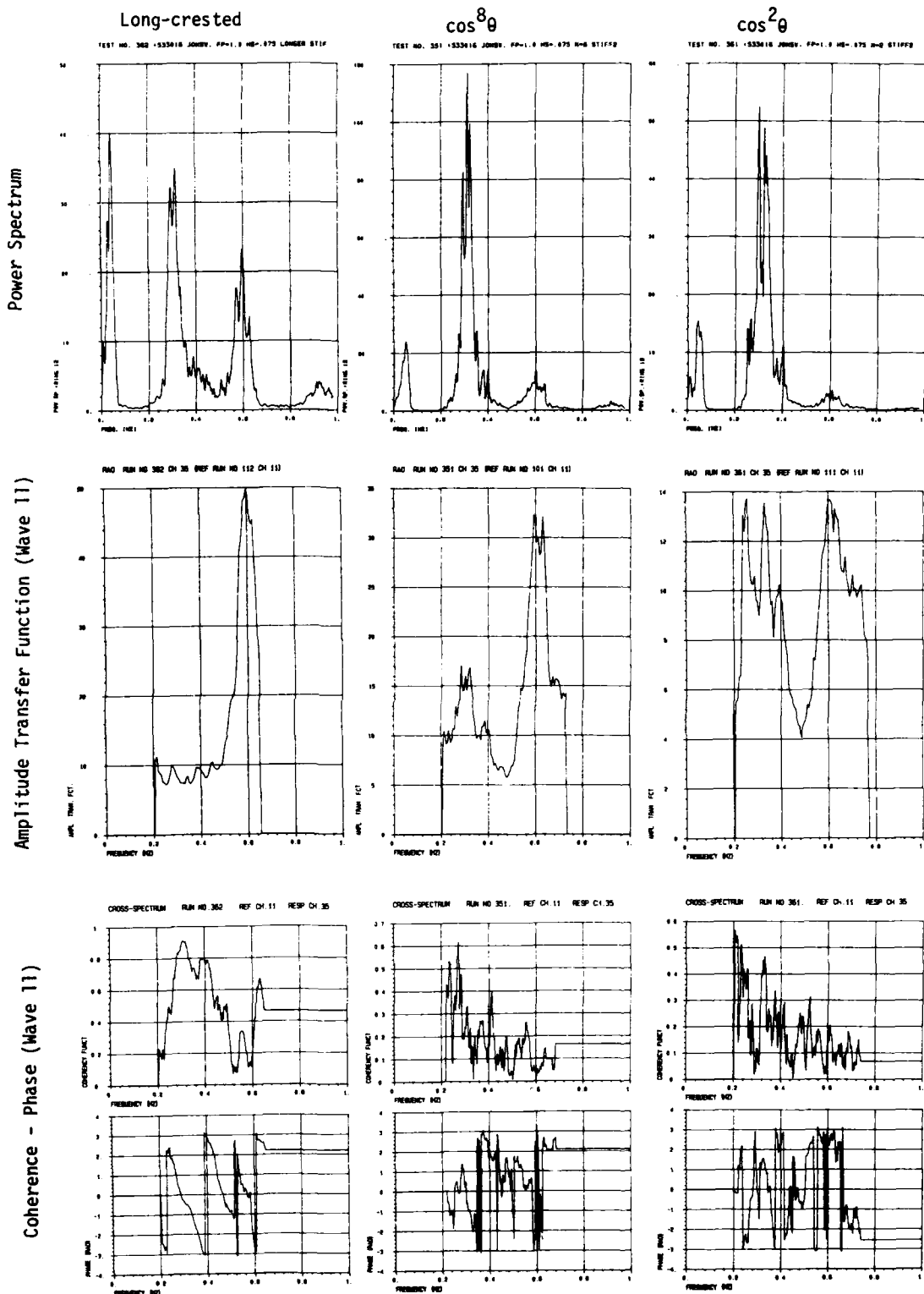


Fig. 3.130

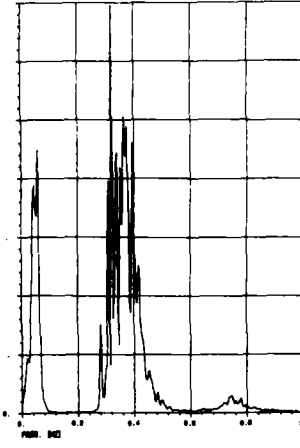
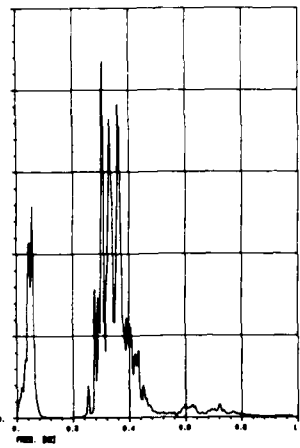
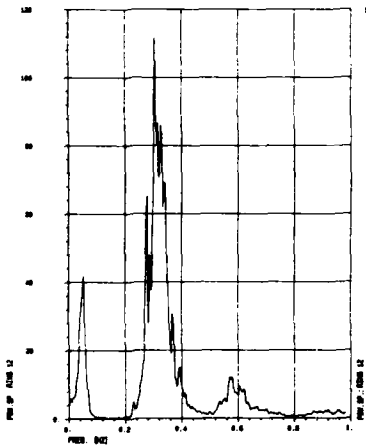
SPECTRAL ANALYSIS FORCE NO.12 Stiff Model Input: JONSWAP $\cos^8 \theta$

$T_p = 3.0\text{s}$ $H_s = 0.93\text{m}$ $\text{Gam} = 2.0$
TEST NO. 357 : 533016 JONSWP. FP=1.05 HS=.093 STIFF2 0-2

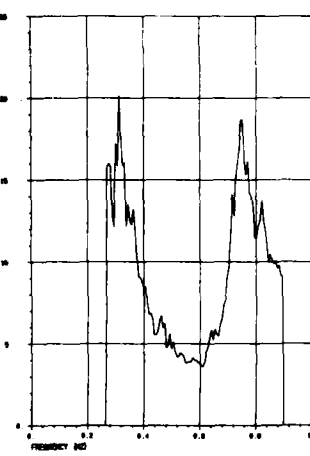
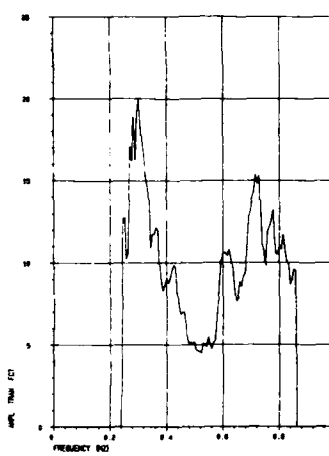
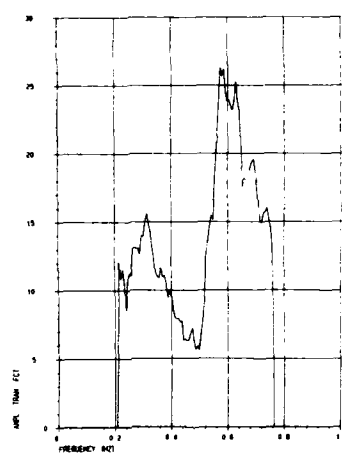
$T_p = 2.8\text{s}$ $H_s = 0.65\text{m}$ $\text{Gam} = 2.0$
TEST NO. 358 : 533016 JONSWP. FP=1.14 HS=.065 STIFF2 0-2

$T_p = 2.4\text{s}$ $H_s = 0.70\text{m}$ $\text{Gam} = 2.7$
TEST NO. 359 : 533016 JONSWP. FP=1.32 HS=.07 STIFF2 0-2

Power Spectrum



Amplitude Transfer Function (Wave 11)



Coherence - Phase (Wave 11)

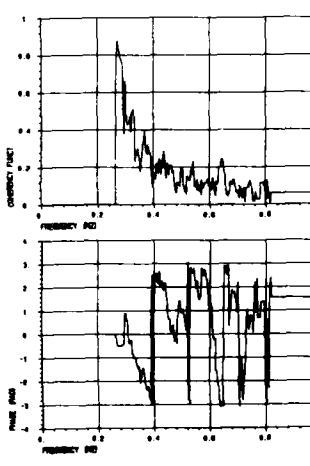
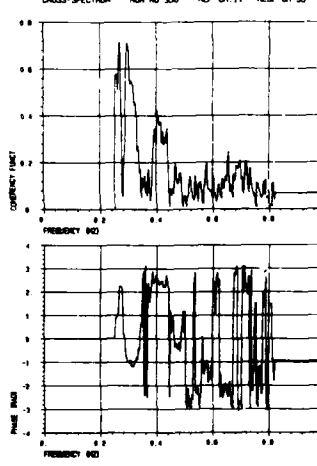
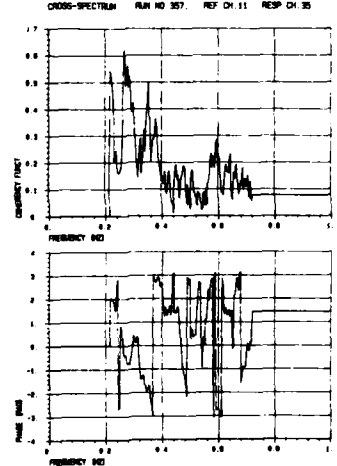


Fig. 3.131

SPECTRAL ANALYSIS FORCE NO.12 Stiff Model Input: JONSWAP $\cos^8 \theta$

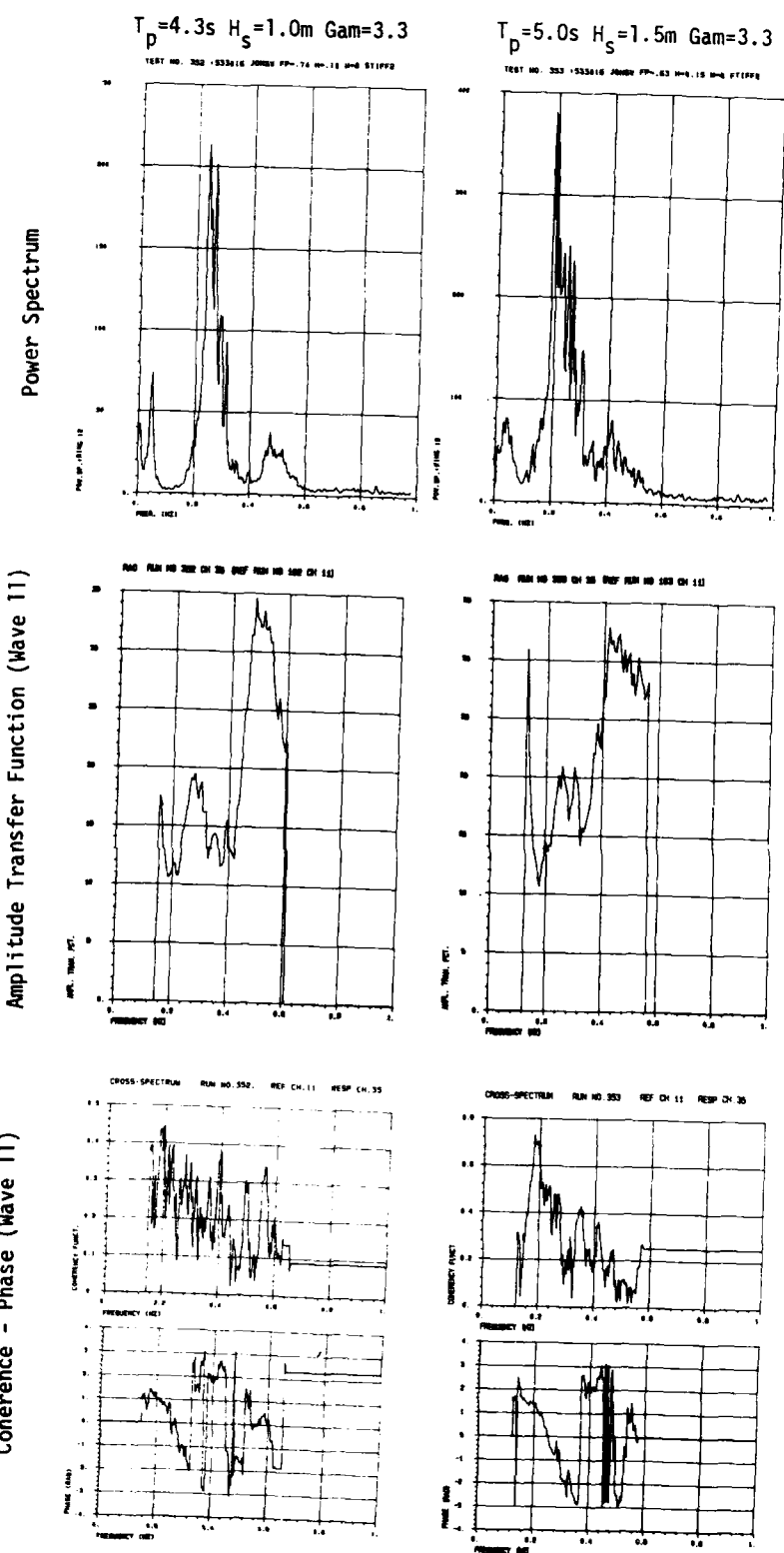


Fig. 3.132

AMPLITUDE STATISTICS FORCE Stiff Model Input: JONSWAP $T_p = 3.2\text{s}$ $H_s = 0.75\text{m}$ $\text{Gam} = 3.3$

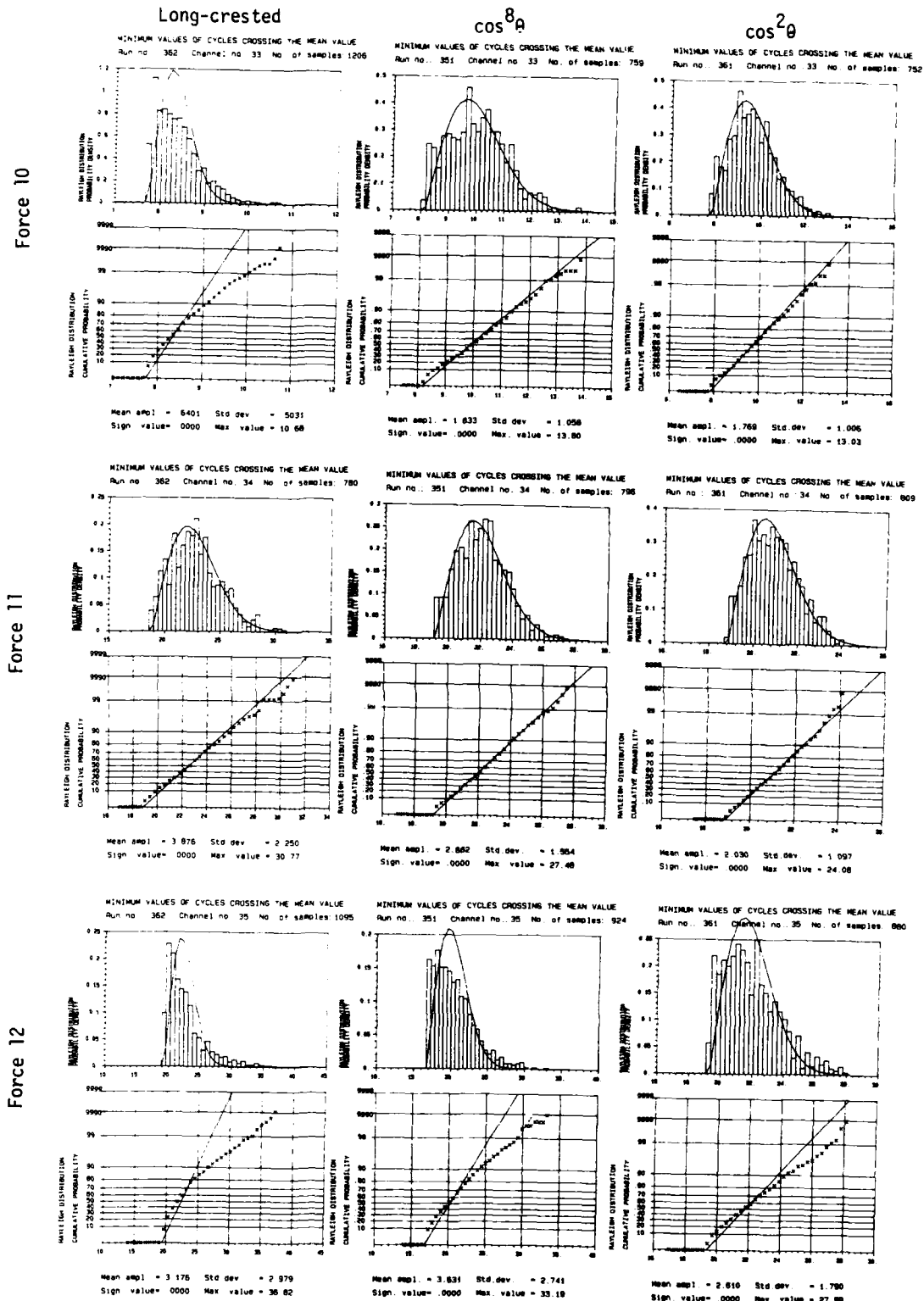
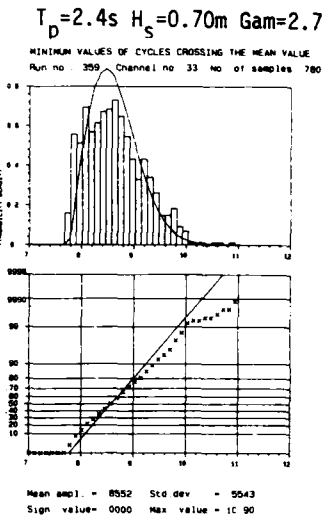
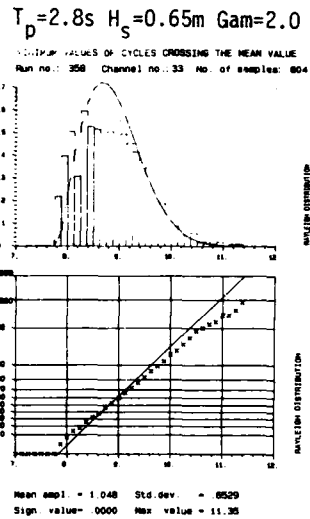
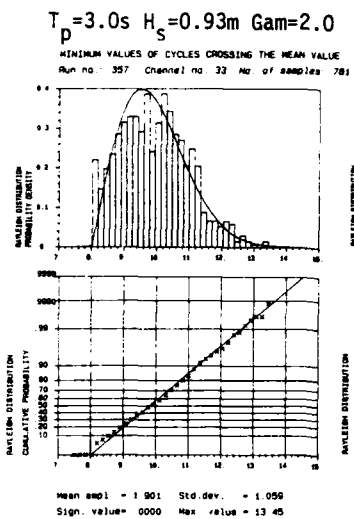


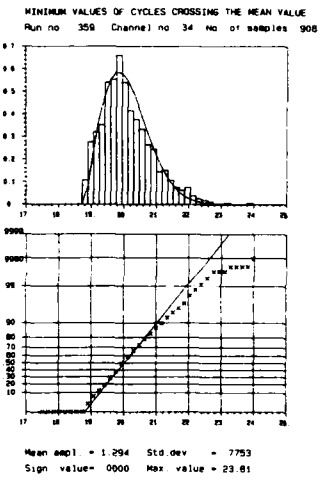
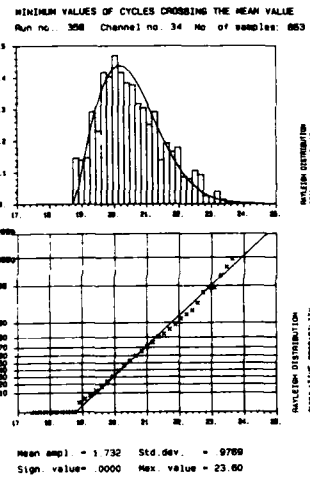
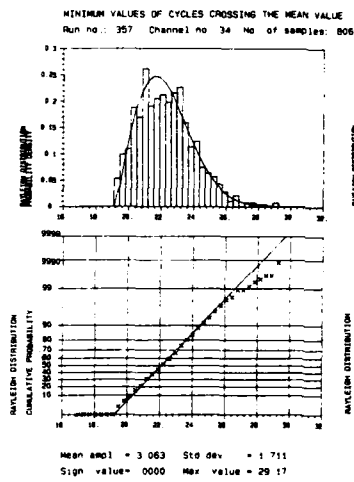
Fig. 3.133

AMPLITUDE STATISTICS FORCE Stiff Model Input: JONSWAP $\cos^8 \theta$

Force 10



Force 11



Force 12

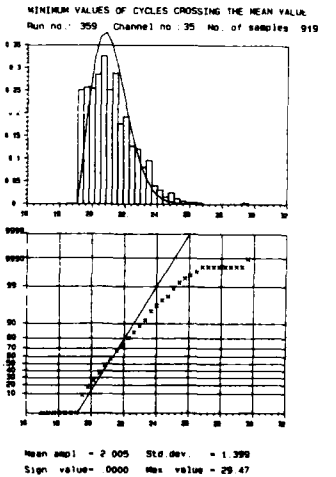
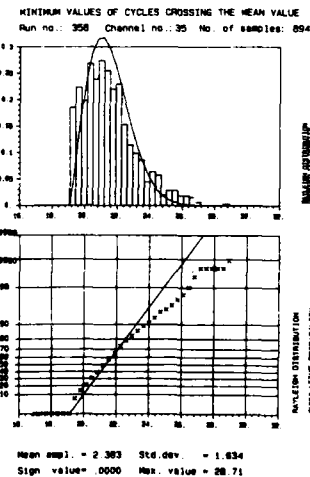
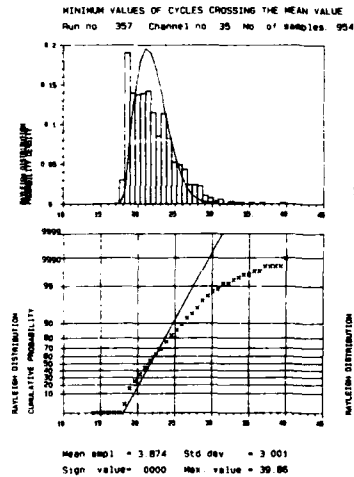


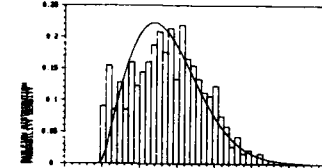
Fig. 3.134

AMPLITUDE STATISTICS FORCE Stiff Model

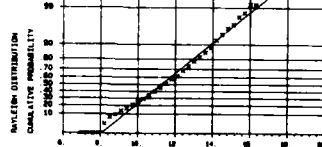
Input: JONSWAP $\cos^8 \theta$

$T_p = 4.3\text{s}$ $H_s = 1.0\text{m}$ $\text{Gam} = 3.3$

MINIMUM VALUES OF CYCLES CROSSING THE MEAN VALUE
Run no : 352 Channel no 33 No. of samples 623

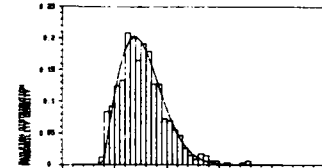


Force 10

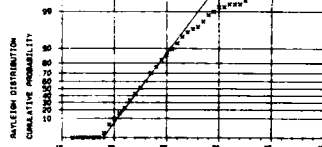


Mean ampl. = 3.414 Std.dev. = 1.900
Sign. value= 0000 Max. value = 17.15

MINIMUM VALUES OF CYCLES CROSSING THE MEAN VALUE
Run no : 352 Channel no 34 No. of samples: 589

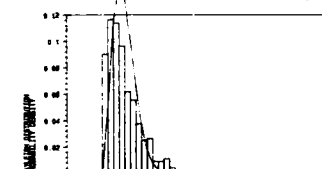


Force 11

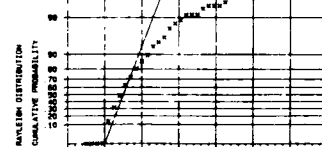


Mean ampl. = 3.745 Std.dev. = 2.225
Sign. value= 0000 Max. value = 32.97

MINIMUM VALUES OF CYCLES CROSSING THE MEAN VALUE
Run no : 352 Channel no 35 No. of samples: 960



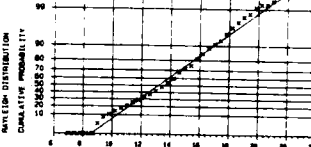
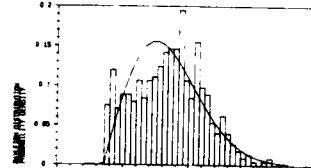
Force 12



Mean ampl. = 5.354 Std.dev. = 4.753
Sign. value= 0000 Max. value = 80.72

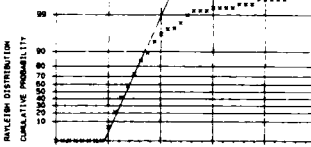
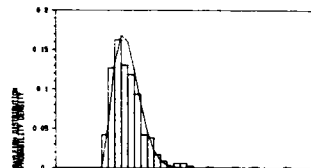
$T_p = 5.0\text{s}$ $H_s = 1.5\text{m}$ $\text{Gam} = 3.3$

MINIMUM VALUES OF CYCLES CROSSING THE MEAN VALUE
Run no : 353 Channel no 33 No. of samples 563



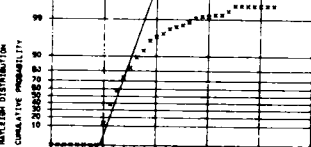
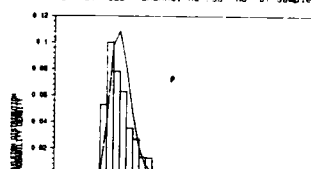
Mean ampl. = 4.874 Std.dev. = 2.626
Sign. value= 0000 Max. value = 21.38

MINIMUM VALUES OF CYCLES CROSSING THE MEAN VALUE
Run no : 353 Channel no 34 No. of samples 568



Mean ampl. = 4.473 Std.dev. = 3.402
Sign. value= 0000 Max. value = 53.94

MINIMUM VALUES OF CYCLES CROSSING THE MEAN VALUE
Run no : 353 Channel no 35 No. of samples 1109



Mean ampl. = 6.883 Std.dev. = 7.044
Sign. value= 0000 Max. value = 86.16

Fig. 3.135

COHERENCE-PHASE ANALYSIS FORCE - FORCE Stiff Model Input: JONSWAP $T_d = 3.2\text{s}$ $H_s = 0.75\text{m}$ $\text{Gam} = 3.3$

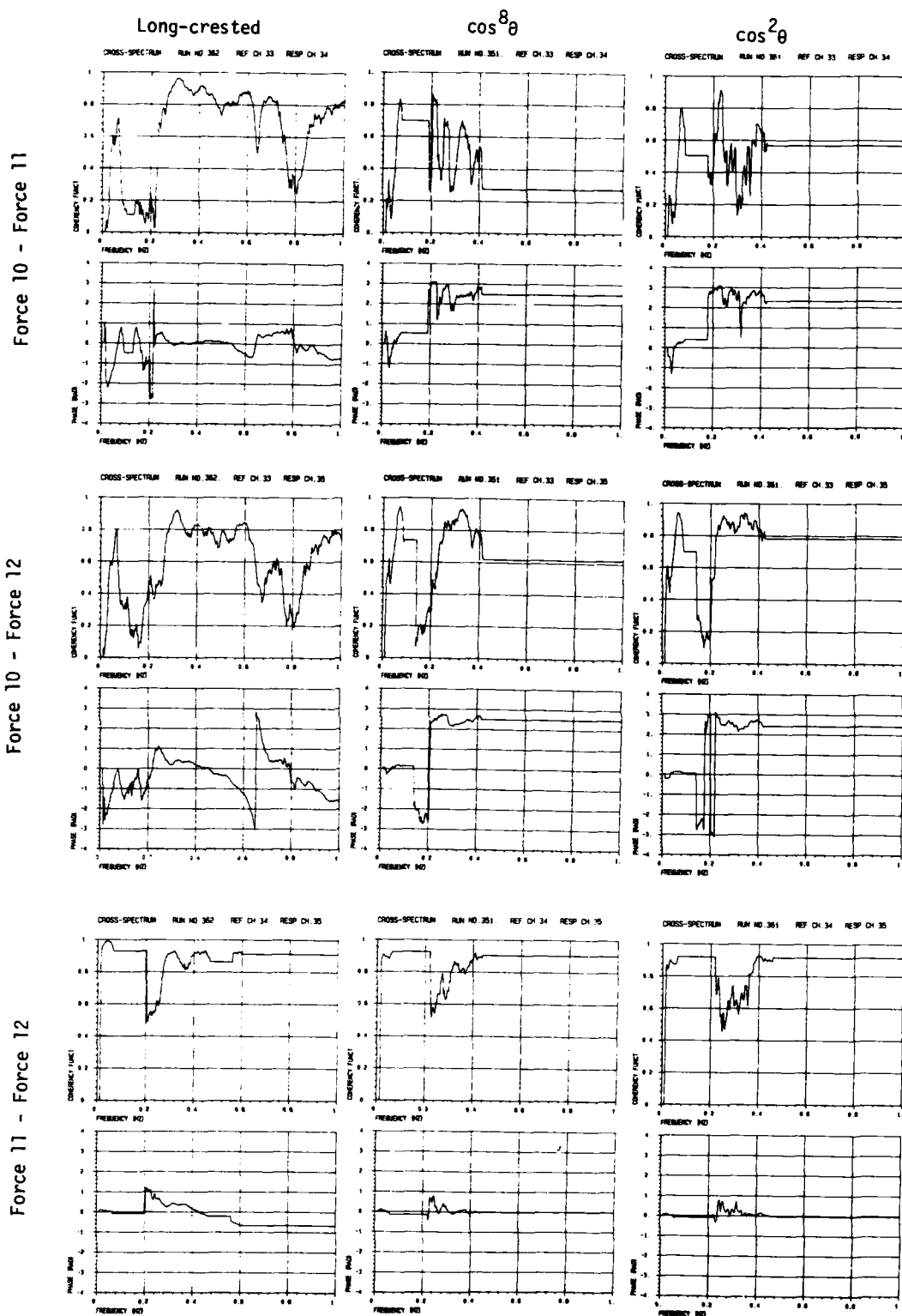


Fig. 3.136

COHERENCE-PHASE ANALYSIS FORCE - FORCE Stiff Model Input: JONSWAP $\cos^8 \theta$

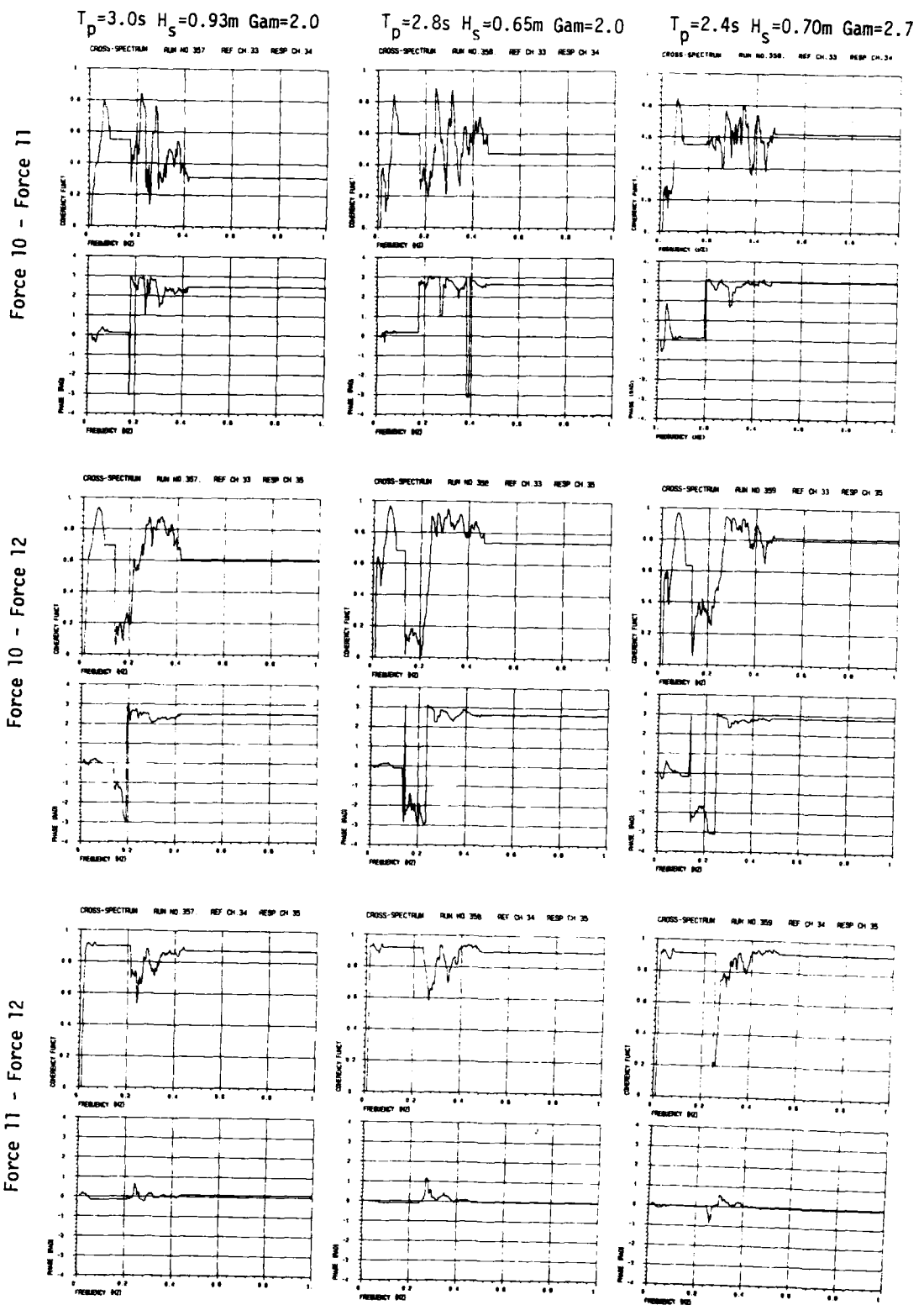


Fig. 3.137

COHERENCE-PHASE ANALYSIS FORCE - FORCE Stiff Model Input: JONSWAP $\cos^8 \theta$

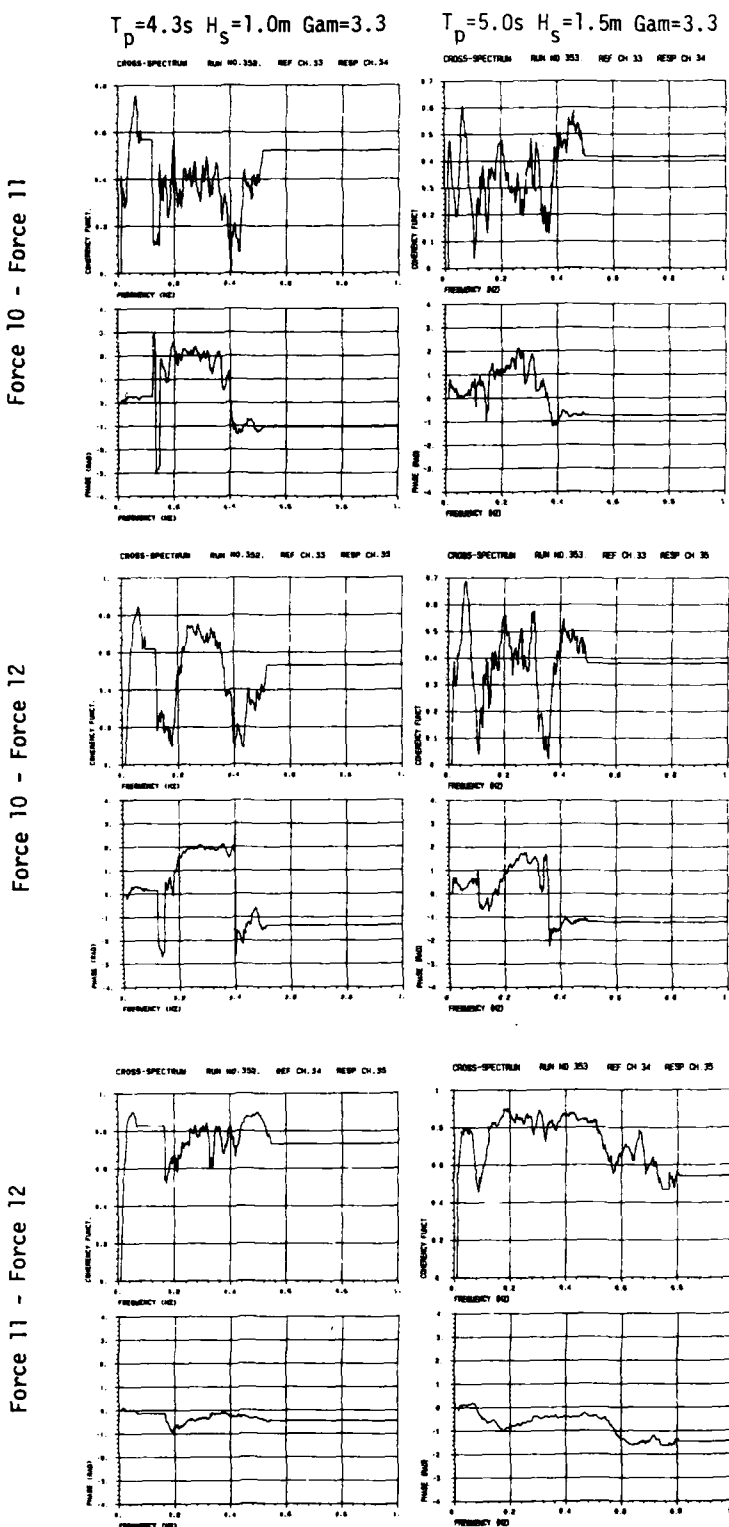


Fig. 3.138

COHERENCE - PHASE ANALYSIS FORCE-MOTION Stiff Model Input: JONSWAF $T_p = 3.2\text{s}$ $H_s = 0.75\text{m}$ $\text{Gam} = 3.3$

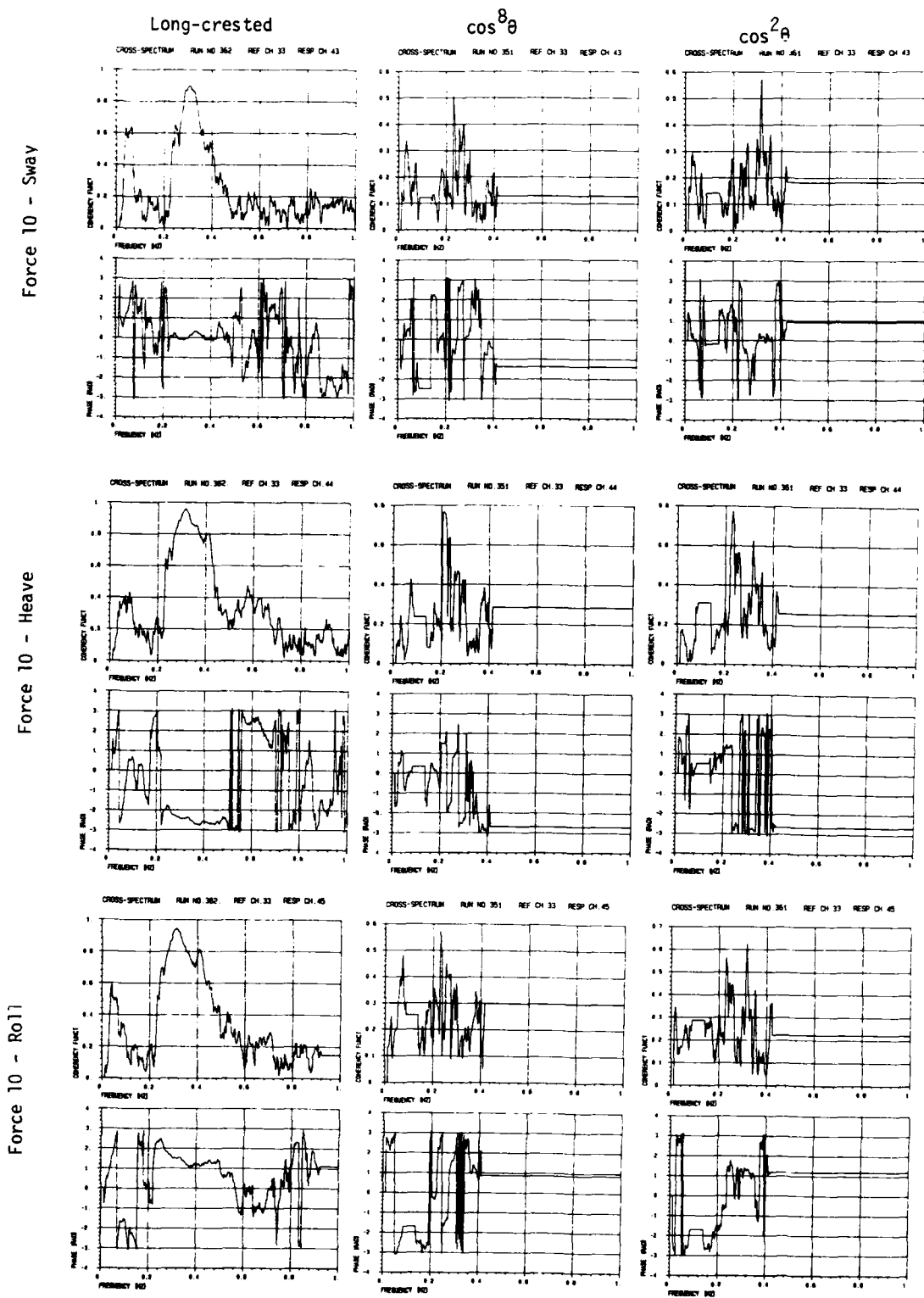


Fig. 3.139

COHERENCE - PHASE ANALYSIS FORCE - MOTION Stiff Model Input: JONSWAP $\cos^8 \theta$

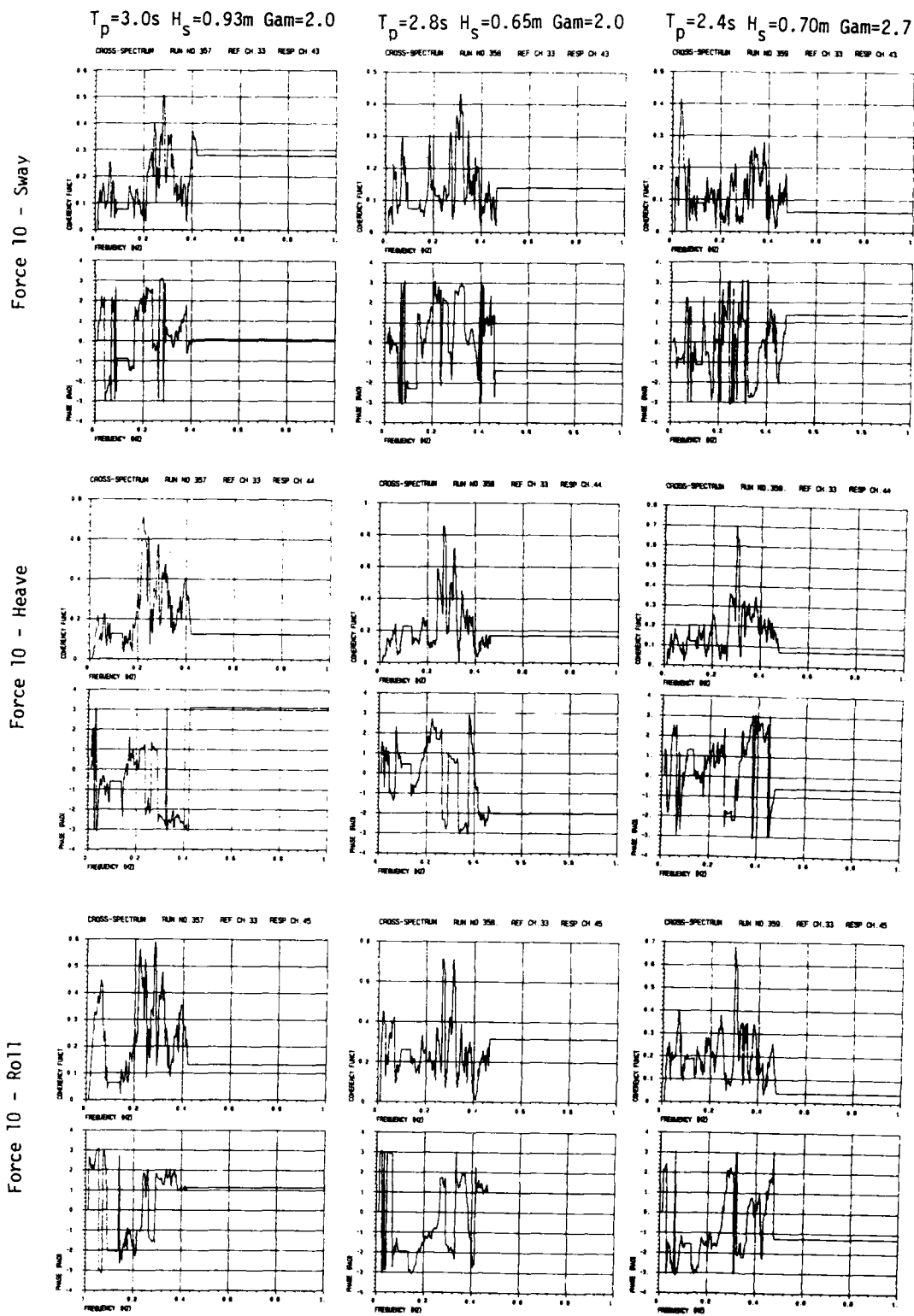


Fig. 3.140

COHERENCE - PHASE ANALYSIS FORCE - MOTION Stiff Model Input: JONSWAP $\cos^8 \theta$

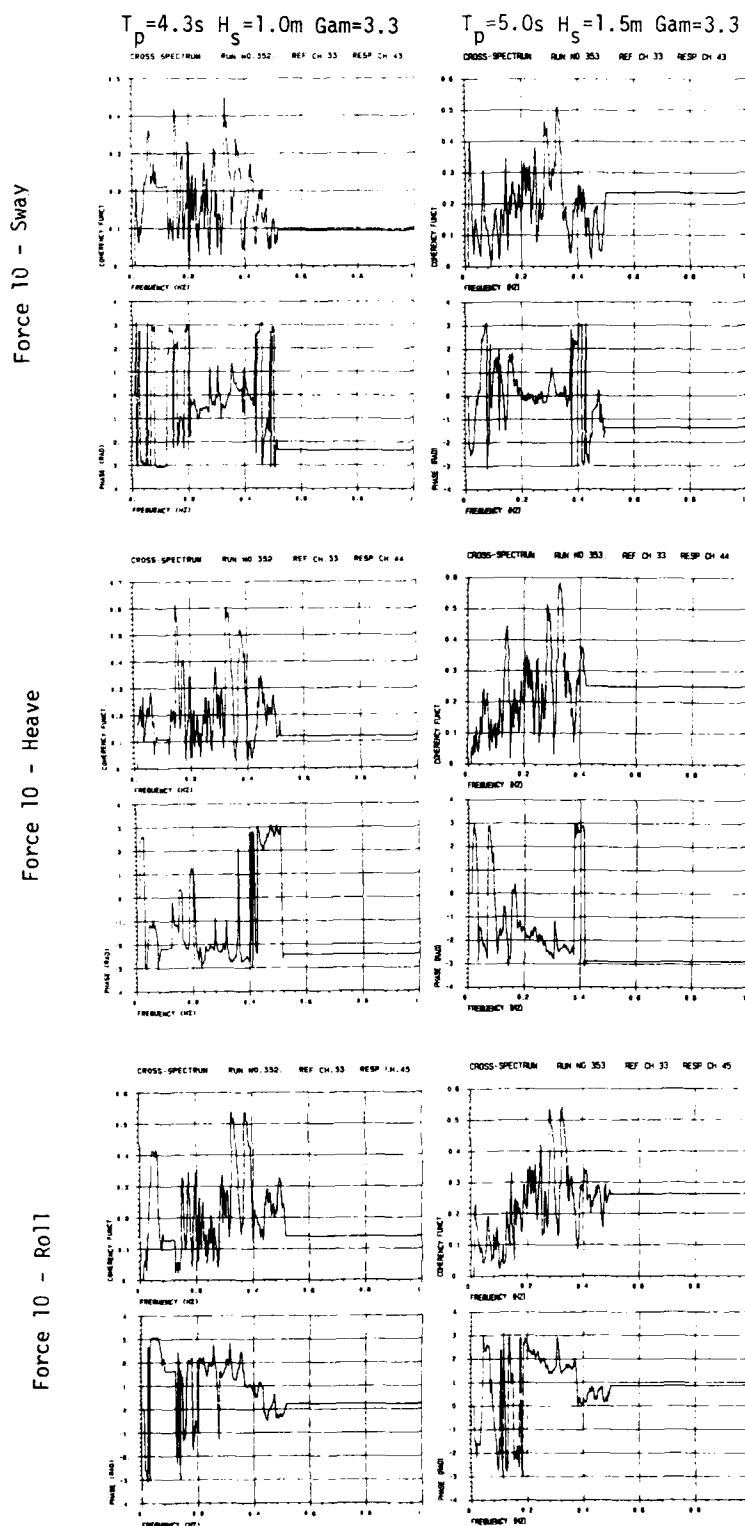


Fig. 3.141

COHERENCE - PHASE ANALYSIS FORCE-MOTION Stiff Model Input: JONSWAP $T_p = 3.2s$ $H_s = 0.75m$ $Gam = 3.3$

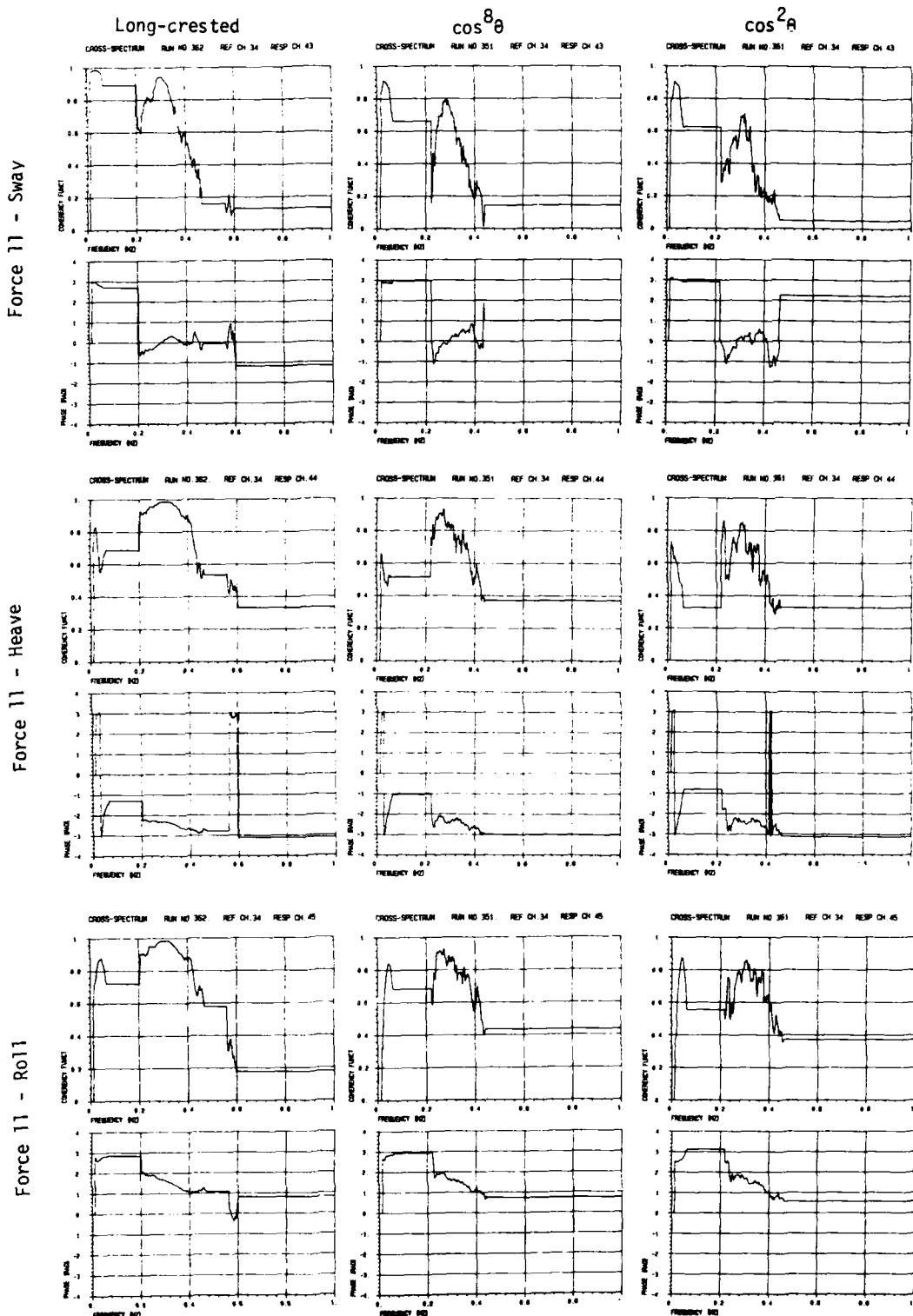


Fig. 3.142

COHERENCE - PHASE ANALYSIS FORCE - MOTION Stiff Model Input: JONSWAP $\cos^8 \theta$

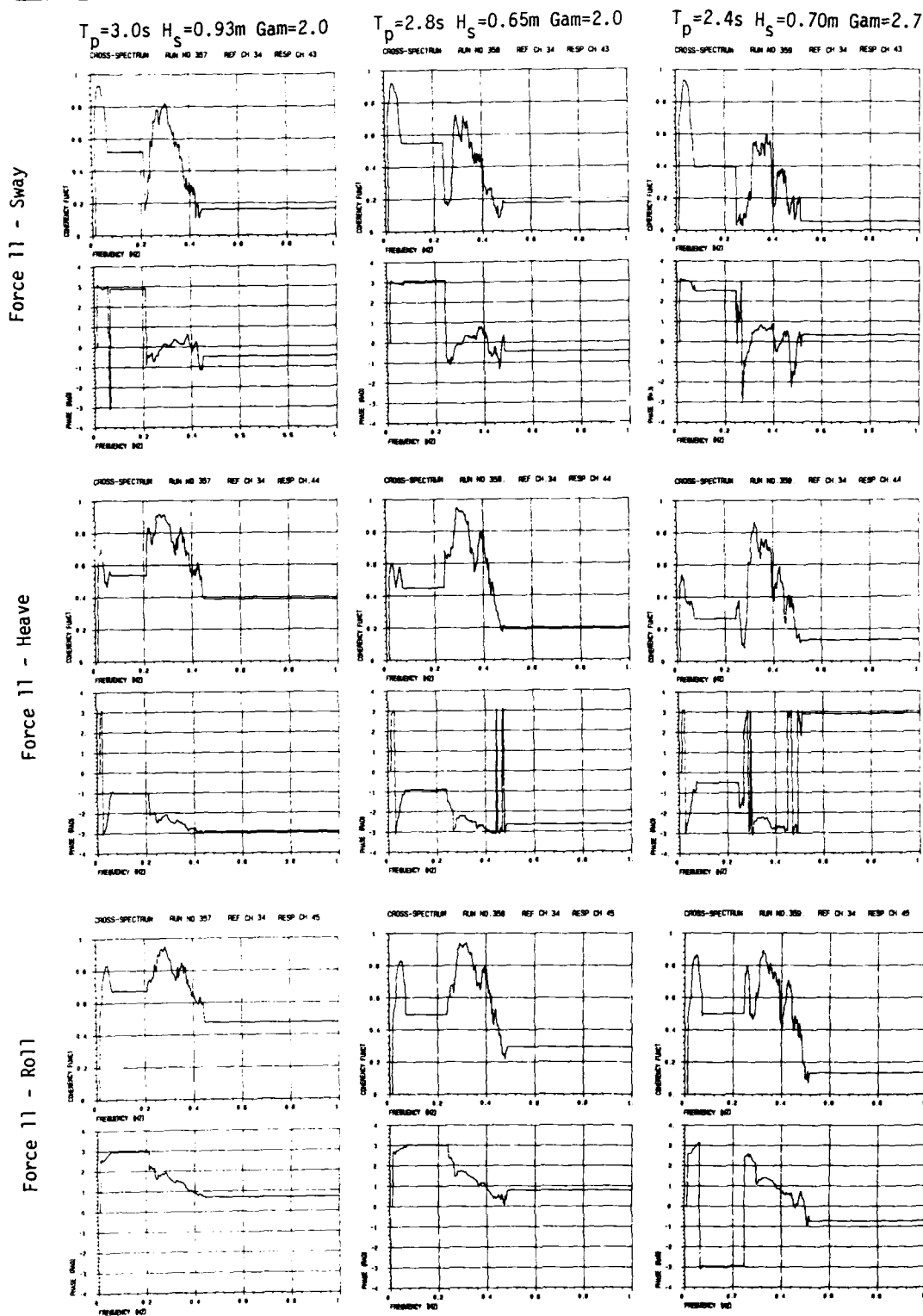


Fig. 3.143

COHERENCE - PHASE ANALYSIS FORCE - MOTION Stiff Model

Input: JONSWAP $\cos^8 \theta_R$

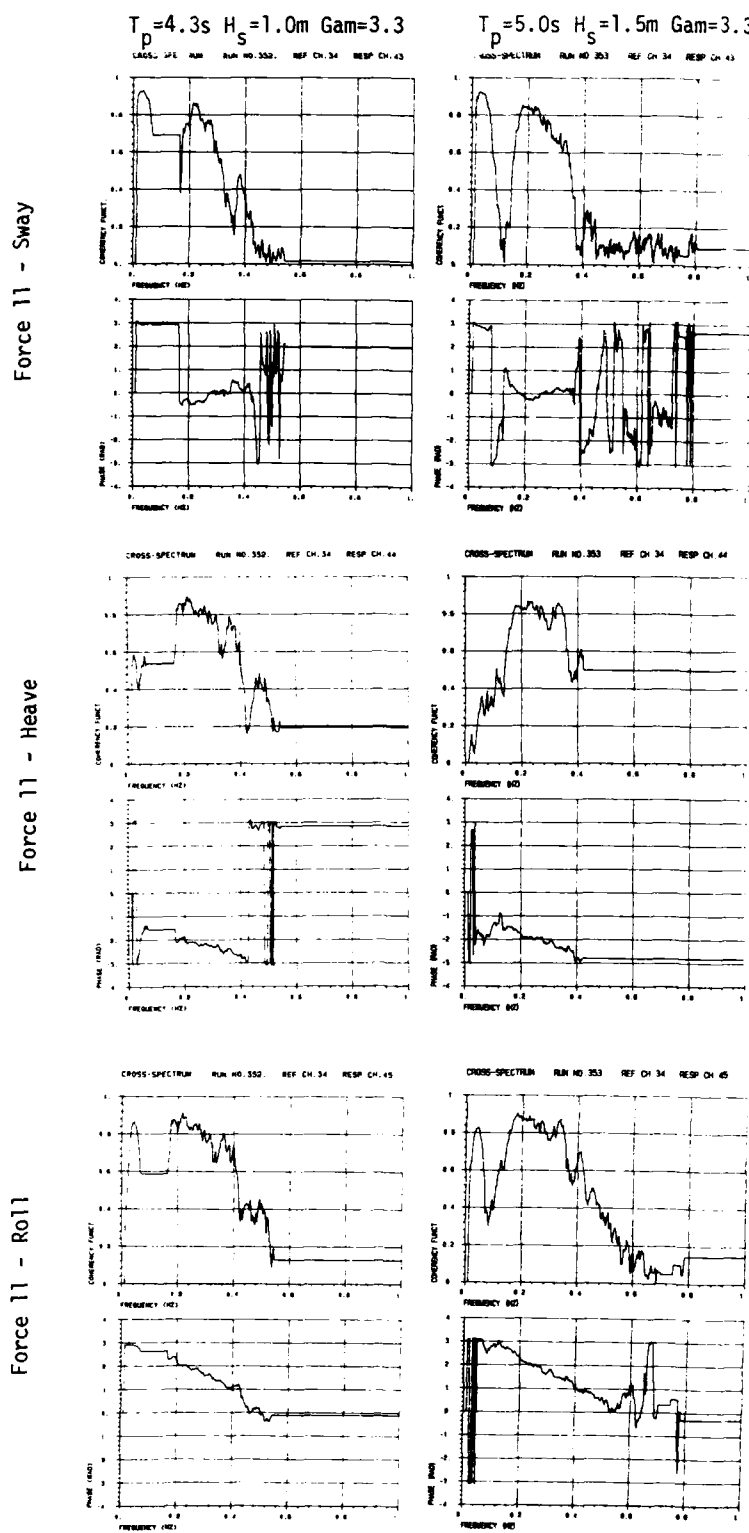


Fig. 3.144

COHERENCE - PHASE ANALYSIS FORCE-MOTION Stiff Model Input: JONSWAP $T_p = 3.2\text{s}$ $H_s = 0.75\text{m}$ $\text{Gam} = 3.3$

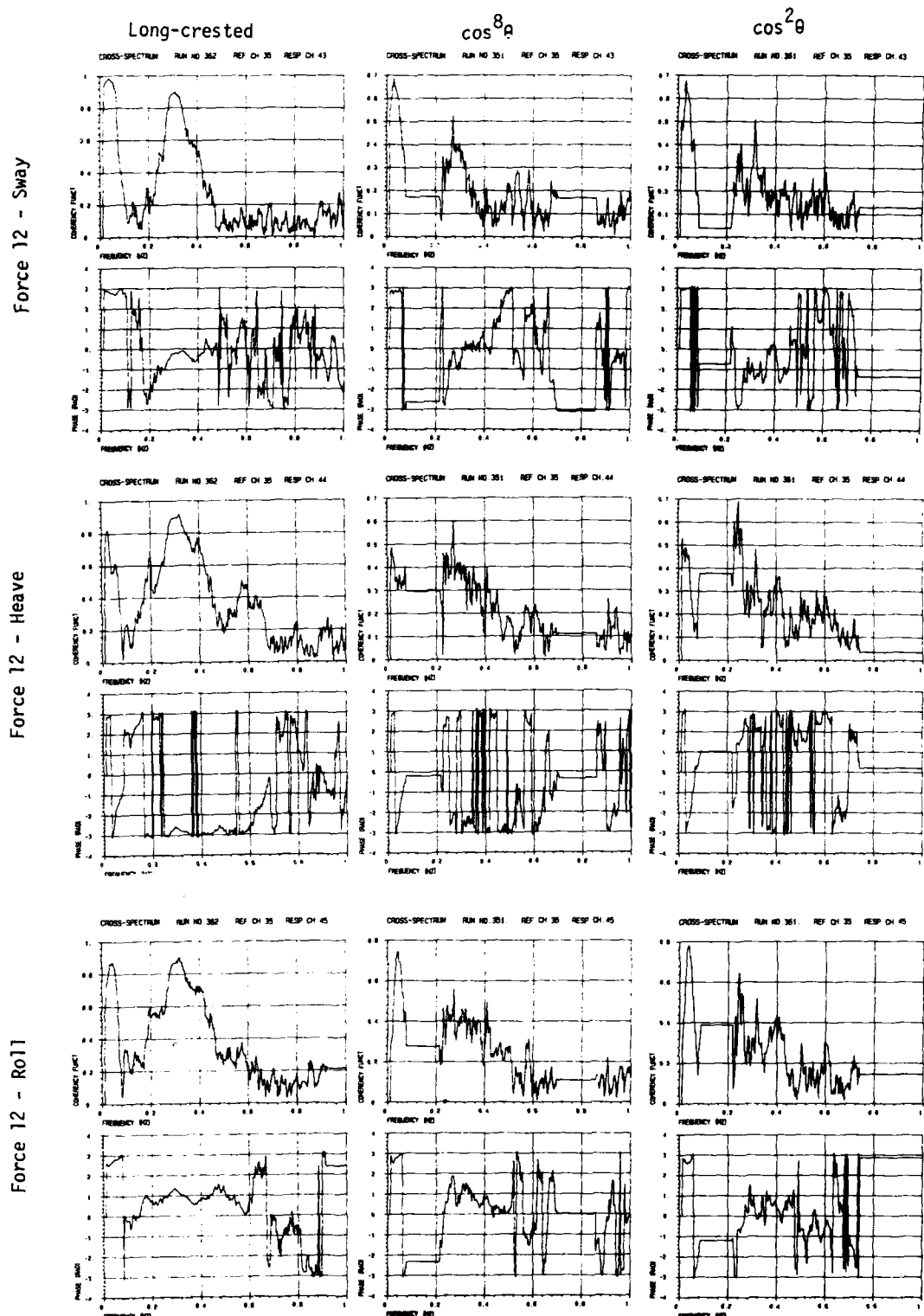


Fig. 3.145

COHERENCE - PHASE ANALYSIS FORCE - MOTION Stiff Model Input: JONSWAP $\cos^8\theta$

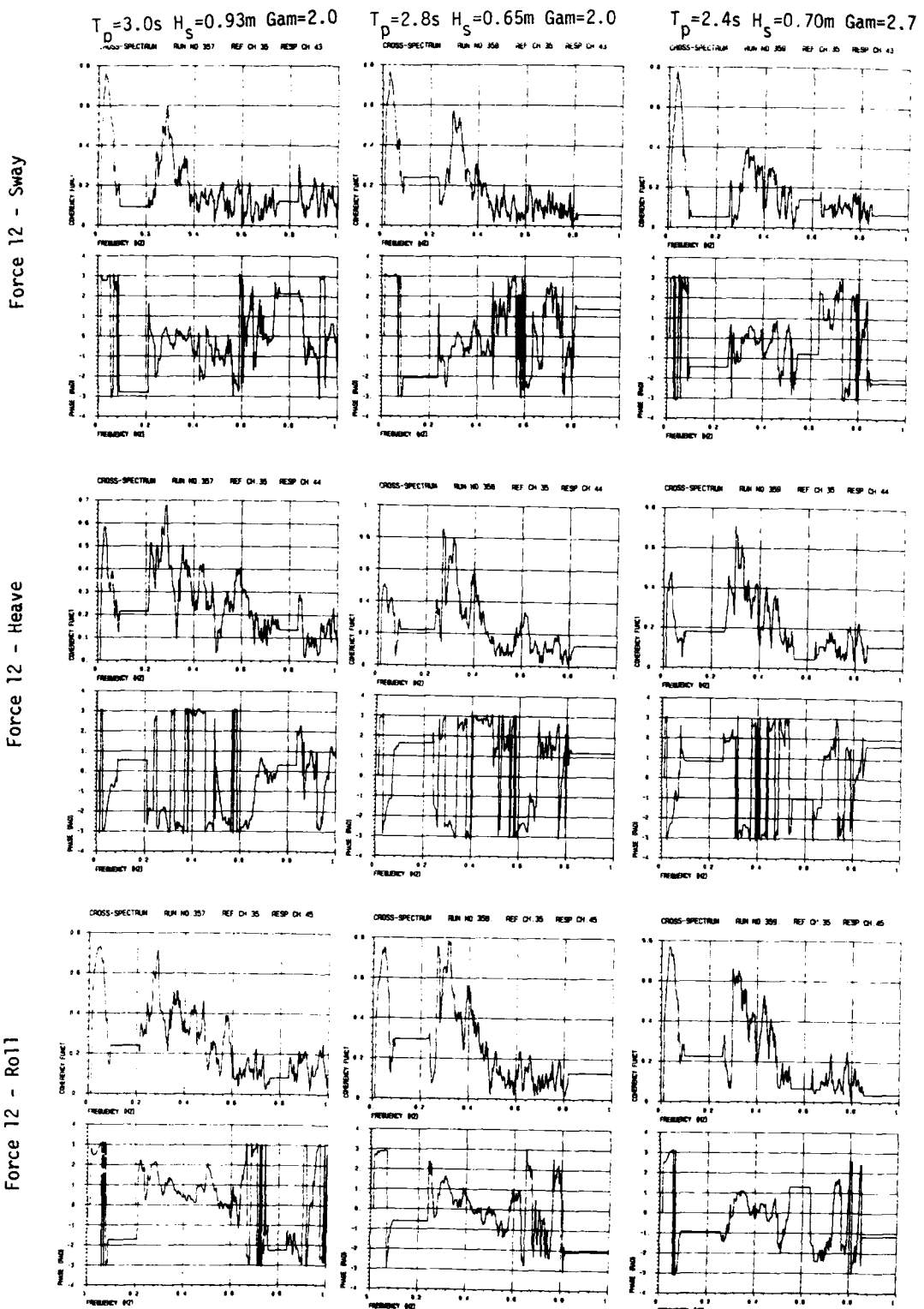


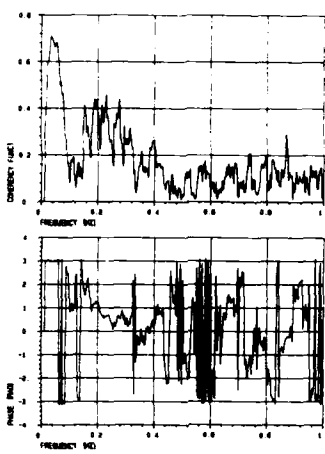
Fig. 3.146

COHERENCE - PHASE ANALYSIS FORCE - MOTION Stiff Model

$T_p = 4.3s$ $H_s = 1.0m$ $\text{Gam} = 3.3$

CROSS-SPECTRUM RUN NO 352 REF CH 35 RESP CH 43

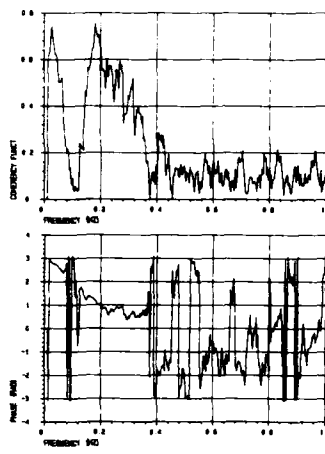
Force 12 - Sway



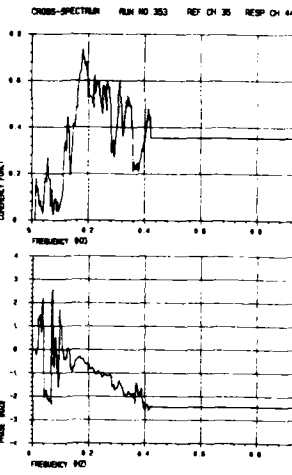
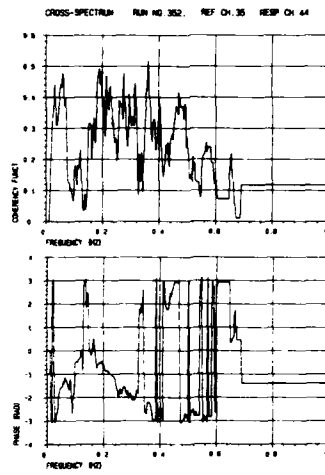
Input: JONSWAP $\cos^8 \theta$

$T_p = 5.0s$ $H_s = 1.5m$ $\text{Gam} = 3.3$

CROSS-SPECTRUM RUN NO 353 REF CH 35 RESP CH 43



Force 12 - Heave



Force 12 - Roll

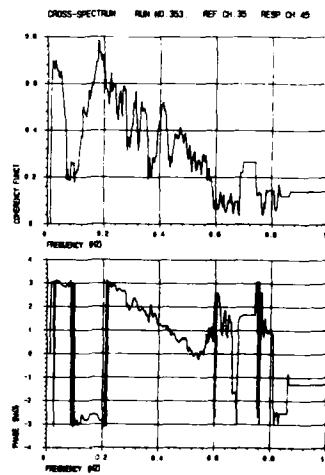
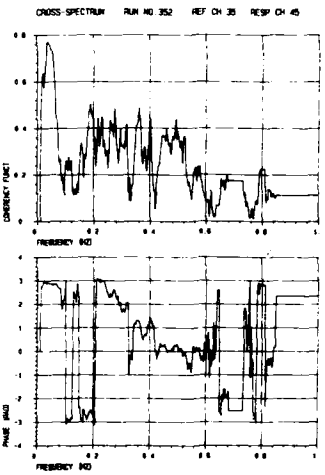


Fig. 3.147

3.2.4 Motions analysis

The following presentation of results for breakwater motions is quite similar to the previous presentation of force results.

First the 3 plots in figs. 3.148 - 3.150 show the maximum and RMS values for sway (y-position), heave (z-position) and roll motion, as a function of the input significant wave height $H_{mo,o}$. Next, 3 plots showing the maximum and the RMS values, normalized by $H_{mo,o}$, as a function of the input peak wave period T_p , are presented (figs. 3.151 - 3.153). Then follow 9 pages (figs. 3.154 - 3.162) with plots of spectra, transfer functions and coherence/phase functions for sway, heave and roll, with wave staff 11 as a reference. Statistics of maxima (or in some cases: minima - see the coordinate system definition in fig. 2.18) of all 6 breakwater motions (surge-sway-heave-roll-pitch-yaw) are then presented and compared to Rayleigh curves (figs. 3.163 - 3.168). Coupling sway-heave, sway-roll and heave-roll is finally illustrated by coherence/phase plots in figs. 3.169 - 3.171.

MAXIMUM AND RMS VALUES VS INPUT SIGNIFICANT WAVE HEIGHT
 SWAY (Y-POSITION) PONTOON 1 STIFF MODEL

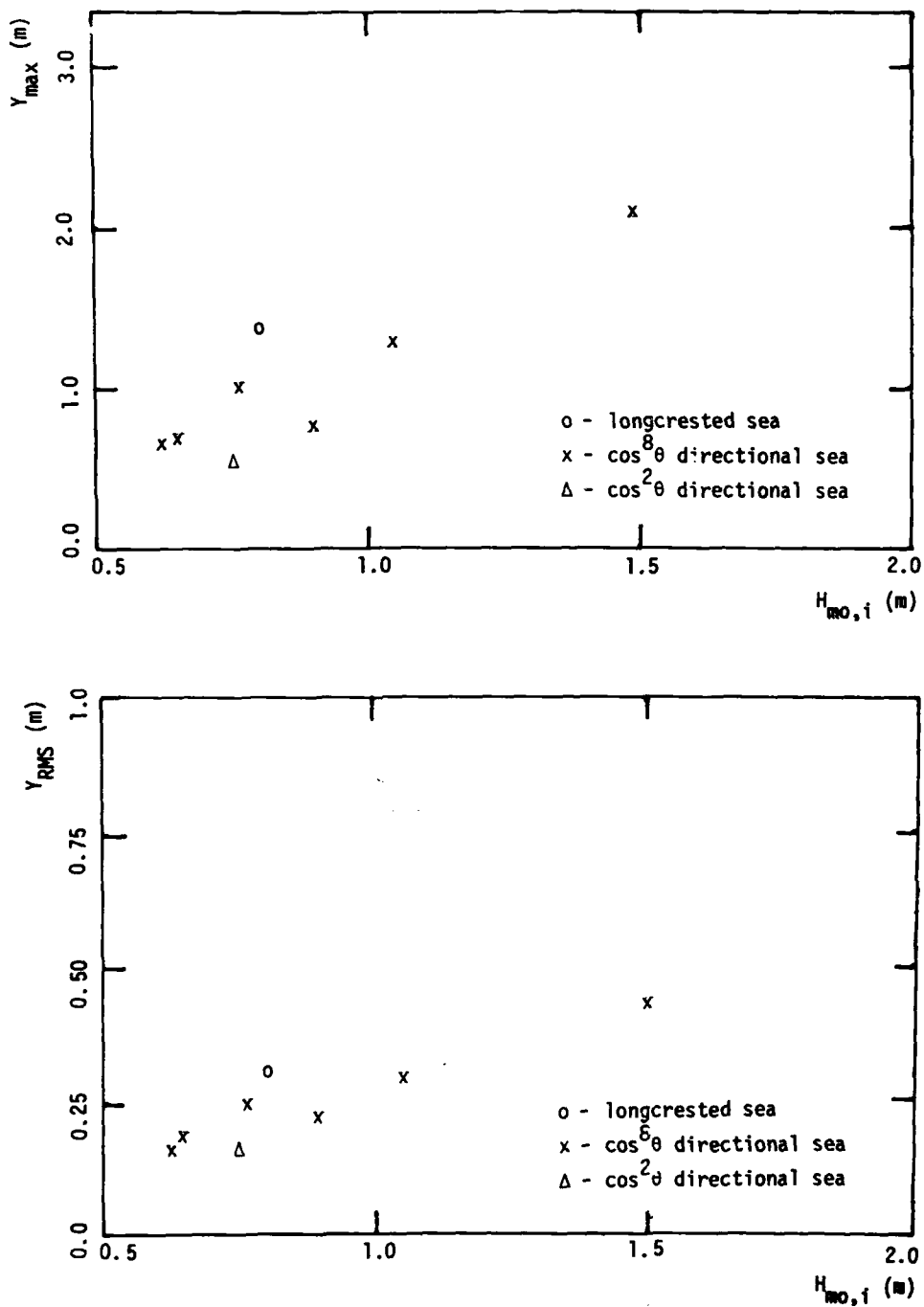


Fig. 3.148

MAXIMUM AND RMS VALUES VS INPUT SIGNIFICANT WAVE HEIGHT
HEAVE (Z-POSITION) PONTOON 1 STIFF MODEL

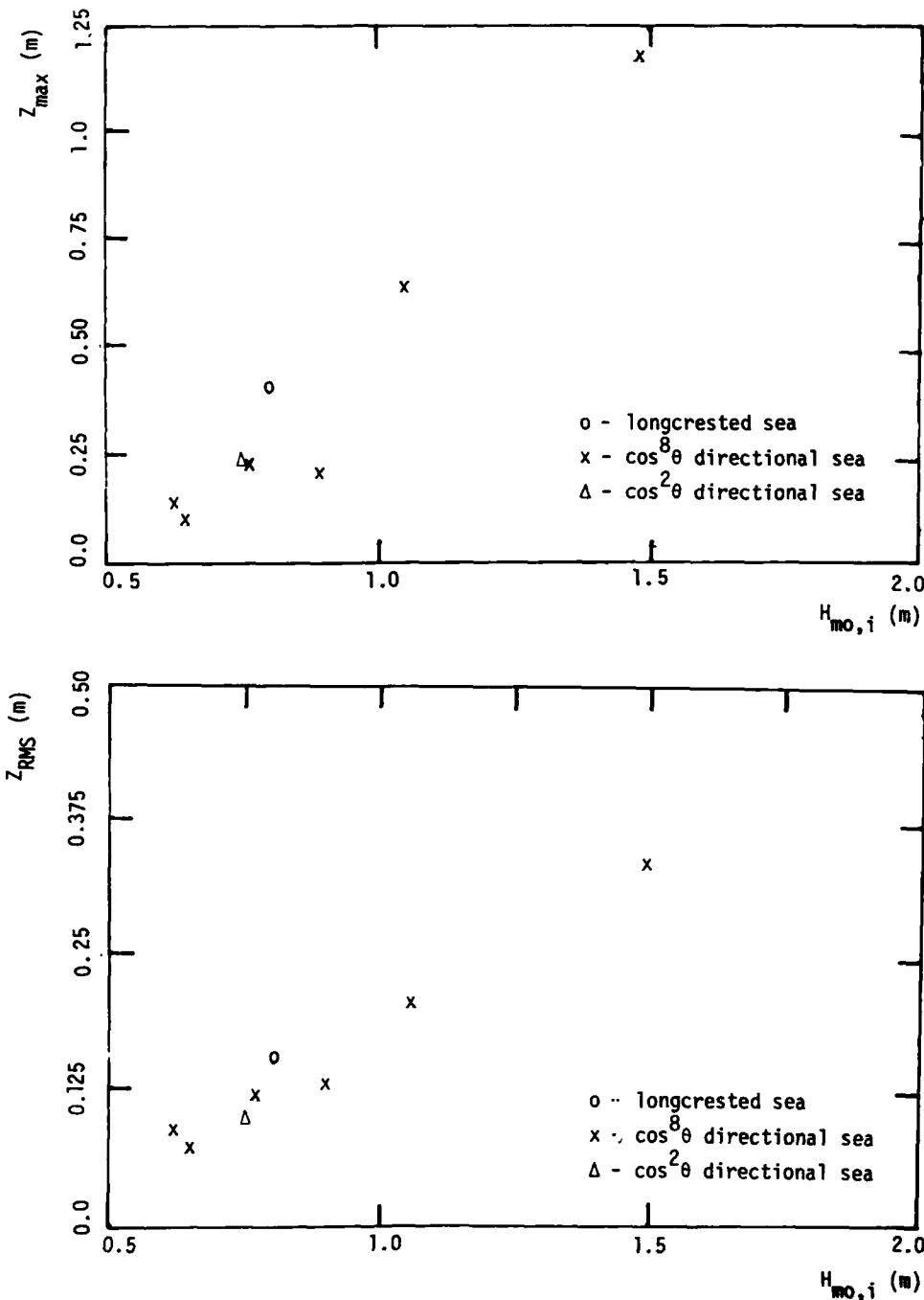


Fig. 3.149

MAXIMUM AND RMS VALUES VS INPUT SIGNIFICANT WAVE HEIGHT
 ROLL PONTOON 1 STIFF MODEL

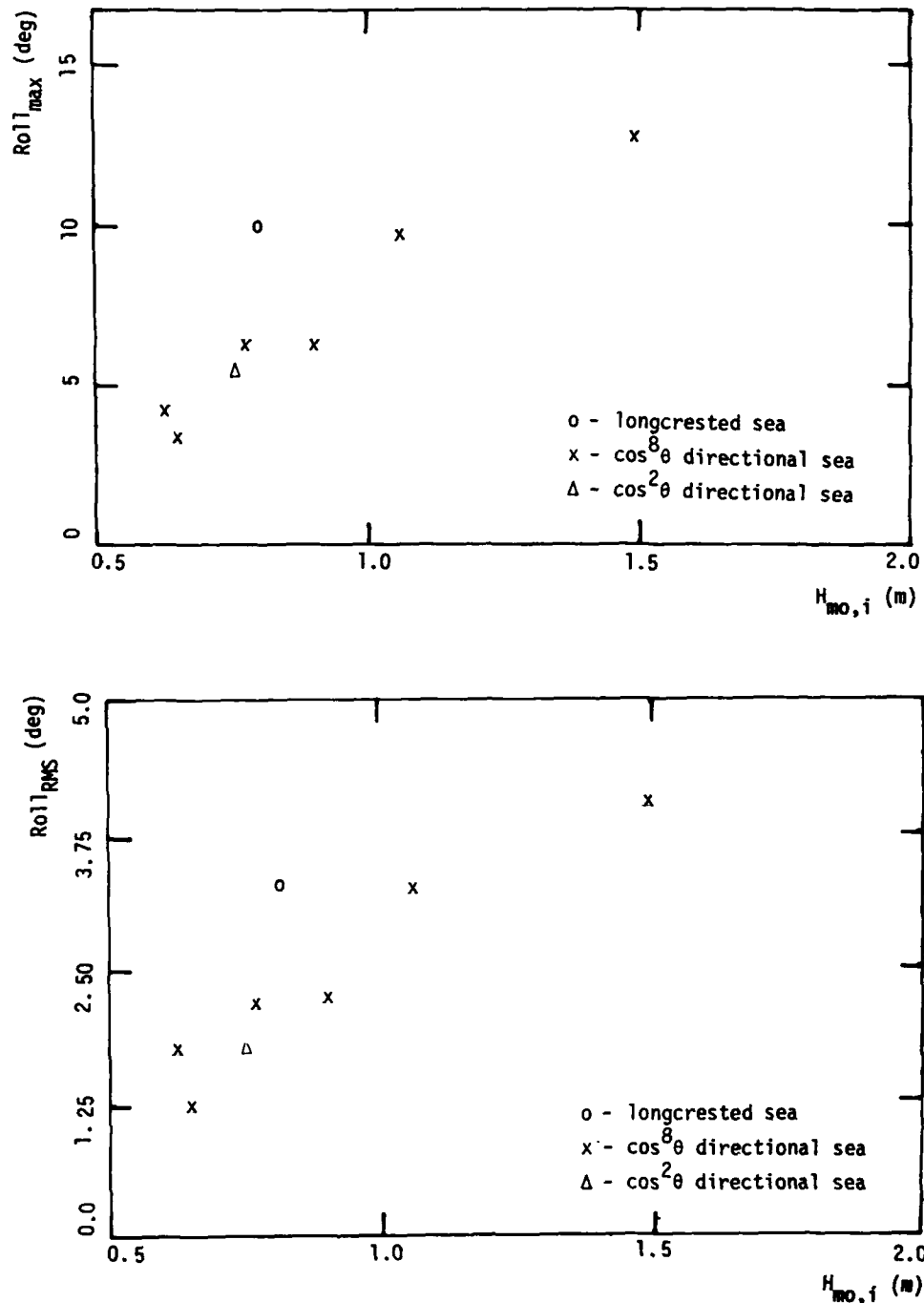


Fig. 3.150

NORMALIZED MAXIMUM AND RMS VALUES VS PEAK PERIOD OF INPUT WAVE
 SWAY (Y-POSITION) PONTOON 1 STIFF MODEL

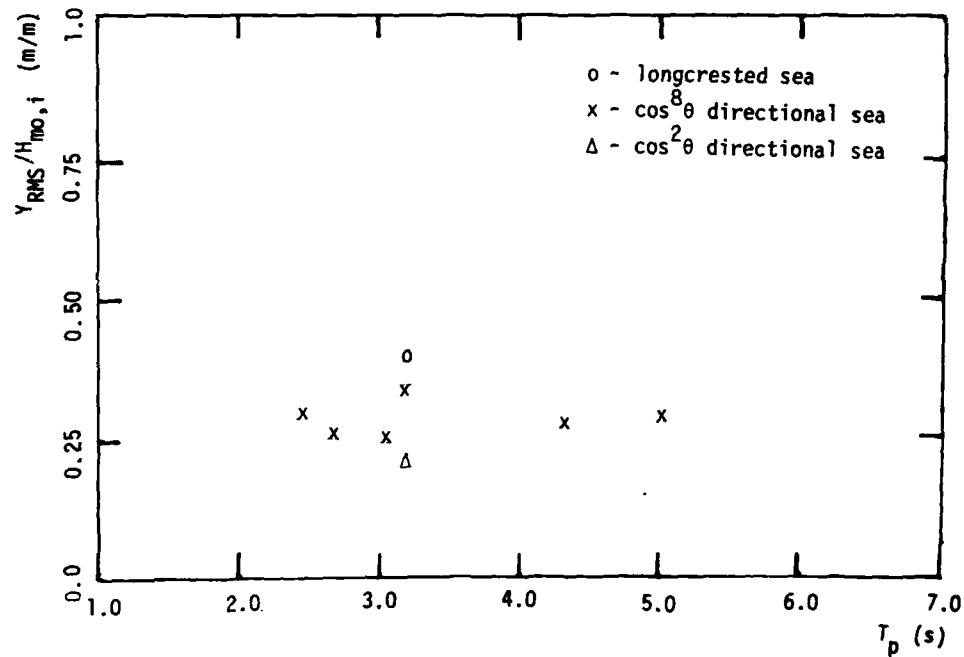
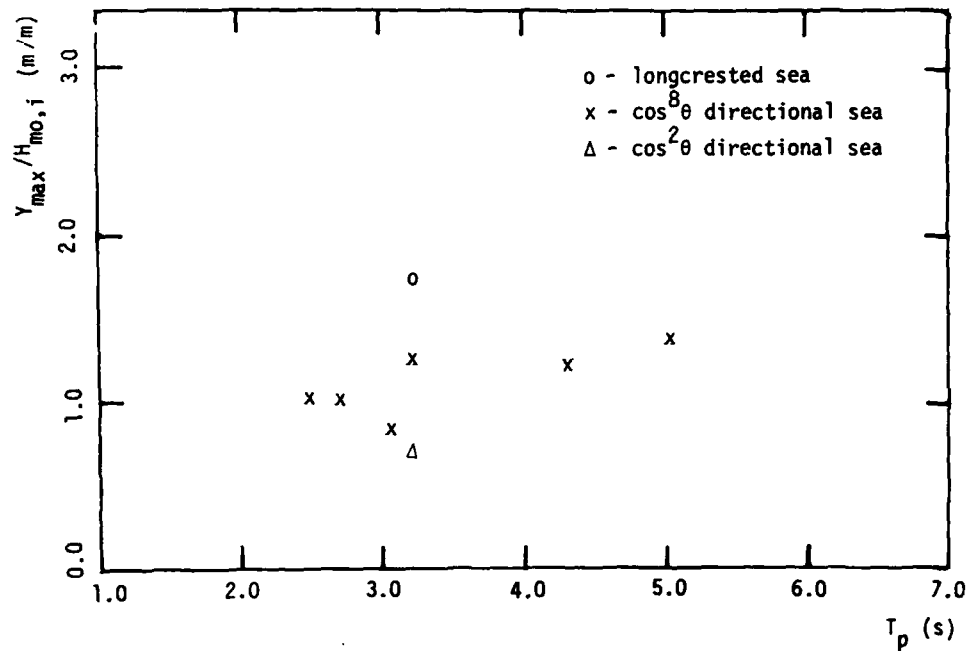


Fig. 3.151

NORMALIZED MAXIMUM AND RMS VALUES VS PEAK PERIOD OF INPUT WAVE
 HEAVE (Z-POSITION) PONTOON 1 STIFF MODEL

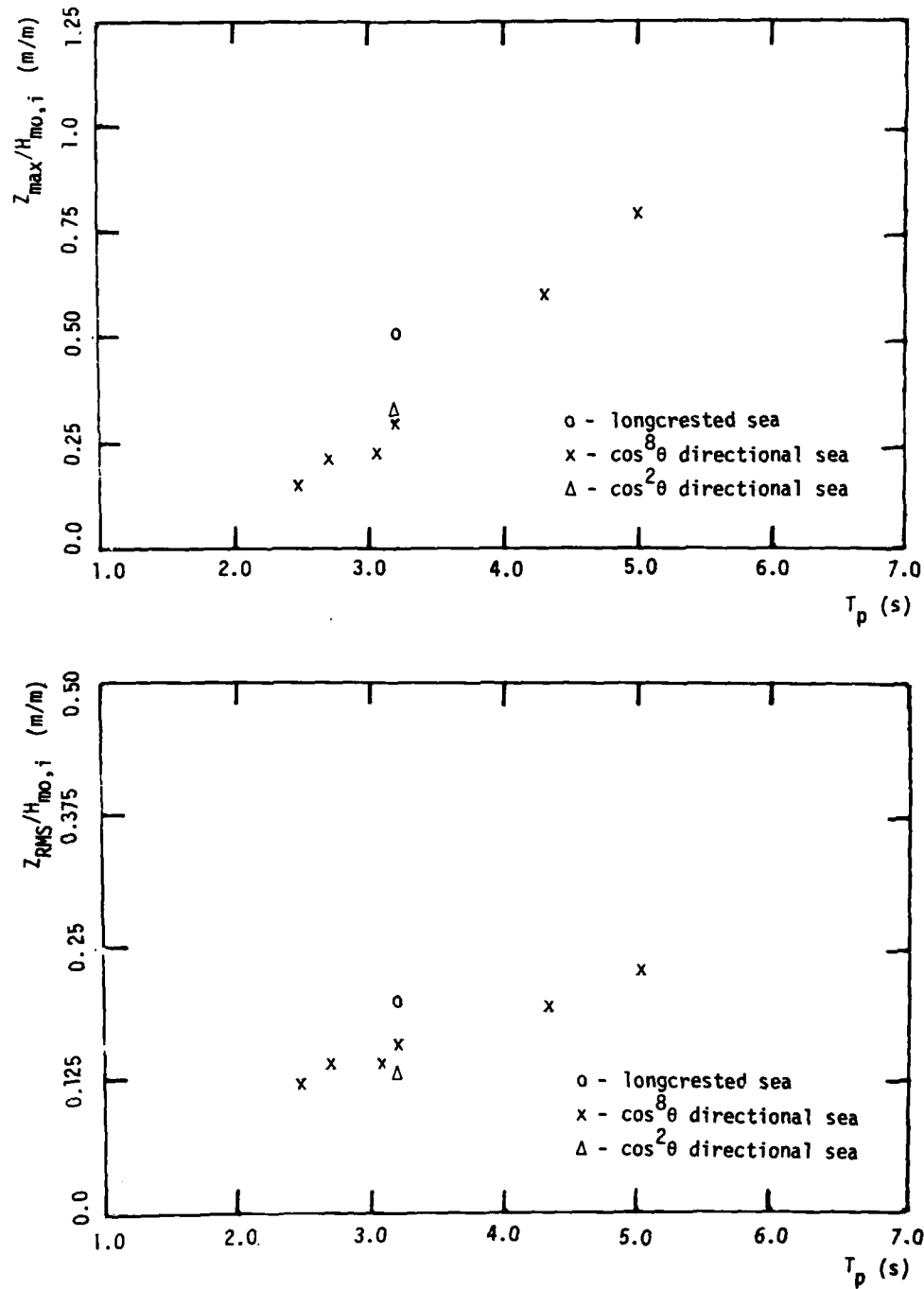


Fig. 3.152

NORMALIZED MAXIMUM AND RMS VALUES VS PEAK PERIOD OF INPUT WAVE

ROLL PONTOON 1 STIFF MODEL

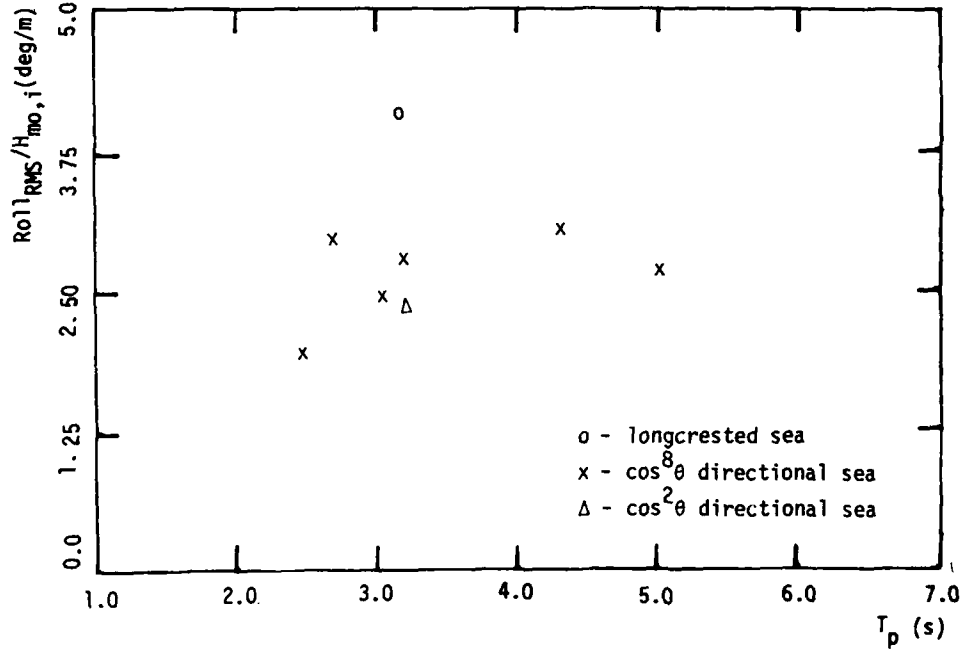
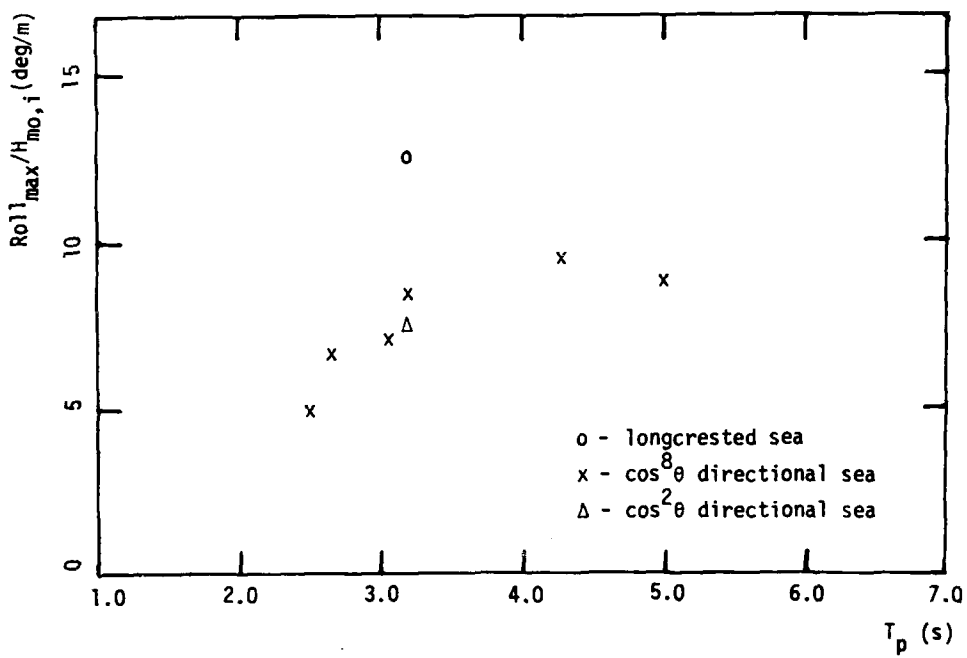


Fig. 3.153

SPECTRAL ANALYSIS SWAY (Y-POS) Stiff Model Input: JONSWAP

$T_p = 3.2\text{ s}$ $H_s = 0.75\text{ m}$ $\text{Gam} = 3.3$

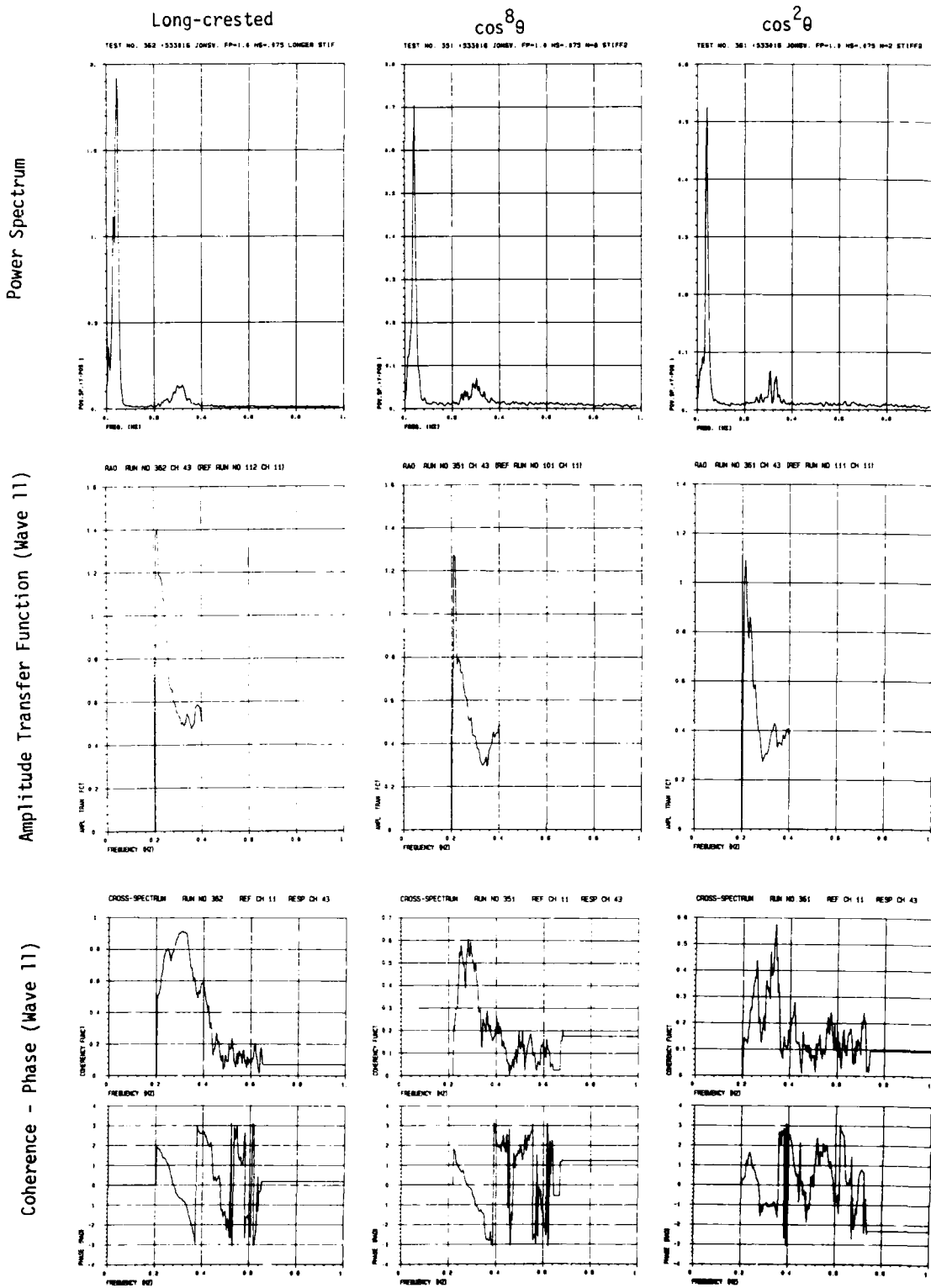


Fig. 3.154

SPECTRAL ANALYSIS SWAY (Y-POS) Stiff Model Input: JONSWAP $\cos^8 \theta$

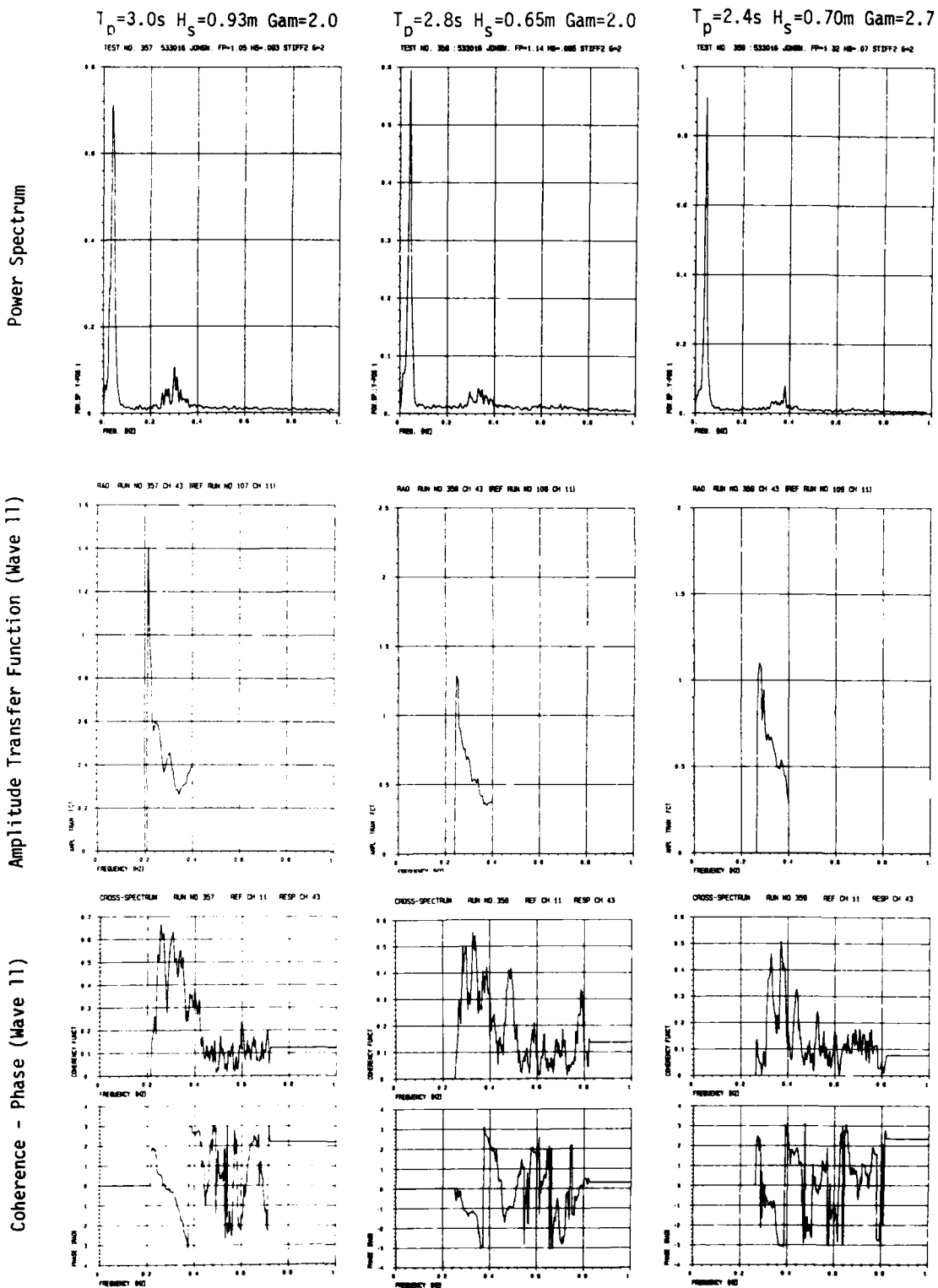
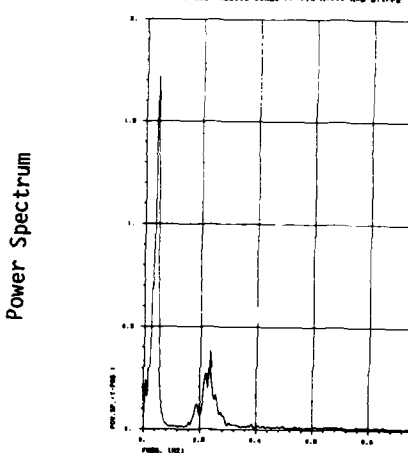


Fig. 3.155

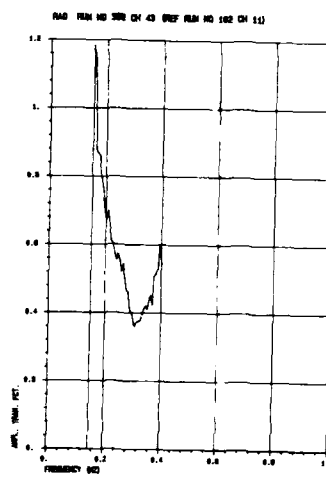
SPECTRAL ANALYSIS SWAY (Y-POS) Stiff Model

$T_p = 4.3\text{s}$ $H_s = 1.0\text{m}$ $\text{Gam} = 3.3$

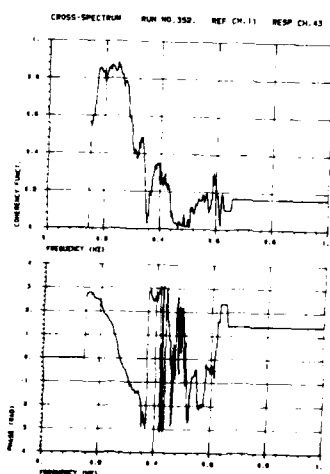
TEST NO. 350-1533410 JONSWAP FP=74 H=1.0m G=3.3 STIFF



Amplitude Transfer Function (Wave 11)



Coherence - Phase (Wave 11)



Input: JONSWAP $\cos^8 \theta$

$T_p = 5.0\text{s}$ $H_s = 1.5\text{m}$ $\text{Gam} = 3.3$

TEST NO. 353-1533410 JONSWAP FP=63 H=1.5m G=3.3 STIFF

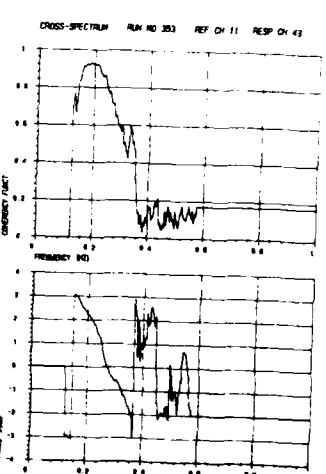
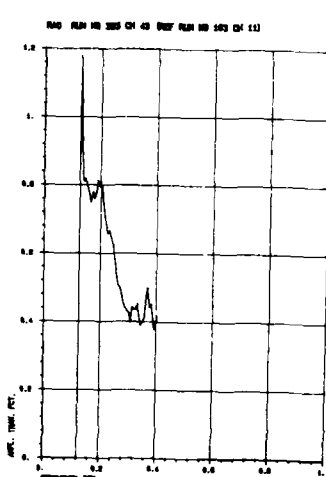
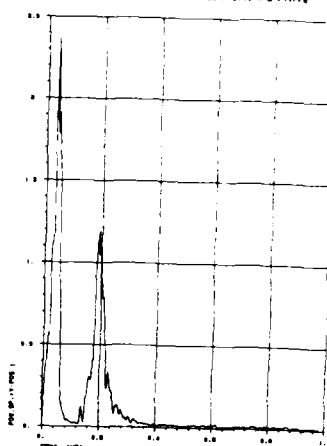


Fig. 3.156

SPECTRAL ANALYSIS HEAVE (Z-POS) Stiff Model Input: JONSWAP $T_p = 3.2\text{ s}$ $H_s = 0.75\text{ m}$ $\Gamma_m = 3.3$

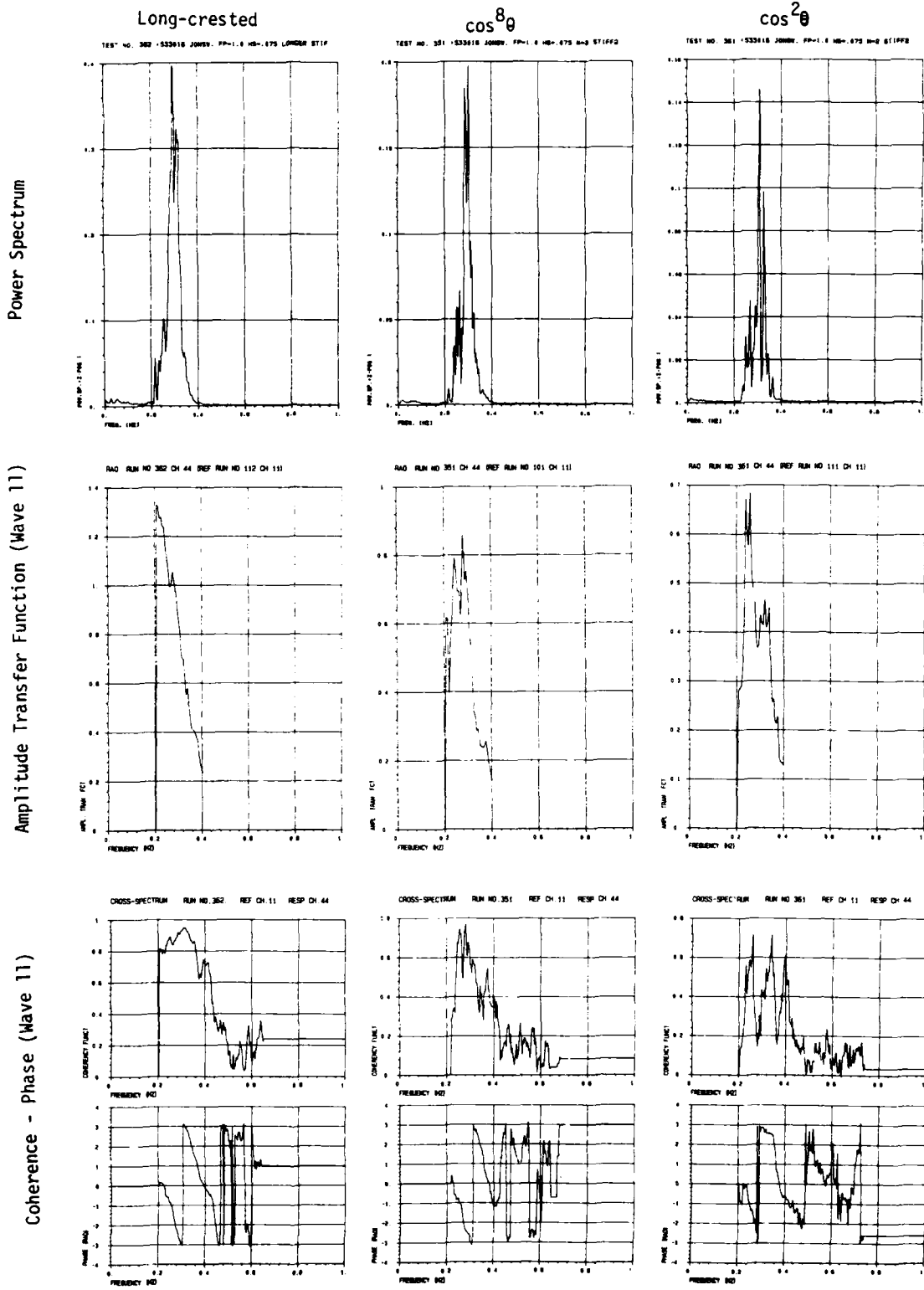


Fig. 3.157

SPECTRAL ANALYSIS HEAVE (Z-POS) Stiff Model Input: JONSWAF $\cos^8 \theta$

$T_p = 3.0\text{ s}$ $H_s = 0.93\text{ m}$ $\text{Gam} = 2.0$

TEST NO. 357 : S33016 JONSWF FP=1.05 HS=.930 STIFF2 G=2

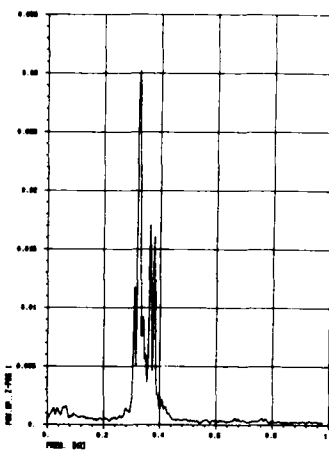
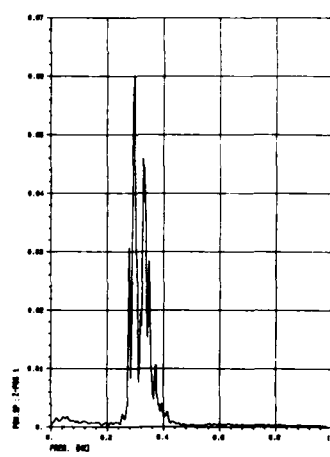
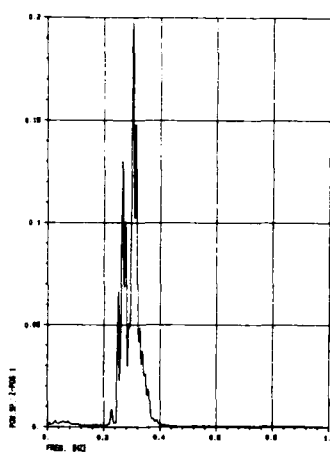
$T_p = 2.8\text{ s}$ $H_s = 0.65\text{ m}$ $\text{Gam} = 2.0$

TEST NO. 358 : S33016 JONSWF FP=1.14 HS=.650 STIFF2 G=2

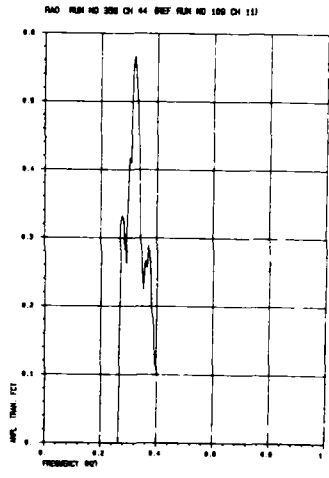
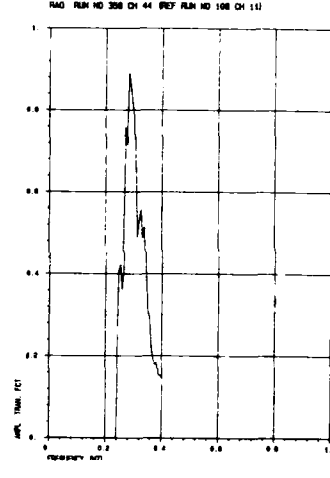
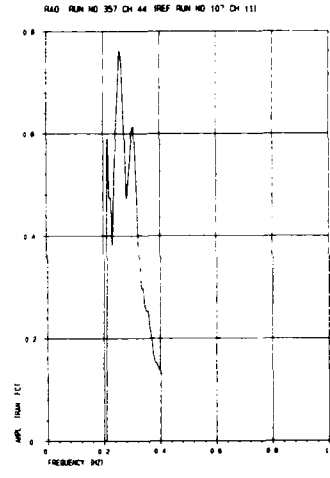
$T_p = 2.4\text{ s}$ $H_s = 0.70\text{ m}$ $\text{Gam} = 2.7$

TEST NO. 359 : S33016 JONSWF FP=1.32 HS=.070 STIFF2 G=2

Power Spectrum



Amplitude Transfer Function (Wave 11)



Coherence - Phase (Wave 11)

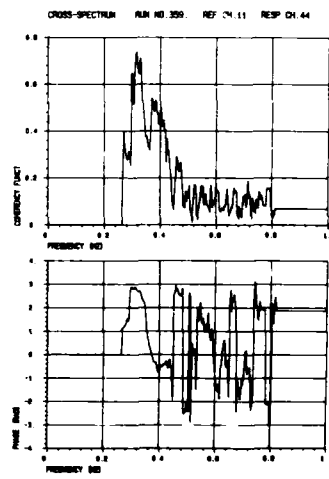
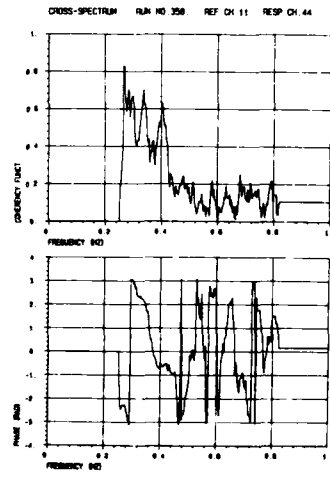
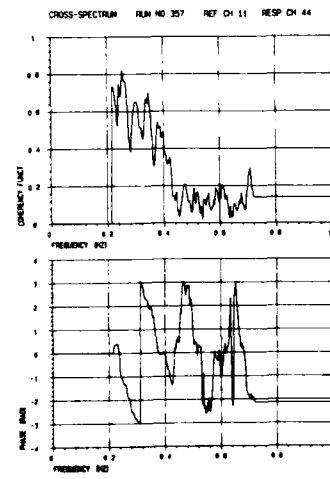


Fig. 3.158

SPECTRAL ANALYSIS HEAVE (Z-POS) Stiff Model Input: JONSWAP $\cos^8 \theta$

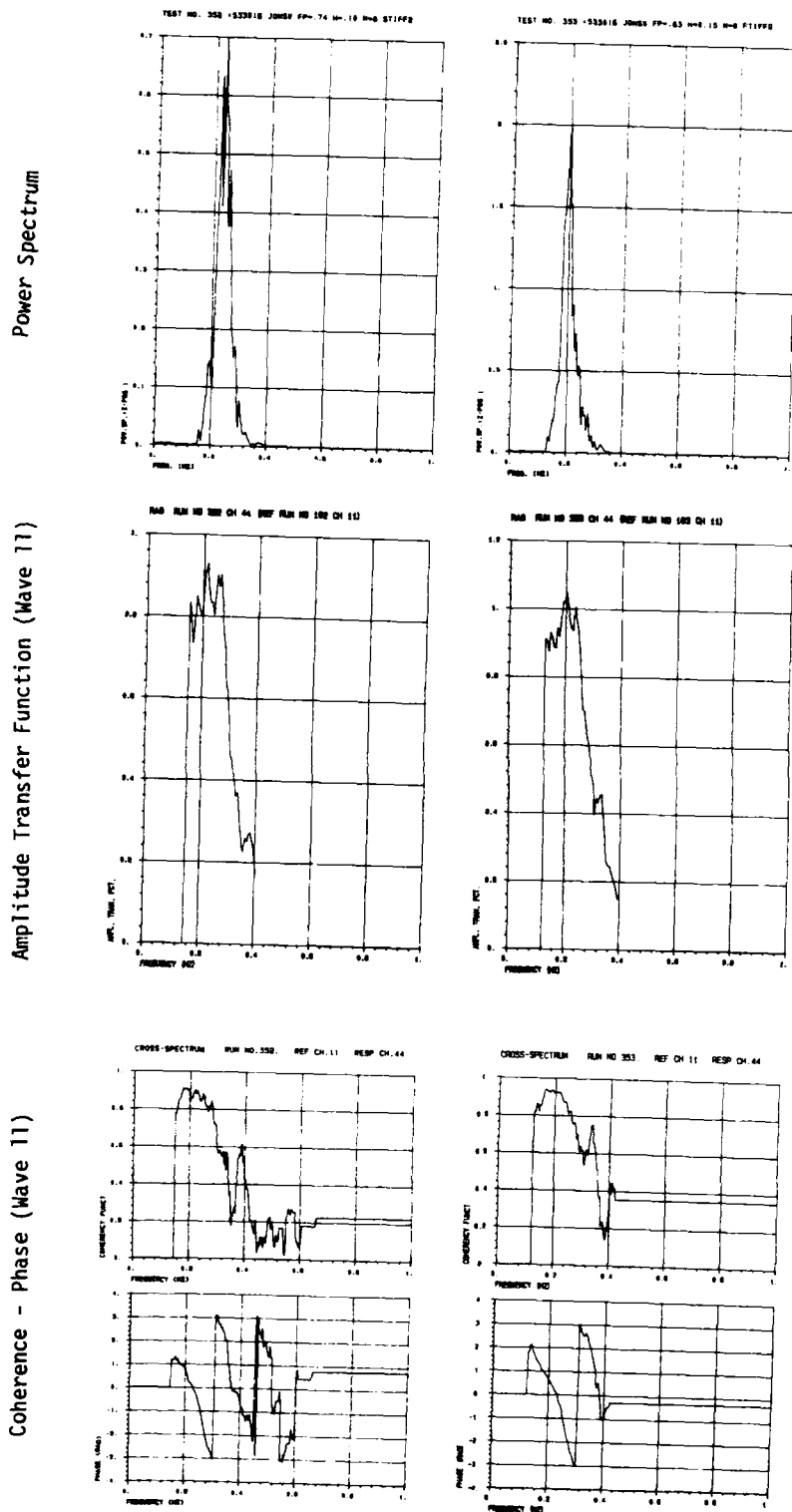


Fig. 3.159

SPECTRAL ANALYSIS ROLL Stiff Model

Input: JONSWAP $T_p = 3.2\text{ s}$ $H_s = 0.75\text{ m}$ $\Gamma_m = 3.3$

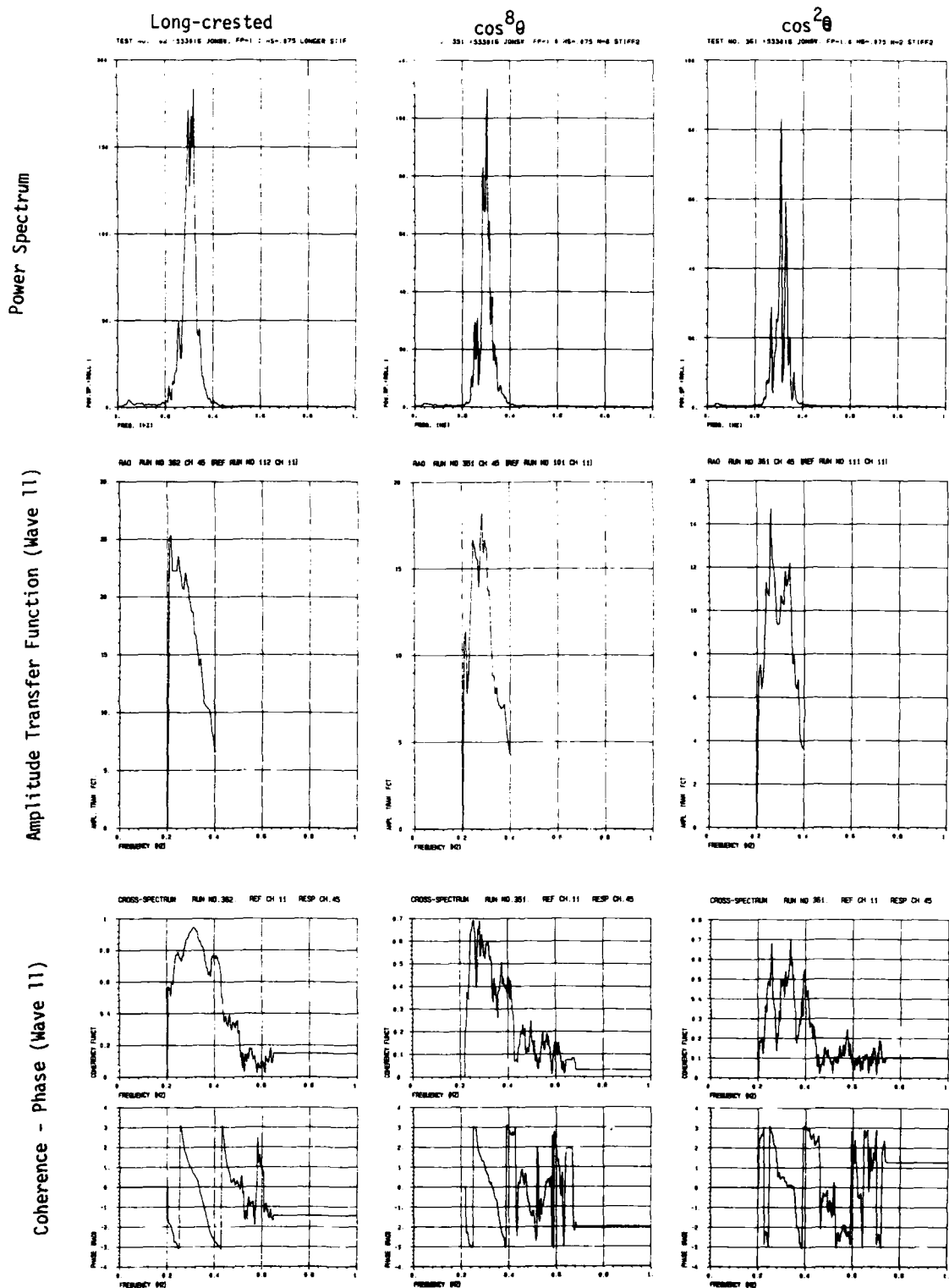
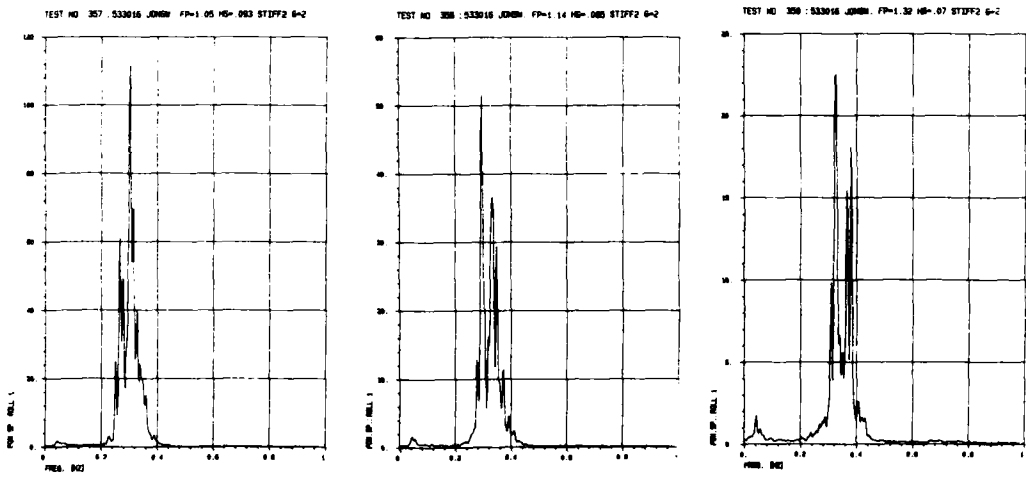


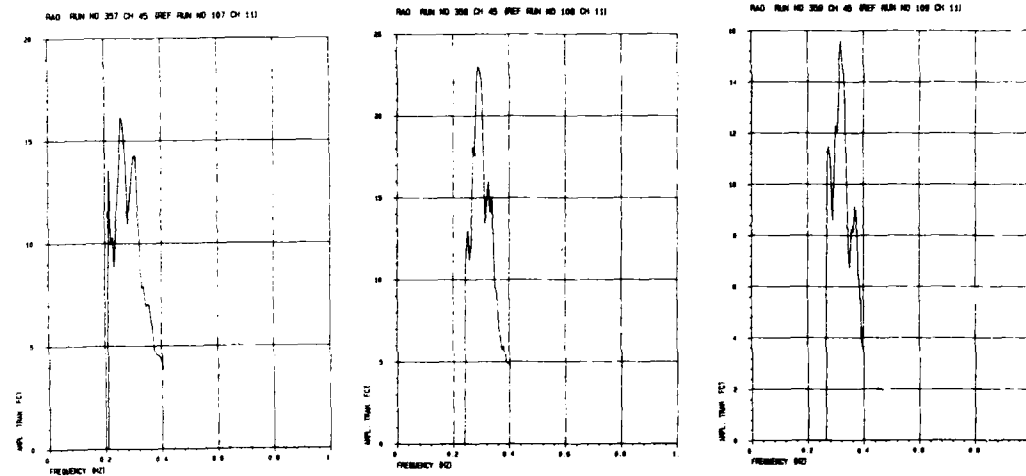
Fig. 3.160

SPECTRAL ANALYSIS ROLL Stiff Model Input: JONSWAP $\cos^8 \theta$

Power Spectrum



Amplitude Transfer Function (Wave 11)



Coherence - Phase (Wave 11)

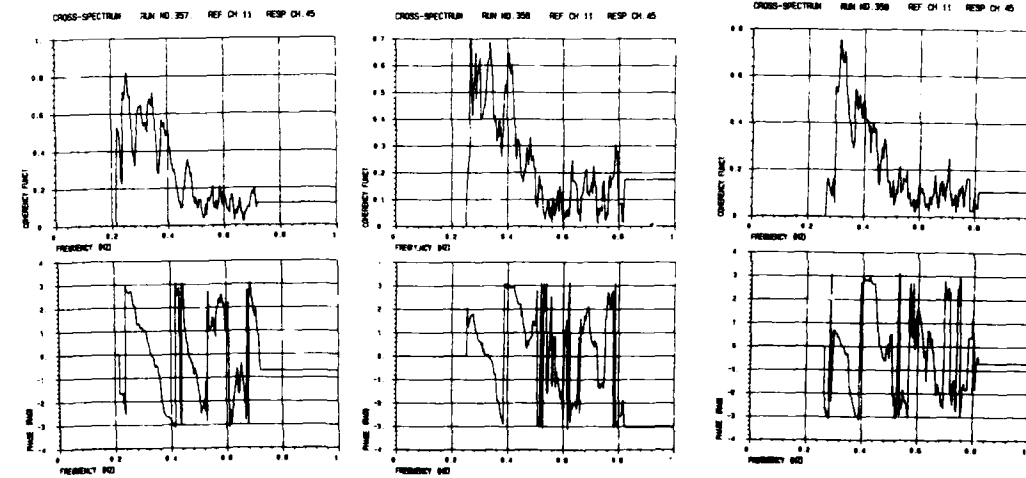


Fig. 3.161

SPECTRAL ANALYSIS ROLL Stiff Model

Input: JONSWAP $\cos^8 \theta$

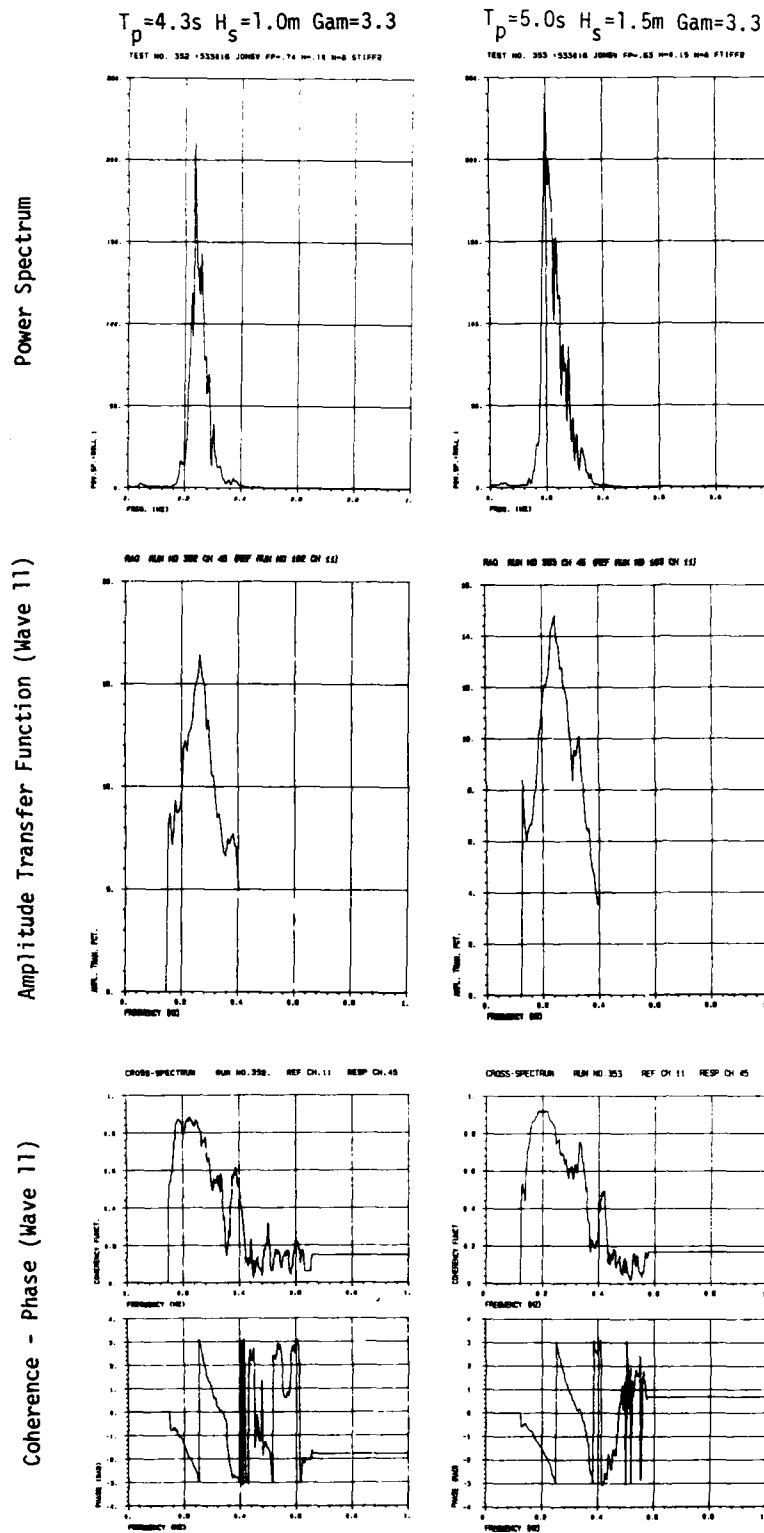


Fig. 3.162

AMPLITUDE STATISTICS MOTION Stiff Model Input: JONSWAP $T_p = 3.2s$ $H_s = 0.75m$ $\Gamma_m = 3.3$

Long-crested

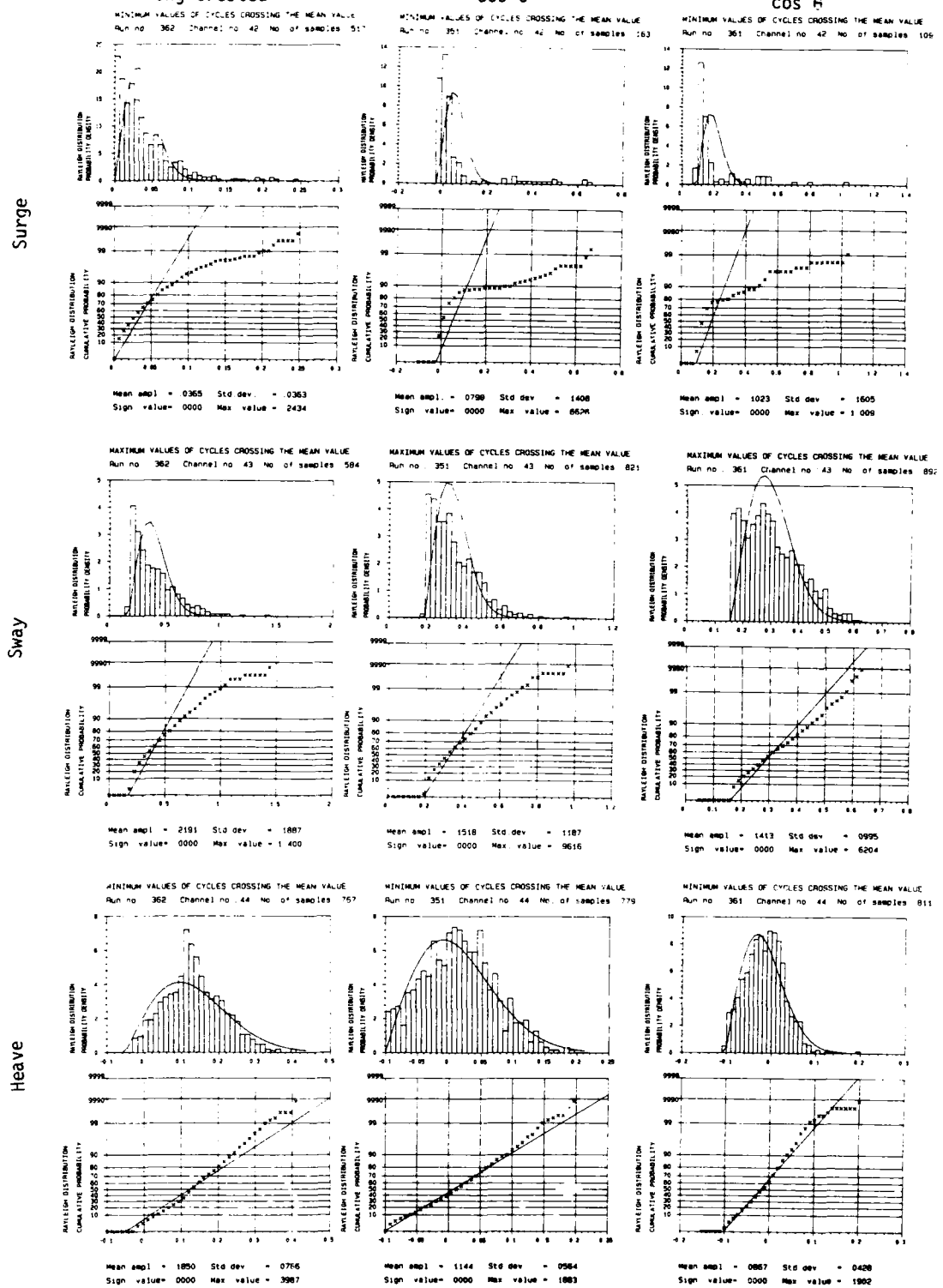


Fig. 3.163

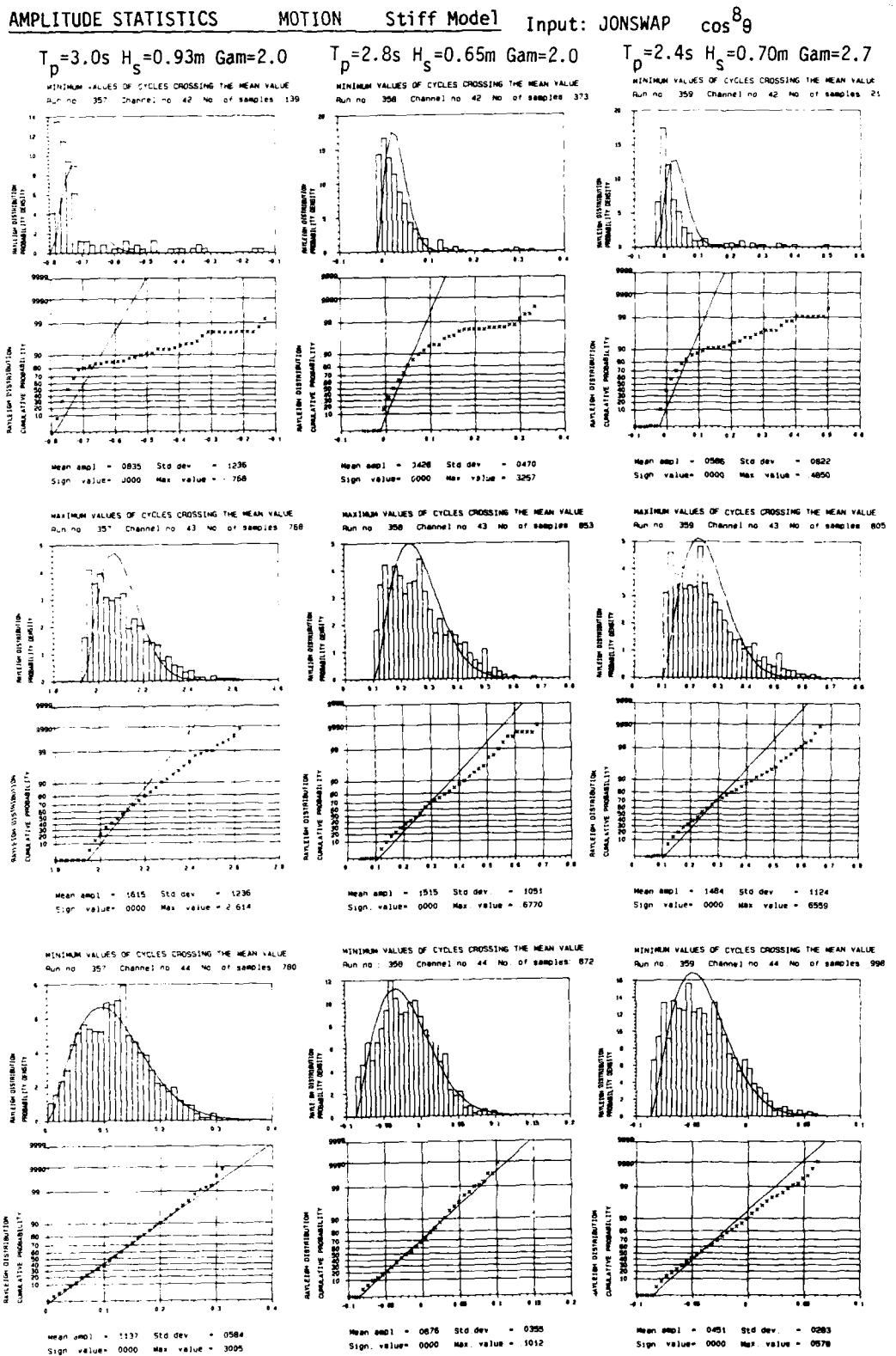


Fig. 3.164

AMPLITUDE STATISTICS MOTION Stiff Model Input: JONSWAP

$\cos^8 \theta$

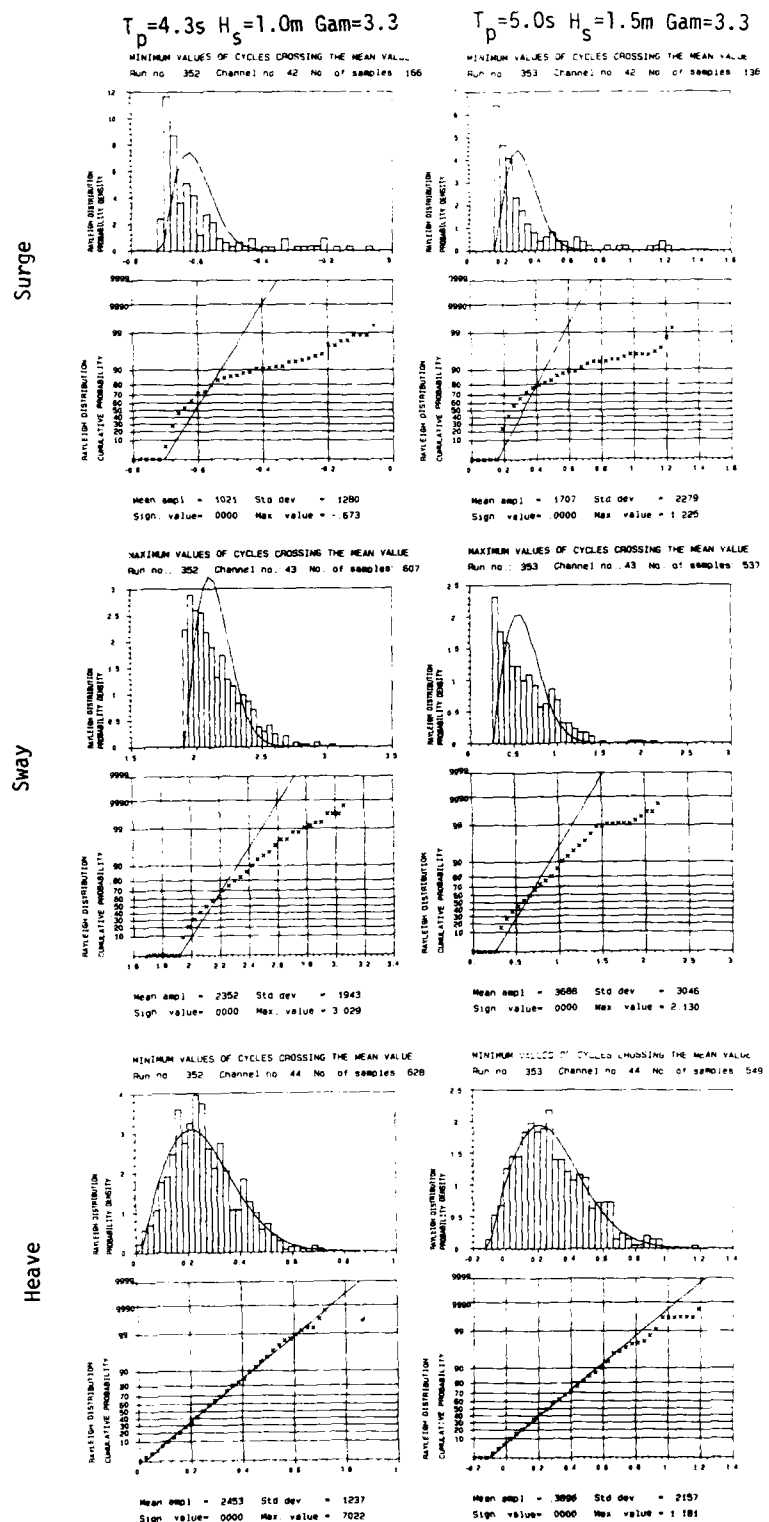


Fig. 3.165

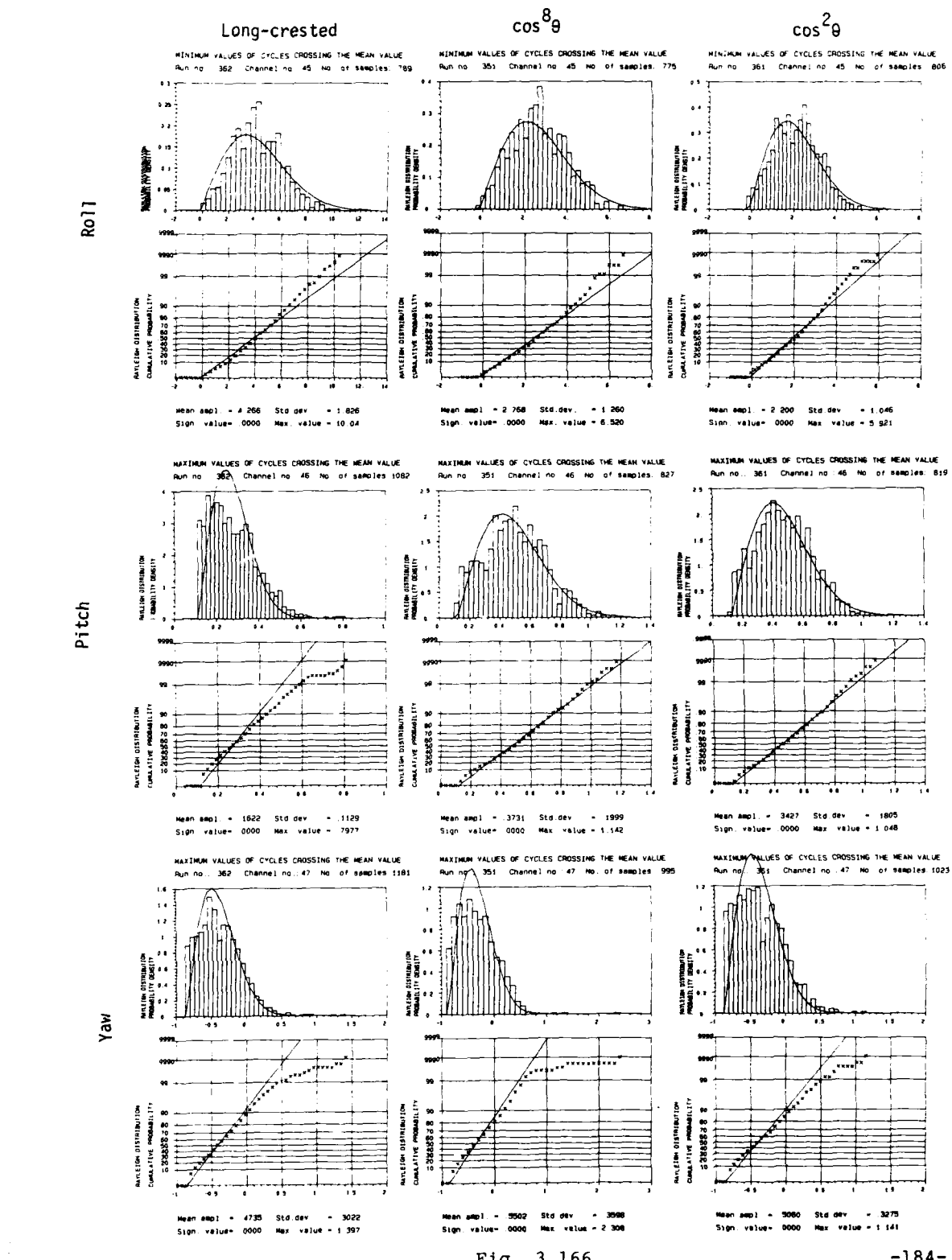


Fig. 3.166

AMPLITUDE STATISTICS MOTION Stiff Model Input: JONSWAP $\cos^8 \theta$

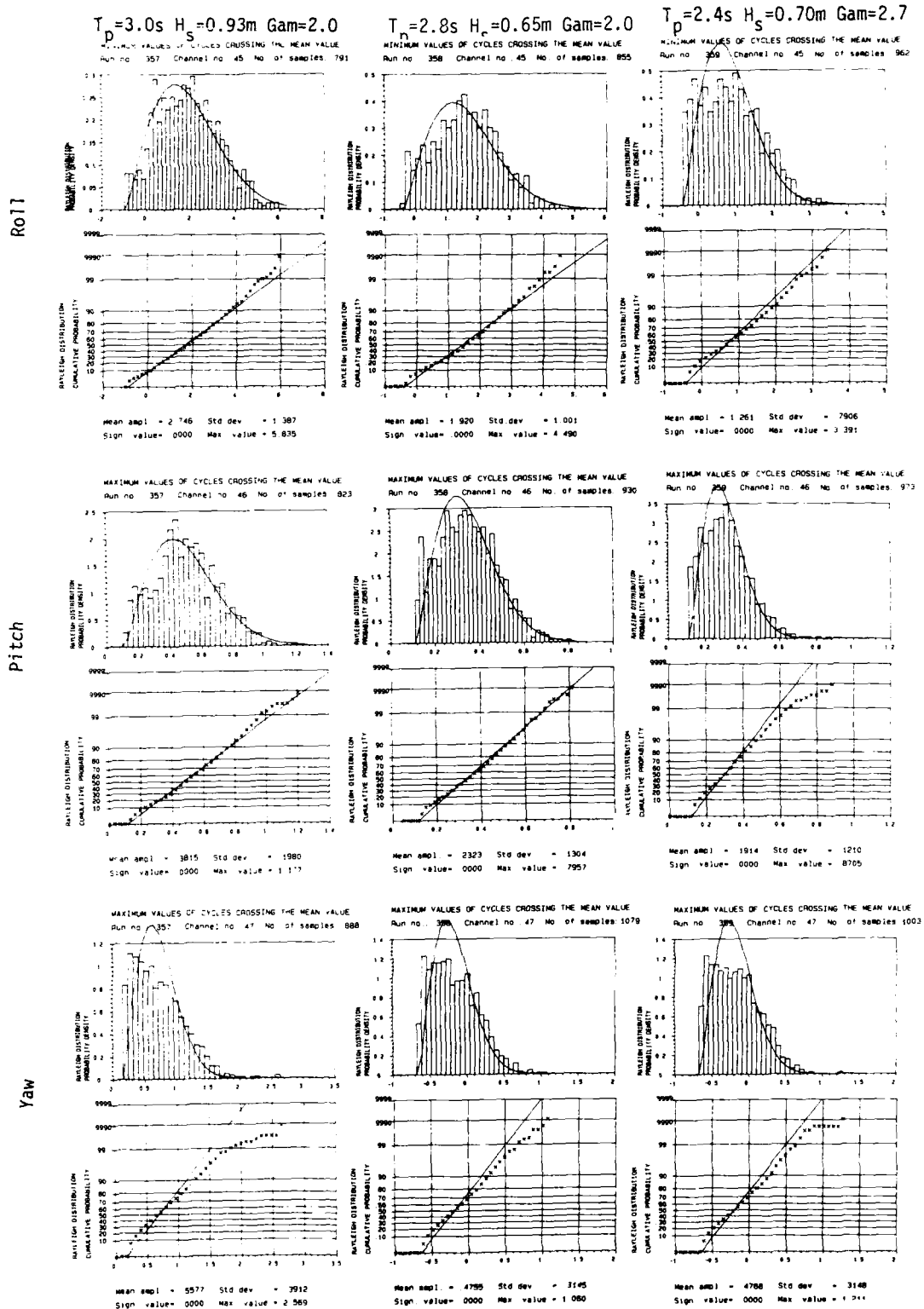


Fig. 3.167

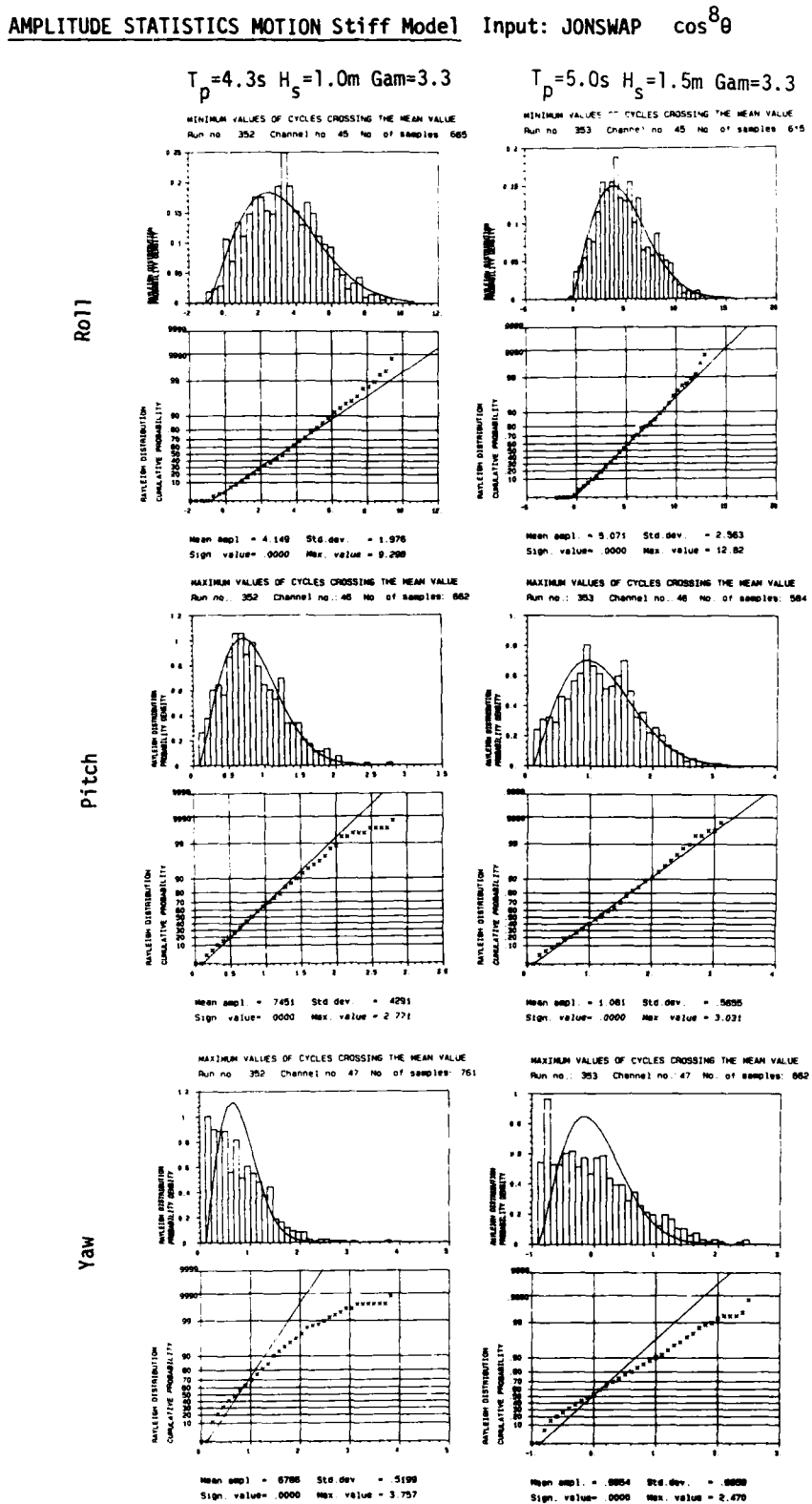


Fig. 3.168

COHERENCE-PHASE ANALYSIS MOTION - MOTION Stiff Model Input: JONSWAP $T_p = 3.2s$ $H_s = 0.75m$ $\text{Gam} = 3.3$

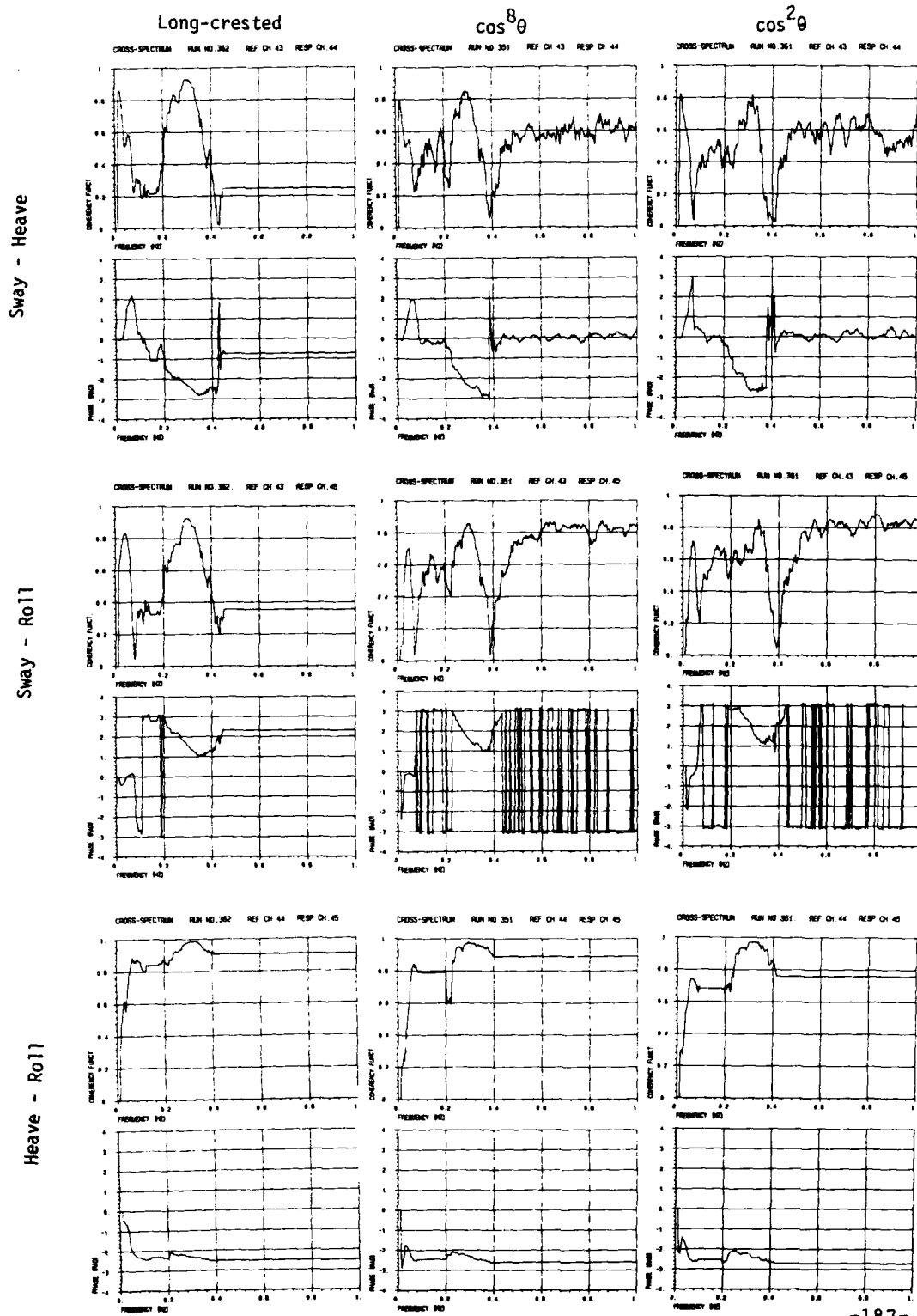


Fig. 3.169

COHERENCE - PHASE ANALYSIS MOTION - MOTION Stiff Model Input: JONSWAF $\cos^8 \theta$

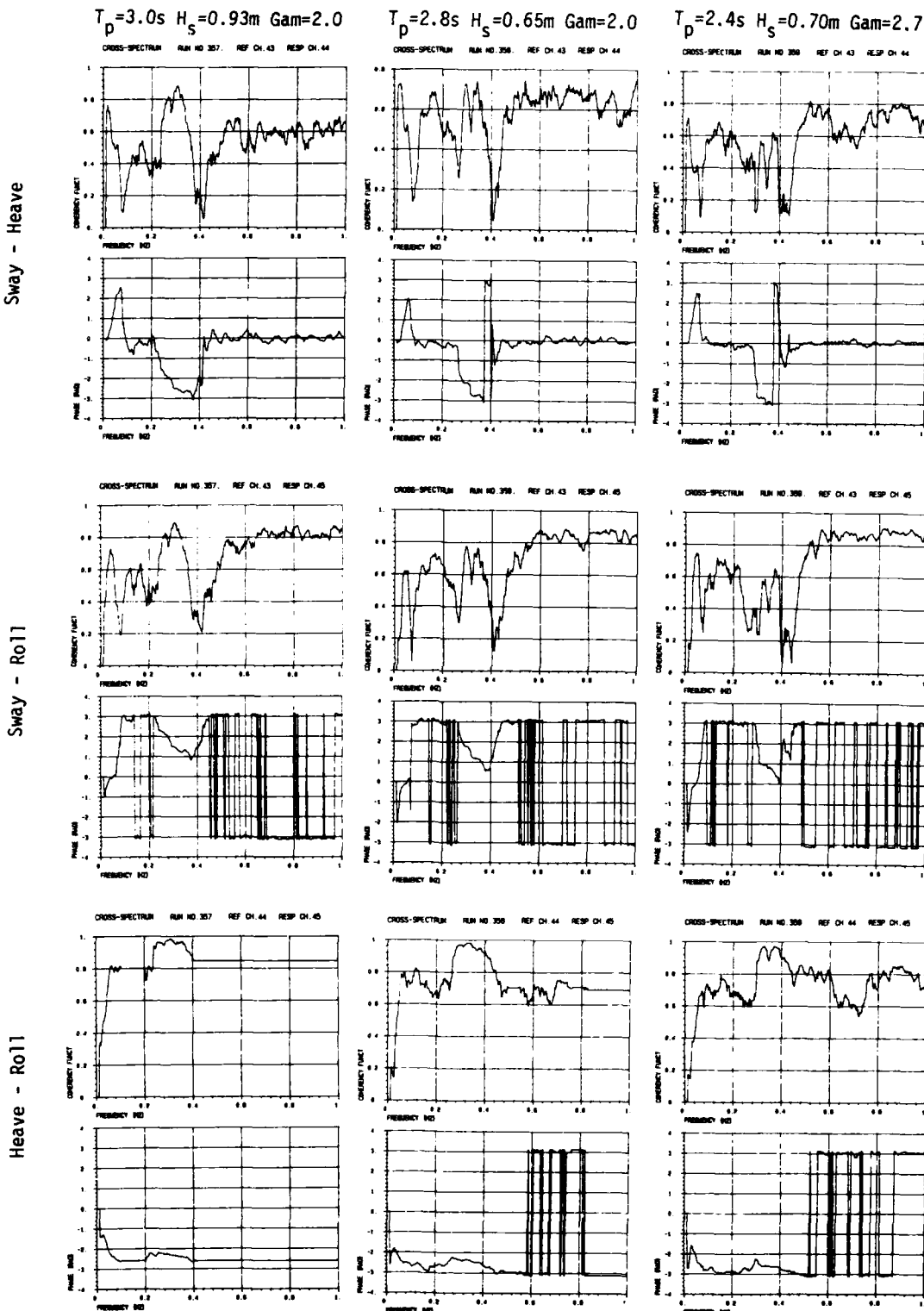


Fig. 3.170

COHERENCE - PHASE ANALYSIS MOTION - MOTION Stiff Model Input: JONSWAP $\cos^8 \theta$

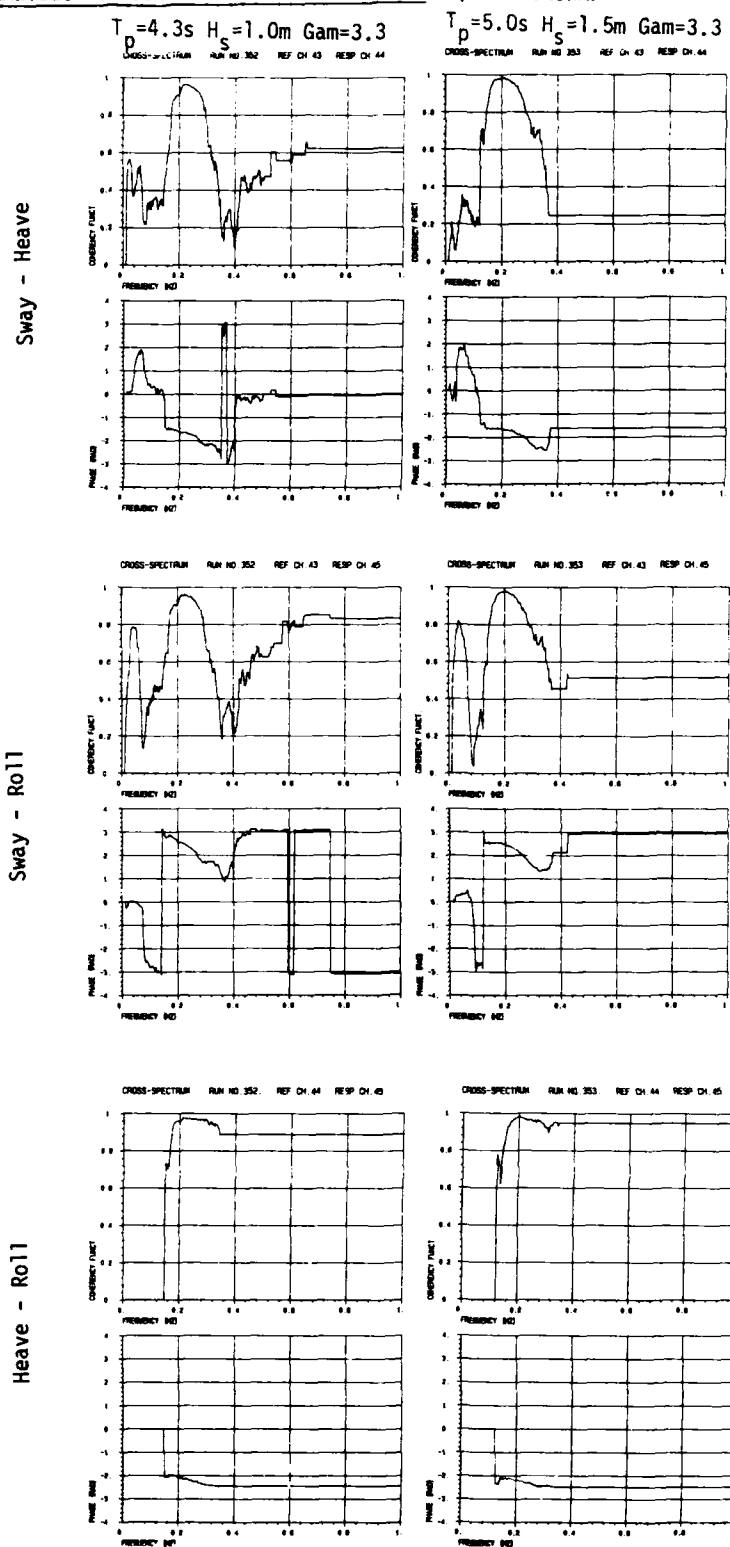


Fig. 3.171

4. COMPUTER SIMULATIONS WITH A SIMPLE NUMERICAL MODEL

4.1. Brief introduction

The linear wave frequency motions of the 2 floating breakwaters (46 m and 138 m long) have been calculated by means of the two dimensional stripe-theory program WAMOF, ref /7/.

Then, the quasistatic line tensions are calculated by means of the mooring analysis program MIMOSA, ref /8/.

Note, however, that the quasistatic line tension is not representative for the total line tension in these tests. Line dynamics due to inertia forces on the clump weights, give the main contribution to the total loads in the anchor lines.

In a more comprehensive theoretical analysis, both the wave frequency and the second order response can be simulated in the time domain. Then, the dynamic line tensions, which include non-linear drag forces and inertia forces on the clump weights, can be simulated from the forced upper end motions.

4.2. System description

4.2.1 Floating breakwaters

Two floating breakwaters have been analysed:

- Floater no 1 consists of two sections, each 23 m long, with rigid connections.
- Floater no 2 consists of six sections, each 23 m long, with rigid connections.

The cross section of the breakwater is plotted in fig. 4.1. The breadth is 4.85 m and the draught is assumed to be 1.1 m.

The main data specified in the computer program WAMOF, are as follows:

	Floater no 1	Floater no 2
Length.	46 m	138 m
Total mass (x)	$2.52 \cdot 10^5$ kg	$7.55 \cdot 10^5$ kg
Radius of gyration, x (x)	1.7 m	1.7 m
----- " ----- , y	13.4 m	39.8 m
----- " ----- , z	13.4 m	39.8 m

(x) Incl. clump weight contribution.

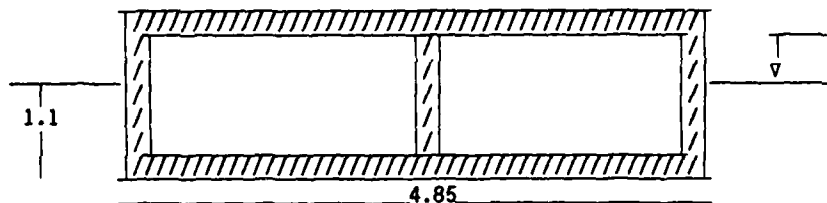


Fig. 4.1 Cross section.

4.2.2 Mooring system data

Each mooring line is divided into three segments as follows:

	Type	Diam.	Weight	Length
Upper segment:	Chain	32 mm	190 N/m	6.1 m
Mean segment:	Wire	35 mm	38.1 N/m	92.7 m
Lower segment:	Chain	32 mm	190 N/m	4.6 m

The weights specified are weights in air. The ratio of submerged weight to the weight in air, is assumed to be 0.87 and 0.81, for chain and wire, respectively.

In addition, a clump weight of 8.9 kN, (submerged) is located approx. 11.9 m from the upper end of the mooring lines.

The average modulus of elasticity is assumed to be $7.0 \cdot 10^{10}$ N/m² for the whole mooring line.

The pretension in each mooring line, with zero external force, is assumed to be 18 kN.

4.2.3 Mooring system

Two different systems are considered:

The first system, floater no 1, has 10 mooring lines, equally distributed along the floater sides. The distance between two neighbour lines is 11.5 m.

The second system, floater no 2, has 26 mooring lines, 13 to each side, and a distance of 11.5 m between each line.

In order to improve the availability of the breakwaters, the mooring lines are crossing each other below the floaters. See fig 4.2.

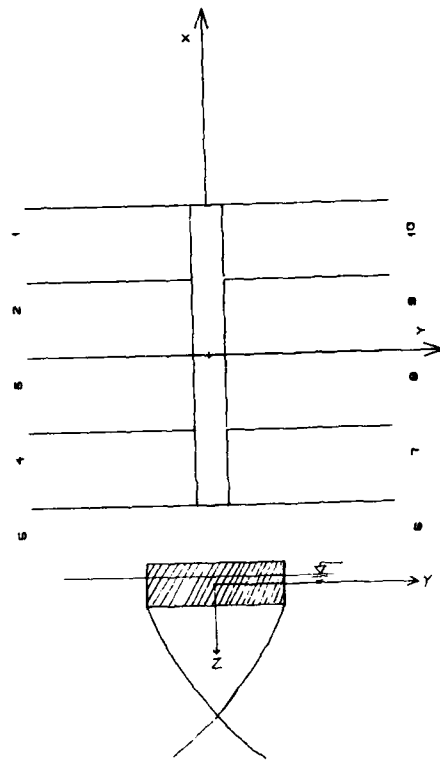


Fig. 4.2 The mooring system (system no. 1).

4.2.4 Wave conditions

The following wave conditions have been analysed:

Run no	Floater no	Hs (m)	Tp (s)	γ	Spreading function
301	1	0.75	3.2	3.3	\cos^8
302	1	1.0	4.3	3.3	\cos^8
303	1	1.5	5.0	3.3	\cos^8
307	1	0.93	3.0	2.0	\cos^8
308	1	0.65	2.8	2.0	\cos^8
309	1	0.65	2.4	2.7	\cos^8
311	1	0.75	3.2	3.3	\cos^2
312	1	0.75	3.2	3.3	long crest
313	1	1.0	6.3	" "	regular waves
315	1	0.75	3.2	" "	" "
501	2	0.75	3.2	3.3	\cos^8
502	2	1.0	4.3	3.3	\cos^8
503	2	1.5	5.0	3.3	\cos^8
509	2	0.65	2.4	2.7	\cos^8
511	2	0.75	3.2	3.3	\cos^2
512	2	0.75	3.2	3.3	long crest
513	2	1.0	6.3	" "	regular waves
515	2	0.75	3.2	" "	" "

Table 4.1 Wave conditions

All irregular wave conditions are modelled by JONSWAP type spectra.

4.3. Results

4.3.1 Wave frequency response

A linear frequency domain response analysis is performed. This means that all statistics are described by the response spectrum, only.

The response spectrum, $S_r(\omega) = H(\omega)^2 \cdot S_w(\omega)$, where

- ω is the wave frequency, (rad/s).
- $H(\omega)$ is the linear motion transfer function
- $S_w(\omega)$ is the actual wave spectrum

$H(\omega)$ is calculated by means of the two dimensional stripe theory program WAMOF, ref /7/. Geometry and mass data are specified as input to WAMOF. The average mooring stiffness, obtained from fig. 4.3, is also given as input.

The calculated motion transfer functions in six degrees of freedom are plotted in section 4.3.3, both for floater no 1 and no 2. The transfer functions are referred to the centre of gravity.

The following resonance periods are calculated:

	Floater no 1	Floater no 2
Surge	-	-
Sway	23.3 s	24.9 s
Heave	3.8 s	3.8 s
Roll	2.8 s	2.8 s
Pitch	3.8 s	3.8 s
Yaw	17.0 s	22.6 s

Results

Results from the wave frequency motion analysis are given in table 4.1 and 4.2.

The following statistical parameters are calculated from the response spectra, $S(\omega)$:

Est. max : Estimated maximum amplitude in 2 hours

Sign. : Significant value

Tz : Zero crossing period

B. width : Band width parameter

The following notations are used for the response components in the centre of gravity:

X11 - Translation in x-direction (surge)

X22 - Translation in y-direction (sway)

X33 - Translation in z-direction (heave)

X44 - Rotation about x-axis (roll)

X55 - Rotation about y-axis (pitch)

X66 - Rotation about z-axis (yaw)

Terminal point no 1, see fig. 4.2, is considered both for floater no 1 and no 2.

WAVE DIR.: 90.0 deg

RUN	PARAM.	STATIST. (m)			(deg)			TERM.P X22
		X11	X22	X33	X44	X55	X66	
301	EST.MAX.:	0.0	0.4	0.2	16.1	0.2	0.2	0.5
	SIGN.:	0.0	0.2	0.1	7.8	0.1	0.1	0.2
	TZ:	3.2	2.9	2.9	2.9	3.8	3.5	2.8
	B.WIDTH:	0.08	0.21	0.29	0.02	0.13	0.14	0.19
302	EST.MAX.:	0.1	0.7	0.5	13.9	1.0	0.7	0.7
	SIGN.:	0.0	0.3	0.2	6.8	0.5	0.4	0.3
	TZ:	4.7	3.8	4.1	2.9	4.4	4.3	3.7
	B.WIDTH:	0.14	0.27	0.27	0.02	0.05	0.06	0.29
303	EST.MAX.:	0.2	1.1	0.9	17.0	1.9	1.2	1.1
	SIGN.:	0.1	0.6	0.4	8.3	1.0	0.6	0.6
	TZ:	5.2	4.4	4.8	2.9	4.9	4.8	2.6
	B.WIDTH:	0.09	0.30	0.25	0.02	0.06	0.08	0.33
307	EST.MAX.:	0.0	0.5	0.3	24.9	0.2	0.2	0.6
	SIGN.:	0.0	0.3	0.1	12.1	0.1	0.1	0.3
	TZ:	3.1	2.7	2.6	2.8	3.5	3.2	2.6
	B.WIDTH:	0.10	0.21	0.28	0.01	0.17	0.14	0.17
308	EST.MAX.:	0.0	0.4	0.2	25.6	0.1	0.1	0.4
	SIGN.:	0.0	0.2	0.1	12.4	0.6	0.7	0.2
	TZ:	2.9	2.6	2.4	2.8	3.2	3.0	2.5
	B.WIDTH:	0.11	0.17	0.24	0.01	0.18	0.12	0.16
309	EST.MAX.:	0.0	0.3	0.2	12.0	0.8	0.9	0.4
	SIGN.:	0.0	0.2	0.1	5.8	0.4	0.5	0.2
	TZ:	2.6	2.3	2.1	2.8	2.4	2.5	2.3
	B.WIDTH:	0.12	0.16	0.15	0.03	0.09	0.07	0.13
311	EST.MAX.:	0.0	0.3	0.2	11.9	0.3	0.3	0.3
	SIGN.:	0.0	0.2	0.1	5.8	0.1	0.1	0.2
	TZ:	3.3	2.9	2.9	2.9	3.7	3.5	2.8
	B.WIDTH:	0.08	0.21	0.29	0.02	0.14	0.14	0.19
312	EST.MAX.:	0.0	0.6	0.3	20.5	0.0	0.0	0.6
	SIGN.:	0.0	0.3	0.1	10.0	0.0	0.0	0.3
	TZ:	0.0	2.9	2.9	2.9	0.0	0.0	2.8
	B.WIDTH:	1.00	0.21	0.29	0.02	1.00	1.00	0.18
313	EST.MAX.:	0.0	0.5	0.5	0.6	0.0	0.0	0.5
	T:	0.0	6.3	6.3	6.3	0.0	0.0	6.3
315	EST.MAX.:	0.0	0.3	0.1	4.4	0.0	0.0	0.3
	T:	0.0	3.2	3.2	3.2	0.0	0.0	3.2

Table 4.2. Wave frequency motion in c.o.g. and in terminal point.
Case 1.

WAVE DIR.: 90.0 deg

RUN	STATIST. PARAM.	(m)			(deg)			TERM.P X22
		X11	X22	X33	X44	X55	X66	
501	EST.MAX. : SIGN. : TZ : B.WIDTH :	0.0 0.0 3.3 0.10	0.4 0.2 2.9 0.21	0.2 0.1 2.9 0.28	15.1 7.3 2.9 0.02	0.0 0.0 0.0 1.00	0.0 0.0 0.0 1.00	0.4 0.2 2.8 0.19
502	EST.MAX. : SIGN. : TZ : B.WIDTH :	0.0 0.0 4.4 0.13	0.7 0.3 3.8 0.27	0.5 0.2 4.1 0.26	12.8 6.3 2.9 0.02	0.0 0.0 0.0 1.00	0.0 0.0 0.0 1.00	0.6 0.3 3.7 0.30
503	EST.MAX. : SIGN. : TZ : B.WIDTH :	0.1 0.0 5.1 0.11	1.1 0.5 4.3 0.30	0.8 0.4 4.7 0.25	15.7 7.6 2.9 0.02	0.1 0.1 5.4 0.10	0.0 0.0 0.0 1.00	1.0 0.5 4.3 0.34
509	EST.MAX. : SIGN. : TZ : B.WIDTH :	0.0 0.0 2.5 0.06	0.3 0.2 2.3 0.16	0.2 0.1 2.1 0.15	10.4 5.1 2.8 0.04	0.0 0.0 0.0 1.00	0.0 0.0 0.0 1.00	0.4 0.2 2.3 0.13
511	EST.MAX. : SIGN. : TZ : B.WIDTH :	0.0 0.0 3.3 0.11	0.3 0.2 2.9 0.21	0.2 0.1 2.9 0.28	11.1 5.4 2.9 0.02	0.0 0.0 0.0 1.00	0.0 0.0 0.0 1.00	0.3 0.2 2.8 0.19
312	EST.MAX. : SIGN. : TZ : B.WIDTH :	0.0 0.0 0.0 1.00	0.6 0.3 2.9 0.21	0.3 0.1 2.9 0.28	19.3 9.4 2.9 0.02	0.0 0.0 0.0 1.00	0.0 0.0 0.0 1.00	0.6 0.3 2.8 0.19
513	EST.MAX. : TZ :	0.0 0.0	0.5 6.3	0.4 6.3	0.6 6.3	0.0 0.0	0.0 0.0	0.5 6.3
515	EST.MAX. : TZ :	0.0 0.0	0.3 3.2	0.1 3.2	4.4 3.2	0.0 0.0	0.0 0.0	0.3 3.2

Table 4.3. Wave frequency motion in c.o.g. and terminal point,
Case 2

The low frequency response, (LF) due to the slowly varying wave drift forces are not calculated in this scope of work.

In order to account for these effects, in calculation of the mooring line tension, the LF-motions should be obtained from the model tests. However, this has not been performed within this work.

In a more comprehensive analysis, both the low frequency and the wave frequency response components, and the corresponding instantaneous line tension can be simulated by means of the time domain simulation program MOSSI, ref /9/.

4.3.2 Mooring analysis

The quasistatic mooring analysis is performed by means of the computer program MIMOSA, ref /8/.

Input to MIMOSA is line data, (see chapter 4.2.2), and static environmental forces or displacements.

The total restoring force, and the tension in the heaviest loaded anchor line are plotted in fig. 4.3 versus the horizontal displacement in the terminal point.

Then the line profile is plotted in fig. 4.4, with a top tension of 18 kN.

RESTORING FORCE AND MAXIMUM LINE TENSION -----

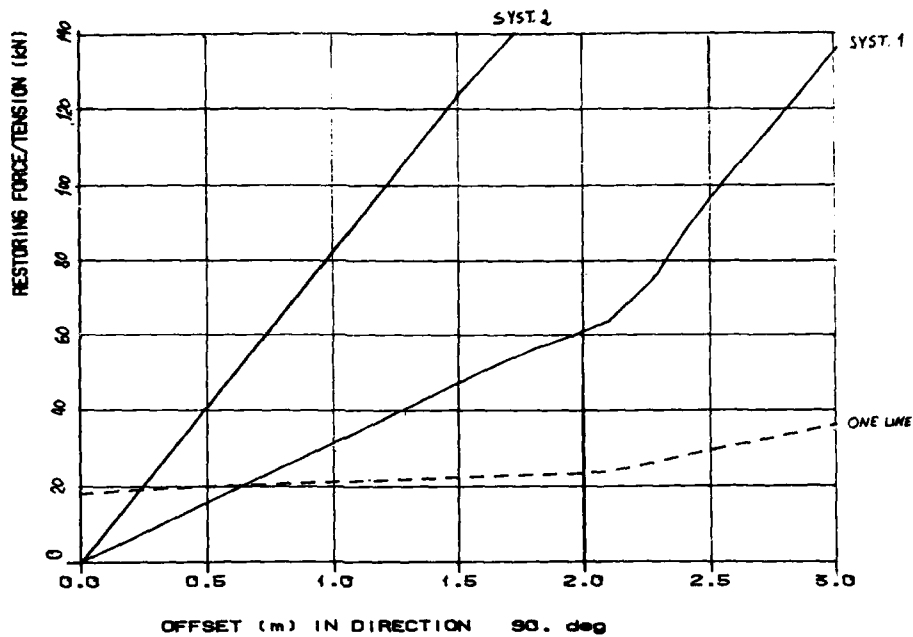


Fig. 4.3 Force displacement characteristic.

The quasistatic line tension in each wave condition is obtained by combining the total horizontal displacement in the terminal point, by the dotted curve in fig. 4.3. The results are given in table 3.3.

It should be stressed that the calculated line tensions do neither include dynamic effects in the mooring lines and the clump weights, nor the low frequency motions of the breakwater.

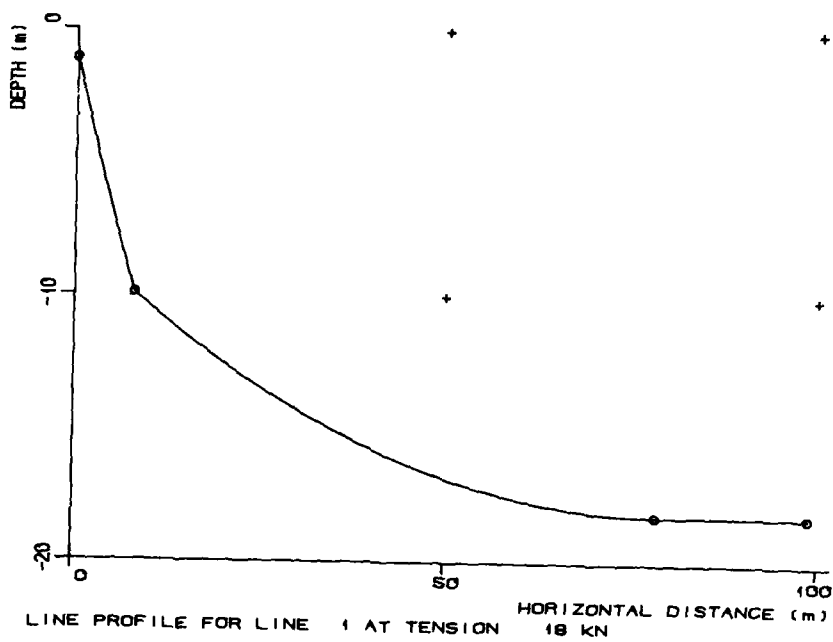


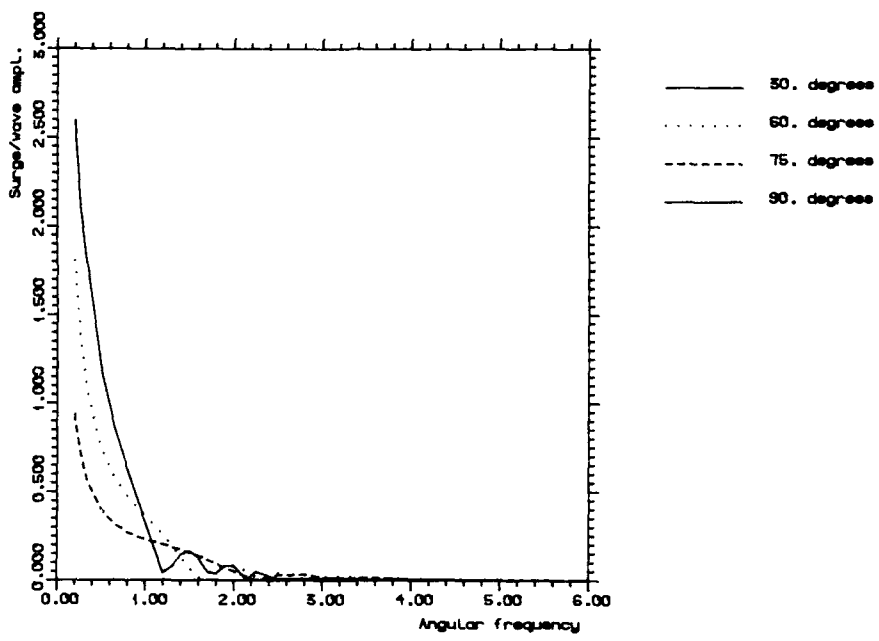
Fig. 4.4. Line profile with a tension of 18 kN.

Run	Static offse (m)	HF- motion (m)	Quasistatic line tension	
301	0.2	0.5	0.7	20
302	0.2	0.7	0.9	22
303	0.3	1.1	1.4	24
307	0.2	0.6	0.8	21
308	0.1	0.4	0.5	20
309	0.1	0.4	0.5	20
311	0.2	0.3	0.5	20
312	0.2	0.6	0.8	21
313	0.0	0.5	0.5	20
315	0.4	0.3	0.7	21
501	0.5	0.4	0.9	22
502	0.6	0.6	1.2	23
503	0.8	1.0	1.8	24
509	0.4	0.4	0.8	21
511	0.5	0.3	0.8	21
512	0.5	0.6	1.1	22
513	0.2	0.5	0.7	21
515	0.9	0.3	1.2	23

Table 4.4 Total terminal point motions, and corresponding quasistatic line tension.

4.3.3. First order motion transfer functions

FLOATER NO. 1



FLOATER NO. 2

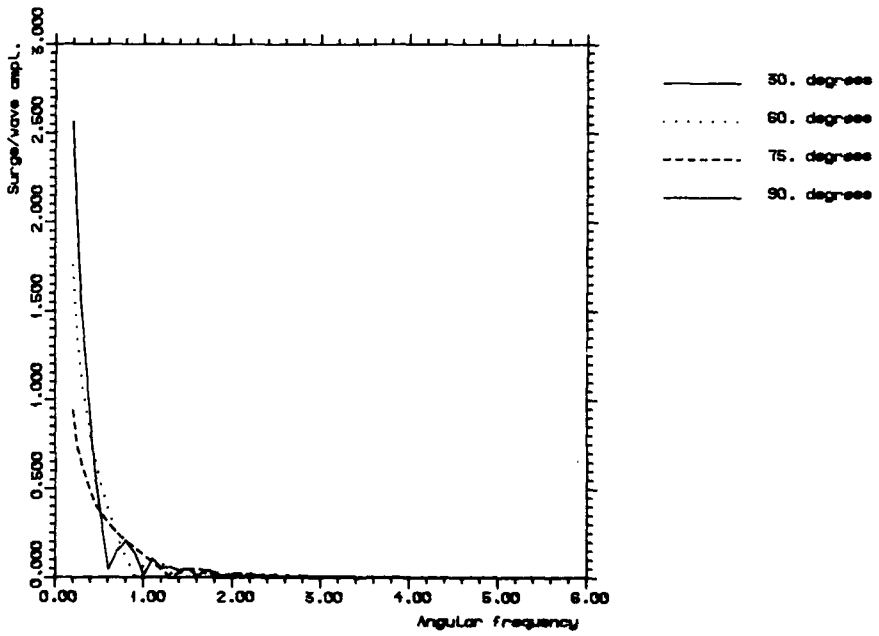
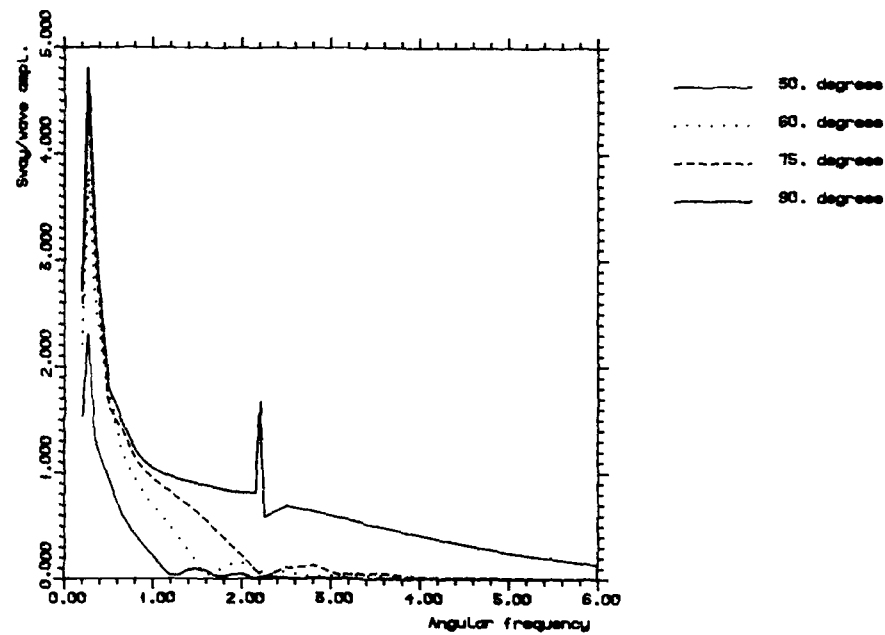


Fig. 4.5 Transfer functions, surge

FLOATER NO. 1



FLOATER NO. 2

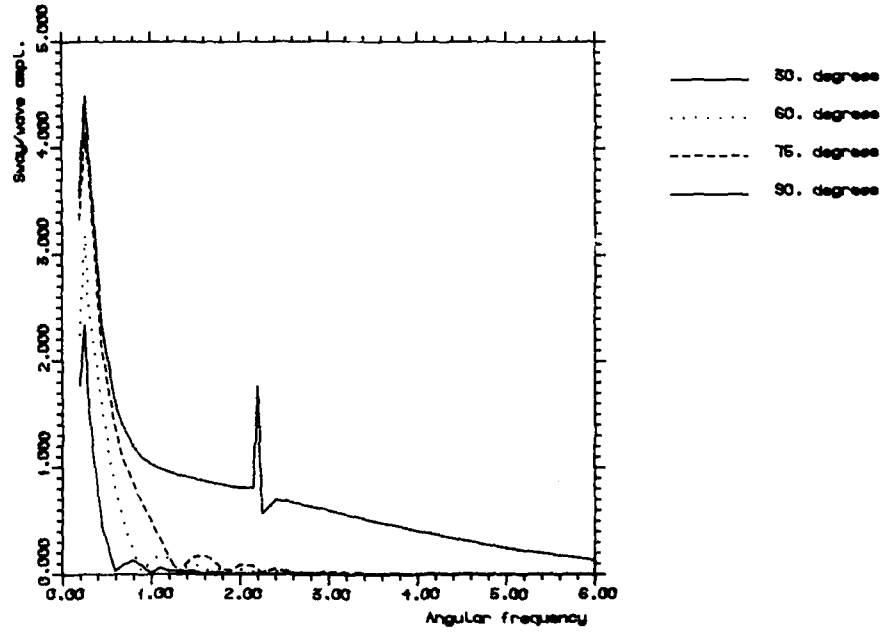
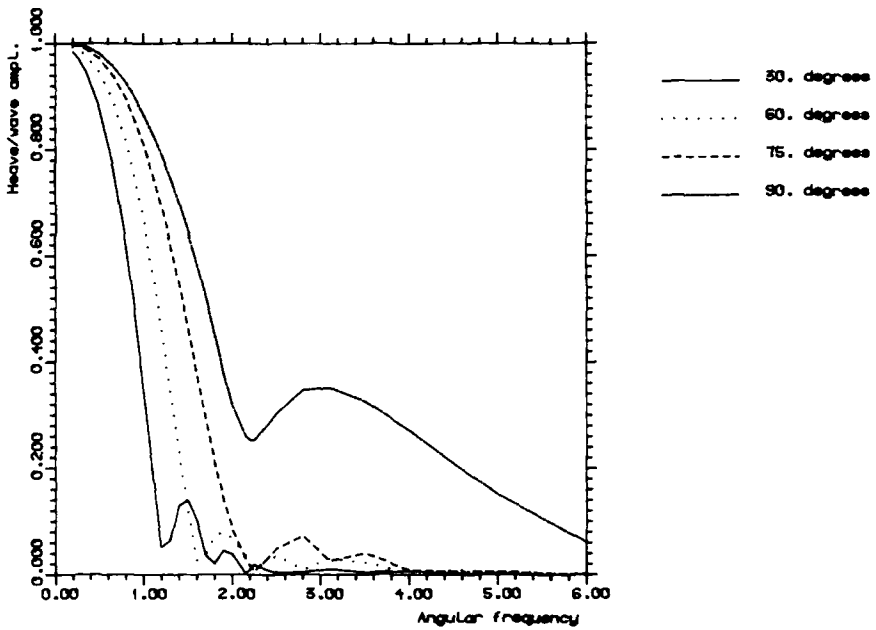


Fig. 4.6 Transfer functions, sway

MOL01



FLOATER NO. 8

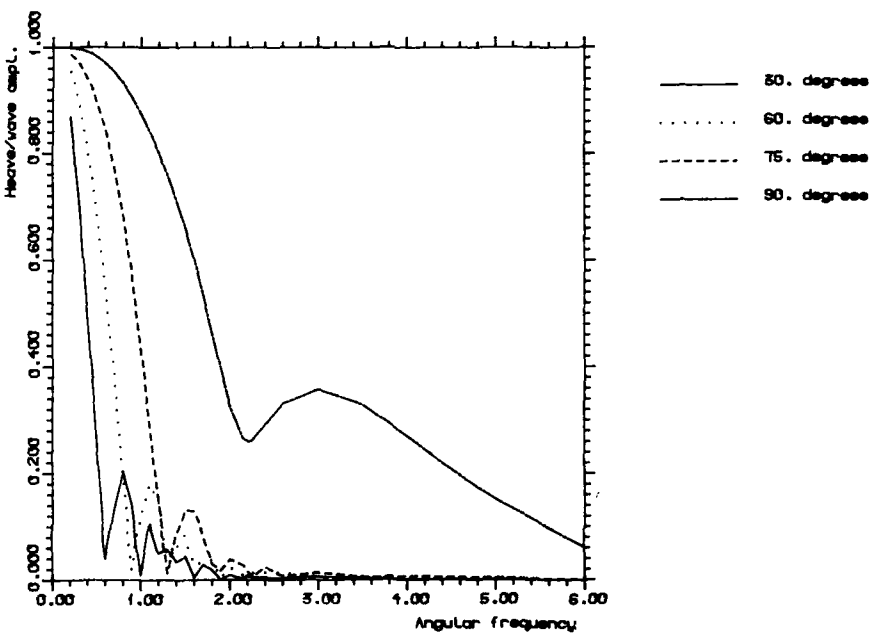
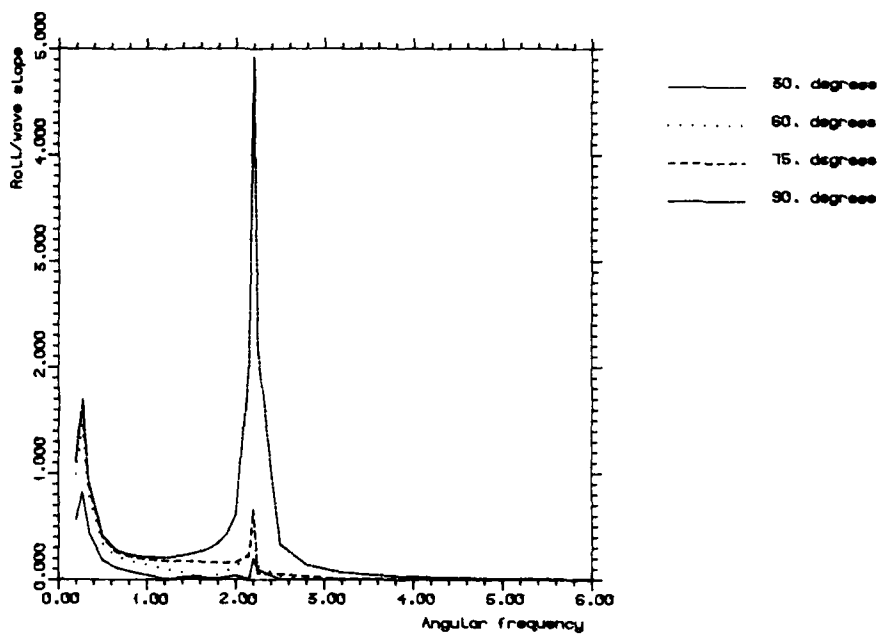


Fig. 4.7 Transfer functions, heave.

FLOATER NO. 1



FLOATER NO. 2

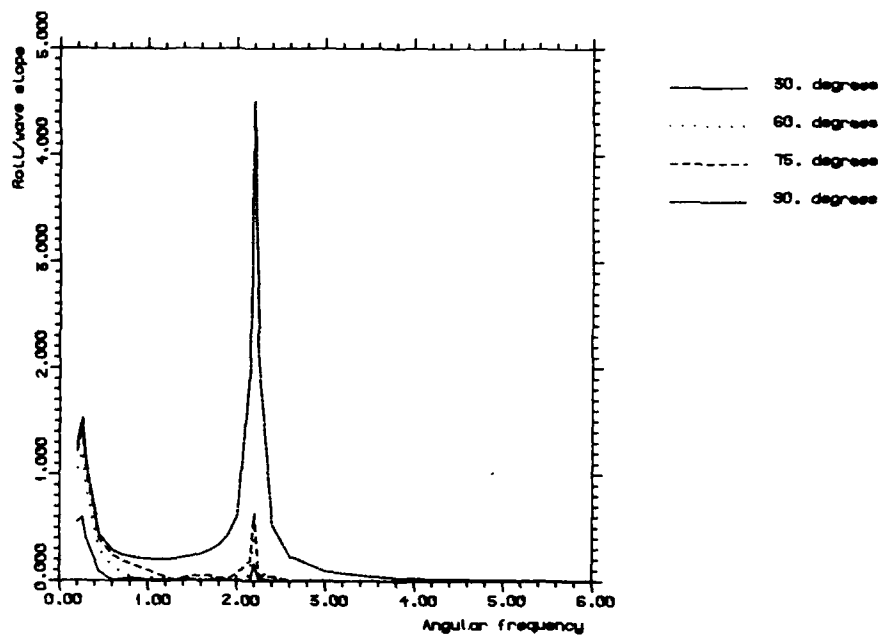
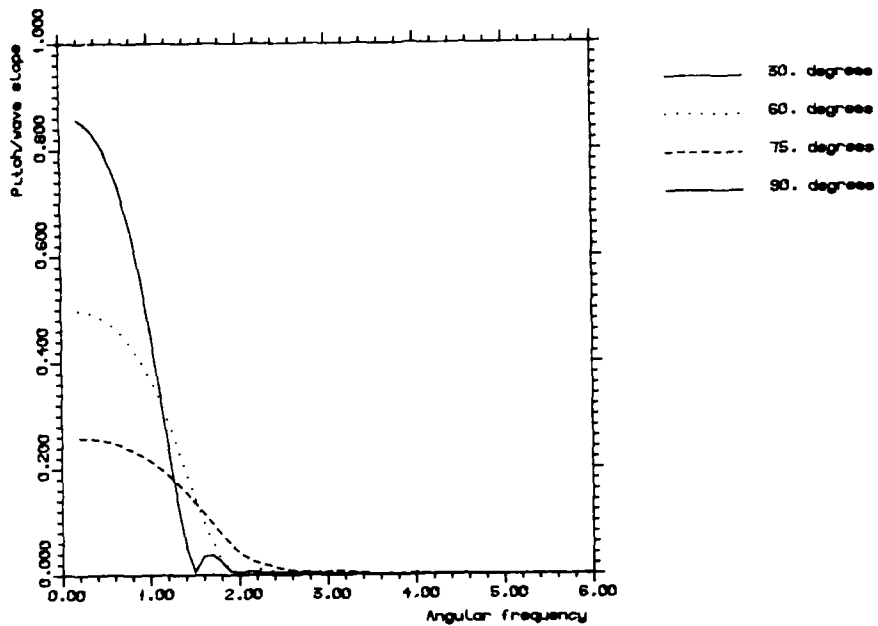


Fig. 4.8 Transfer functions, roll.

FLOATER NO. 1



FLOATER NO. 2

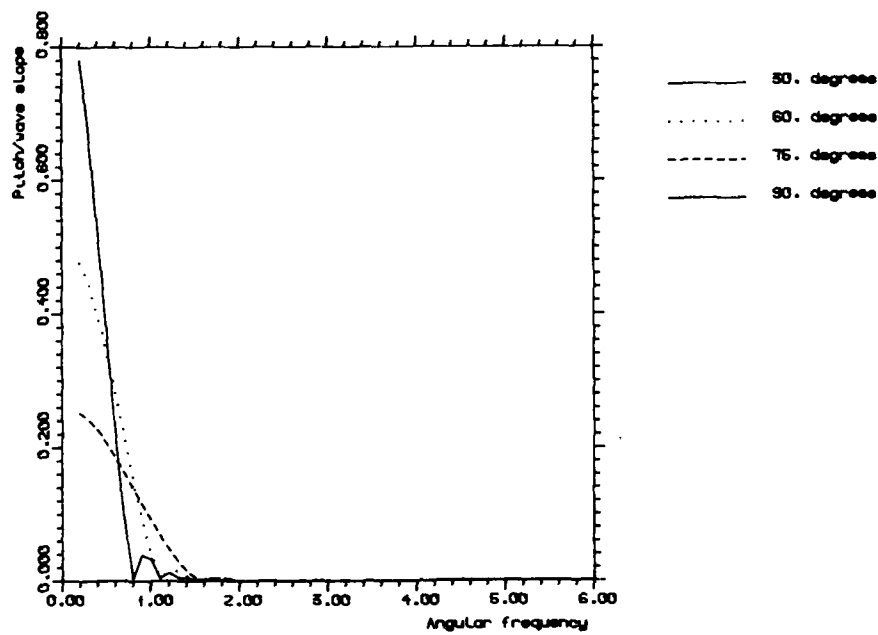
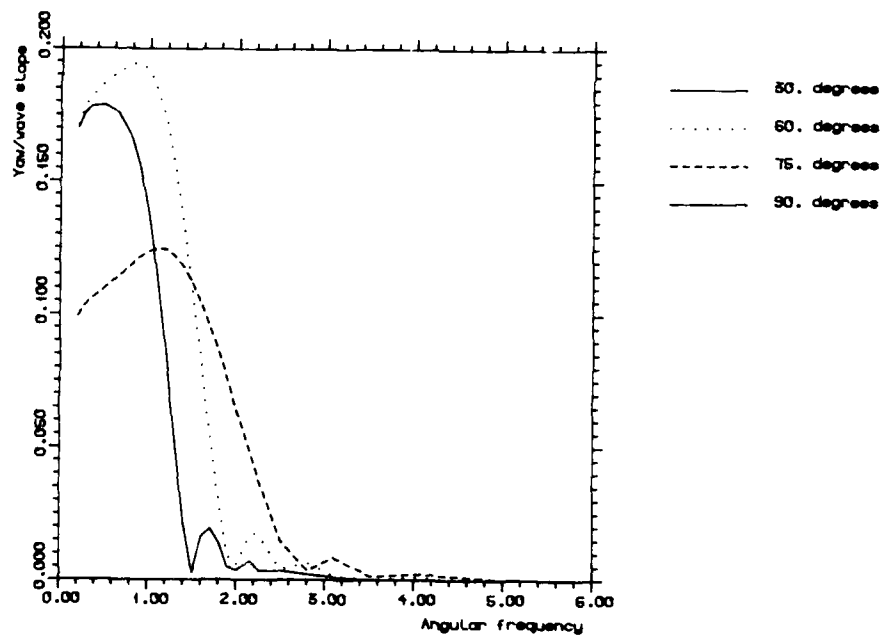


Fig. 4.9 Transfer functions, pitch.

FLOATER NO. 1



FLOATER NO. 2

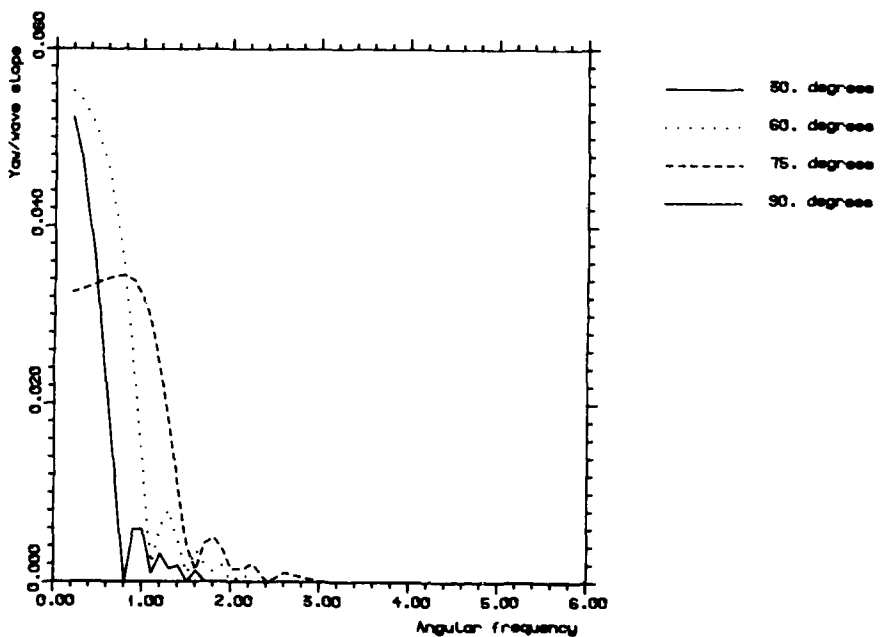


Fig. 4.10 Transfer functions, yaw.

5. DISCUSSION AND CONCLUSIONS

The results show clearly that the wave periods chosen for the experiment cover exactly the critical range of the tested breakwater. The shortest waves (peak period irregular waves 2.4s fullscale) are very efficiently reduced by the breakwater, with relatively small mooring line forces (max ~ 30 kN in a single line) and motions. The largest waves (peak period irregular waves 5.0s full scale, regular wave period 6.3s) are more or less unaffected by the breakwater and may cause critically large forces (max ~ 100-200 kN in a single line) and motions. Thus the experiment serves well as a test of the performance of such a breakwater, in addition to being used as a verification of prototype results.

As indicated through this observation, it is also clear that the wave period is one of the most critical parameters in a floating breakwater problem, for a given breakwater geometry. This is reasonable, since the mechanisms governing the hydrodynamical problem depends particularly on the breakwater size (width) relative to the wavelength, and on the roll motion resonance period.

Other important parameters of the problem are the significant wave height, the shortcrestedness of the waves, and the type of connection (coupling) between the pontoons (in the present case: fendered or stiff). In addition, the breakwater is certainly sensitive to the mean wave direction Θ_m , although that dependence has not been tested in the model experiment - Θ_m is 90° to the breakwater long axis in all the test runs.

The wave reduction analysis shows that the breakwater is reasonably efficient for sea states with peak periods 4s or shorter (full scale). For short-crested waves, the range of the breakwater extends to somewhat longer waves (more reflection for non-perpendicular wave contributions). The stiff model is slightly more efficient than the fendered one. One should also note that a significant part of the transmitted wave energy lies in the overharmonic range (non-linear energy transport).

The analysis of the waves in front of the model shows that the breakwater works as a reasonably good reflector. This causes local and temporary standing wave situations in front, with rough sea and fairly high wave crests due to Stoke's non-linearities. Other main mechanisms contributing to the wave reduction are wave dissipation and wave absorption (excitation of roll motion near resonance).

Wave height statistics and wave grouping are seen to follow the theoretical predictions fairly well, regardless of the model present or not. Long-crested waves

are seen, however, to be slightly more grouped than shortcrested.

The mooring line force analysis shows that in shortcrested waves, the maximum force of a test run is generally larger for the fendered model than for the stiff model. This is mainly due to the y-shaped coupling of central mooring lines, connecting pontoon 1 and 2 (see section 2.2). The chains coupled together in the y-couplings restore the relative motions between the 2 pontoons. Restoring forces of that kind are often very abrupt and non-linear. Thus the y-coupling is perhaps a weak point of the fendered breakwater. However, for the sea states with longest waves (~ 5s), the max. forces are more governed by the common motion of the pontoons, as in the case with the stiff breakwater.

The force spectra show significant non-linear components, both in the low-frequency and the high-frequency regions. The higher harmonics are partly due to nonlinear characteristics of the mooring lines at large displacement values (for moderate displacements the characteristics of the lines are expected to be close to linear - see chapter 4). The dynamics of the clump-weights probably also contribute in the higher-frequency range, as well as in the wave frequency region. For the fendered model, additional significant high-frequency non-linearities occur in the restoring force of the y-coupled chains, as a result of relative pontoon motions (see above). The low-frequency non-linearities arise from slow-drift motions of the breakwater. These motions turned out to be fairly large (see the discussion of motions analysis below).

Short-crestedness of the waves affect the fendered and stiff model differently. Results from tests in sea states having similar scalar spectra (with peak period around roll resonance) but different directional spectra (long-crested, $\cos^8\theta$ and $\cos^2\theta$) show that in the fendered model case, the force maximum is generally larger in short-crested than in long-crested waves. This is due to more irregular pontoon motions, in particular the larger relative motion between the pontoons. With the stiff model, however, there is a moderate decrease in force maxima due to short-crestedness.

In the linear (1. order) frequency range, the force transfer functions shows a significant peak around 3s (full scale), which is close to the roll resonance of a free floating pontoon.

The results for the force statistics confirm the non-linearities observed from the spectral plots. Predictions based on Rayleigh curves generally underestimate the extreme values.

From the analysis, and in particular by means of the coherence-phase analysis, it may be concluded that the mooring forces are to a large extent governed by the following effects:

- low-frequency sway motion
- roll motion
- pitch motion
- Yaw motion (stiff model)
- inertia forces and dynamical behaviour of clump weights
- relative motion between pontoons

The influence from the clump-weights on the forces is perhaps most easily seen in the coherence/phase-plots between force 11 and sway. Here the relative phase shifts from 180 deg. for low-frequency oscillations, to 0 deg. for wave-frequency oscillations. Thus for sway oscillations in the 2 - 5s range, the maximum forces occur when the model is closest to the wavemaker. This must be due to the clump-weights (inertia forces).

The importance of effects other than those obtained from regular waves and linear theory is very well demonstrated through the tests in long, regular waves (see the Data Reports), $H = 1.0\text{m}$ $T = 6.3\text{s}$. The maximum forces measured there were 22-24 kN full scale, (Static force = 18 kN), while tests in irregular waves with $T_p = 4 - 5\text{s}$, $H_s = 1 - 1.5\text{m}$, gave force maxima larger than 100 kN.

Spectral analysis of motions show that horizontal components (surge, sway and to a certain extent, yaw) are more or less dominated by non-linear slowdrift oscillations, with the linear components observed as smaller, "distorting" effects. This slow-drift motion arises from slow drift excitation forces combined with the damping properties of the moored system. The statistical analysis strongly confirm the picture of non-linear motions. It is observed that it is clearly unsatisfactory to fit the statistics with Rayleigh distributions, which may predict extreme values to be less than half of the measured values. The shape of the statistical distribution observed for the sway motion amplitude is, with a few exceptions, fairly close to a negative exponential function (χ^2 -distribution with 2 degrees of freedom), for which the standard deviation is equal to the mean deviation from the mean value.

In the spectral and statistical plots of vertical motional components (heave, roll and pitch) a more linear behaviour is observed. Transfer functions show that for the short-crested sea states, the roll motion has a resonance around 3.0s, which is in agreement with the resonance observed for a free floating pontoon (chapter 2). For the long-crested sea state, there is no obvious resonance peak for the roll motion, although the transfer function agrees reasonably with the short-crested cases. We also note that the statistics of the roll motion in some cases deviate somewhat from linear (Rayleigh) predictions: extreme values may be significantly lower than obtained from linear theory. It may seem that the roll motion is slightly locked to a certain amplitude range.

The results show that short-crestedness reduce the sway, heave and roll motions, and increase the surge, pitch and, to a certain degree, the yaw motions. (Theoretically, both surge, pitch and yaw should be zero in long-crested sea perpendicular to the breakwater. The experiment shows, however, some motion for these components).

The coherence/phase plots between motional components show a significant coupling between sway, heave and roll, except between sway and roll for short and very short-crested waves. In the linear (wave-frequency) region, the sway-heave dependence gradually shifts from the surface-slope-determined 90° phase delay for long waves, to a 180° delay for shorter waves (i.e. wave periods shorter than the roll resonance). Sway and roll are $\sim 150^\circ$ out of phase for long waves, while the delay reduces to $\sim 60^\circ$ - 90° for short waves. Heave and roll seem to be more or less locked to each other, with a relative phase $= -135^\circ$ for all wave periods, i.e. max. roll occurs always shortly before the breakwater is on a wave top. The wave short-crestedness does not seem to have any significant influence on these motional couplings, except from a moderately increasing decoupling with increasing short-crestedness, particularly for sway/roll. Phases are more or less unaffected.

Note that for small horizontal motions, especially sway and yaw, there is present a noticeable white noise arising from the optical measuring system. Motions less than 1 cm (model scale) are difficult to resolve with the actual model location in the Ocean Basin. Change of location, e.g., could increase resolution but the location was chosen to give optimal conditions for generation of short-crested waves. This noise was the reason for filtering at 3 Hz (model scale), but still the presented sway and yaw spectra and transfer functions for the smallest waves should be interpreted with care. Coherence/phase information between motional components should be ignored in frequency ranges where there is very little motional energy.

This report also includes a minor task with numerical simulations of the stiff breakwater motions. Significant simplifications made in the numerical model are the ignorance of the clumpweight dynamics, and of the slow-drift motions. The resulting transfer functions agree moderately well with the measured ones for sway, heave and roll, when one takes into account the simplifications made. Absolute values in sway and heave transfer functions show moderate (~ 50%) discrepancies. The numerically calculated roll resonance is 2.8s while the measured one is around 3.3s. The numerical peak is much sharper than the measured. For the sway motion, a peak in the numerically computed transfer function is observed at 20-25s, which agrees with the measured non-linear slow-drift resonance.

Accurate computer simulations with the actual breakwater should include the above mentioned ignored effects, since they are considered to be quite essential to the problem.

6. REFERENCES

1. Nelson, E.E. and Broderich, L.L., "Floating Breakwater Prototype Test Program: Seattle, Wash.", Final Report, Misc. Paper CERC-86-3, US Army Corps of Engineers, Wash. DC, 1986.
2. Stansberg, C.T., Otterå, G.O. and Slåttelid, O.H., "Model Tests with Floating Breakwaters - Long Models", MARINTEK Report, Trondheim, Norway 1987.
3. Tørum, A., "Model Tests on the CERC Full Scale Tend Floating Breakwater", MARINTEK Proposal No. 533010.01, Trondheim, Norway 1986.
4. Abelseth, L., Fløbak, T., Rensvik, E. and Røtvold, Ø., "NHL - Ocean Laboratory, Developments in Instrumentation and Measuring Systems", Proceedings, International Symposium on Hydrodynamics in Ocean Engineering, Norwegian Institute of Technology, Trondheim, Norway 1981, p.p. 1171-1191.
5. Stansberg, C.T., "Statistical Analysis of Slowdrift Responses", Journal of Energy Resources Technology, Vol. 105, 1983, P.P. 310-316.
6. Pinkster, J.A., "Low-Frequency Second Order Wave Forces on Vessels Moored at Sea", Proceedings, 11th Symposium on Naval Hydrodynamics, London 1976.
7. WAMOF - A Computer Program for Calculation of Hydrodynamic Forces and Coefficients. Users Manual, MARINTEK, Trondheim, Norway.
8. MIMOSA - A Quasistatic Mooring Analysis Program. Users manual, MARINTEK, Trondheim, Norway.
9. MOSSI - Simulation of Motions of Moored and/or Dynamically Positioned Structures. Users Manual, MARINTEK, Trondheim, Norway.